UNIVERSITY OF CALIFORNIA,
IRVINE

Brain-Computer Interface Systems for Neurorehabilitation

DISSERTATION

submitted in partial satisfaction of the requirements
for the degree of

DOCTOR OF PHILOSOPHY

in Biomedical Engineering

by

Christine E. King

Dissertation Committee:
Professor Zoran Nenadic, Chair
Professor David J. Reinkensmeyer
Professor Frithjof Kruggel

2014

DEDICATION

To my parents, sister, and Patrick.

TABLE OF CONTENTS

LIST OF FIGURES

LIST OF TABLES

ACKNOWLEDGMENTS

I would like to thank my funders, the Roman Reed Spinal Cord Injury Research Fund of California (RR 08-258 and RR 10-281), the National Science Foundation (NSF-1134575, NSF-1056105, and NSF-1160200), the Institute of Clinical and Translational Science at the University of California, Irvine, and the American Academy of Neurology.

I would also like to thank my colleagues at the Center for Biomedical Signal Processing and Computation, Po T. Wang, Colin M. McCrimmon and Dr. An H. Do, as well as my advisor, Dr. Zoran Nenadic, for all their contributions and help with my thesis work.

Finally, I would like to acknowledge the publishers of our previous work, the Journal of Neuroengineering and Rehabilitation (BiomMed Central), the Journal of Neural Engineering (IOP Science), and the Medical Engineering and Physics Journal (Elsevier).

CURRICULUM VITAE

Christine E. King

EDUCATION

Doctorate of Philosophy in Biomedical Engineering – August, 2014
UNIVERSITY OF CALIFORNIA, IRVINE, Irvine, CA
Dissertation: *Brain-Computer Interface Systems for Neurorehabilitation*
Advisor: Professor Zoran Nenadic

Master of Science in Biomedical Engineering – September, 2010
UNIVERSITY OF CALIFORNIA, IRVINE, Irvine, CA
Thesis: *Towards the Development of High-Performance Electroencephalogram (EEG) Based Brain-Computer Interface (BCI) Systems*
Advisor: Professor Zoran Nenadic

Master of Science in Mechanical Engineering – May, 2009
MANHATTAN COLLEGE, Riverdale, NY
Thesis: *Redundant Manipulator for Power Wheelchair Used by BCI Unit*
Advisor: Professor Reza Jazar

Bachelor of Science in Mechanical Engineering – May, 2008
MANHATTAN COLLEGE, Riverdale, NY
Magna Cum Laude
Minor in Mathematics

Regents Diploma – June, 2004
SUFFERN HIGH SCHOOL, Suffern, NY
Completed high school in three years

PROFESSIONAL EXPERIENCE

UNIVERSITY OF CALIFORNIA, IRVINE, Irvine, CA
Writing Tutor for the Graduate Resource Center, June 2011 – January 2013

- Tutored writing for fellowships, grants, theses, and other technical reports in engineering and all other graduate fields

Teaching Assistant in Biomedical Engineering Department, January – March 2011

- Taught EEG Lab for Biomedical Engineering Laboratory
- Assisted in teaching Organ Transport Systems

HRL LABORATORIES, LLC., Malibu, CA
Intern in the Information Systems Sciences Laboratory, June – August 2012

- Designed an electroencephalogram (EEG) based brain-computer interface (BCI) driven virtual reality car using imagination of foot movement
- Researched cognitive workload for cognitive threat detection warning system that used rapid serial visual discrimination

LUCIUS PITKIN, INC., New York, NY
Intern for Con Edison, May – August 2009

- Conducted experiments on water hammer

MANHATTAN COLLEGE, Riverdale, NY
Graduate Assistant in Mechanical Engineering Department, January 2008 – May 2009

- Assisted in teaching Thermal–Fluids Laboratory
- Taught Manufacturing Laboratory

Manhattan College Writing Center, September 2006 – May 2008

- Math and engineering tutor

Undergraduate Research, September 2006 – May 2008

- Research and analysis conducted on stresses in willow trees using IDEAS with Dr. Zella Kahn-Jetter and Dr. Lance Evans
- Used Labview to analyze and test baby dummies for shaken baby syndrome research with Dr. Graham Walker
- Designed and built a prototype of a device to assist wheelchair users over curbs with advisor Dr. Bahman Litkouhi
- Designed an experiment to test an unknown material using emissivity and radiation with advisor Dr. Mohammad Naraghi

RYAN CONSULTING ENGINEERS, New York, NY
Design Engineer in HVAC, December 2007 – September 2008

- Used AutoCad to draft electrical, plumbing, HVAC, fire alarm, and asbestos design

ROYAL NATIONAL ORTHOPEDICS HOSPITAL, Stanmore, England
Intern in ASPIRE Centre of Orthopedics, May – August 2007

- Analyzed wheelchair propulsion data, created finite element analysis on femur, tested forced plate for spinal cord injury patients

ROCKLAND COUNTY AMERICORPS, New City, NY
AmeriCorps Member, May – August 2006

- Assisted in building an ADA compliant trail along the Appalachian Trail

RICARDO CONSULTING ENGINEERS, Shoreham-by-Sea, West Sussex, England

Intern in Diesel Development Department, May – August 2005

- Created cost estimation database for manufacturing parts of engines, researched oil data for diesel engines, experimented with engines for reasons behind failure in a test bed

RESEARCH INTERESTS

Brain-computer interface (BCI) systems, neural engineering, neuroscience, robotics, neurorehabilitation, wearable sensors, assistive devices, control systems, biomedical signal processing, electroencephalography (EEG), electrocorticography (ECoG), machine learning.

FELLOWSHIPS AND AWARDS

First Place Winner of the UCI IEEE EMBS Industry Night Poster Contest, 2014

UCI Graduate Student Research and Travel Grant Award Recipient, 2014

First Place Winner of the OCGWIS Spring Conference PhD Oral Presentations, 2014

Center of Cognitive Neuroscience and Engineering (CENCE) Graduate Merit Fellowship Recipient, 2013

Travel Award for the 2013 International BCI Meeting, 2013

Travel Award for the BMBI Workshop at the IEEE EMBC 2012 Conference, 2012

The Brother Aubert Medal for Mechanical Engineering, 2008

Presidential Scholarship, LaSallian Honor Society, 2004 – 2008

Honors Enrichment Program, 2004 – 2008

Pi Tau Sigma, Mechanical Engineering Honors Chapter, 2004 – 2008

Epsilon Sigma Pi Honors Society, 2004 – 2008

Tau Beta Pi Engineering Honors Society, 2004 – 2008

PROFESSIONAL MEMBERSHIPS

The Institute of Electrical and Electronics Engineers (IEEE), IEEE Engineering in Medicine and Biology Society (EMBS), American Society of Mechanical Engineers (ASME), Rehabilitative Engineering and Assistive Devices Society of North America (RESNA)

UNIVERSITY EXPERIENCE

UNIVERSITY OF CALIFORNIA, IRVINE

Writing Tutor for the Graduate Resource Center, 2011 – 2013

Backup Housing Assistant for Palo Verde Housing Community, 2011

Teaching Assistant for the Biomedical Engineering Department, 2010 – 2011

Secretary for IEEE EMBS Society, 2010 – 2013

MANHATTAN COLLEGE

Graduate Assistant for the Mechanical Engineering Department, 2008 – 2009

Math and Engineering Tutor for Manhattan College, 2006 – 2008

Mechanical Engineering Student Advisory Committee, Member, 2006 – 2008

VOLUNTEER WORK

Rocket Science Tutors, 2010 – 2014

ROCKET SCIENCE TUTORS, McFadden, MacArthur Intermediate School, and Century High School, Santa Ana, CA

- Tutored 12 – 16 year olds science in after school program and several other outreach program days
- Performed outreach demos at UCI, Youth Leadership Summit in Santa Ana, CA, at the Boys and Girls Club of America in Santa Ana, CA, and at Century High School in Santa Ana, CA

Coordinator: Nino Polizzi

Outreach at University of California, Irvine, 2009 – 2014

UNIVERSITY OF CALIFORNIA, IRVINE, Irvine, CA

- Outreach demos of P300 spelling device and anthropomorphic robotic arm for middle school, high school, and community college students

Coordinator: Debra Mauzy-Melitz

Volunteer at Helen Hayes Hospital, 2003 – 2008

HELEN HAYES HOSPITAL, Haverstraw, NY

- Assisted in recreational and cultural activities and data entry in the Gait and Cardiopulmonary Laboratories

INVITED TALKS

Brain Driven Electrical Stimulation for Overground Walking, June 2014
15th Annual UC Systemwide Bioengineering Symposium, Irvine, CA

Brain-Computer Interface Driven Functional Electrical Stimulation System for Presentations Overground Walking: A Case Report, May 2014
American Academy of Neurology Annual Meeting, Philadelphia, PA

Noninvasive Brain-Computer Interface Driven Functional Electrical Stimulation Device for Ambulation, April 2014
Orange County Graduate Women in Science 2014 Spring Conference, Irvine, CA

Mind Controlled Rehabilitation, February 2013
UC Irvine Salon TED Talk, Irvine, CA

Noninvasive Brain-Computer Interface Driven Hand Orthosis, June 2011
IEEE EMBS Conference 2011, Boston Massachusetts

BCI-Controlled Walking Simulator for a BCI-Driven FES Device, June 2010
RESNA 2010 Annual Conference, Las Vegas, NV

THESES AND DISSERTATIONS

C.E. King. Brain-Computer Interface Systems for Neurorehabilitation. Ph.D. Dissertation in Biomedical Engineering, University of California, Irvine, Irvine, CA, 2014.

C.E. King. Towards the Development of High-Performance Electroencephalogram (EEG) Based Brain-Computer Interface (BCI) Systems. M.S. Thesis in Biomedical Engineering, University of California, Irvine, Irvine, CA, 2011.

C.E. King. Redundant Robotic Manipulator for Power Wheelchair Used by BCI Unit. M.S. Thesis in Mechanical Engineering, Manhattan College, Riverdale, NY, 2009.

JOURNAL PUBLICATIONS

R.D. Flint, P.T. Wang, Z.A. Wright, **C.E. King**, M.O. Krucoff, S.U. Schuele, J.M. Resenow, F.P.K. Hsu, C.Y. Liu, J.J. Lin, M. Sazgar, D.E. Millett, Z. Nenadic, A.H. Do, M.W. Slutzky. Extracting kinetic information from human motor cortical signals. *NeuroImage*, 2014 (in press).

C.E. King, K.R. Dave, P.T. Wang, M. Mizuta, D.J. Reinkensmeyer, A.H. Do, S. Moromugi, Z. Nenadic. Performance assessment of a brain-computer interface driven

hand orthosis. *Ann. Biomed. Eng.*, 2014 (in press).

P.T. Wang, **C.E. King**, A.H. Do, Z. Nenadic. Pushing the communication speed limit of a noninvasive BCI speller. *ArXiv Preprint*, 2012.

A.H. Do, P.T. Wang, **C.E. King**, S.N. Chun, Z. Nenadic. Brain-computer interface controlled robotic gait orthosis: a case report. *J. Neuroeng. Rehabil.*, 10(111), 2013 (highly accessed).

C.E. King, P.T. Wang, L.A. Chui, A.H. Do, Z. Nenadic. Operation of a brain-computer interface walking simulator by users with spinal cord injury. *J. Neuroeng. Rehabil.*, 10(77), 2013.

P.T. Wang, **C.E. King**, L.A. Chui, A.H. Do, Z. Nenadic. Self-paced brain-computer interface control of ambulation in a virtual reality environment. *J. Neural Eng.*, 9(5), pp. 056016, 2012.

A.H. Do, P.T. Wang, **C.E. King**, A. Abiri, Z. Nenadic. Brain-computer interface controlled functional electrical stimulation system for ankle movement. *J. Neuroeng. Rehabil.*, vol. 8(49), 2011 (highly accessed).

P.T. Wang, **C.E. King**, A.H. Do, Z. Nenadic. A durable, low-cost electrogoniometer for dynamic measurement of joint trajectories. *Med. Eng. Phys.*, 33(5), pp. 546-552, 2011.

CONFERENCE PUBLICATIONS

C.E. King, P.T. Wang, C.M. McCrimmon, C.C.Y. Chou, A.H. Do, Z. Nenadic. Brain computer interface driven functional electrical stimulation system for over-ground walking in spinal cord injury participant. *In Proc. of the 36th Annual International Conference of the IEEE Engineering in Medicine and Biology Society*, (accepted).

C.M. McCrimmon*, **C.E. King***, P.T. Wang, S.C. Cramer, Z. Nenadic, A.H. Do. Brain-controlled functional electrical stimulation for lower-limb motor recovery in stroke survivors. *In Proc. of the 36th Annual International Conference of the IEEE Engineering in Medicine and Biology Society*, (accepted).

*Authors contributed equally.

P.T. Wang, **C.E. King**, C.M. McCrimmon, S.J. Shaw, D.E. Millett, C.Y. Liu, L.A. Chui, Z. Nenadic, A.H. Do. Electrocorticogram encoding of upper extremity movement duration. *In Proc. of the 36th Annual International Conference of the IEEE Engineering in Medicine and Biology Society*, (accepted).

P.T. Wang, **C.E. King**, A. Schombs, J.J. Lin, M. Sazgar, F.P.K. Hsu, S.J. Shaw,

D. Millett, C.Y. Liu, L.A. Chui, Z. Nenadic, A.H. Do. Electrocorticogram encoding of upper extremity movement trajectories. *In Proc. of the 6th International IEEE EMBS Conference on Neural Engineering*, pp. 1429-1432, 2013.

P.T. Wang, E.J. Puttock, **C.E. King**, A. Schombs, J.J. Lin, M. Sazgar, F.P.K. Hsu, S.J. Shaw, D.E. Millett, C.Y. Liu, L.A. Chui, A.H. Do, Z. Nenadic. State and trajectory decoding of upper extremity movements from electrocorticogram. *In Proc. of the 6th International IEEE EMBS Conference on Neural Engineering*, pp. 969-972, 2013.

P.T. Wang, **C.E. King**, S.J. Shaw, D. Millett, C.Y. Liu, L.A. Chui, Z. Nenadic, A.H. Do. A co-registration approach for electrocorticogram electrode localization using post-implantation MRI and CT of the head. *In Proc. of the 6th International IEEE EMBS Conference on Neural Engineering*, pp. 525-528, 2013.

A.H. Do, P.T. Wang, **C.E. King**, A. Schombs, S.N. Chun, Z. Nenadic. Brain-computer interface controlled robotic gait orthosis. *In Proc. of the 5th International Brain-Computer Interface Meeting*, Article ID 127, 2013.

P.T. Wang, **C.E. King**, A. Schombs, J.J. Lin, M. Sazgar, F.P.K Hsu, S.J. Shaw, D.E. Millett, C.Y. Liu, L.A. Chui, Z. Nenadic, A.H. Do. Electrocorticographic gamma band power encodes the velocity of upper extremity movements. *In Proc. of the 5th International Brain-Computer Interface Meeting*, Article ID 120, 2013.

A.H. Do, P.T. Wang, **C.E. King**, A. Schombs, J.J. Lin, M. Sazgar, F.P.K Hsu, S.J. Shaw, D.E. Millett, C.Y. Liu, A.A. Szymanska, L.A. Chui, Z. Nenadic. Sensitivity and specificity of upper extremity movements decoded from electrocorticogram. *In Proc. of the 35th Annual International Conference of the IEEE Engineering in Medicine and Biology Society*, pp. 5618-5621, 2013.

A.H. Do, P.T. Wang, **C.E. King**, A. Schombs, S.C. Cramer, Z. Nenadic. Brain-computer interface controlled functional electrical stimulation device for foot drop due to stroke. *In Proc. of the 34th Annual International Conference of the IEEE Engineering in Medicine and Biology Society*, pp. 6414-6417, 2012.

C.W. Lee, **C.E. King**, S.-C. Wu, A.L. Swindlehurst, and Z. Nenadic. Signal source localization with tetrodes: Experimental verification. *In Proc. of the 33rd Annual International Conference of the IEEE Engineering in Medicine and Biology Society*, pp. 67-70, 2011.

C.E. King, P.T. Wang, M Mizuta, D. Reinkensmeyer, A.H. Do, S. Moromugi, and Z. Nenadic. Noninvasive brain-computer interface driven hand orthosis. *In Proc. of the 33rd Annual International Conference of the IEEE Engineering in Medicine and Biology Society*, pp. 5786-5789, 2011.

P.T. Wang, **C.E. King**, L.A. Chui, Z. Nenadic, and A.H. Do. BCI controlled walking

simulator for a BCI driven FES device. *In Proc. of RESNA Annual Conference*, Las Vegas, Nevada, June 26-30, 2010.

C.E. King, R. Jazar, G. Walker. 6R manipulator robotic arm for a power wheelchair used by BCI unit. *11th ASME Summer Bioengineering Conference*, Lake Tahoe, CA, 2009.

ABSTRACTS

C.E. King, P.T. Wang, C.M. McCrimmon, C.C.Y. Chou, A.H. Do, Z. Nenadic. Noninvasive brain-computer interface driven functional electrical stimulation system for overground walking. *In Proc. of the 15th Annual UC Systemwide Bioengineering Symposium*, Irvine, CA, 2014.

C.E. King, C.M. McCrimmon, P.T. Wang, C.C.Y. Chou, A.H. Do, Z. Nenadic. Noninvasive brain-computer interface driven functional electrical stimulation device for ambulation. *In Proc. of the Orange County Graduate Women in Science 2014 Spring Conference*, Irvine, CA, 2014.

C.E. King, C.M. McCrimmon, P.T. Wang, C.C.Y. Chou, Z. Nenadic, A. H. Do. Brain-computer interface driven functional electrical stimulation system for overground walking: a case report. *In Proc. of the American Academy of Neurology 2014 Annual Meeting*, Philadelphia, PA, 2014.

A.H. Do, P.T. Wang, **C.E. King**, A. Schombs, Z. Nenadic, S.C. Cramer. Brain-computer interface controlled functional electrical stimulation as a novel approach to improving foot-drop after stroke. *In Proc. of the 2013 International Stroke Conference*, Honolulu, HI, 2013.

A.H. Do, P.T. Wang, **C.E. King**, S.N. Chun, Z. Nenadic. Brain-computer interface controlled robotic gait orthosis. *In Proc. of the 34th Annual International Conference of the IEEE Engineering in Medicine and Biology Society Workshop on Brain-Machine-Body Interfaces*, San Diego, CA, 2012.

P.T. Wang, **C.E. King**, A.H. Do, Z. Nenadic. Breaking the communication speed limit: a high-performance noninvasive BCI speller. *In Proc. of the 34th Annual International Conference of the IEEE Engineering in Medicine and Biology Society Workshop on Brain-Machine-Body Interfaces*, San Diego, CA, 2012.

A.H. Do, P.T. Wang, A. Abiri, **C.E. King**, and Z. Nenadic. Brain-computer interface control of functional electrical stimulation to restore foot dorsiflexion. *The 1st UC Irvine School of Medicine Clinical Basic & Translational Science Festival*, Irvine, CA, 2011.

A.H. Do, P.T. Wang, A. Abiri, **C.E. King**, and Z. Nenadic. Brain computer inter-

face control of functional electrical stimulation to restore foot dorsiflexion. *The 63rd American Academy of Neurology Annual Meeting*, Honolulu, HI, 2011.

Z. Nenadic, P.T. Wang, **C.E. King**, A.H. Do, L.A. Chui. Asynchronous brain-computer interface control of ambulation simulator. *Soc. Neurosci. Abstr.* 40:294.6, San Diego, CA, 2010.

C.E. King, P.T. Wang, Z. Nenadic, A.H. Do. BCI controlled walking simulator for a BCI driven FES device. *The 39th Neural Interfaces Conference*, Long Beach, CA, 2010.

A.H. Do, P.T. Wang, **C.E. King**, L.A. Chui, Z. Nenadic. Asynchronous BCI control of walking simulator. *The 4th International BCI Meeting*, Asilomar, CA, 2010.

C.E. King, R. Jazar, G. Walker. 6R manipulator robotic arm for a power wheelchair used by a BCI unit. *4th Frontiers in Biomedical Devices Conference & Exhibition (sponsored by ASME Emerging Technologies)*, Irvine, CA, 2009.

FEATURED NEWS ARTICLES

BCI Controls Robotic Leg Orthosis, The O&P EDGE, OandP.com, September 7, 2012, <http://tinyurl.com/oxfy2vp>.

Mind-Controlled Robotic Legs Could Help the Paralyzed Walk (VIDEO), Betsy Isaacson, The Huffington Post, September 6, 2012, <http://tinyurl.com/ae954hw>.

Man Walks With Aid of Brain-Controlled Robotic Legs, Tanya Lewis, Wired Science, September 5, 2012, <http://tinyurl.com/cwxrct9>.

Researchers Tout Progress with Brain-Controlled Robotic Legs, Donald Melanson, Engadget, September 4, 2012, <http://tinyurl.com/czbzfpm>.

Team Reports Brain-Controlled Ambulation in Robotic Leg Test, Nancy Owano, Phys.org, September 4, 2012, <http://tinyurl.com/nea99dk>.

ABSTRACT OF THE DISSERTATION

Brain-Computer Interface Systems for Neurorehabilitation

By

Christine E. King

Doctor of Philosophy in Biomedical Engineering

University of California, Irvine, 2014

Professor Zoran Nenadic, Chair

This dissertation seeks to develop novel neurorehabilitative therapies and neuroprostheses for restorative treatments in stroke and spinal cord injury (SCI) individuals. Since standard physiotherapies and substitutive solutions only provide a limited degree of restoration of the lost motor behavior in these individuals, novel brain-computer interfaces (BCI) have been sought. To develop BCI systems for stroke and SCI individuals, a high-performance electroencephalogram (EEG) based BCI system was developed and tested under several conditions. This system utilized data-driven decoding methodologies to obtain real-time control of several external devices. The external devices that were integrated and tested with this BCI system include a hand orthosis for stroke individuals with hand weakness, a noninvasive functional electrical stimulation (FES) system for the treatment of post-stroke foot drop, a virtual reality training environment to assess attempted or kinesthetic motor imagery of walking control strategies, a robotic gait orthosis mounted on a treadmill for ambulation training after SCI, and a noninvasive FES device for overground walking for those with paraplegia due to SCI. The BCI systems directed towards the treatment of stroke individuals focused on elementary motor behaviors common in chronic stroke individuals: foot drop and hand weakness (i.e. grasping and extension of the hand). On the other hand, the BCI systems for SCI individuals focused on ambulation after paraplegia.

Finally, all systems were tested in both able-bodied individuals and those with stroke or SCI to assess the performance, safety, and applicability of these devices.

All BCI systems allowed individuals to control the external devices purposefully in real time. Furthermore, the BCI driven neurorehabilitative therapies and neuroprostheses presented here allowed for stroke and SCI individuals to obtain real-time control of the desired motor behavior using intuitive control strategies after only minimal training, and individuals were able to maintain this high level of control after several days to months. This provides preliminary evidence that neurorehabilitative therapies and implantable neuroprostheses in stroke and SCI individuals are feasible. If future studies are successful, these systems may provide noninvasive training platforms for implantable neuroprostheses or noninvasive neurorehabilitative therapies for stroke and SCI individuals, thus becoming novel restorative treatments.

Chapter 1

Introduction and Background

1.1 Introduction

Brain-computer interface (BCI) systems have the potential to restore lost motor functions in individuals with stroke, spinal cord injury (SCI), and traumatic brain injury [9]. In a typical BCI system, electrophysiological signals are recorded from the brain, analyzed in real time, and then translated into control commands for various computer applications [7, 91], robotic manipulators [64, 105, 136], functional electrical stimulation (FES) devices [103, 112], and other electro-mechanical devices. Thus, in most biomedical applications where BCI technology has been implemented, the goal has been for individuals who suffer from severe paralysis or locked-in syndrome to be able to communicate via their brain waves and BCI computer [41].

Although BCI technology has been traditionally driven by applications for communication [41], this technology may also be used in motor restoration and neurorehabilitation. This may be done by strengthening the motor pathways between the brain and desired motor output through some form of neural plasticity or Hebbian learn-

ing [119]. Specifically, rehabilitation of the damaged pathways can foster reconnection of damaged neural circuits through strengthening the residual synaptic connections by coactivation of pre- and postsynaptic neurons [119]. By allowing the user's neural activity associated with the motor intention to be coupled with the desired motor behavior, the synaptic connections between the brain, spinal motor pools, and output motor neurons, can be strengthened.

The concept of using BCI systems to restore lost motor functions by combining brain intention with desired motor behaviors has been explored in our preliminary work [30, 34, 83, 81, 145] as well as in other research laboratories [17, 24, 64, 91, 100, 103, 105, 112, 136]. These studies typically focused on restoring motor behaviors in individuals with stroke and SCI, and they used both invasive and noninvasive methods to acquire brain signals. Additionally, the output devices that control motor behaviors in these individuals typically included FES systems, virtual reality environments, and robotic exoskeletons or manipulators. By augmenting or restoring the lost motor behaviors through the use of these technologies with BCI systems, neurorehabilitative therapies and the potential for functional motor improvements from BCI systems, as well as their applications towards neuroprostheses, have been explored.

This dissertation seeks to develop BCI systems that explore neurorehabilitative therapies and neuroprostheses for individuals with SCI and stroke. By integrating our high-performance noninvasive electroencephalogram (EEG) based BCI system with output devices that control motor behaviors such as FES systems and robotic orthoses, we have been able to successfully develop BCI systems for the treatment of foot drop, hand weakness, as well as systems for overground ambulation. The following sections and chapters will introduce BCI systems, applications of our BCI, and stroke and SCI neurorehabilitation. Then, the common methodologies of our BCI systems will be described, followed by an in-depth review of the BCI systems our

laboratory has developed for stroke and SCI neurorehabilitation. Finally, the future work of these systems will be examined, as well as the future direction of BCI systems for neurorehabilitation.

1.2 Background

1.2.1 Overview

BCI systems have traditionally been used as a means of communication for those who have severe paralysis or are affected by locked-in syndrome [41]. However, more recently, they have been used in motor restoration and the neurorehabilitation of stroke [5, 15, 24, 118], SCI [44, 64, 112], and traumatic brain injury individuals [66]. The following sections will introduce BCIs, as well as some conventional applications using BCI system developed by our laboratory. Then, the concept of motor restoration and neurorehabilitation will be discussed to show how our BCI system can be applied to the field of neurorehabilitation to restore motor movement in stroke and SCI individuals.

1.2.2 Brain-Computer Interface Systems

In a typical BCI system, electrophysiological signals are recorded from the brain, analyzed in real time, and then translated into control commands for various applications (Fig. 1.1[1]) [41]. In most biomedical applications of this technology, the goal has been for individuals who suffer from severe paralysis to be able to bypass the disrupted motor pathways by operating prostheses directly from the brain. In addition, BCI systems have become a valuable scientific tool for the biomedical field, as they allow

brain functions to be studied in the context of brain-machine interactions.

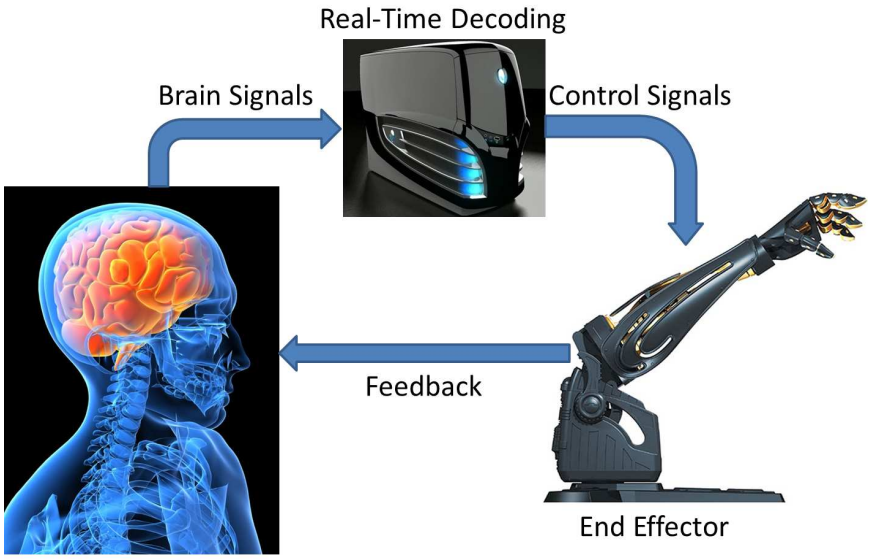

Figure 1.1: Schematic of a typical BCI system.

Based on the way BCIs acquire brain signals, these systems can be classified as either invasive or noninvasive. Invasive BCIs utilize either electrocorticogram (ECoG) signals, where electrodes are placed beneath the dura (on the surface of the brain), or action/local field potentials, which are recorded by intracortical electrode implants. Even though these signals have higher spatio-temporal resolution and better signal-to-noise ratios than scalp EEG recordings [92], obtaining these signals carry significant health risks. Thus, the majority of BCI devices use noninvasive EEG to acquire brain signals.

EEG signals are generated by cortical inhibitory and excitatory postsynaptic nerve cell potentials that summate in the cortex and extend to the scalp surface, where they are recorded as voltages [46]. Typically, these scalp-mounted electrodes are arranged in an array (examples shown in Figs. 1.2 and 1.3), conditioned and amplified using a bioamplifier, and then digitized for computer analysis, which usually involves further signal processing and statistical data analysis. Once these signals are processed, a machine learning algorithm or pattern recognition technique is used to extract infor-

mation from the EEG data to control various devices (Fig. 1.1), such as a computer cursor [100, 161], virtual keyboard for communication [125, 129, 130, 135, 138], virtual reality environment [7, 91], FES devices [103, 112], robotic manipulators [64, 105, 136], or other electromechanical devices.

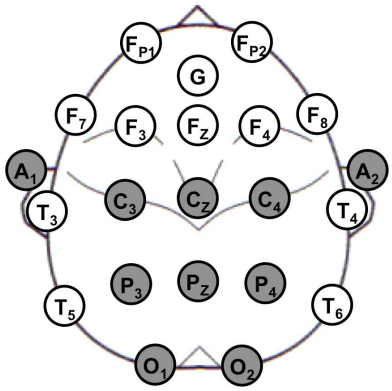

Figure 1.2: Layout of 19 EEG electrodes according to the 10-20 International Standard, where electrodes are placed at 10% and 20% intervals according to the nasion, inion, and left and right preauricular reference locations [72].

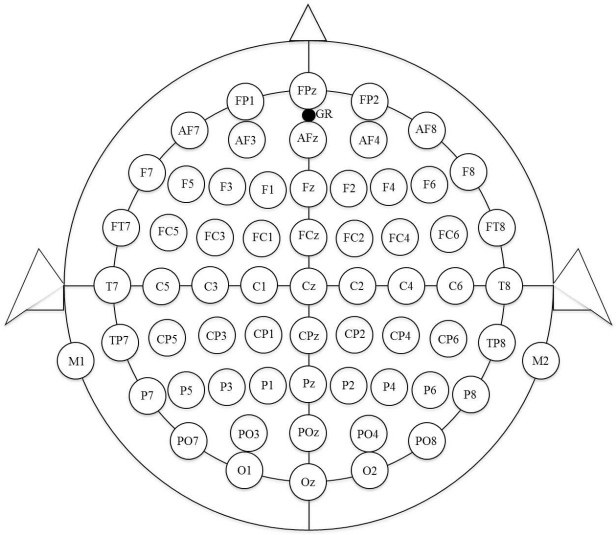

Figure 1.3: Layout of 64 EEG electrodes arranged according to the 10-10 International Standard, where electrodes are placed at 10% intervals according to the reference locations.

One of the most common and widely studied application of EEG based BCI systems is the virtual keyboard for communication, or the P300 speller system [41, 159]. Originally developed by Farwell and Donchin, [45], P300 speller systems rely on the P300 evoked potential [134], a positive deflection in EEG signals observed predominantly over the parietal lobe that occurs ∼300 ms after the presentation of an infrequent task-relevant stimulus, to control a virtual keyboard. These systems utilize the visual oddball paradigm [45], where participants are instructed to pay attention to a target stimulus in a random sequence of target and non-target stimuli presented on a computer screen. The participant's intentions can then be decoded in real time by detecting the presence of a P300 potential that coincides with the illumination of

the target letter on the virtual keyboard. By repeatedly illuminating the letters in a randomized fashion and detecting the corresponding P300 potentials, letters can be selected individually from a virtual keyboard to convey messages. These systems are potentially useful for individuals who suffer from locked-in syndrome [10] (i.e. those who suffer from quadriplegia and anarthria with the preservation of consciousness and vertical eye movement [132]) that cannot use residual movement based communication systems.

Other widely studied BCI applications attempt to restore motor function in individuals affected by paralysis due to stroke [5, 15, 24, 118], SCI [44, 64, 112], or traumatic brain injury individuals. These systems sometimes utilize 1-D [86] and 2-D [161] (sometimes even 3-D [100]) cursor systems to train an individual to control his/her sensory motor rhythms so that they are eventually able to control the cursor, and in turn the electromechanical device, purposefully in real-time. Other types of these systems attempt to use actual or imagined movement to control a BCI system through the use of sophisticated signal processing and machine learning algorithms [11, 103, 112]. However, these systems may require extensive training, so further investigation in movement based BCI systems for motor restoration is required.

Cue vs. Self-Paced BCI Systems

In addition to being classified as either invasive or noninvasive, the BCI applications mentioned above can also be classified into cue or self-paced BCI systems. In a cue-paced BCI system, the user is only allowed to assume control of a device upon presentation of a cue (i.e. outside of this time window, the BCI is not engaged). On the other hand, self-paced BCI systems allow the participant to make their own decisions on when to initiate control of the BCI. Another difference between cue-paced

and self-paced BCIs is that the former uses spatio-temporal features, while the latter uses spatio-spectral features to classify brain data. For instance, spatio-temporal features are used in the P300 speller system because oddball and non-oddball EEG signals are event-related potential [134] (as mentioned in Section 1.2.2) that are time-locked to the stimuli. Conversely, self-paced BCI systems rely on spatio-spectral features as there is no time-locked stimuli to be locked to during real-time operation, only the user's intention (e.g. imagery or attempted movement).

Self-paced BCI systems developed in our laboratory (Fig. 1.4) can be further categorized as: i) motor imagery based, and ii) movement based. Motor imagery based BCI systems require the participants to generate motor imagery (mental rehearsal of a motor act or attempting the motor act without any motor output) in order to control the output device. On the other hand, movement based BCIs require the participants to use actual movement or residual movement to control the output device. These BCIs will potentially target populations of users with preserved residual movement (e.g. stroke survivors who suffer from foot drop or incomplete motor SCI), while motor imagery based BCIs are targeted towards participants with complete motor paralysis.

Despite the differences between self-paced and cue-paced BCIs, both types of systems utilize signal acquisition, an open-loop training procedure, and classification (these procedures will be described in Chapter 2). The details of our cue-paced BCI system, the P300 speller [148], will be presented in Section 1.2.3 below, followed by a description of the current research efforts in our invasive self-paced BCI study, the ECoG-Robot project. The other projects presented in Fig. 1.4 (projects 3–7) will be examined in the latter chapters, as they represent the current efforts towards the neurorehabilitation of stroke and SCI individuals.

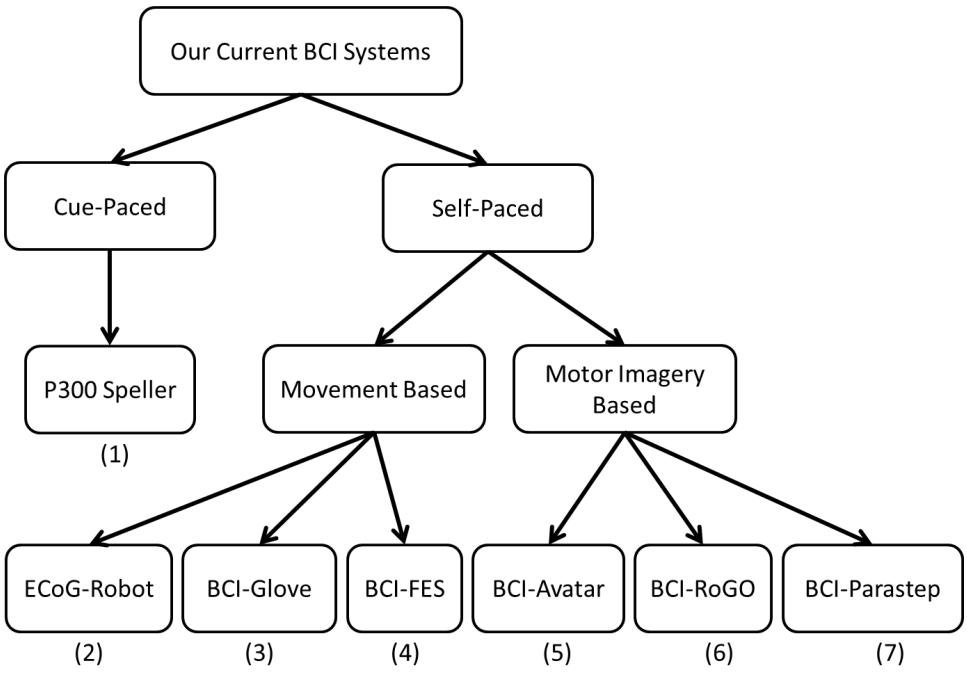

Figure 1.4: Overview of the BCI systems currently in development by our laboratory.

1.2.3 Cue–Paced BCI Research

As mentioned in Section 1.2.2, one of the most robust and well studied EEG based BCI communication systems is the P300 speller [41, 159]. However, in addition to the P300 speller, there are other more recent applications to cue-paced BCI research, such as BCIs that utilize the steady-state visual evoked potential (SSVEP) [2, 48, 101, 109, 166]. An SSVEP is elicited using a visual flickering stimulus (examples shown in Fig. 1.5) that is modulated at a fixed frequency [101], and is characterized by an increase in EEG activity over the occipital and parietal lobes at the specified stimulus frequency. Typically, the flickering stimulus is generated using white fluorescent light whose luminance is modulated between 6 – 13.5 Hz [101, 104]. The neural response to these frequencies can be then be utilized in BCIs by having various visual targets flashing at specific frequencies, each associated with a particular command [143]. This has been successfully performed by various laboratories [2, 48, 101, 109, 166, 167], and it has been shown that SSVEP based BCI systems can obtain information transfer

rates (ITR, see definition in Appendix B.4) between 0.03 – 1.13 bits/sec [143].

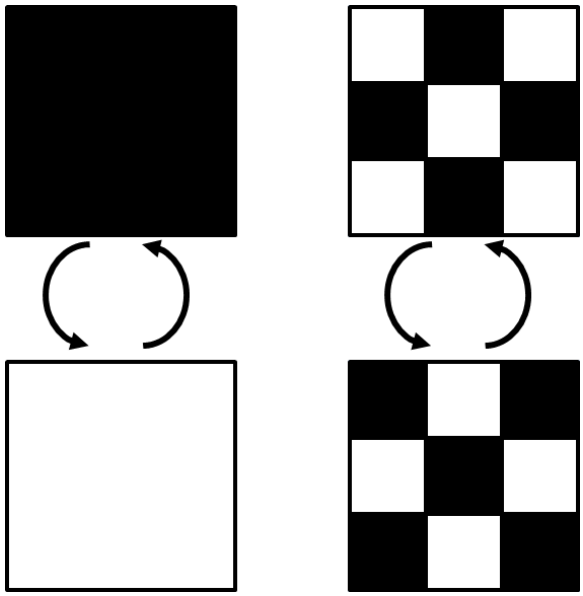

Figure 1.5: Typical visual presentation for an SSVEP based BCI system, depicting both the plain stimulus (left) and checkerboard stimulus (right) designs (e.g. those described in [143, 166]).

Similar to SSVEP based BCI systems, P300 speller systems can also achieve high ITRs (i.e. communication rates). Specifically, it was hypothesized in [45] that a P300 speller BCI system could achieve ITRs as high as 0.2 bit/s (or 2.3 characters/min). However, while subsequent studies (e.g. [55, 87, 138, 161]) have managed to optimize the original BCI spelling system and thus significantly improve its performance beyond this value, the achieved ITRs are still relatively modest and fall well below those of communication and/or control systems such as SSVEP [48] or systems that rely on residual motor function (e.g. eye movements [70]). Whether used in spelling, computer cursor movement, or other applications, it is generally accepted that the ITR limit of EEG based BCIs is $\sim$1 bit/sec [159], which remains a major obstacle to their adoption in both clinical and non-clinical applications. Thus, the goal of our P300 speller research [148] was to determine if our BCI system could achieve ITRs higher than those previously reported. This research allowed our lab to determine how our BCI system's performance compares to other laboratories.

P300 Speller System

The cue-paced P300 speller system developed by our laboratory [148] investigated the ITRs of able-bodied participants with little to no prior BCI experience. To this end, 6 able-bodied participants performed 3 experimental sessions on 3 different days over the course of 1 – 3 weeks. Within each daily session, participants performed BCI spelling experiments at 3 different speeds, where a short training procedure was performed followed by 1 – 3 online spelling sessions at each speed. The following sections will briefly describe the experimental protocols, and will show how the results of the study verified the high ITRs and performances of our P300 speller system.

Methods

As described in [148], each participant completed 3 experimental sessions over the course of 1 – 3 weeks in which participants performed P300 spelling experiments at 3 different interface speeds (see Table 2 in [148]). For each speed, a short training procedure was performed, followed by 1 – 3 online spelling sessions. Briefly, a training procedure was first performed by having the participant pay attention to a specific character from the speller matrix for 30 s (see Fig. 1.6 for the speller interface) while their EEG was recorded at the following electrode locations: C3, Cz, C4, P3, Pz, P4, O1, and O2 (see Fig. 1.2 in Section 1.2.2). Within this time frame, 42 characters were illuminated randomly in groups of 6 in a block randomized fashion, i.e. after a single cycle consisting of 7 illuminations, all 42 characters have been illuminated exactly once. Upon completing the cycle, the groups were re-randomized, and the whole procedure was repeated for 30 s. After this 30 s procedure, a short pause ensued, during which the participant was instructed to pay attention to another character, and the whole procedure was repeated for a total of 10 training characters. The whole

training session lasted ∼7 min for each speed.

Figure 1.6: Screen capture showing the matrix of characters in the P300 speller interface [148]. The illuminated characters are bold-faced and highlighted in pink. The typing prompt (yellow) shows the spelling progress.

For the online spelling sessions described in [148], participants were instructed to *correctly* spell the following sentence: **THE QUICK BROWN FOX JUMPS OVER THE LAZY DOG***. This sentence contains 44 characters, including spaces and the symbol * at the end to exit the interface, and is an English-language pangram, i.e. each letter of the English alphabet appears at least once in the sentence. In the case of a typing error, participants used the backspace symbol (<) to delete erroneously selected characters, and then proceeded with the correct sequence of letters.

To spell the above sentence in a free-spelling mode [10] (meaning that participants could choose letters rather than "copy spell" a pre-defined sequence), the BCI computer illuminated characters in groups of 6 in the same manner as done in the training sessions. In response to each illumination, an EEG trial was processed in real time and classified (see Chapter 2 for specific methods). The interface continued illuminating

these characters until an oddball trial was detected, in which the BCI computer then transitioned to a single-letter pattern where individual characters from the selected group were illuminated. Once an individual character was selected by classifying it as oddball, the interface highlighted the selected character and paused for 3 s to let the participant know of the decision. Note that the order in which the groups of letters and individual characters illuminated was based on the character's relative frequencies in the English language [148]. Finally, the interface included the selected character in the typing prompt (see Fig. 1.6) so that the participant could track his/her spelling progress.

To determine the online performance of each session, the BCI system was modeled as a binary communication channel (see Fig. 1.7) whose inputs are user intentions: o (select the highlighted character–oddball) and e (do not select the highlighted character–non-oddball), respectively, and whose output are the decoded intentions: $\hat{o}$ (select character) and $\hat{e}$ (do not select character). The transition probabilities between inputs and outputs was estimated from the training procedure.

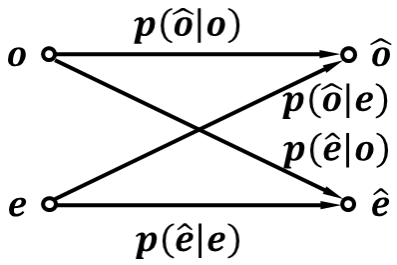

Figure 1.7: Our P300 speller system [148] described as an asymmetric noisy communication channel [21].

Using the communication model in Fig. 1.7, the amount of information per transmission is given by the mutual information between inputs and outputs [21], i.e.

$$I(\text{in}, \text{out}) = H(\text{out}) - H(\text{out}|\text{in}) \tag{1.1}$$

The explicit formula for calculating Eq. 1.1 is given in Appendix B.4. The ITR can then be calculated as: ITR $= BI(\text{in}, \text{out})$, where B is the number of transmissions (i.e. character illuminations) per unit of time.

For each online session, the total time T to correctly type the benchmark sentence (44 characters) was recorded by the BCI computer. The total time included the 3 s pause after each selection that allowed participants to be notified of their selection, track their typing progress, and visually locate the next desired character. This was true regardless of whether a correct or incorrect selection was made. In addition, the participants were required to correct the incorrect selections by backspacing. While in this case, the selection of $<$ (backspace) represents an intended action, so backspaces were *not* counted as correct selections since their purpose is to merely rectify previously committed error(s). As stringent as these requirements are, they set a standard for the definition of ITR that is completely immune to bit rate manipulations. More formally, practical, error-free ITR is defined as

$$\text{ITR} = \frac{N_c}{T} \log_2 |\mathcal{A}| \tag{1.2}$$

where N_c is the number of correctly typed characters (44 in this study), and $|\mathcal{A}|$ is the size of the alphabet ($|\mathcal{A}| = 42$ in this study).

Results

The performances from the training sessions described in [148] revealed that classification rates as high as 97.4% (Table 3 in [148]) were achieved (see Chapter 2 and Appendix A for methods). Furthermore, event-related potential analysis (obtained by averaging oddball and non-oddball trials) consistently revealed that participants utilized both the N200 and P300 potential, which were most visible on the occipital

lobe ∼190 ms post-stimulus and ∼290 ms post-stimulus, respectively (see Fig. 1.8). This is consistent with previously reported findings, e.g. [87] and [129].

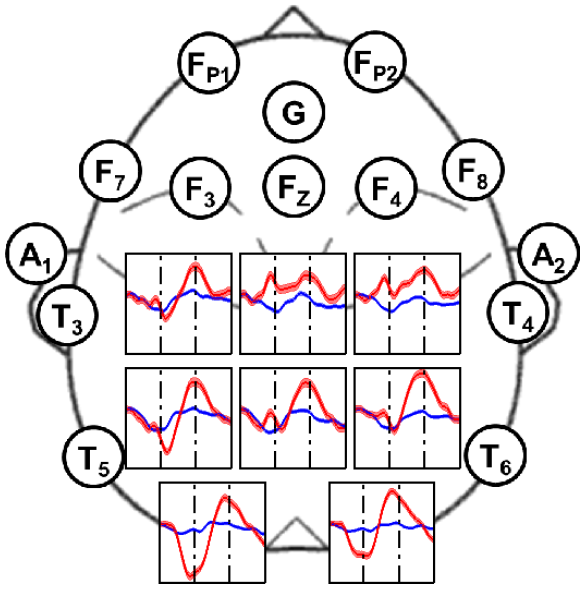

Figure 1.8: Event-related potential of oddball (red) and non-oddball (blue) trials for Participant 2, collected at the slow interface speed [148]. The error bars represent the standard error of mean. Each panel is 18 μV $\times$ 300 ms, with the grid lines corresponding to 200 and 300 ms post-stimulus.

In the online sessions, the ITR of each participant was determined by the total time taken (T) to correctly type the 44-character sentence and the formula presented in Eq. 1.2. This performance measure revealed that all participants were able to achieve their best results at the highest interface speed and were able to complete the task within a 3.45 – 4.51 min time window (see Table 4 in [148]). Additionally, participants were able to reach practical, error-free ITR values as high as 1.146 bit/s (Table 4). This bit rate corresponds to correctly typing 12.75 characters per min, which includes the time taken to backspace as well as the pause time for each character selection. A movie of this high spelling performance can be seen at `<http://www.youtube.com/user/UCIBCI>`, where the video is titled "High-performance EEG based BCI Speller".

The high online performances indicate that participants who used our P300 speller system can achieve ITRs considerably higher than those previously reported (see

Table 5 in [148] for a comparison with prior studies [55, 87, 138, 161]). The best ITRs achieved for the 6 participants are shown in Fig. 1.9. The figure also illustrates how the achieved online performances compare to the theoretical lower and upper bounds, given by the Fano bounds and channel capacity, respectively. This demonstrates that the communication speed limit of P300 speller systems can be pushed using advanced signal processing and information theoretic techniques. However, Fig. 1.9 also shows that further improvement in performance is theoretically possible.

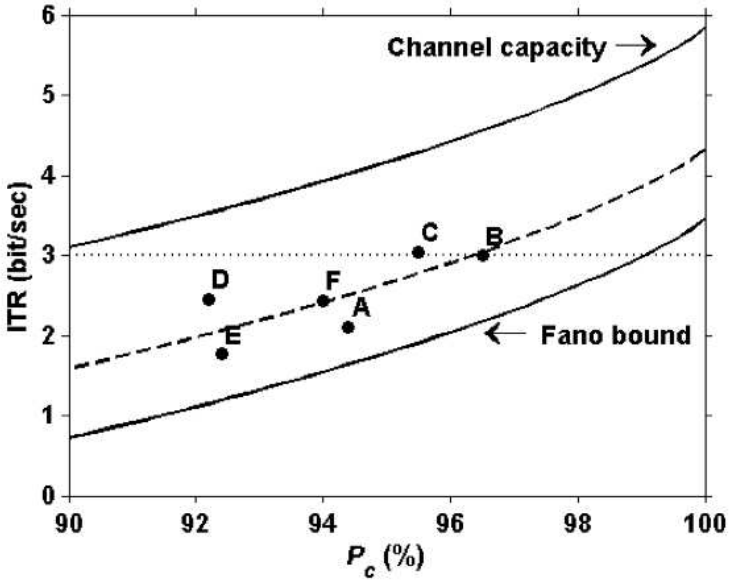

Figure 1.9: ITRs and classification accuracies for the 6 participants (A – F) in the P300 speller study [148]. Note that the channel capacity (the upper limit of ITR) and Fano Bounds (the lower limit of ITR) are shown, and the participants' ITRs are within these bounds.

Discussion

The results presented above disprove the assumption regarding the upper bound on ITRs achievable by EEG based BCIs [126, 161]. Particularly, our P300 speller system allows characters to be selected in an error-free fashion, with ITRs in excess of 3 bit/s (c.f. Fig. 1.9), which is 3 times higher than the best bit rates achieved with similar spelling systems [138], and nearly 3 times higher than those achieved with BCI 2-D

cursor control [161] or SSVEP [48].

While superior online performances were achieved in this study, the P300 speller system using our BCI has not been fully optimized. For example, as the users underwent multiple experimental sessions, they became familiar with the character layout (see Fig. 1.6), and felt that further reduction of the post-selection pause time (e.g. from 3 to 2 s) would not compromise the spelling accuracy. This step alone would reduce the total spelling times by at least 43 s, and would increase the practical, error-free ITRs by $> 25\%$. Furthermore, implementation of a full word completion similar to current text-messaging systems could further significantly increase the practical bit rates. These improvements are straightforward and require very little development effort, although some user training may be required.

In conclusion, the presented P300 speller system allows for error-free selection of characters with sustained, online bit rates that are several-fold higher than those that have been achieved with similar spelling systems. By using the ITR calculations presented in Appendix B.4, we were able to quantitatively compare our online results to other laboratories [55, 87, 138, 161] to better understand our system's performance. More importantly, the results invalidate the common assumption that ITRs of EEG based BCI spelling systems are limited to $\sim$1 bit/sec [126, 159]. Since the parameters of the present system were not completely optimized, it can be hypothesized that further substantial improvements of both character selection and error-free ITRs can be achieved. Many of these improvements are straightforward, while others may require some user training. The results of this study also have significant implications on the viability and adoption of EEG based BCIs in other applications.

1.2.4 Invasive BCI Research

Due to the promising results of our P300 speller system research, our laboratory has also performed extensive research on self-paced BCI systems. Particularly, we have performed research using invasive ECoG recordings in humans for the "ECoG-Robot" project depicted in Fig. 1.4 in Section 1.2.2 [37, 149, 150, 152]. This research focuses on the ability of ECoG data to decode elementary upper extremity movements as a means of determining appropriate control strategies for a BCI-controlled upper extremity prosthesis or robotic manipulator. The reason for using a more invasive recording technique (Fig. 1.10) instead of the more common and non-invasive EEG technique in this research is because ECoG signals offer higher spatial resolution and better signal quality [157]. This is important in movement based studies because it yields superior signal characteristics that could allow for faster communication rates [157] and multiple degrees of freedom for control [115]. Furthermore, although action and local field potentials (LFPs) have an even higher resolution [62, 65] than ECoG (Fig. 1.10 from [25] and [160]), they rely on intracortical implantation of micro-electrodes, which is a more invasive surgical procedure. Thus, since ECoG has both better long-term signal stability properties than LFPs and a higher spatial resolution than EEG, it may provide an ideal signal modality for a BCI-controlled upper extremity prosthesis.

Other neurophysiological signal modalities, such as functional imaging techniques (e.g. functional magnetic resonance (fMRI), functional near infrared spectroscopy (fNIRS), magnetoencephalogram (MEG), or positron emission tomography (PET)) also fall inferior to ECoG for decoding elementary upper extremity movements. Most notably, fMRI, fNIRS MEG, and PET are very expensive to perform and require bulky equipment [127]. Furthermore, these functional imaging techniques all rely on the measure of an increase in blood flow corresponding to increased brain activity.

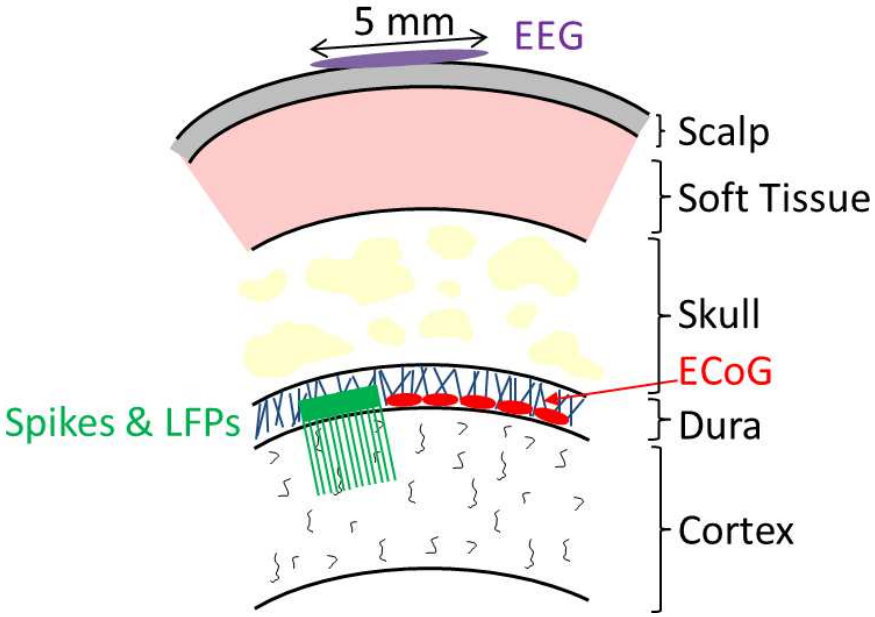

Figure 1.10: Neurophysiological signal modalities within the brain, which is further described in [25, 160].

This is problematic, as these technologies can only detect relatively slow changes in brain function, thus not making them ideal choices for fast communication [127] from a BCI system.

ECoG Based BCI Research

The purpose of the ECoG based research on decoding elementary upper extremity movements was to develop decoding and control strategies for a BCI-controlled upper extremity prosthesis. In order to create a viable BCI prosthesis for upper extremity tasks, movements such as finger movement [88, 94, 153], reaching [19, 154] and grasping [19, 164] are insufficient for restoring upper extremity movement functions, and in turn, restoring independence to users. Moreover, the Functional Independence Measure ^{TM} [162] indicates that tasks required for independent living, such as dressing,

toileting, and transferring, require complex upper extremity movements and unique configurations. Thus, an ideal BCI-controlled upper extremity prosthesis will require at least 6 degrees-of-freedom to restore independence to a user, as this requirement was empirically determined in [120] for the above tasks.

The several studies outlined below examine the representation of 6 elementary finger, hand and arm movements in ECoG signals, and whether these movements can be distinguished from one another. To accomplish this, the ability to decode idling periods as well as movement periods were elucidated, as prior studies (e.g. [8, 88, 94]) have omitted this non-movement state. In addition, we improved on the ability to decode movement trajectories continuously in real-time for each elementary movement. Finally, the ability to distinguish between different elementary movements and joints was investigated to determine whether a BCI control strategy for a 6 degrees-of-freedom upper extremity robotic manipulator using ECoG can be developed.

Methods

Participants undergoing subdural ECoG electrode implantation over the primary motor cortex (M1) for epilepsy resection surgery evaluation were recruited for this study from both the University of California, Irvine Medical Center and the Rancho Los Amigos National Rehabilitation Center (see Fig. 1.11 for an example electrode placement). Up to 64 channels of ECoG data were recorded (see Chapter 2 in Section 2.2 for signal acquisition), and the signals were acquired at 2048 Hz with common average referencing. The participants performed 6 elementary arm movements on the side contralateral to their ECoG electrode implant: **(1)** pincer grasp and release, **(2)** wrist flexion and extension, **(3)** forearm pronation and supinaton, **(4)** elbow flexion and extension, **(5)** shoulder forward flexion and extension, and **(6)** shoulder internal and external rotation. For the pincer grasp and wrist flexion/extension movements,

the movement trajectory (position, velocity) was measured using a custom-made goniometer built by our laboratory [147]; for the remaining movements, the trajectories were measured using a gyroscope (Wii Motion Plus, Ninetendo, Kyoto, Japan) and microcontroller unit (Arduino, Smart Projects, Turin, Italy). The ECoG and trajectory data were synchronized using a common pulse train sent to both acquisition systems. Finally, for each movement type, the participant was tasked with performing 4 sets of 25 continuous movement repetitions, with each set intervened by a 20 – 30 s idling period.

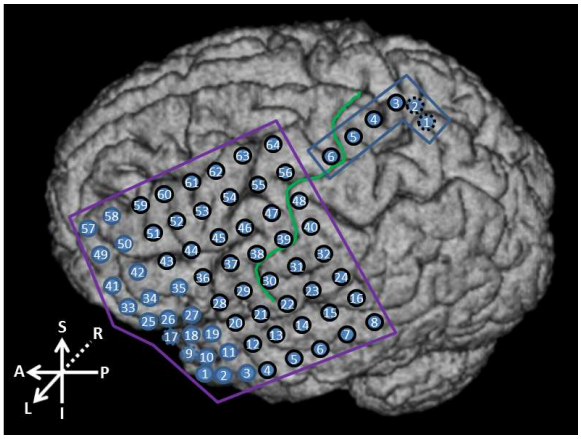

Figure 1.11: Magnetic resonance image (MRI) of a participant in [149] (© 2013 IEEE) with ECoG electrodes localized using the technique described in [151].

For each movement type, a decoding model consisting of a state decoder followed by a trajectory decoder was developed [150, 152]. This allowed us to examine both the non-movement versus movement states, as well as our ability to decode movement continuously in real time. To develop these decoding models for each movement type, the temporal relationship between the μ (8 – 12 Hz), β (13 – 30 Hz), low-γ (30 – 50 Hz) and high-γ (80 – 160 Hz) band powers and trajectories was explored in [152]. This was done by first calculating the logarithmic instantaneous power in each band:

$$P_n(t) = \log |f(x_n^2(t))| \tag{1.3}$$

where $x_n(t)$ is the bandpass filtered ECoG signal (μ, β, low-γ, high-γ bands) at channel n, and $P_n(t)$ is its power, enveloped by a 1.5 Hz low-pass filter, $f(.)$ [149, 150, 152]. Note that taking the logarithm of the powers equalized the otherwise disparate power levels, especially between the μ and high-γ bands. This avoided skewing the parameters of the state decoder described in [152] and Section 2.5 in Chapter 2. Subsequently, $P_n(t)$ was segmented into flexion, extension, and idling epochs to examine the instantaneous power during these different states [149]. This was done by analyzing the cross-correlations (Appendix B.2) during each movement or non-movement type (idling epochs were calculated at zero lag) for all channels across participants [149].

In addition to examining the instantaneous power, $P_n(t)$ at flexion, extension, and idling epochs, each of the band powers' ability to decode the trajectories was also examined. This led to the use of the high-γ band power (80 – 160 Hz) in [150], as the instantaneous powers in this band were visually correlated with the trajectory for several movement types. Specifically, a combination of classification and regression was used to decode the state and movement trajectories from this band power. This approach resulted in trajectory decoding accuracies (i.e. cross-correlations, Appendix B.2) as high as 0.69. However, these accuracies were relatively modest and had to be improved in order to better translate this feature into a control strategy for a BCI-controlled 6 degree-of freedom upper extremity prosthesis.

The trajectory decoding of the high-γ band instantaneous power was improved in [152] through the use of a continuous decoder, constrained by a dynamic movement model, to decode the movement state trajectories. To this end, a Kalman filter based tra-

jectory decoder was developed using the following dynamic model:

$$\begin{aligned} x_{k+1} &= Ax_k + w_k \\ y_k &= Cx_k + n_k \end{aligned} \tag{1.4}$$

where $x_k \in \mathbb{R}^{2\times 1}$ is the state consisting of the angular position, θ, and velocity, $\dot{\theta}$, k is the current time step, $Ain\mathbb{R}^{2\times 2}$ is the state matrix, and $w_k \sim \mathcal{N}(0, \Sigma_w)$ is zero-mean Gaussian process noise with covariance Σ_w. Similarly, $y_k \in \mathbb{R}^{c\times 1}$ is the output (note that $y_k = P_k$), $C \in \mathbb{R}^{c\times 2}$ is the output matrix, and $n_k \sim \mathcal{N}(0, \Sigma_n)$ is zero-mean Gaussian measurement noise with covariance Σ_n. Both A and C are computed from the data according to [163]. The Kalman filter was then constructed to compute the position and velocity at the next time step [163]:

$$\begin{aligned} \Sigma_{k+1} = &\quad [I - L_{k+1}C]\left[A\Sigma_k A^{\mathrm{T}} + \Sigma_w\right] \\ L_{k+1} = &\quad \left[A\Sigma_k A^{\mathrm{T}} + \Sigma_w\right] C^{\mathrm{T}} \left[C\left[A\Sigma_k A^{\mathrm{T}} + \Sigma_w\right] C^{\mathrm{T}} + \Sigma_n\right]^{-1} \end{aligned} \tag{1.5}$$

where Σ is the *a posteriori* error covariance and L is the optimal gain.

To assess the performance of the Kalman filter based decoder as well as our state decoder (described in Section 2.5 of Chapter 2), the reconstructed trajectories, $\hat{\theta}$ and $\dot{\hat{\theta}}$, were compared to the trajectories measured by the electrogoniometer or gyroscope, θ and $\dot{\theta}$ [152]. This was accomplished by calculating the fraction of correctly decoded idle and movement states, P_c, and the correlation coefficient of the movement, ρ_M. Then, to determine the overall performance of both decoders using a single number, a performance measure, PM, was developed:

$$PM = \frac{\rho_M n_M + P(I|I) n_I}{n_M + n_I} \times 100\% \tag{1.6}$$

where n_M and n_I are the number of movement and idle state samples, respectively,

and $P(I|I)$ is the probability of correctly decoding the idling state.

The state and trajectory decoder described in [152] led to high state and decoding performance measures, PM, across multiple degrees of freedom. However, the ability to decode movement states across multiple joints and distinguish between movement types still required investigation. To accomplish this task, the sensitivity and specificity of models for each elementary upper extremity movement were formally tested in [37]. The sensitivity was defined as the accurate detection of movement of a particular joint, while the specificity was defined as the ability to distinguish movements from one another.

For each of the 6 decoding models developed in [152] of each movement type, the output of the classifier (details given in Appendix A.4) was compared to the class identity of the test data, which generated the following confusion matrix:

Model\Test	$\mathcal{I}_a$	$\mathcal{M}_a$
$\mathcal{I}_a$	$P(\mathcal{I}_a\|\mathcal{I}_a)$	$P(\mathcal{I}_a\|\mathcal{M}_a)$
$\mathcal{M}_a$	$P(\mathcal{M}_a\|\mathcal{I}_a)$	$P(\mathcal{M}_a\|\mathcal{M}_a)$

(1.7)

The sensitivity of the model, defined as $P(\mathcal{M}_a|\mathcal{M}_a)$, represents the probability of decoding model a correctly classifying the occurrence of movement during task a. For example, the highly sensitive model for the pincer grasp and release movement would classify all epochs of pincer grasp movements as the movement class. Similarly, $P(\mathcal{I}_a|\mathcal{I}_a)$ represents the probability of correctly classifying the occurrence of idling during the same task.

To assess the specificity of model a, ECoG data corresponding to task b ($b \neq a$) were

classified using model a. This procedure generated the following confusion matrix:

Model\Test	$\mathcal{I}_b$	$\mathcal{M}_b$
$\mathcal{I}_a$	$P(\mathcal{I}_a \mid \mathcal{I}_b)$	$P(\mathcal{I}_a \mid \mathcal{M}_b)$
$\mathcal{M}_a$	$P(\mathcal{M}_a \mid \mathcal{I}_b)$	$P(\mathcal{M}_a \mid \mathcal{M}_b)$

(1.8)

Specificity was then defined as $1 - P(\mathcal{M}_a|\mathcal{M}_b)$, where $P(\mathcal{M}_a|\mathcal{M}_b)$ represents the probability of model a classifying movement b as movement a — an undesirable outcome. For example, $P(\mathcal{M}_{\mathrm{PG}}|\mathcal{M}_{\mathrm{W}})$ would be high if the pincer grasp (PG) movement model frequently classified the wrist flexion and extension (W) movement as pincer grasp movement, indicating the low specificity of the model. Note that this definition deviates from specificity in the classical sense, which is defined as $P(\mathcal{I}_a \mid \mathcal{I}_a)$. Hence, a more appropriate name would be "cross-specificity," although the term specificity will be used in the results and discussion of this research since the contextual distinction is clear [37].

Results

Visual inspection of the μ (8 – 12 Hz), β (13 – 30 Hz), low-γ (30 – 50 Hz), and high-γ (80 – 160 Hz) instantaneous powers [152] revealed a burst of high-γ power that was time-locked to every flexion or extension event, while the power $P(t)$ during idling appeared noisy and chaotic. This resulted in a high positive cross-correlation for flexion epochs, a low correlation for idling epochs, and a high negative cross-correlation for extension epochs [149]. As seen in [149] and Fig. 1.12, the high cross-correlations using the high-γ power over the M1 brain area revealed that this band power strongly encodes for upper extremity movements, and can be used to determine the state of the movement (i.e. idle versus move).

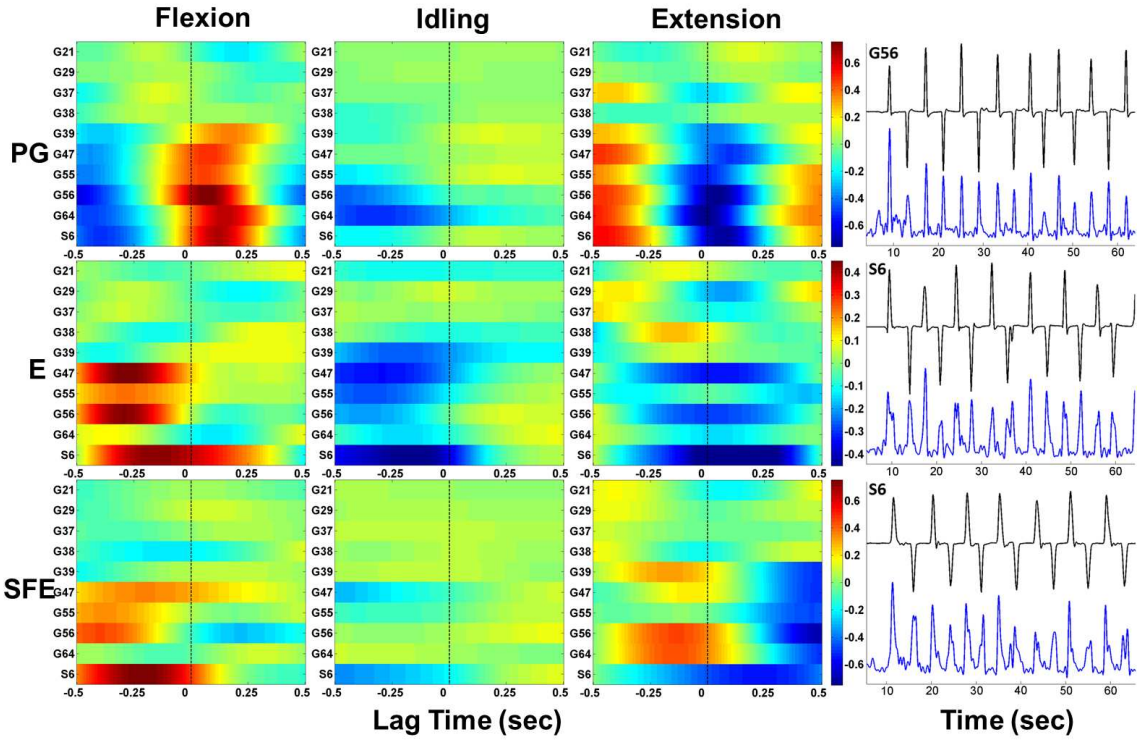

Figure 1.12: Lag-correlation diagram of Participant S2 for pincer grasp (top), elbow flexion and extension (middle) and shoulder forward flexion and extension movements. For each M1 electrode, the colors represent the cross-correlation at various lag times. The dotted line indicates the initiation of movement. On the right is a representative segment of $P(t)$ (blue trace) and corresponding velocity, $\dot{\theta}(t)$ (black), at the best M1 electrode [149] (© 2013 IEEE).

Further investigation of the high-γ instantaneous power in [150] resulted in the use of classification and regression to decode trajectories of the movement state from this input feature. This resulted in cross-correlations as high as 0.69, and trajectories representative of Fig. 1.13. Also, the high classification accuracy of movement versus idle state using this feature resulted in being able to detect wrist movements in real time to drive the "wrist" of a robotic arm (video can be seen at `<http://www.youtube.com/user/UCIBCI>`, where the video is titled "Electrocorticogram (ECoG) based Brain-Computer Interface (BCI)"). However, as mentioned previously, the trajectory decoding results presented in [150] and Fig. 1.13 were relatively modest and required further improvement.

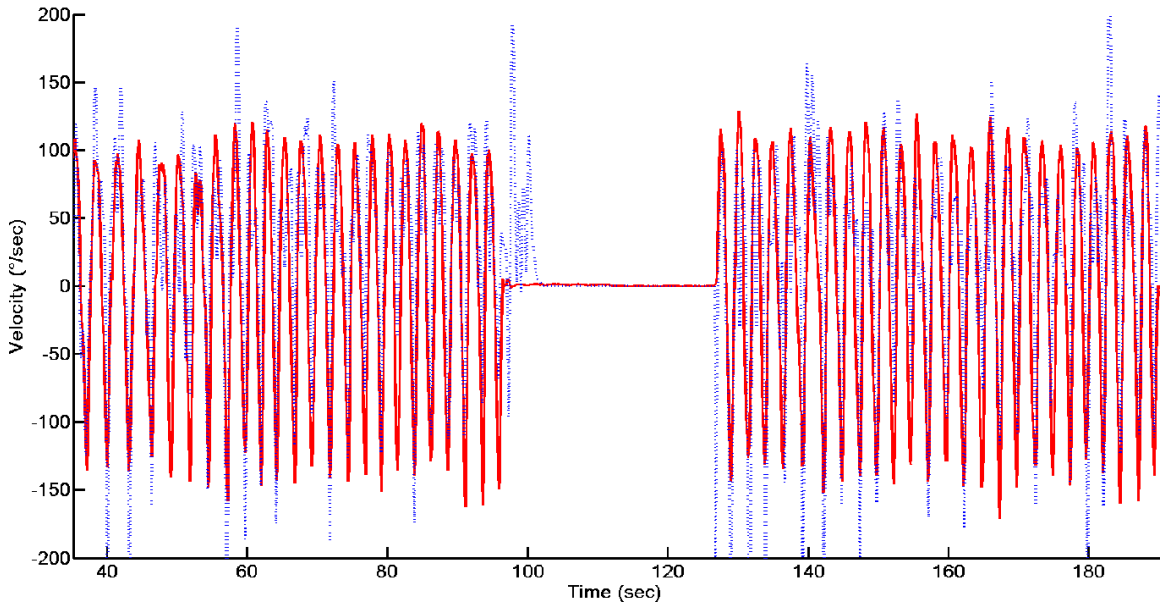

Figure 1.13: ECoG-decoding from regression using the high-γ instantaneous power approach (blue dashed line) and measured (red solid line) velocities during the shoulder flexion and extension movement for Participant S2 [150].

Based on the results described in [149] and the state and trajectory decoding results described in [150], the trajectory decoding of the high-γ instantaneous power was improved in [152] through the use of a Kalman filter based trajectory decoder. This resulted in decoded trajectories representative of Fig. 1.14, and cross-correlations as high as 0.76. In addition, the performance measures, PM, resulted in high state and trajectory decoding accuracies, reaching accuracies as high as 91% for the pincer grasping movement for Participant 3 [152].

The performances and cross-correlations of the Kalman filter based approach [152] in comparison to the regression approach [150] revealed that the improved approach outperformed the regression approach by a wide margin (average: $\sim$83%). For example, the average cross-correlation of the Kalman filter based approach was 0.70 and 0.68 for position and velocity, respectively, while the average correlation of the velocity using the regression approach was 0.58. This represents a significant improvement with respect to velocity decoding, and led to relatively accurate trajectory decoding

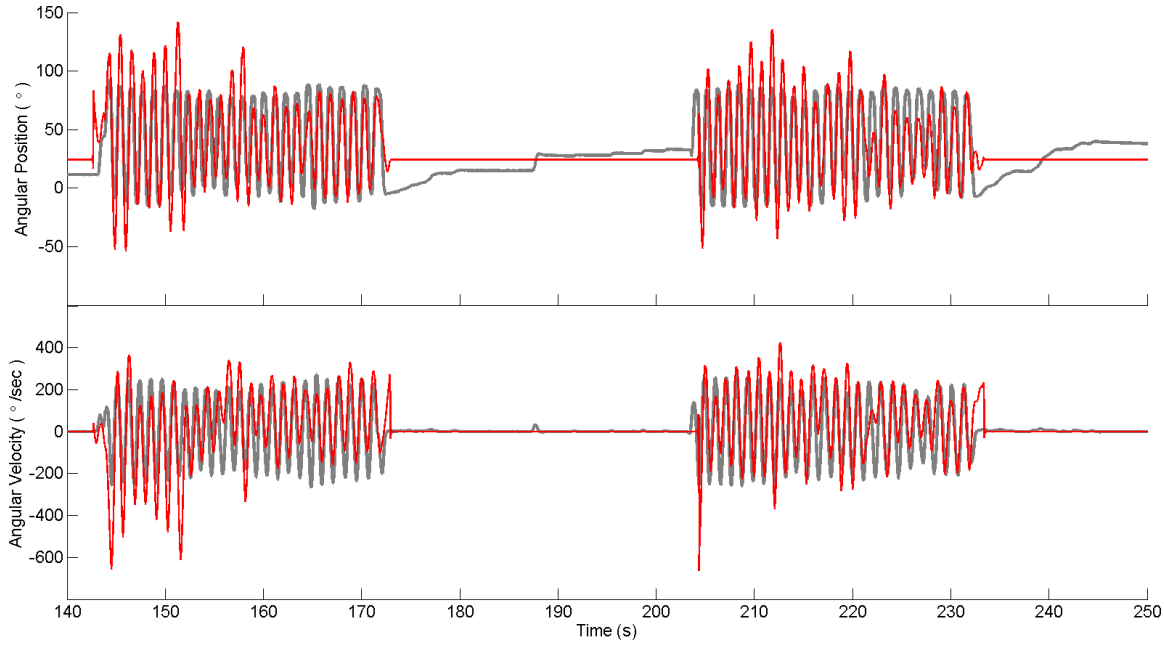

Figure 1.14: ECoG-decoded from the Kalman filter decoding approach (red thin line) and measured (gray thick line) velocities during the pincer grasping movement for Participant 3 [152] (© 2013 IEEE).

results.

Despite the accurate results presented in [152] and the improvement in trajectory decoding, the ability to decode movement states across multiple joints and distinguish between different joint movements still required investigation. This resulted in a formal sensitivity and specificity test [37] for each upper extremity movement. The results of this study revealed that the movements in all 6 tasks could be detected with high sensitivity across participants (see the sensitivity Table I in [37]). Specifically, the average sensitivity across all models for Participant S1 was 0.95 ± 0.03, and ranged from 0.90 – 0.98. This was true for Participant S2 as well, who had an average sensitivity of 0.98 ± 0.02 and ranged from 0.95 to 1.00.

Unlike the sensitivity of the decoding models, the specificity of the individual models was very low. For example, the shoulder forward flexion and extension model classified all instances of elbow movement as shoulder forward flexion/extension movements,

yielding zero specificity (see $P(I_{SFE}|M_E)$ in Table I in [37]). This means that a BCI designed to decode shoulder movement could be operated by elbow movement, potentially confusing the user's movement intentions. However, the pincer grasping model was specific with respect to shoulder flexion/extension movement, as it had a specificity of 0.57. Furthermore, on average, the specificity of all models with respect to all movements was 0.11±0.12 for Participant S1; for Participant S2, the average specificity was 0.19±0.26. These average specificities are very low, and the specificity during idling were very low, indicating that the ECoG signals during idling were very similar across tasks. This is expected, however, given that idling behavior is similar across tasks, so the low specificity of idling is considered a positive outcome.

Discussion

The results presented in [149] and shown above indicate that the high-γ instantaneous power, $P(t)$, is an important input feature for BCI decoding algorithms of upper extremity movements from ECoG signals. Furthermore, when $P(t)$ is only visually inspected, the pattern of high-γ bursts (Fig. 1.12) can be seen with each flexion and extension event. This indicates that such an input feature may significantly boost the decoding accuracies of BCI algorithms. Also, the high classification accuracy of movement versus idle state using this feature elucidates the ability to decode the state of the movement. However, further examination of the trajectory decoding of the movement using this feature was required and performed in [150] and [152].

Using the regression based trajectory decoding approach in [150], efforts towards developing an appropriate trajectory decoding approach using the high-γ band instantaneous power was improved and resulted high classification accuracies of idle versus movement. However, the trajectory decoding cross-correlations were relatively modest, so further improvement through the use of a Kalman filter based design was

necessary [152]. This new method for trajectory decoding resulted in relatively high state and trajectory decoding accuracies (i.e. performance measures, PM). In addition, the Kalman filter based approach outperformed the regression approach by a wide margin, demonstrating the improvement in decoding model design. Even though these results improved the trajectory decoding model design, the specificity of the decoder, or the ability to distinguish between movement types, was challenging using ECoG recordings and our BCI decoding design. This warrants further investigation in whether resolving movement states across multiple joints is possible.

The sensitivity and specificity results presented in [37] indicate that the decoding model design is capable of high sensitivity for idle versus movement, but has low specificity. In other words, the decoding model of each movement has a tendency of confusing other movement types as its own movement. Only in some cases was this confusion somewhat lower; however, the increased specificity for these instances is likely due to the somatotopic, anatomical separation of finger from shoulder representation areas on M1. Conversely, the somatotopic proximity of neighboring upper extremity joint representation areas may explain why ECoG high-γ features underlying other movements appear to be similar and confuse the decoding models. To alleviate this issue, the BCI upper extremity prosthesis may require the use of mini- or micro-ECoG grids, or other neurophysiological signal acquisition techniques that offer higher resolution signals.

In addition to the specificity issue described in [37], there are other issues underlying the development of a BCI-controlled 6 degree-of-freedom upper extremity prosthesis. First, the Kalman filter based trajectory decoder [152] would sometimes overshoot the measured trajectory, which could be problematic during development because the prosthesis itself imposes physical constraints. This overshoot can be mitigated by imposing boundary conditions to the trajectory decoder that conform to the phys-

ical constraints of the prosthesis. Secondly, the ability to decode multiple degree-of-freedom movements largely depended on the grid placement, which caused some participants to have only 1 or 2 degree-of-freedom movements accurately decoded. As previously mentioned, this may be improved through the use of higher resolution neurophysioligical signals such as micro- or mini-ECoG, which may further facilitate proper 6 degrees-of-freedom BCI control of an upper extremity prosthesis. Finally, even though the specificity of the decoding models may be improved through the use of other methods or signal acquisition techniques, it will likely result in a reduction in specificity. This problem can be avoided by sacrificing some degrees of freedom, however, this may limit the applicability of a BCI-controlled upper extremity prosthesis.

In conclusion, the findings in [37], [149], [150], and [152] suggest that the high-γ power band of ECoG signals can be used to accurately decode both the state and trajectory for several movement types. The ability to decode these movements may lead to BCI control of a 6 degrees-of-freedom upper extremity prosthesis, however, further research in the specificity of movement types is required. Through research using mini- or micro-ECoG, the decoding models presented above may increase in specificity by increasing the separability of upper extremity movements across electrodes, which in turn may provide a better decoding resolution.

1.2.5 BCI Systems for Neurorehabilitation

In addition to our ECoG-Robot research described above and depicted in Fig. 1.4, our laboratory has focused on other self-paced BCI applications, particularly applications for neurorehabilitation and motor recovery. Our high performance BCI system can be used in neurorehabilitation applications by simultaneously activating the motor

brain areas via our BCI, and the lower motor neurons of a damaged pathway via an external device, such as a FES system. This may foster reconnection of the damaged neural circuits through strengthening the synaptic connections by coactivation of pre- and postsynaptic neurons [119]. In other words, by allowing the user's neural activity associated with the motor intention to be coupled with the desired motor behavior, the synaptic connections between the brain, spinal motor pools, and output motor neurons, can be strengthened. The following sections will describe the theory behind these concepts, and how they can be exploited for the neurorehabilitation of stroke and SCI individuals.

Neural Plasticity and Hebbian Learning

The concept of neurorehabilitation stems from the theories underlying neural plasticity, which is defined as any change in neuron structure or function that is observed either directly from measures of individual neurons or inferred from measures taken across populations of neurons [155]. This definition specifies measurable change in neuron structure or function, thus changes in behavior on their own are not a measure of neural plasticity. Although these behavioral changes are mediated by neural plasticity, they are not direct measures, and do not tell us exactly how the central nervous system is adapting to the therapy. Conversely, neural plasticity measures alone do not tell us how the behavior is adapting during the therapy. Therefore, we need both sets of information to determine how neural plasticity supports improvements in motor function associated with neurorehabilition [155]. BCI systems may offer one such novel approach by providing both sets of information through EEG or other neurophysiological signal acquisition techniques, and through functional behavior measures before, during, and after the BCI therapy.

The use of neural plasticity to induce behavioral change originated from the theory

of Hebbian learning [61]. Specifically, Hebbian learning plays an important role in neural plasticity by strengthening synaptic connections when pre- and postsynaptic neurons are coactive [61]. This may be accomplished when two neurons or groups of neurons that have been disconnected by a lesion are activated at the same time (see Fig. 1.15 from [119]). Simultaneous activation will take place if both neurons are separately connected to a circuit whose neurons themselves are functionally interconnected. When this circuit of neurons is activated, the two neurons that are disconnected from each other are simultaneously activated [119]. Thus, Hebbian learning may help explain how partially lesioned neural circuits can regain the original pattern of connections, and therefore the cortical functions that they subserve may be regained. Furthermore, there is abundant evidence [29, 136] that supports the Hebbian principle that *"cells that fire together, wire together"*. This is an important concept in neural plasticity and neurorehabilitation, as it helps define the framework for therapies that attempt to optimize recovery mechanisms and allow for the greatest functional gain.

There are other theories of neural plasticity in addition to Hebbian learning that may explain how partially lesioned neural circuits can regain the original pattern of connections, and thus regain the desired motor function. For instance, mechanisms that support rapid plasticity may be the uncovering of latent or existing connections, activating existing but silent synapses [12]. In addition, morphological changes such as neurogenesis, synaptogenesis, or synaptic remodelling may provide a new substrate and space for neuroplastic changes [12]. However, there is overwhelming evidence that long-term potentiation and long-term depression, or changes in synaptic efficacy within the cortex and elsewhere in the nervous system, plays an important role in neural plasticity and motor learning. These concepts are closely related to Hebbian learning, as long-term potentiation and depression observations help explain the key mechanisms required to observe Hebbian learning across neurons by allowing for

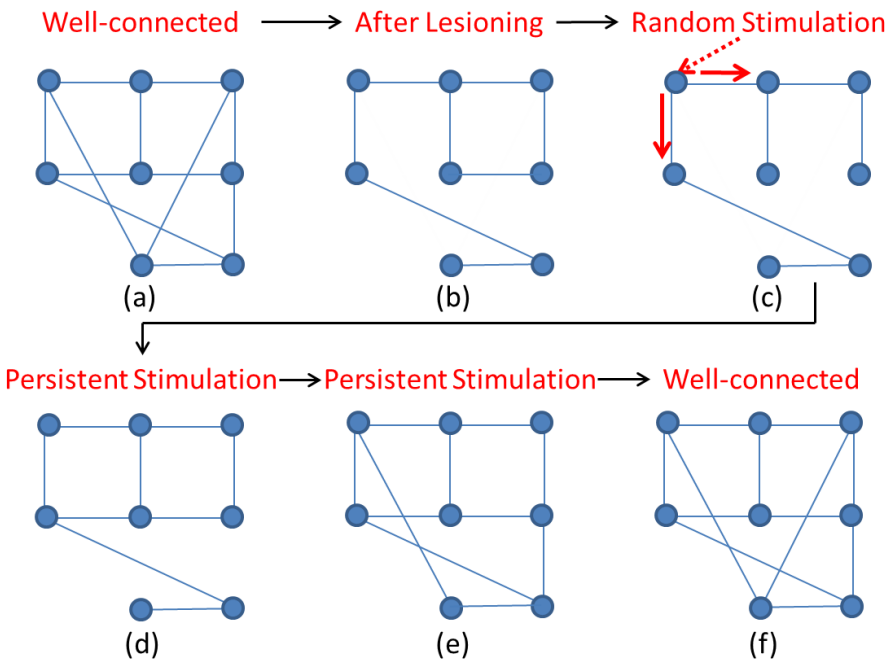

Figure 1.15: Illustration of autonomous reconnection through Hebbian learning, similar to the process presented in [119]. Circles represent neural groups, and lines represent tracts in the neural circuit. (A) A well-connected, intact neural circuit, (B) After lesioning (by brain damage), the same circuit is still connected but not very densely, (C) Some neural groups become activated through an external random process, (D) The activation spreads through the circuit, where a Hebbian learning process forms connections, (E) The process continues until the circuit is well connected in (F).

activity-dependent bidirectional modification of synaptic strength [16].

The application of Hebbian learning and other neural plasticity concepts in neurorehabilitative therapies is not a trivial task. First, although there have been major advances in neuroscience, we are still far from understanding the brain circuitry at a level needed to place new neurons and synapses in the right places to restore lost function after damage. Furthermore, identifying the specific neural circuits that encode for a particular movement or experience may be difficult to identify [155]. This is because behaviors such as a motor task can engage multiple brain areas. For example, learning a skilled hand movement engages the primary motor cortex, supplementary motor cortex, premotor cortex, cerebellum, somatosensory cortex, and several sub-

cortical areas. Finally, because neural plasticity is a dynamic process involving a complex cascade of molecular, cellular, and structural events that change over time, it is difficult to observe neural plasticity and its behavioral relevance during a therapy even though functional and neural measures exist.

In addition to the above issues, neurorehabilitation therapies face several confounding variables that can contribute to the level of functional improvement when treating neurological injury or disease, such as stroke or SCI. These variables include the individual's health status, age, lifestyle, time after injury, and the nature and locus of the central nervous system injury [155]. These factors compound to produce an extremely diverse range of impairments even within the same injury domain (e.g. stroke or SCI), and may lead to further heterogeneity in the way residual brain areas or spinal cord connections adapt to the injury and potentially respond to the therapy through neural recovery and compensation. However, different neural strategies, such as restoration, recruitment, and training, can take advantage of the inherent functional redundancy within the brain [155], thus inducing some form of neural plasticity.

Neurorehabilitative therapies that focus on motor recovery utilize all of the aforementioned strategies to induce neural plasticity. Specifically, these types of therapies are based on the hypothesis that synaptic plasticity mediates rehabilitation-dependent functional reorganization within the central nervous system. Furthermore, since there are many confounding variables and strategies for neurorehabilitation, we must recognize the importance of individualizing the therapy for each participant, and characterize the specific behavioral and neural impairment profiles to guide this individualization. By developing specific therapies for each individual, we may maximize the opportunity for neural plasticity and ultimately enhance functional outcomes.

Stroke Neurorehabilitation

The concept of using BCI systems as neurorehabilitative therapies for motor recovery of stroke individuals has been explored by several research laboratories [5, 14, 15, 24, 118, 142]. These BCI-driven devices utilize movements of an orthosis [15, 118], robotic manipulator [5, 14, 142] or directly via FES [24] to provide real time feedback during simultaneous motor imagery or attempted movement. Specifically, the motor imagery or attempted movement behaviors of an individual produce specific spatio-temporal or spatio-spectral patterns of cortical oscillations, mainly observed over the sensorimotor areas. These potentials or rhythms can be recorded via EEG [5, 24, 118, 142], magnetoencephalogram [15], or both [14], and then decoded and classified via a computer to provide real time feedback to the user. By simultaneously activating the brain areas of motor behavior with real time movement feedback, these systems may re-engage the damaged neural circuits within the motor cortex by positively affecting neuroplastic changes associated with the brain lesion [131].

There are different design strategies used in BCI neurorehabilitation to exploit learning mechanisms in the post-stroke brain. For instance, one design strategy for a BCI system for the neurorehabilitation of stroke would be to promote neuroplasticity by coupling a conditioned stimulus, such as a target on a cursor screen, and an unconditioned stimulus attached to a response, such as movement of an orthosis [15, 118] or robotic manipulator [5, 14, 142]. Specifically, these BCI designs require spatio-temporal patterns of cortical activity (i.e. event-related potentials) to be linked to a specific task (i.e. target reaching with a screen cursor [14, 15]) and the external device to be connected to the task. These cue-paced BCI systems [14, 15] simulate the contingency between the cortical neuronal activation (the event-related potential) and the spinal or subcortical neuronal activation (the movement induced by the external device triggered by the target stimulus). This may facilitate new activations

between the cortical and subcortical neurons, and consequently motor functional recovery. However, this particular paradigm does not require specific motor actions or behaviors of the participant, as these event-related potentials can be driven by other movements or strategies by the user, thus negatively affecting neuroplastic changes.

Another example of a BCI design for stroke neurorehabilitation is a BCI system that is integrated with a FES system for finger extension [24]. This BCI task requires attempted or imagined finger movement to be integrated with FES of the finger that then aids him/her in the motor action via an orthodromic response (i.e. in the anterograde direction, or away from the soma of the stimulating neuron). Additionally, the electrical stimulation feedback from the antidromic response in the motor nerve fibers (towards the soma) may reach the anterior horn cell, and possibly further up the neuraxis [122] (Fig. 1.16 from [122]). This may help reinforce the connection between the attempted or imagined finger movement with the desired movement by promoting associations in secondary brain regions. If this task is repeated several times, the probability of excitation of the perilesioned areas increases as the probability of enhancing the desired movement increases. The association between the attempted or imagined movement and the antrodimic stimulation towards the secondary brain areas may facilitate functional recovery by increasing the probability of the desired motor behavior.

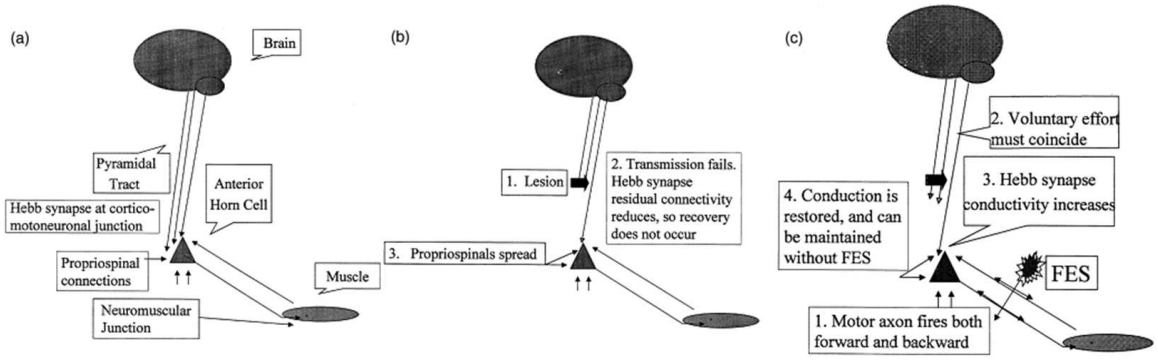

Figure 1.16: Cartoon of the potential connections for neural plasticity within the central nervous system after performing a BCI driven FES based therapy [122].

It is still unclear how these BCI experimental designs influence brain plasticity. At present, due to the wide heterogeneity of stroke individuals and their different lesion sizes and locations [131], it is difficult to delineate how BCI systems influence the promotion of neuroplasticity. Furthermore, it is unclear how the timing and duration of the BCI driven feedback affects the functional outcomes of the therapy. Studies on BCI based neurorehabilitative therapies for stroke should therefore consider using objective assessments of brain function to understand the persistent functional changes in the brain induced by the BCI neurorehabilitative therapy. Understanding how the brain reorganizes during a BCI based therapy may be crucial in understanding the mechanisms underlying motor improvement, and may facilitate *restorative* [39] rather than *substitutive* treatments for stroke recovery.

The facilitation of motor movement restoration after stroke is an important concept in determining the design of BCI systems for stroke neurorehabilitation. Motor behaviors can be substituted, compensated, or restored (i.e. recovered) using different rehabilitation concepts. A motor behaviors can be substituted through alternative motor elements, it can be compensated through adaptation of remaining motor elements, or it can be recovered or restored through reacquisition of the motor behavior [93]. For example, through substitutive rehabilitative methods, the motor behavior of walking can be substituted by a wheelchair to provide ambulation after stroke. However, this does not lead to the reacquisition of motor behaviors. Thus, all BCI designs should attempt to restore or recover lost motor behaviors through influencing neuroplasticity of the post stroke brain by coupling intention to the desired motor behavior.

SCI Neurorehabilitation and Neuroprostheses

Although SCI and stroke both involve the central nervous system, they differ in the possibility to restore the disrupted neuronal connection through BCI neurorehabili-

tative therapies. Particularly, spinal cord injuries are characterized by an irreparable nerve lesion at the spinal level, while in stroke, the lesion occurs where tissues are known to be plastic, such as cortical and subcortical structures of the brain [131]. Thus, restoring movement in individuals with SCI requires a bypass of the spinal injury through incomplete or spared connections, while restoring movement in stroke individuals would requiring positively affecting neuroplastic changes associated with the brain lesion [131]. This is important in the design of BCI neurorehabilitative therapies for SCI, as only *incomplete* SCI individuals may have any restorative benefits from a *neurorehabilitative* therapy, while complete injury individuals may only benefit from the BCI as a *neuroprosthesis*.

There has been considerable progress in the field of BCI systems for incomplete and complete motor SCI individuals [64, 91, 103, 112]. These studies utilized invasive [64] or noninvasive [91, 103, 112] techniques to acquire brain signals related to motor imagery tasks. Although noninvasive techniques are easier to perform and are safer, invasive techniques may provide a more direct channel of communication between the central nervous system and the prosthetic device [50]. In addition to the varying recording techniques, the aforementioned studies used different types of movement feedback or virtual reality feedback [91] as their interface of the BCI. For instance, the study in [64] used a robotic arm to provide upper extremity movement feedback to tetraplegic individuals, while the studies in [103] and [112] used FES. Depending on the end effector type (virtual reality feedback [91] or robotic arm movement [64] versus FES [103, 112]), these studies also differed in the designs of the BCI driven therapy.

The BCI systems in [112] and [103] relied on FES of the upper extremities to provide movement feedback and antidromic stimulation. Specifically, the study in [112] used EEG based BCI-controlled functional electrical stimulation of the fingers, hand, and

forearm to allow a tetraplegic participant perform a reach and grasp task. This was accomplished by performing different phases of repetitive foot motor imagery to trigger different functions of the noninvasive FES device. The experiment resulted in successful reach and grasp movements by the individual, and allowed the user to drink a cup of water. However, this study relied on foot motor imagery to control the device, so this BCI design may lead to maladaptive neuroplasticity in the brain if used as a neurorehabiliative therapy.

The study in [103] performed grasping patterns of the hand using a FES device. The stimulation device used in this study was the Freehand system (NeuroControl Corporation, Valley View, OH), an FDA-approved, 8-channel, implantable FES system. This device was set to perform lateral grasping movements, resulting in 3 grasp phases of stimulation. These phases were triggered by a "brain switch", or the detection of only one brain pattern from EEG to initiate all phases of the stimulation. Unfortunately, the control strategy for the "brain switch" used in this study also relied on foot motor imagery.

The aforementioned BCI studies [103, 112] have successfully allowed for upper extremity movements in SCI individuals. However, these studies relied on unintuitive control strategies [103, 112]. In order to design a BCI neurorehabilitative therapy or an assistive device for this population, the BCI system should use intuitive control strategies, such as grasping imagery for an upper extremity movement, to prevent any maladaptive neuroplastic changes. Also, prior BCI studies on SCI individuals have mostly focused on tetraplegic individuals and restoring movements to the upper extremities [64, 103, 112]. Lower extremity movements, such as foot movement or ambulation, on SCI individuals with paraparesis or monoparesis has yet to be investigated.

1.3 Significance of Work

1.3.1 Significance

The research presented in this dissertation uses our high-performance BCI system to develop neurorehabilitative therapies and assistive devices for both SCI and stroke individuals. Due to the heterogeneity of these injuries, the potential functional motor improvements are unknown. However, by promoting neuroplasticity and functional reorganization in these patient populations using our BCI system, our devices may lead to motor function improvements and increased independence. This may in turn improve their quality of life beyond that of current rehabilitation.

This dissertation also contributes significantly to the field of neurorehabilitation by focusing on lower extremity movements. By testing the feasibility of BCI systems for lower extremity movements in both stroke and SCI individuals, the potential applications for neurorehabilitation in these populations have increased. Particularly, our BCI system was applied to ambulation applications in SCI individuals. Since most technological approaches for ambulation have been sought to substitute for the lost motor functions, such as robotic exoskeletons [49], FES systems [52], or spinal cord stimulators [60], there has yet to be any restorative treatments for walking. By applying our BCI to different ambulation applications, our research may lead to novel restorative approaches to walking, improving the quality of life in SCI individuals.

1.3.2 My Contributions

This dissertation represents a collaborative work performed by our laboratory. I was mainly responsible for building and testing prototypes, conducting all BCI experi-

ments, assisting with technical debugging, performing post-hoc analyses, writing the manuscripts, and presenting our work at conferences. My colleague, Po T. Wang, wrote the BCI software and assisted with technical debugging, prototyping, post-hoc analyses, and writing the manuscripts. Finally, our co-principal investigators, Dr. Zoran Nenadic and Dr. An H. Do, provided conceptual design, funding and support, recruited participants, and assisted with the experiments and writing the manuscripts. All projects were performed as a team effort, although my primary research focused on the neurorehabilitation of ambulation after SCI (Chapter 4), while Po T. Wang focused on our invasive BCI research (Section 1.2.4 above).

Chapter 2

Common Methodologies

2.1 Overview

The following chapters will discuss our current efforts towards BCI systems for stroke and spinal cord injury (SCI) neurorehabilitation. These systems (projects 3–7 in Fig. 1.4) are all self-paced BCI systems, where they allow participants to generate motor imagery or movements to control the output device in a self-paced manner (i.e. they can decide when to initiate control). In order to allow participants to control these output devices, our BCI systems use noninvasive electroencephalogram (EEG) signals to acquire brain signals (Section 2.2). Then, through a brief open-loop training procedure (Section 2.3), a prediction model for the classification of EEG signals into "Idle" or "Move" states is developed using data-driven dimensionality reduction techniques (Section 2.4). Once a prediction model is developed, a brief online calibration procedure is performed (Section 2.5) to find the optimal parameters

for online operation. Finally, self-paced or cue-paced online tests (Section 2.6) are performed to assess the performance of the system by the user (Section 2.7). Note that some of these tests are performed in a cue-paced manner to be able to perform a complete feasibility assessment of the system, or are performed because the design of the BCI system itself is cue-paced (i.e. the P300 speller system in Section 1.2.3 of Chapter 1).

2.2 Experimental Setup and Data Acquisition

With the exception of our research using electrocorticogram (ECoG) signals (Section 1.2.4), our BCI systems typically use EEG signals to acquire neurophysiological information. Specifically, signals are acquired by a 19-channel (for the P300-Speller system in Section 1.2.3) or 63-channel (for all of our other EEG based BCIs) EEG cap arranged according to the 10-20 (19-channel cap) or 10-10 (63-channel cap) International Standard, respectively. A layout of these caps can be seen in Fig. 1.3 of Chapter 1. In addition to these layouts, the chosen electrodes using 32 channels of the 64 channel cap for the BCI systems described in Chapter 3 and 4 are shown below in Fig. 2.1. This subset of electrodes removed "hat band" electrodes to prevent electromyogram (EMG) artifacts from contaminating the EEG signals during movements. The setup for the wireless EEG system that utilizes Bluetooth capabilities only allows for 24 EEG signals to be recorded wirelessly, so the chosen electrodes shown in Fig. 2.1 are utilized. This setup ensures that most of the brain areas can be recorded by the EEG, and it also focuses on the motor cortex region, as these electrodes are known to be important for imagined and attempted movement.

For the 19-channel cap, the EEG cap used (Compumedics USA, Charlotte, NC) has 19 sintered Ag-AgCl electrodes, as optimal electrode locations to detect the P300

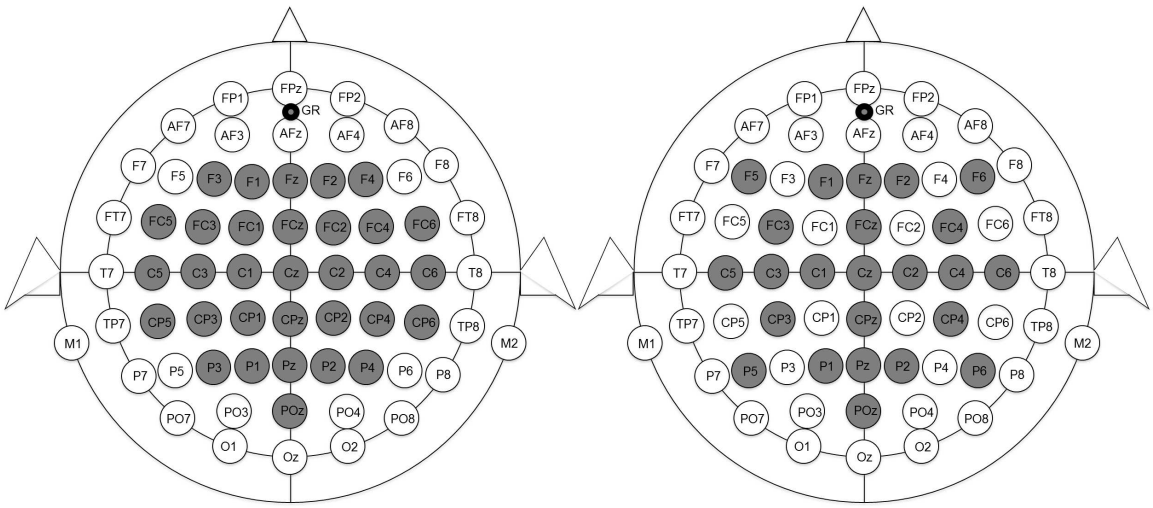

Figure 2.1: EEG channels chosen for the 32 channel EEG setup for wired transmission, and for the 24 channel setup for wireless EEG transmission. Note that these layouts excluded "hat band" electrodes, which are susceptible to EMG artifacts.

evoked potential are already known. However, for the self-paced BCI systems, a relatively novel BCI research field with not fully understood EEG features, a 63-channel EEG cap with sintered Ag-AgCl electrodes (MediFactory BV, Heerlen, The Netherlands) is used. Also, since some of these systems utilize actual movement to control the BCI system, the 64-channel cap is immune to motion artifact because the actively shielded electrodes minimize the electromagnetic interference due to cable movements and mechanical vibrations. Finally, both EEG caps require conductive gel (Compumedics USA, Charlotte, NC) to be applied to all electrodes and the 30-Hz impedance between each electrode and the reference electrode must be maintained at < 5–10 kΩ.

Once an EEG cap is mounted and the impedances between the electrodes and reference electrode are reduced, the EEG signals are amplified, band-passed filtered, and digitized. For the 19-channel EEG system, this is done using a system of linked single-channel EEG bioamplifiers (EEG100C, Biopac Systems, Goleta, CA), and the signals are subsequently digitized using the MP150 data acquisition system (Biopac Systems). For the BCI systems discussed in the remaining chapters that used the

63-channel EEG cap, the signals are acquired using two linked 32-channel bioamplifiers (NeXus-32, Mind Media, Roermond-Herten, The Netherlands) to amplify (gain: 20), filter (0.01 – 50 Hz), and digitize (sampling rate: 256 Hz, resolution: 22 bits) the EEG signals in a common average reference mode and synchronized with other physical sensor acquisition systems (see Fig. 2.2 for the data acquisition schematic). Finally, EEG signals from both systems are acquired using several Matlab scripts (MathWorks, Natick, MA).

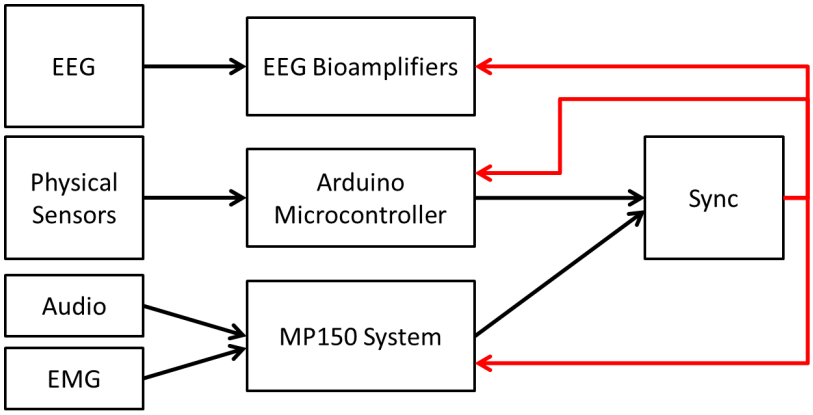

Figure 2.2: Schematic of our current data acquisition systems. EEG data, physical sensor data, and audio data are all synchronized by a common pulse train sent by either the MP150 or Arduino microcontroller (SmartProjects, Turin, Italy) systems. The common pulse train is then routed back to the data channel of the EEG bioamplifier and other acquisition systems to synchronize all data.

After mounting the EEG cap and preparing the signals for data acquisition, physical sensors are mounted to detect the attempted or actual movement by the participant and/or output device. These physical sensors include electrogoniometers [147], gyroscopes (L3G4200D, STMicroelectronics, Geneva, Switzerland), a Wii motion plus (Nintendo, Kyoto, Japan), a laser distance meter (411D Laser Distance Meter, Fluke Corporation, Everett, WA), or EMG sensors (Biopac Systems). For the motor imagery based BCI systems, an audio signal is used to determine the cue given to the participant (Fig. 2.2), and assuming the motor imagery or idling task is being followed by the participant. Finally, all neurophysiological, physical sensor, and audio data is

synchronized by a common pulse train (the "sync" in Fig. 2.2) generated by either an Arduino microcontroller (SmartProjects, Turin, Italy) or an MP150 data acquisition system (Biopac Systems).

2.3 Training Procedure

To develop a prediction model for the classification of EEG signals, the BCI systems require participants to undergo a short 10–20 min training session while EEG signals associated with a cognitive process (e.g. P300 response, motor imagery, motor movement) are recorded in an open-loop manner. More specifically, participants are seated in a chair 0.8–1.0 m from a monitor while computer cues (Fig. 2.3) instruct the user to perform a cognitive process while EEG data is recorded without providing any feedback to the user. Then, the recorded EEG signals are combined/synchronized using the M150 system or Arduino microcontroller, and segmented into class-labeled trials using several Matlab scripts.

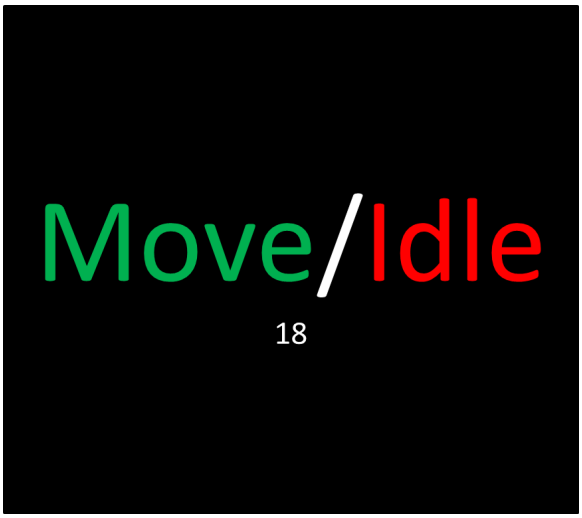

Figure 2.3: Example interface for the offline training session for BCI systems using textual cues with visual feedback applied after each trial, in this instance, after each "Idle" or "Move" trial.

During the training procedure, participants are asked to remain still and refrain from making any excessive movements or blinking. The experimenter monitors the EEG, physical sensors, as well as the audio and synchronization signals while the participant performs the movement or motor imagery tasks. This is performed to prevent any excessive movement artifacts or blinking that may contaminate the EEG training data for subsequent decoding model generation. If consistent movements or blinking are observed, then the participant is asked to repeat the entire training procedure without making the undesired movements. Finally, if excessive EMG artifacts are observed during the training procedure due to face, neck and jaw muscles, these channels are physically removed from the amplifier as well as from the analysis, as common average referencing and feature extraction are susceptible to these artifacts.

2.4 Decoding Model Generation

2.4.1 Feature Extraction

Once the training procedure is completed and the EEG data is saved for offline analysis, a prediction model to classify "Class 1" and "Class 2" EEG signals is developed. Briefly, the EEG and labeling signals are first aligned and merged using the synchronization signal, and an iterative artifact rejection algorithm [30] is used to exclude EEG channels with excessive EMG artifacts from further analysis. This is done by removing those channels whose EEG amplitude exceeded an outlier voltage threshold in more than 25% of the total trials. The outlier threshold voltage is nominally set to 6 standard deviations from the mean, and is adaptively changed to keep the number of outlier trials below a pre-specified number (5% of all trials). This procedure is repeated until no more channels can be removed. To minimize the effect of outliers

on statistical estimates, robust (i.e. median-based) mean and standard deviations are used [69]. Finally, upon artifact removal, the EEG data from the remaining channels are split into each class using the audio signal or physical sensors for subsequent signal processing and feature extraction.

Since both computer-paced and self-paced BCI systems use the same signal processing and pattern recognition techniques, both systems use the methodologies described in Appendix A. Specifically, both systems use a combination of classwise principal component analysis (CPCA) [27], and approximate information discriminant analysis (AIDA) [26] or Fisher's linear discriminant analysis (LDA) [47], to reduce the dimension of the input data and extract its salient features. These pattern recognition and dimensionality reduction techniques typically result in the extraction of 1D spatio-temporal or spatio-spectral features. A schematic of the individual steps to this process are shown in Fig. 2.4.

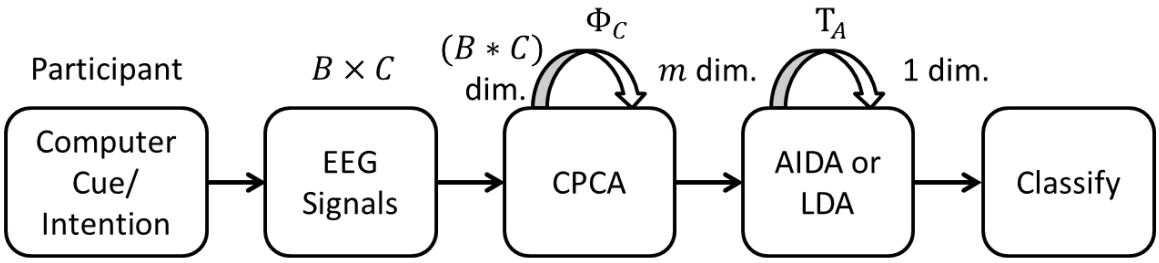

Figure 2.4: Schematic of our current data-driven methods for feature extraction and classification. Note that there are C channels and B time (frequency) samples per channel in our cue-paced BCIs (self-paced BCIs), respectively.

For binary pattern recognition problems, CPCA projects high-dimensional data onto a pair of subspaces locally adapted to individual classes. Due to its nonlinear (piecewise linear) nature, CPCA is well-suited for pattern recognition problems where high-dimensional data are confined to a low-dimensional manifold, such as a binary classification. In addition, unlike principal component analysis and other nonlinear dimensionality reduction techniques [121], CPCA is a supervised learning technique,

as it takes advantage of the known class labels (see Appendix A.3 for details on the methodology).

In addition to CPCA, AIDA and LDA enhance the class separability of the remaining m dimensions while reducing the dimension of the data. AIDA is an approximation of an information-theoretic technique [106] that seeks a low-dimensional data projection by maximizing the mutual information between the class labels and data. Unlike other computationally expensive information-theoretic techniques [106, 137], AIDA and LDA retains the computational simplicity characteristics of linear, second-order techniques. More specifically, the feature extraction matrix of AIDA, $\mathbf{T}_{DA}$ described below, is found through eigenvalue/eigenvector decomposition (details in Appendix A.3).

Using the AIDA, LDA, and CPCA methods described above, the resulting low-dimensional spatio-temporal/spatio-spectral features can be extracted by:

$$f^{\star} = \mathbf{T}_{DA}\mathbf{\Phi}_{C}(\mathbf{d}) \tag{2.1}$$

where $\mathbf{d} \in \mathbb{R}^{B\times C}$ is a single-trial of EEG data (B– the number of frequency bins, C– the number of EEG channels), $\mathbf{\Phi}_{C} : \mathbb{R}^{B\times C} \rightarrow \mathbb{R}^{m}$ is a piecewise linear mapping from the data space into an m-dimensional CPCA-subspace, and $\mathbf{T}_{DA} : \mathbb{R}^{m} \rightarrow \mathbb{R}$ is an LDA or AIDA transformation matrix. A detailed description of the CPCA, AIDA, LDA, and related information-theoretic feature extraction techniques can be found in [27, 26, 47, 106], and a recap of these techniques is given in Appendix A.3.

2.4.2 Classification

For all of our BCI systems, the Bayesian classifier is implemented as the following rule:

$$\frac{P(C_1|f^\star)}{P(C_2|f^\star)} \begin{array}{c} C_1 \\ > \\ < \\ C_2 \end{array} 1 \tag{2.2}$$

where $P(C_1\,|f^\star)$ and $P(C_2\,|f^\star)$ are the posterior probabilities of "Class 1" and "Class 2" given the observed feature, $f^\star$, respectively. Note that these posterior probabilities were calculated from the Bayes rule assuming Gaussian probability density functions with equal variances. Eq. 2.2 is read as: "classify $f^\star$ as Class 1 if $P(C_1\,|f^\star) > P(C_2\,|f^\star)$, and vice versa." A detailed description of the Bayesian classifier as well as how to calculate the posterior probabilities for classification are given in Appendix A.4.

The performance of the Bayesian classifier (Eq. 2.2), expressed as a classification accuracy, can be assessed by performing stratified 10-fold cross-validation [85]. Briefly, the EEG trials are randomly separated into 10 groups (folds) while the data from 9 of the 10 folds is used to train the parameters of CPCA, the choice of AIDA or LDA and its corresponding parameters, and the Bayesian classifier. The data from the remaining fold is then transformed into the feature domain and classified. This is repeated until all 10 folds are exhausted, each time designating a different fold for classification. The number of misclassified trials are then used to calculate the probabilities of omission and false alarm errors. Finally, to estimate the standard deviation of these errors, the 10-fold cross-validation procedure is repeated 5 to 10 times, each time re-randomizing the grouping of trials into folds. Once this is completed and a

performance is determined, the resulting parameters of the CPCA, choice of AIDA or LDA procedure and its corresponding transformation matrix ($\mathbf{T}_{DA}$), and the Bayesian classifier are saved for real time operation.

Once the features are extracted and a decoding model is generated, the linear Bayesian classifier is implemented as a binary state machine for online BCI operation. As a binary state machine (Fig. 2.5), these classes can be generally denoted as "Class 1" (C_1) and "Class 2" (C_2) in Eq. 2.2. Note that for our P300 speller system, the classes are defined as oddball or non-oddball (see Section 1.2.3 in Chapter 1). Similarly, for the BCI systems for gait and ambulation (Chapter 4), the classes are defined as attempted walking motor imagery or idling. For the BCI systems for stroke neurorehabilitation (Sections 3.3 and 3.2 in Chapter 3), the two classes are defined as idling or actual movement.

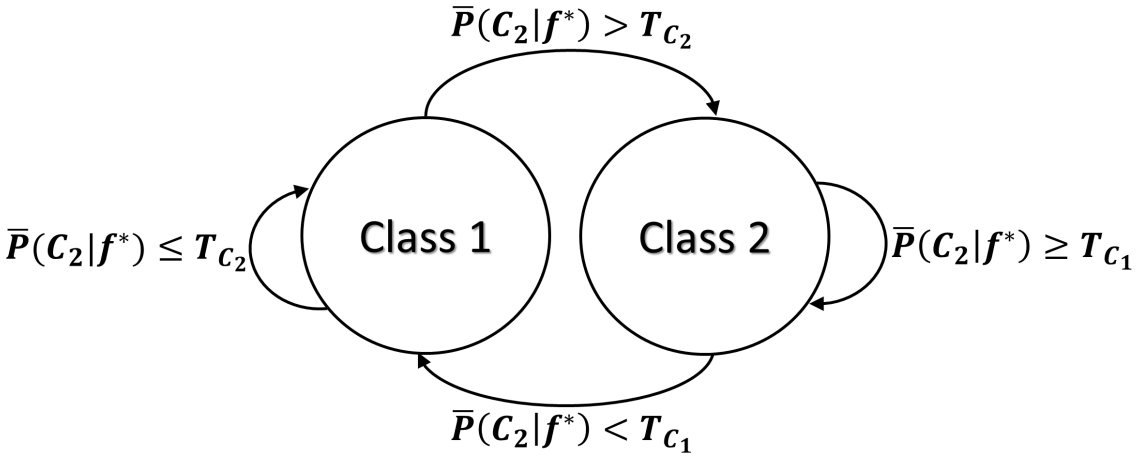

Figure 2.5: Schematic of our binary state machine, with classes "Class 1", C_1, and "Class 2", C_2. Note that the posterior probability, $\bar{P}(C_2|f^\star)$, is averaged over a sliding average window of 1–2 s to reduce false transitions between states.

As depicted in Fig. 2.5 above and the hysteresis shown below (Fig. 2.6), two thresholds are used to transition between each class. Specifically, the BCI system transitions to the "Class 1" state when $\bar{P}(C_2|f^\star) < T_{C_1}$, and transitions to the "Class 2" state when $\bar{P}(C_2|f^\star) > T_{C_2}$. Otherwise, the system remains in the current state. Note that these

separate thresholds are utilized to reduce the number of false alarms and omissions during online operation.

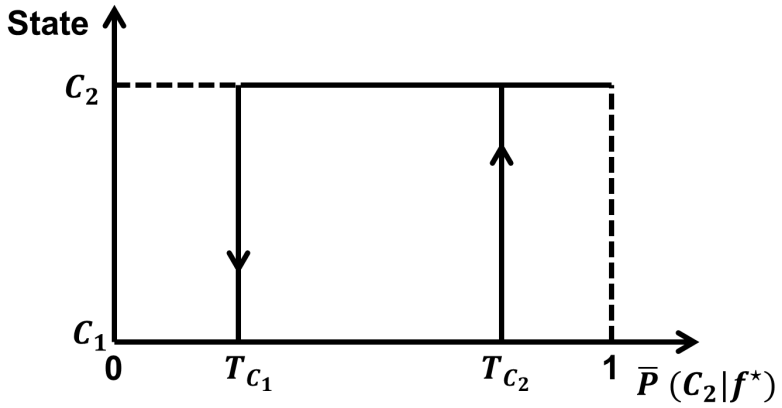

Figure 2.6: Hysteresis of our binary state machine, with thresholds T_{C_1} and T_{C_2} to transition from "Class 1" and "Class 2". The BCI system transitions to the "Class 1" state when $\bar{P}(C_2|f^\star) < T_{C_1}$, and transitions to the "Class 2" state when $\bar{P}(C_2|f^\star) > T_{C_2}$.

2.5 Online Calibration

Prior to online testing for the self-paced BCI systems described in the remaining chapters, a brief 2 – 5 min calibration procedure is performed to determine the optimal parameters for online operation. This step is necessary to reduce noise during online BCI operation and to minimize the mental workload of the user. To this end, segments of EEG data are acquired every 0.25 s and the most recent data segments are combined into a data window with a duration of AD. This sliding window duration can be varied to make faster or more reliable decisions based on the EEG data. The EEG data window of duration AD is then used as the input for the feature extraction techniques described in Section 2.4.1. The posterior probabilities, $P(C_1|f^\star)$ and $P(C_2|f^\star)$, are calculated using the Bayes rule in Eq. 2.2. To reduce the false alarms and omission rates as well as make faster or more reliable decisions during

online operation, the posterior probabilities are also averaged over a sliding window duration of PD, $\bar{P}(\cdot|f^\star)$. In addition, the posterior probability is compared to the two thresholds mentioned above, T_{C_1} and T_{C_2}, to initiate state transitions (see Figs. 2.5 and 2.6).

The values of T_{C_1} and T_{C_2}, as well as other parameters for online operation (e.g. sliding window durations PD and AD), are determined from the short calibration procedure and brief familiarization session. Specifically, during both procedures, the system is set to run in the online mode (with the external device disabled) as the participant alternates between "Class 1" and "Class 2" states for 2 – 5 min. The values of $\bar{P}$ are then plotted in a histogram after the calibration procedure to empirically determine the values of T_{C_1} and T_{C_2}. A sample histogram can be seen in Fig. 2.7. Note that ideally, $\bar{P}(C_2|f^\star \in C_1)$ and $\bar{P}(C_2|f^\star \in C_2)$ should cluster around 0 and 1, respectively. However, as long as these probabilities are separable, online BCI control should be achievable.

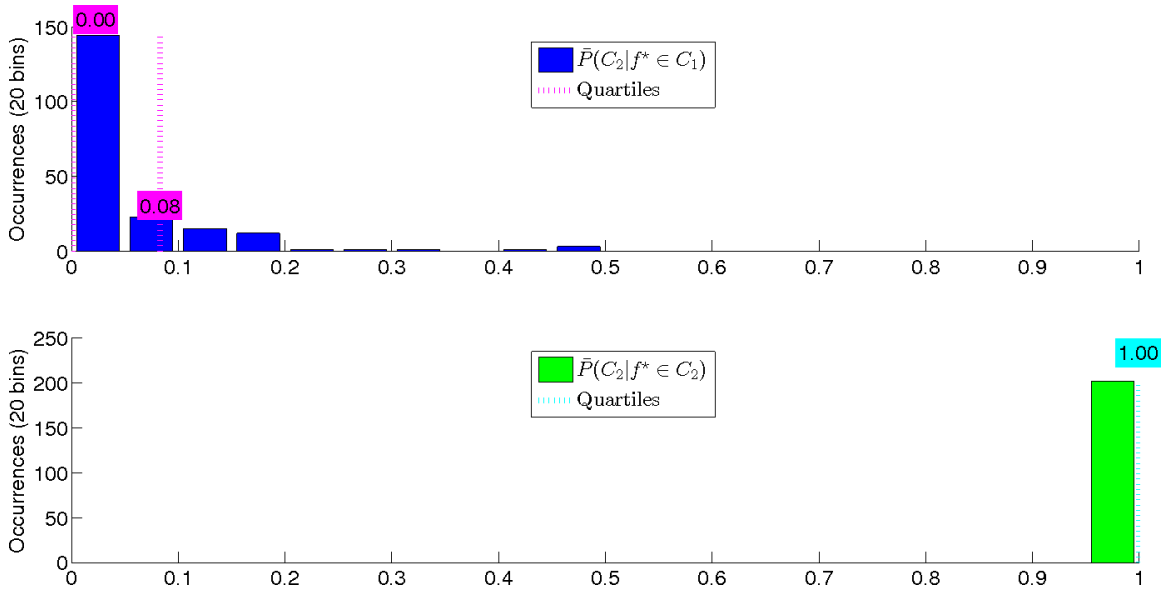

Figure 2.7: Histogram of an online calibration session where $\bar{P}(C_2|f^\star \in C_1)$ are the averaged posterior probabilities of "Class 2" given the features belong to "Class 1", and $\bar{P}(C_2|f^\star \in C_2)$ are the posterior probabilities of "Class 2" given the features belong to "Class 2".

The brief familiarization online session with posterior probability feedback while the external device is still disabled is performed after the histogram plotting session to further fine-tune the threshold values T_{C_1} and T_{C_2}, as well as the sliding window durations AD and PD. The two thresholds, T_{C_1} and T_{C_2}, are initially set as $T_{C_1} = \text{median}\{P(C_2|f^\star \in C_1)\}$ and $T_{C_2} = \text{median}\{P(C_2|f^\star \in C_2)\}$. Then, based on the participant's feedback and verbal cues given to the participant, the operator adjusts these thresholds and the values of PD and AD as necessary. This step is implemented to smooth the noisy state transitions, reduce false alarms and omissions, and allow for faster and more reliable detection of both states.

2.6 Online Experiments

2.6.1 Online Signal Analysis

During online BCI operation, 0.25 s segments of EEG data are acquired and the averaged posterior probabilities are calculated as explained above. For the self-paced BCI systems, projects 3 – 7 in Fig. 1.4 and those described in the remaining chapters, the power spectral densities (PSD) are calculated using the Fast Fourier Transform (FFT) over a sliding data window with the empirically determined duration AD (see Appendix A for details). This is then used as the input for the feature extraction techniques described in Section 2.4.1. The posterior probabilities, $P(C_1|f^\star)$ and $P(C_2|f^\star)$, are calculated using the Bayes rule in Eq. 2.2, and averaged over the determined sliding window duration PD. Then, the averaged posterior probability, $\bar{P}(\cdot|f^\star)$, is compared to the determined thresholds T_{C_1} and T_{C_2} to make state transitions or remain in the current state. Note that these decisions are made in a self-paced manner, meaning the user can decide when to initiate state transitions through active

movement or mental imagery.

Unlike the self-paced BCI systems, the cue-paced BCI systems in our laboratory, such as our P300 speller system, utilize spatio-temporal features for classification of oddball or non-oddball (see Section 1.2.3 in Chapter 1). This is because the P300 speller system relies on the presentation of a cue followed by an event-related potential to classify neurophysiological data into oddball or non-oddball states. Thus, the EEG data does not need to use FFT to transform the data into the frequency domain; rather, a 400 ms sliding window of data is used as the input for feature extraction and classification in the temporal domain. Then, once 1-D features are extracted, the instant posterior probabilities are calculated using the Bayes rule in Eq. 2.2, and compared to a threshold that was determined using the training EEG data. Specifically, this threshold represents the ratio of the costs associated with false alarm and omission errors so that the Bayesian classifier minimizes the total risk function [42, 148]. Finally, since the ratio of each class is not equal in the case of the P300 speller system, the classifier with this determined threshold prefers to make non-oddball decisions over oddball decisions, thus defaulting to make reliable target letter decisions and reducing the number of false alarms, or undesired letter selections, during online spelling.

2.6.2 Real-Time Experiments

To determine the performance of our BCI systems, several different online tests are performed. For a complete feasibility assessment of a system and to determine the level of real-time control of the BCI system, participants are often asked to perform alternating epochs of "Class 1" or "Class 2", i.e. "Idle" or "Move", given computerized textual cues [30, 34, 83] similar to Fig. 2.3. Although these BCI systems are considered

self-paced systems, computerized cues are used to assess purposeful control and the level of system performance given the known intended tasks. In addition, several physical sensors and/or an audio signal are recorded and synchronized with the BCI system (Section 2.2) to assess the performance of the output device and/or intended movement. For the P300 speller system, the complete assessment of participants' control is determined by having participants copy-spell a sentence that is free of errors [148] (Section 1.2.3 of Chapter 1). On the other hand, to assess the performance of BCI systems in a self-paced manner, other BCI studies in our laboratory use goal-oriented tasks with virtual reality games [32, 81, 146, 145] or overground courses [80]. The details of these goal-oriented task will further be described in Section 4.3 and 4.5 of Chapter 4.

2.7 Performance Assessment

To assess the performance of the BCI systems in the remaining chapters, several statistical tests are used. For the BCI systems that utilized computerized textual cues to assess the performance, these systems compare epochs of intended movement and BCI mediated movement. To accomplish this, there are two different methods for comparing intention and movement. For the motor imagery studies or those where movement intention is desired albeit ineffective (e.g. stroke or SCI studies), the intended movement is determined by the state of the BCI and an audio signal sent during each "Move" class epoch given by the computerized textual cues. Conversely, for those studies where actual movement is used to control the BCI system, the readings from the physical sensors are used to determine epochs of movement and idling using a threshold crossing. A time series, x, describing intended movement, is

thus defined as:

$$x[i] = \begin{cases} -1, & \text{if} \quad i \in C_1 \\ 1, & \text{if} \quad i \in C_2 \end{cases} \tag{2.3}$$

where $i = 1, 2, \ldots, N$, and N is the number of samples in the physical sensor trace. A time series, y, describing the output control device movement, is defined in a similar manner. The normalized cross-covariance function between the time series x and y is then calculated as:

$$\rho_{xy}(m) = \begin{cases} \frac{\sum_{n=1}^{N-m} x_{n+m} y_n}{N-m} & m \geq 0 \\ \frac{\sum_{n=1}^{N+m} x_n y_{n-m}}{N+m} & m < 0 \end{cases} \tag{2.4}$$

where $m \in [-N+1, N-1]$ is the lag between the sequences x and y. The latency between the two sequences is then found as the lag with maximal cross-covariance, i.e. $m^\star = \arg\max_{-L \leq m \leq L} \rho_{xy}(m)$, where L is the lag cutoff. Subsequently, the temporal correlation between x and y is found to be: $\rho^\star_{xy} = \rho_{xy}(m^\star)$. A detailed description of this performance measure can be found in Appendix B.2.

In addition to assessing the performance of the BCI system through cross-correlation, the sequences x and y are also analyzed for false alarms and omissions (see Appendix B.5). A false alarm is defined as any BCI-mediated movement during a non-movement intention epoch (as determined by the physical sensors or audio signal and Eq. 2.3). Conversely, an omission is defined as the absence of any BCI-mediated movements within a movement intention epoch.

To assess the significance of the online performances, an auto-regressive model is

defined as [34]:

$$\begin{aligned} X_{k+1} &= \alpha X_k + \beta W_k \quad X_0 \sim U(0,1) \\ Y_k &= h(X_k) \end{aligned} \tag{2.5}$$

where X_k is the state variable, $W_k \sim U(0,1)$ is uniform white noise, Y_k is the simulated posterior probability, and h is a piecewise linear saturation function that ensures $y_k \in [0,1]$. The coefficients α and β are determined so that the mean, $\mu\{Y_k\}$, and the "one off" lag correlation coefficient, $\rho(Y_{k+1}, Y_k)$, match those of the posterior probability sequence, $\bar{P}$, observed in the online sessions. The simulated posterior probabilities, $\{Y_k\}$, are then fed into the binary state machine (Fig. 2.5 in Section 2.4.2), resulting in a simulated sequence of "Class 1" and "Class 2" (i.e. "Idle" and "Move" in the remaining Chapters) states. The cross-correlation between the intended movement and the simulated BCI states is then calculated as explained above and in Appendix B.2. This procedure is repeated for several Monte Carlo runs, typically 10,000 runs, for each online session. The details of this procedure can be seen in Appendix B.3. Finally, an empirical p-value is then defined as the fraction of Monte Carlo runs that achieved a higher temporal correlation than the online session's $\rho^{\star}_{xy}$.

Chapter 3

Stroke Neurorehabilitation

3.1 Overview

The BCI systems for stroke neurorehabilitation, projects 3 and 4 in Fig. 1.4, utilize attempted or actual movement to initiate the movement of an external device. The BCI-Glove study mentioned in Fig 1.4, also described as the BCI driven hand orthosis, utilizes actual movement of the hand to control the orthosis. In addition, the BCI-functional electrical stimulation (FES) system (project 4 in Fig. 1.4), also known as the BCI-FES system for foot dorsiflexion, utilizes actual foot movement in able-bodied individuals and attempted, albeit ineffective, movement in stroke individuals to operate the FES of the tibialis anterior to initiate foot dorsiflexion. Note that both of these studies only focus on one type of attempted movement that is simple, and both studies assess both the movement as well as the idle state (i.e. non-movement) of each of these behaviors. The reason behind utilizing both movement and non-movement states to control the BCI systems is to prevent potential positive feedback from occurring during activation of the external device.

In order to develop these systems as a stroke neurorehabilitative therapy, each movement or non-movement state is controlled in real time over a long period of time (e.g. each epoch of the states lasts for several seconds). The reason for this sustained movement or non-movement is due to the need for coactivation to occur during each state, thus hopefully capitalizing on the Hebbian learning and neuroplasticity principles that can lead to functional improvement (Section 1.2.5 of Chapter 1). Furthermore, since significant latency can occur between the attempted movement and non-movement caused by the BCI driven external device, the sustained movement or non-movement state allows for the potential coactivation of the upper and lower motor neurons to occur during the steady state response of the system.

3.2 BCI Driven Hand Orthosis

A common functional deficit that affects more than one third of chronic ($>$ 6 months post-ictus) stroke survivors is distal upper extremity weakness, i.e. hand weakness [74]. Despite intensive treatment and spontaneous recovery, significant functional recovery of hand weakness after the first 6–8 months in these individuals is uncommon [43], and there are only limited treatments for chronic individuals (e.g. bilateral arm training [97], constraint-induced movement therapy [139, 158], or both [96]). Also, these therapies often require the individual to have residual movements in their hand (for constraint-induced therapy, a minimum of 20° of active wrist extension and 10° of finger extension [139]), and thus are not applicable for stroke individuals with severe upper extremity weakness. Therefore, to address these issues, novel treatments such as BCI neurorehabilitative therapies for chronic stroke individuals with distal upper extremity weakness have been sought.

To develop a BCI neurorehabilitative therapy for chronic stroke individuals with

hand weakness, the underlying attempted (albeit ineffective for those with severe limb weakness) neurophysiological activity must be coupled with the same movement from an output device, such as an FES system or an orthosis. This has been tested by several other laboratories using different output devices and control strategies, for instance, a magnetoencephalogram based BCI driven hand orthosis [15], a BCI-FES system for finger movement [24], and a BCI driven and arm orthoses [118]. However, these existing BCI upper extremity systems require bulky and expensive equipment [15], extensive training (e.g. days [118] or weeks [24]), selection of brain areas based on able-bodied anatomy [24, 118], or do not account for BCI control during both movement and non-movement states [15, 118]. In order for a more applicable neurorehabilitative treatment, a BCI system should be inexpensive, operable after only minimal training, able to accommodate for brain remodeling after stroke, and controllable during both movement and non-movement states.

The methods described below demonstrate that purposeful real-time control of an electroencephalogram (EEG) based BCI system during both movement and non-movement states can be achieved after ∼20 min of training [78, 83]. Furthermore, the data-driven decoding approach described in Chapter 2 allows for participant-specific brain areas to control the BCI system, which can accommodate for brain remodeling after stroke.

3.2.1 Methods

Overview

The BCI system described in Chapter 2 was integrated with a hand orthosis [102]. However, in order to determine the feasibility of such a system as a neurorehabilitative therapy, this device was tested on several able-bodied participants in a contralateral

control paradigm [78, 83]. This entailed participants performing voluntary movements of one hand to elicit BCI control of the orthosis mounted on the opposite (contralateral) hand (see Fig. 3.1 for an overview schematic of the system and contralateral control paradigm). Note that unlike an ipsilateral control paradigm, this approach separates voluntary and BCI-mediated hand orthosis movements, thus facilitating an accurate performance assessment of the system. Finally, to assess the attainment of purposeful control using this paradigm, participants' performances of the online sessions were compared to Monte Carlo simulations (described in Appendix B.3).

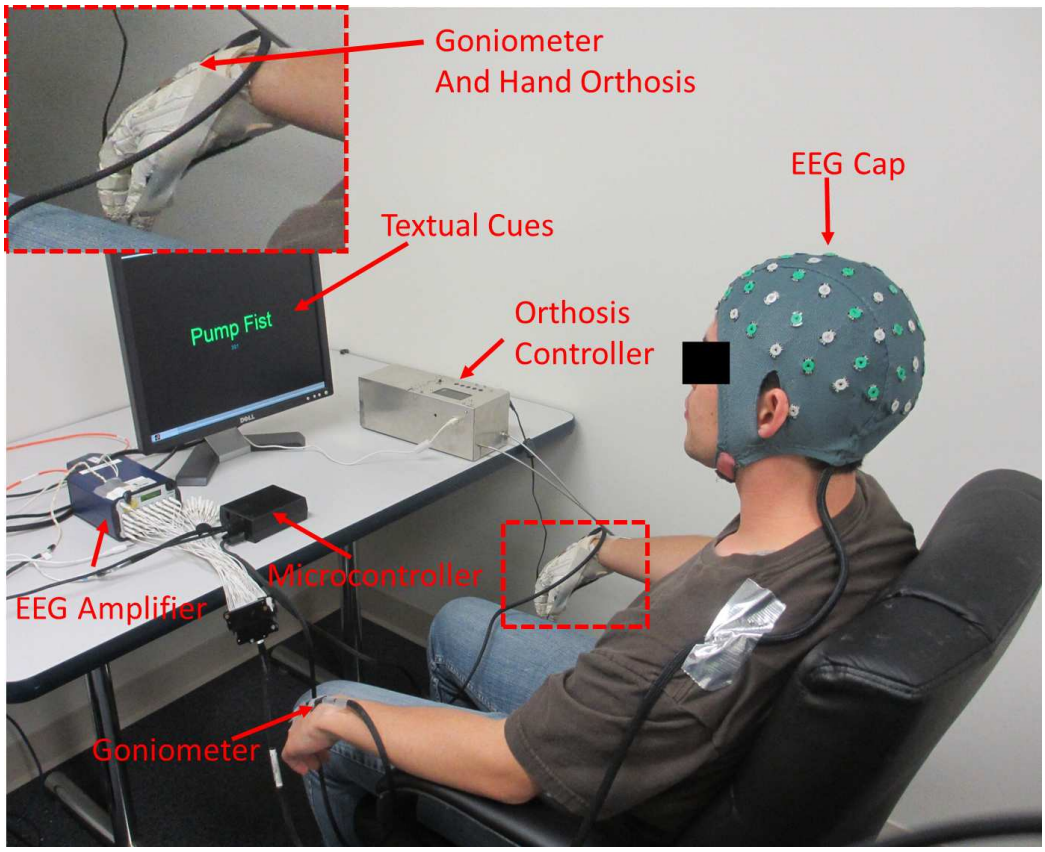

Figure 3.1: Schematic of the BCI driven hand orthosis system [78]. The participant performs repetitive hand grasping of one hand to elicit BCI driven hand orthosis movement of the other hand. Shown in the schematic are the EEG cap and amplifier, the 2 electrogoniometers mounted on each hand to measure hand movement via a microcontroller, a monitor to display textual cues, and the orthotic glove and controller [102] used to control the grasping and extension of the opposite hand.

Participant Recruitment and Data Acquisition

This study [78, 83] was approved by the University of California, Irvine Institutional Review Board. Able-bodied participants who are generally healthy with no history of neurological conditions were recruited and gave their informed consent to participate.

As described in Section 2.3 of Chapter 2, each participant was seated in a chair $\sim$1 min from a computer monitor that displayed textual cues (Fig. 2.3 in Section 2.3). EEG was recorded using the 63-channel EEG cap described in Section 2.2 of Chapter 2. With the exception of the 1st participant, whose methods and results are described in [83], all other participants used the 32 electrodes shown in Fig. 2.1 of Section 2.2 of Chapter 2. Finally, except for Participant 3, whose 30-Hz impedances between each electrode and the reference electrode were $\sim$50 KΩ, all other participants had their impedances reduced to $<$10 KΩ. The EEG signals were then streamed in real-time to a computer and re-referenced in a common average mode using the NeXus-32 bioamplifier (MindMedia, Roermond-Herten, The Netherlands).

The voluntary and orthosis-mediated movements were measured by custom-made electrogoniometers [147] mounted on the metacarpophalangeal joint of the middle fingers (see Fig. 3.1). However, unlike in [147], the 2 bi-directional flex sensors that were integrated with voltage dividers were acquired using an Arduino Uno micro-controller (Arduino, SmartProjects, Turin, Italy). The electrogoniometer system was then synchronized with the EEG system by a common pulse train generated by the microcontroller (see Fig. 2.2 and Section 2.2 of Chapter 2). Finally, custom-written Matlab (MathWorks, Natick, MA) programs were used for data acquisition and analysis of all systems.

Training Procedure and Decoding Model Generation

To generate EEG decoding models for each participant, each participant was instructed via computerized textual cues (shown in Fig. 2.3 of Section 2.3 in Chapter 2) to perform 200 6-s-long alternating epochs of idling and repetitive hand grasping while their EEG and electrogoniometer signals were recorded [78, 83]. Specifically, when instructed to "Grasp", the participants pumped their fist contralateral to the hand orthosis at a comfortable pace. When instructed to "Idle", participants relaxed their hand and remained still. The hand with the orthosis remained idle the entire time. The total duration of this procedure lasted ∼20 min.

Once the training procedure was performed, EEG decoding models were developed using the methods described in Section 2.4 of Chapter 2. Briefly, the EEG and electrogoniometer signals were first aligned and merged using the synchronization signal generated by the microcontroller. The EEG data were then segmented into ∼5.25-s-long trials of "Idling" and "Grasping" using the electrogoniometer signals. Note that the 1^{st} 0.75 s of each training epoch were removed to avoid the effect of visual response from the cues. In addition, those channels whose voltages were excessively contaminated with electromyogram (EMG) artifacts were removed using the iterative artifact rejection algorithm described in Section 2.4.1 of Chapter 2. The power spectral densities (PSD) of the remaining channels and trials were calculated in 2-Hz bins from 8-30 Hz (6-30 Hz for Participant 1 in [83]) using the Fast Fourier Transform (FFT) described in Appendix A.1. The dimension of the input data was then reduced using classwise principal component analysis (CPCA, described in Appendix A.3 and Section 2.4.1), and discriminating features were extracted using either approximated information discriminant analysis (AIDA) or linear discriminant analysis (LDA), described in the same appendix and section mentioned above). Once the single-trial data were reduced to a 1-D spatio-spectral feature, the linear Bayesian classifier de-

scribed in Section 2.4.2 of Chapter 2 and in Appendix A.4 was designed in the feature domain to classify the input feature as "Idle" or "Grasp". The performance of the Bayesian classifier, expressed as a classification accuracy, was assessed using stratified 10-fold cross-validation described in Section 2.4.2 of Chapter 2 and in Appendix B.1. Finally, this cross-validation procedure was also used to determine the parameters and methods for the participant-specific EEG decoding model for online BCI operation.

Online Signal Analysis and Calibration

During online BCI operation, segments of EEG data were acquired every 0.25 s and the most recent data segments were combined into a data window with a duration of AD, as described in Section 2.5 of Chapter 2. The PSDs of this data window were then used as the input for the feature extraction techniques described in Appendix A.3 and Section 2.4.1 of Chapter 2. Finally, the posterior probabilities were calculated using the Bayes rule (Eq. 2.2 in Section 2.4.2 of Chapter 2, and in Appendix A.4), and were averaged over a sliding window with a duration of PD, as described in Section 2.5 of Chapter 2.

To determine the optimal parameters for online operation, and to minimize the false state transitions of the binary state machine (Figs. 2.5 and 2.6 in Section 2.4.2 of Chapter 2), a brief calibration procedure was performed. As previously mentioned, this was performed by allowing the BCI system to run in the online mode (with the hand orthosis disabled) while the participant alternated between idling and voluntary hand grasping for $\sim$5 min. The two thresholds were initially set as the median of the posterior probabilities given the known class of the input feature, and were fine-tuned using a brief familiarization online session without feedback (see Section 2.5 of Chapter 2). Finally, the durations AD and PD were also fine-tuned during the brief familiarization online session to minimize the false state transitions and latency

between the voluntary hand movement and BCI system's binary state machine response.

BCI Driven Hand Orthosis Integration and Online Performance Assessment

The electrically actuated, cable-driven hand orthosis described in [102] consists of a leather glove with a finger actuation system and a controller (see Fig. 3.2). Prior to online experimentation, this device was mounted on each participant. The parameters of the orthosis were then set to a 0% voltage value for flexion and a 100% voltage value for extension for all participants (i.e. the absolute minimum and maximum potential flexion and extension voltage values the orthosis device was capable of), since these participants were all able-bodied and could fully flex/extend their hand [78, 83]. Furthermore, note that both right-hand and left-hand orthoses were available during the time of the study. However, regardless of their handedness, the orthosis used was determined based on the availability of the device. Finally, to assess the real time control of the BCI driven hand orthosis, electrogoniometers [147] were mounted over both the hand orthosis and the opposite hand, as explained above, and their signals were recorded during the online performance assessment sessions.

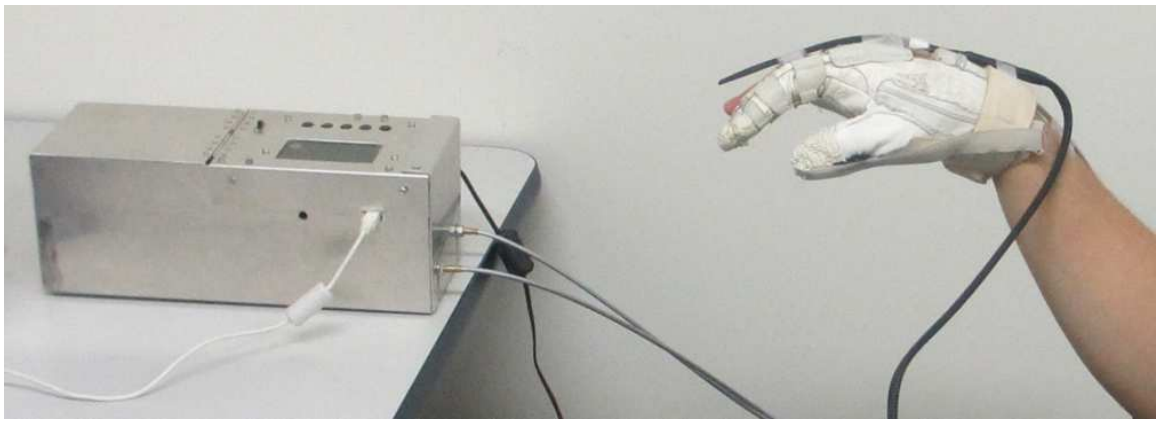

Figure 3.2: Image of the hand orthosis [102] used in the study [78, 83].

After calibrating the BCI and hand orthosis, participants operated the BCI system in real time over multiple online sessions while their EEG and electrogoniometer data were recorded. For each online session, participants were instructed via the computerized textual cues to perform 20 alternating 10-s-long epochs of idling and voluntary hand grasping for a total of 200 s. The transition to the "Idle" state resulted in the extension (opening) of the hand orthosis, while the transition to the "Grasp" state triggered the grasping (clenching) of the orthosis.

To assess the performance of each online session, cross-correlation analysis between the electrogoniometer signals corresponding to the voluntary and orthosis-mediated movements was performed. This procedure is described in Appendix B.2 and Section 2.7 of Chapter 2. In addition to the maximal temporal correlation and the lag with maximal cross-correlation, the number of false alarms and omissions were calculated for each online session. A false alarm was defined as the initiation of a BCI driven hand orthosis response within any idling epoch of the opposite hand. Conversely, an omission was defined as the absence of a BCI driven hand orthosis response within any voluntary hand grasping epoch. A detailed description of how the false alarms and omissions were calculated can be found in Appendix B.5 and Section 2.7 of Chapter 2.

To determine the significance of the online performances, an autoregressive model described in [34], Section 2.7 of Chapter 2, and Appendix B.3, was defined. This model generated simulated and randomized posterior probabilities that matched the posterior probability sequence observed during the online session. The simulated posterior probabilities were then fed into the binary state machine described in Fig. 2.5 of Section 2.4.2 of Chapter 2, resulting in a simulated sequence of "Idle" and "Grasp" states. The cross-correlation between the voluntary movement electrogoniometer data and the simulated BCI states was then calculated as explained in Appendix B.2. This

procedure was repeated for a total of 10,000 Monte Carlo runs for each online session. An empirical p-value was then defined as the fraction of Monte Carlo runs that achieved a higher temporal correlation than the online session being analyzed.

3.2.2 Results

Six able-bodied participants gave their informed consent to participate in the study [78]. Their demographic data are shown in Table 3.1. Note that the hand orthosis for each participant was not chosen based on handedness; rather, it was based on which of the two devices was available at the time of the experiment.

Table 3.1: Demographic data of the study participants, including gender, age, handedness (i.e. preferred hand), hand used for the orthosis, and hours of BCI experience [78]. Note that Participant 1 has more detailed data described in [83] (© 2011 IEEE).

Participant	Sex	Age	Handedness	Orthosis Hand	Hours BCI Experience
1	F	24	Left	Left	10
2	M	21	Left	Right	0
3	F	20	Right	Right	0
4	M	20	Right	Right	0
5	M	22	Right	Right	0
6	M	21	Right	Right	0

Offline Performances

After the participants underwent the offline training procedure (described in Section 2.3 of Chapter 2), participant-specific EEG decoding models were generated as described in Section 2.4.1 of Chapter 2 and Appendix A.3. Each participant's chosen parameters, number of retained EEG channels, and optimal methods are given in Table 3.2. Cross-validation (described in Section 2.4.2 of Chapter 2 and Appendix B.1) of these models resulted in classification accuracies that ranged from 83.7% to 98.7%

(Table 3.2), all significantly above the chance level (50%). Finally, the average offline classification accuracy across all participants was 92.5±4.8% ($n = 6$).

Table 3.2: Offline decoding accuracy (chance = 50%) and parameters across participants. The frequency range, feature extraction method (AIDA or LDA), and number of channels are listed, as these parameters were participant-specific [78, 83]. Note that Participant 1 used a 64 channel EEG system [83], while all other participants used a 32 channel EEG system [78].

Participant	Freq. Range (Hz)	Method	No. Channels	Decoding Accuracy
1	6-30	CPCA+AIDA	63	95.3±0.6%
2	8-30	CPCA+AIDA	29	95.5±0.5%
3	8-30	CPCA+LDA	23	83.7±1.2%
4	8-30	CPCA+LDA	30	98.7±0.4%
5	8-30	CPCA+AIDA	31	92.0±0.8%
6	8-30	CPCA+LDA	32	89.8±0.6%

The EEG decoding models revealed that salient features for classification for Participant 1 were over the C3 electrode at 19 Hz (i.e. the β-band) [83]. The feature extraction maps, depicting this salient feature, can be seen in Fig. 3.3. Note that this participant performed voluntary right hand grasping to control the BCI hand orthosis system. This resulted in a salient feature over the contralateral (left) side of the brain, electrode C3, and a less salient feature over the ipsilateral (right) side of the brain, over electrode C4.

For those participants who performed left hand grasping [78], the EEG decoding models revealed salient features over the C4 and C6 electrodes from 9–19 Hz (i.e. the μ and low-β bands) [78]. A representative example of these salient features can be seen in Fig. 3.4 for Participant 5. Particularly, Participant 2 had salient features over the C4 electrode at 9 Hz, Participant 3 had salient features over the C4 and C6 electrodes at 11 Hz, Participant 4 had salient features over the CP3 and CP5 electrodes at 13 Hz, Participant 5 had salient features over the C6 electrode at 11 Hz (Fig. 3.4), and Participant 6 had salient features over the C6 electrode at 19 Hz. With the exception of Participant 4, all participants' salient EEG features were over

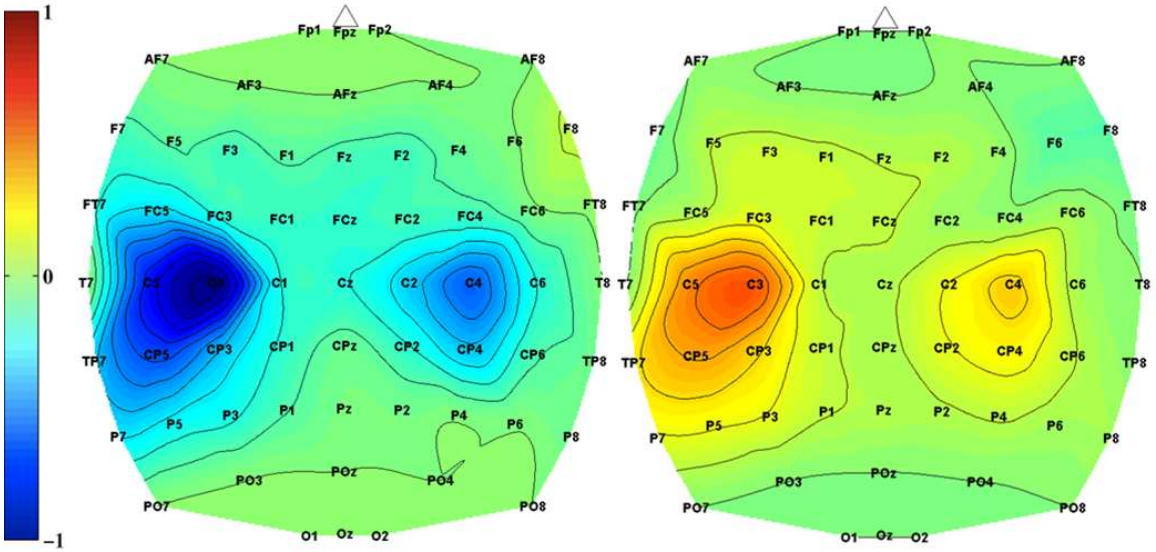

Figure 3.3: Representative feature extraction matrices (CPCA+AIDA) in the 18–20 Hz bin shown as images [83] (© 2011 IEEE). Two images underlie the piecewise linear structure of the CPCA feature extraction method. Dark colors (red, +1, and blue, -1) represent the areas that were most informative for encoding the differences between idling and contralateral hand grasping.

the side of the brain contralateral to the voluntary moved hand [78]. In addition, the power spectra and signal-to-noise ratio for Participant 5 at electrode C6 during the idling and grasping tasks are shown in Fig. 3.5. Note the desynchronization in the μ-band (8 – 12 Hz) between the idling and grasping tasks, a consistent feature that is also present in the offline EEG decoding model in Fig. 3.4.

Online Calibration

The short calibration procedure (methods described in Section 2.5 of Chapter 2) performed to minimize the false state transitions of the binary state machine revealed highly separable distributions of the posterior probabilities, $\bar{P}(G|f^{\star} \in G)$ and $\bar{P}(G|f^{\star} \in I)$, where G denotes the "Grasp" state and I denotes the "Idle" state. Representative histograms are shown in Fig. 3.6 for Participant 1 [83] and Participant 4 [78]. Note that in an ideal situation, $\bar{P}(G|f^{\star} \in G)$ and $\bar{P}(G|f^{\star} \in I)$ should cluster

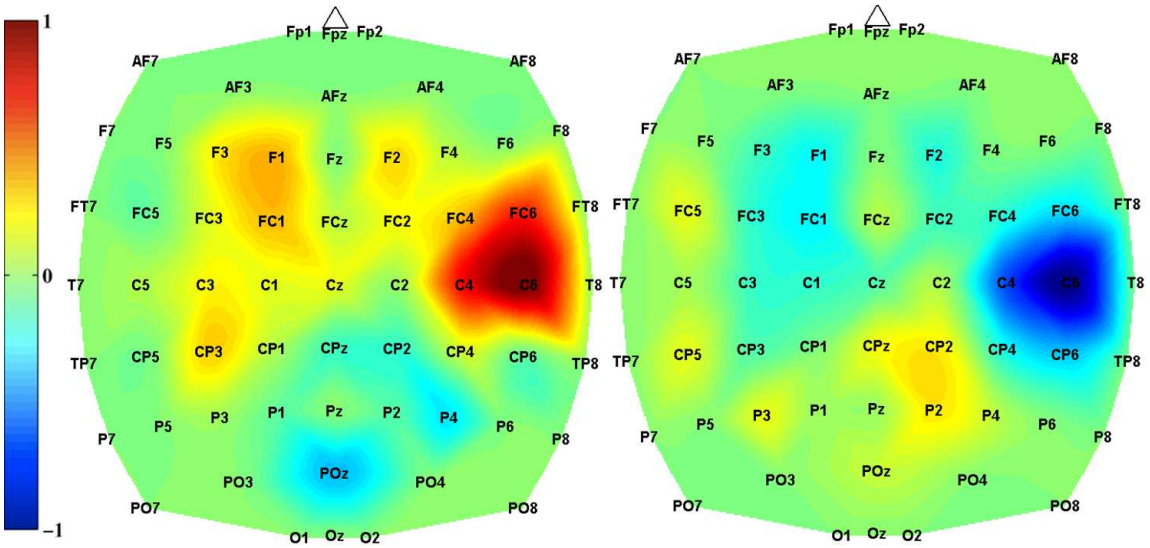

Figure 3.4: Representative feature extraction matrices in the 10–12 Hz bin shown as images for Participant 5 [78]. Dark colors (red, +1, and blue, -1) represent the areas that were most informative for encoding the differences between idling and contralateral hand grasping.

around 1 and 0, respectively. This, in turn, resulted in state transition thresholds that were highly separable (Table 3.3). For example, the average idle threshold across participants was 0.42±0.19, while the average grasp threshold was 0.83±0.12. Finally, with the exception of Participant 3 who had high impedances (< 50 KΩ) during the EEG mounting procedure, the analysis and posterior probability averaging durations, PD, presented in Table 3.3, were relatively consistent across participants.

Table 3.3: Calibration parameters for online BCI operation as determined by the calibration session. The analysis duration (AD), posterior probability averaging duration (PD), idle threshold (T_I), and grasping threshold (T_G) are shown for all participants [78, 83].

Participant	AD (s)	PD (s)	T_I	T_G
1	0.75	1.50	0.10	0.70
2	1.00	2.00	0.42	0.90
3	2.25	4.50	0.55	0.70
4	1.00	2.00	0.60	0.99
5	1.00	2.00	0.30	0.78
6	0.75	1.50	0.57	0.92

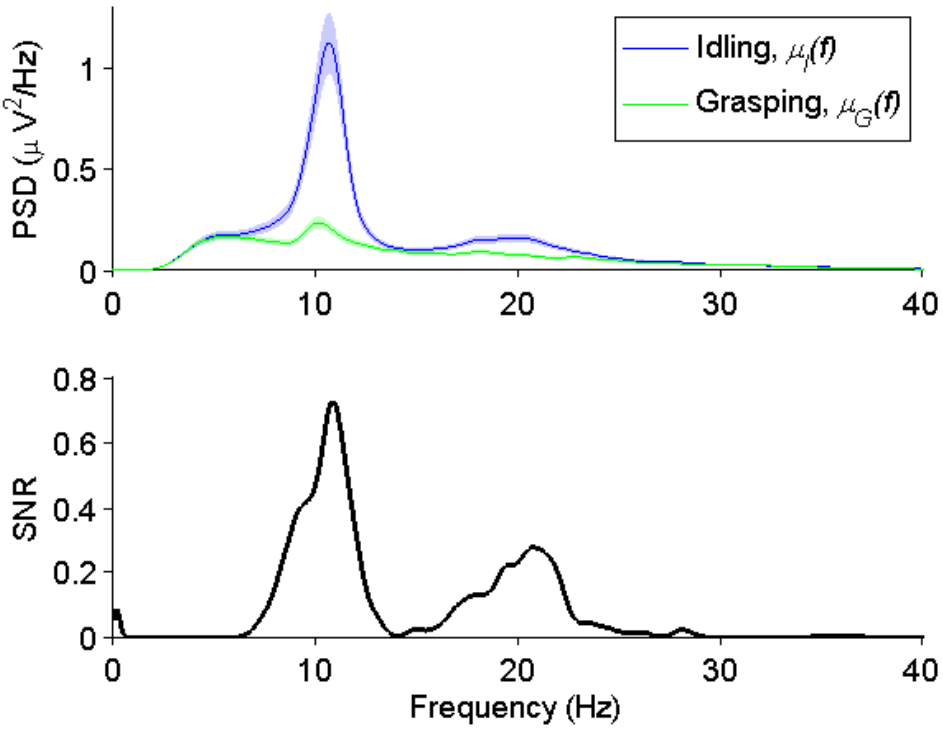

Figure 3.5: Representative (Participant 5 from [78]) PSDs at electrode C6. Red and blue traces denote the average ($n = 100$) power spectra of EEG signals under idling and grasping conditions, respectively. Black trace represents the signal-to-noise ratio (SNR), defined as: $SNR(f) = \frac{(\mu_I(f)-\mu_G(f))^2}{\sigma_I^2(f)+\sigma_G^2(f)}$, where f is the frequency, $\mu_I(f)$ and $\mu_G(f)$ are the average powers at frequency f under idling and grasping conditions, respectively, and $\sigma_I^2(f)$ and $\sigma_G^2(f)$ are the corresponding variances.

Online Performances

After the calibration procedure, all participants operated the BCI driven hand orthosis system in real time for 5 – 7 online sessions (mean: 5.83, standard deviation: 0.75) [78]. The results of the online performances are presented in Table 3.4. The overall average cross-correlation across participants and sessions was 0.58 (standard error of the mean: 0.13), with a corresponding lag of 2.49 (0.61) s. The average maximum cross-correlation across participants and sessions was 0.67 (0.12), with a lag of 2.49 (0.88) s. In addition, the overall average number of false alarms and omissions were 1.91 (1.42) and 0.37 (0.60), respectively. Given that the durations of the "Idle" and "Grasp" states of an online sessions were 100 s, these values correspond to the

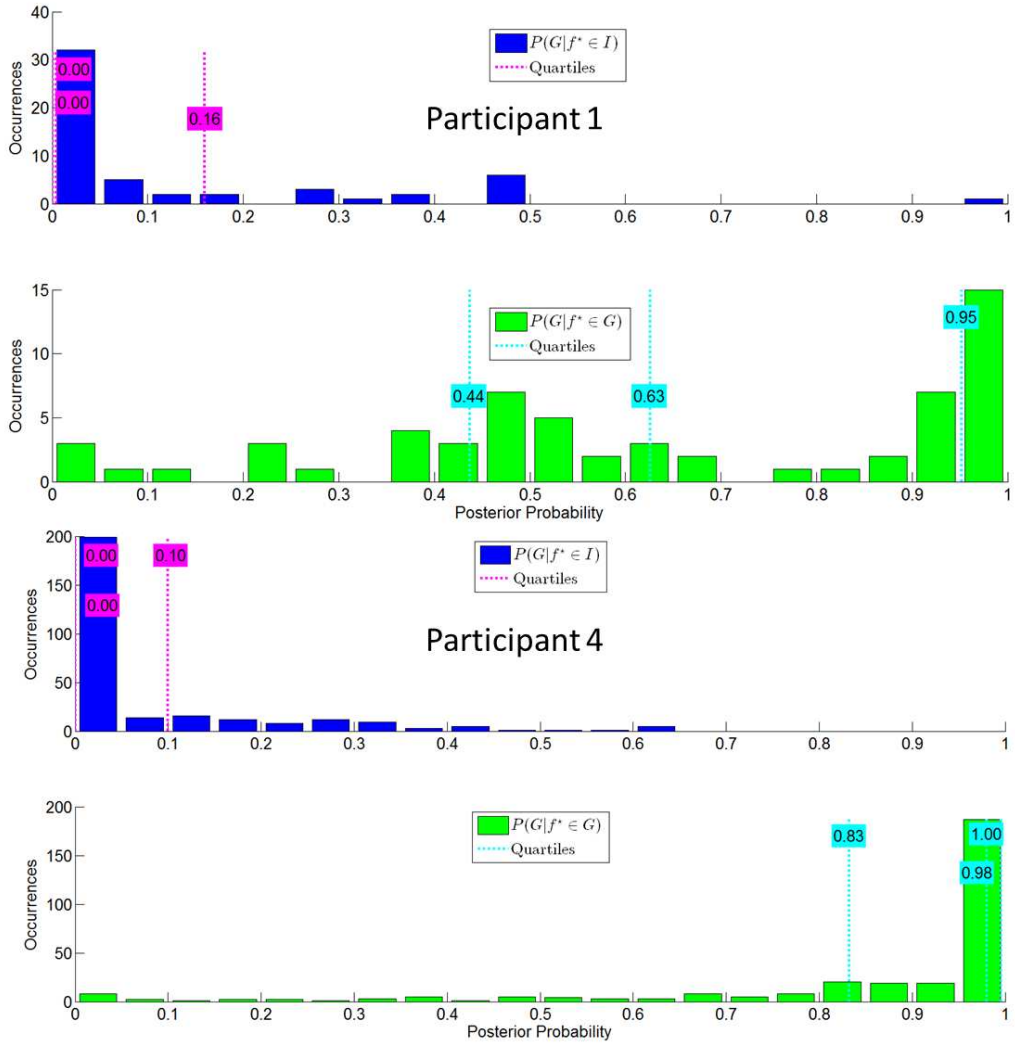

Figure 3.6: Representative histograms of Participant 1 (top) [83] (© 2011 IEEE) and Participant 4 (bottom) [78].

following error rates: 1.15 (0.85) false alarms per minute, and 0.22 (0.36) omissions per minute.

Individual session's performances ranged from a 0.35 cross-correlation at a 2.75 s lag with 1 false alarm and 1 omission (Participant 3, session 1) to a 0.84 cross-correlation at a 2.31 s lag with 1 false alarm and 0 omissions (Participant 1, session 5) [78, 83]. A representative performance (the best online session for Participant 2) is shown in Fig. 3.7. The statistical tests described in Appendix B.3 revealed that all but

Table 3.4: Online performances of each participant (Pt.), including the number of online sessions performed (No. Sess.), average cross-correlation coefficient (ρ) and lag in s, maximum cross-correlation coefficient and lag in s, average number of false alarms (FA), and average number of omissions (OM). Standard error of the mean (SE) are reported in the parentheses [78].

Pt.	No. Sess.	Avg. $\rho^\star$ mean (SE)	Lag (s) mean (SE)	Max. $\rho^\star$	Lag (s)	No. FA mean (SE)	No. OM mean (SE)
1	6	0.77 (0.06)	2.15 (0.31)	0.84	2.31	1.50 (0.55)	0.33 (0.82)
2	6	0.61 (0.07)	2.44 (0.23)	0.73	2.13	0.67 (1.21)	0.33 (0.52)
3	5	0.43 (0.06)	3.35 (0.45)	0.49	4.00	1.17 (1.17)	0.60 (0.55)
4	7	0.50 (0.08)	2.98 (0.26)	0.63	3.00	3.00 (2.33)	0.43 (0.79)
5	6	0.64 (0.06)	2.26 (0.33)	0.71	1.94	3.00 (1.27)	0.00 (0.00)
6	5	0.52 (0.06)	1.70 (0.30)	0.60	1.56	1.80 (0.84)	0.60 (0.55)
Avg.	5.83 (0.75)	0.58 (0.13)	2.49 (0.61)	0.67	2.49	1.91 (1.42)	0.37 (0.60)

one cross-correlation (the 4$^{\text{th}}$ session for Participant 6) were statistically significant (p-value $< 10^{-4}$).

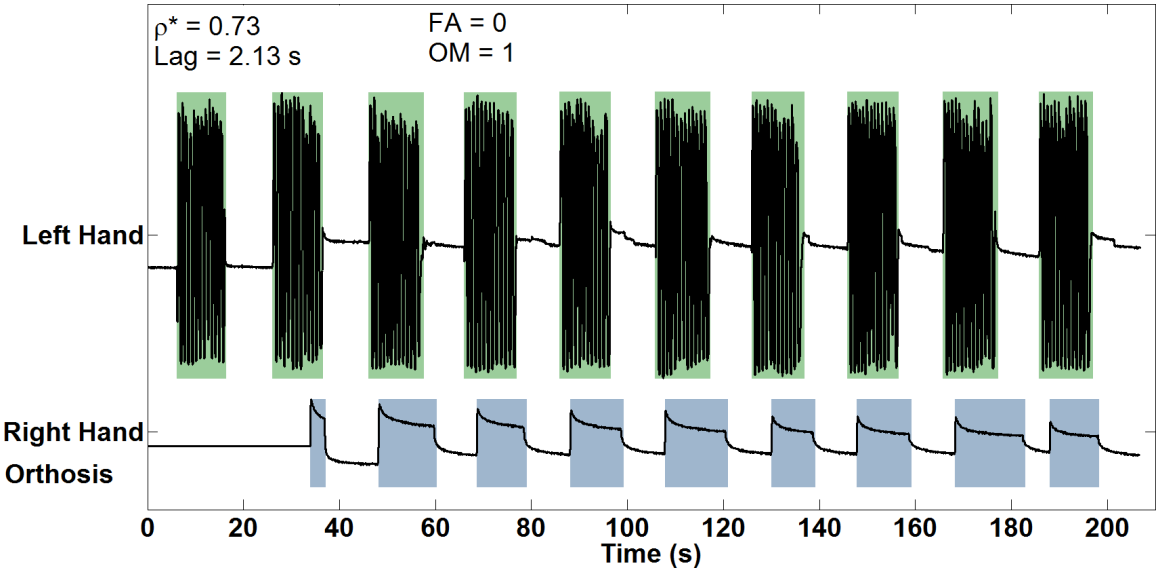

Figure 3.7: Representative electrogoniometer traces of the 4$^{\text{th}}$ online session of Participant 2 [78]. Traces show 1 omission and 0 false alarms for this online session, with a maximum cross-correlation of 0.73 at a 2.29 s lag.

3.2.3 Discussion

The results of this study show that able-bodied participants were able to operate the BCI driven hand orthosis with purposeful (i.e. above the chance level, 50%) performances throughout the entire experiment (except for a single session for Participant 6) [78]. Furthermore, all participants were able to operate the BCI after only ∼25 min of training and calibration, obtaining immediate real time, online control of the orthosis during both movement and non-movement states [78, 83]. These findings suggest that a BCI driven hand orthosis for the neurorehabilitation of stroke individuals with hand weakness may be feasible.

Offline Performances

The offline classification accuracies were very high across participants, and this translated into immediate online control of the system without the need for extensive training [78, 83]. Moreover, the participant with the lowest performance was Participant 3, who had unusually high impedances during the EEG mounting procedure, and this performance (83.7%) was still well above the chance level (50%). These high classification accuracies also translated into high online performances, indicating that no overfitting occurred in the design of the decoding models.

The EEG decoding models across participants revealed that similar features were responsible for encoding the differences between idling and voluntary repetitive hand grasping. Particularly, the EEG power in the μ (8–12 Hz) and β (13–30 Hz) bands over the motor cortex contralateral to the voluntarily moved hand played a prominent role in classifying the two states [78, 83]. The modulation of the EEG power in these bands likely corresponds to activity within the primary motor cortex's hand representation area and/or supplementary motor area. While this is not surprising from

an anatomical standpoint, it should be noted that the EEG decoding models were not anatomically constrained, and so these observations highlight the physiological and anatomical plausibility of our data-driven decoding methodologies described in Chapter 2 and Appendix A.3. Finally, these spatio-spectral EEG features are consistent with classical upper extremity movement theory, and prior EEG [6, 113, 114] and functional magnetic resonance imaging [6] studies.

Online Performances

The results achieved online demonstrate that BCI-mediated hand orthosis movement can be reliably controlled using a contralateral control paradigm in a population of able-bodied individuals [78, 83]. More importantly, the statistically significant cross-correlations across sessions and participants (except for a single online session) throughout the entire study suggest that control of this system can be maintained over time. These results also demonstrate that very high correlation coefficients are achievable (e.g. Participant 1 in [83]), although this participant had more prior BCI experience. This suggests that additional practice with the BCI could further improve performance. Finally, the false alarm rate (i.e. movement during non-movement states) across participants was higher than the omission rate (i.e failing to move within a movement state); however, both types of errors were very low, as the average error rates across participants did not exceed 1.8 false alarms per minute and 0.36 omissions per minute [78].

3.2.4 Conclusion

This study suggests that a BCI driven hand orthosis system to treat hand weakness in stroke individuals may be feasible [78, 83]. With minimal training and BCI experience,

able-bodied participants were able to operate the BCI driven hand orthosis in real time throughout the entire experimental day. Future studies will require testing this device in a population of stroke individuals using attempted, albeit ineffective, hand grasping of the stroke affected hand to control the BCI-hand orthosis. However, this will be further elaborated upon in Section 5.2.1 of Chapter 5.

3.3 BCI-FES System for Foot Dorsiflexion

Despite spontaneous recovery and intensive physiotherapy in stroke survivors, over 30% of these chronic individuals are affected by gait functional impairments, with foot drop often being the primary cause [75]. Ankle-foot orthoses and FES devices can mitigate this condition, however, they are cumbersome to use and can cause discomfort. More importantly, the benefits of these devices disappear upon their removal. Hence, novel methods that can provide lasting neurological and functional gait improvements are necessary [23].

As previously mentioned in Section 3.2 above, there has been a recent increased interest in using BCI systems to improve motor outcomes after stroke [5, 14, 15, 24, 118, 142]. For instance, the results from [24] demonstrated that a BCI-controlled FES system for hand grasping led to the improvement of hand function in a stroke survivor. This improvement may have been due to the participant's robust BCI-FES control, which allowed for simultaneous activation of the post-infarct cortex and peripheral neuromuscular system, thus promoting neural plasticity and Hebbian learning mechanisms (Section 1.2.5 of Chapter 1). Ultimately, simultaneous activation through BCI-FES therapies may reduce motor impairment, and may eventually translate into sustained functional gains in chronic stroke survivors.

To develop a neurorehabilitative therapy for the treatment of foot drop in stroke survivors, the underlying attempted, albeit ineffective, neurophysiological activity of foot movement must be coupled with the peripheral neuromuscular system via FES. Specifically, the voluntary attempted foot movement must be coupled with the electrical stimulation feedback from the antidromic response of the FES in the motor nerve fibers (towards the soma), potentially reaching the anterior horn cell and further up the neuraxis (see Fig. 1.16 in Section 1.2.5 of Chapter 1) [122]. Thus, to accomplish this goal, our laboratory developed a BCI-FES system for the treatment of foot drop in which the movement and non-movement states of the system are controlled in real time over a long period of time (i.e. several seconds). This sustained control may promote coactivation between the intended movement and antidromic response, and may mitigate the latency issues between the BCI response and actual movement, thus promoting neural plasticity and Hebbian learning mechanisms to occur during BCI-FES operation.

3.3.1 Methods

The BCI-FES system developed for the treatment of foot drop in stroke survivors was first tested in an able-bodied population as a proof-of-concept study [30, 31], then in a small population of chronic stroke individuals with foot drop [36, 38]. In addition, two of the participants in the study using a small population of chronic stroke survivors were long-term users of a commercial FES system for foot drop (L300, Bioness, Valencia, CA), providing a control for the potential improvement due to FES alone versus our proposed BCI-FES therapy. Given the successful results from these studies, this device is now being tested for safety in a Phase I clinical trial in a larger population of chronic stroke individuals over a much longer therapy duration ($\sim$20 participants, 12 weeks). However, much of these results will not be presented,

as the Phase I clinical trial is still ongoing.

Overview

For the proof-of-concept study on an able-bodied population [30, 31], our EEG based BCI system was integrated with a noninvasive FES system for the lower extremities (see Fig. 3.8 for a schematic of the setup). To assess the performance of the BCI-FES system and whether purposeful control can be obtained, a contralaterally-controlled FES paradigm, similar to the BCI driven hand orthosis control paradigm described in Section 3.2, was utilized. In other words, able-bodied participants performed repetitive foot dorsiflexion of the opposite foot to trigger FES of the tibialis anterior muscle of the other foot so as to achieve its dorsiflexion. To accomplish this real time BCI task, participants underwent a short 20 min training procedure to develop a participant-specific EEG decoding model, followed by several online sessions using computerized textual cues, where the real time performance of the integrated BCI-FES system was tested.

The BCI-FES studies that included chronic stroke survivors [36, 38] utilized the same BCI-FES system described in Fig. 3.8 for foot dorsiflexion. However, participants utilized attempted, albeit ineffective, repetitive foot dorsiflexion of the stroke affected foot to induce BCI-FES mediated foot dorsiflexion of the same foot. To accomplish this, the training procedure was reduced to 10 min to allow for faster online operation and to reduce fatigue due to attempted foot dorsiflexion by the user. Then, following the same feature extraction techniques (described in Section 2.4.1 of Chapter 2), a participant-specific EEG decoding model was developed. Several online sessions using computerized textual cues were then used to assess the online performance of the system and the participant's ability to induce BCI-FES mediated foot dorsiflexion and idling using this attempted foot dorsiflexion strategy. The online sessions were

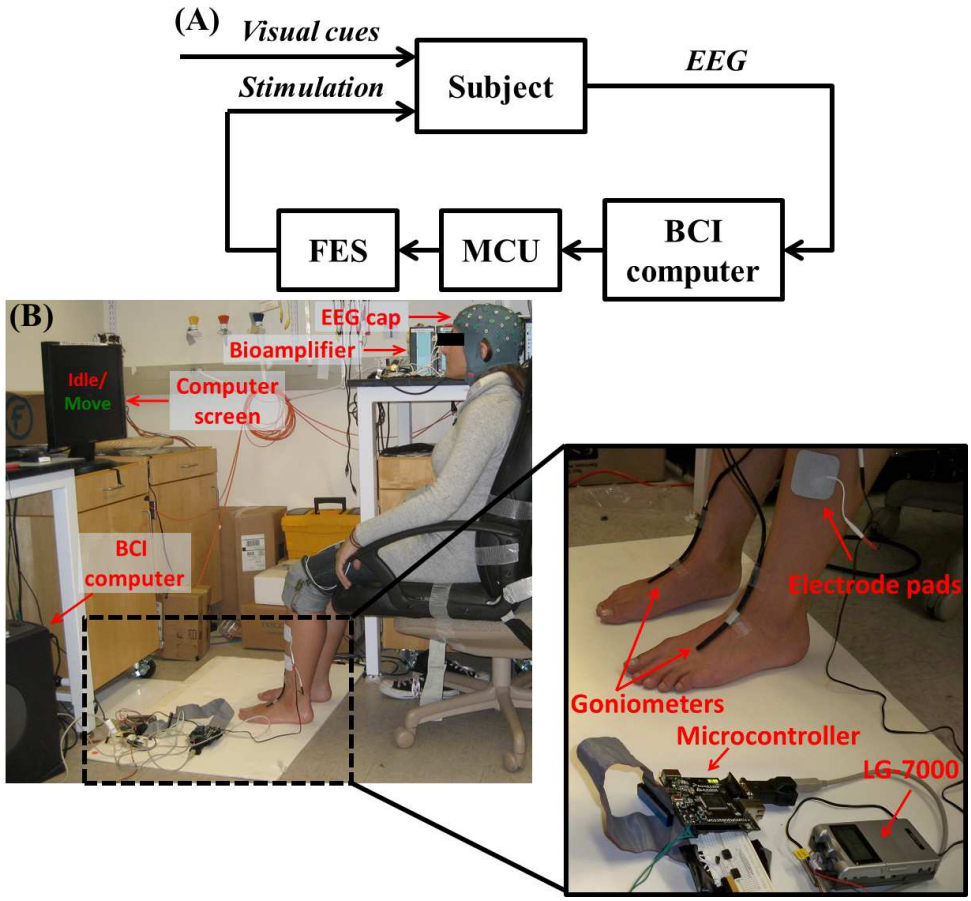

Figure 3.8: (A) Block diagram of the integrated BCI-FES system. (B) Experimental setup showing the participant performing foot dorsifiexion in response to visual cues displayed on the computer screen. The inset shows the microcontroller connected to the neuromuscular stimulator and the placement of surface FES electrodes. Also visible is a pair of custom-made electrogoniometers [147], used for measurement of both executed and BCI-FES mediated foot dorsifiexion [30].

repeated for up to 1 hour, or until the participant was fatigued and could not continue. This entire experimental procedure was repeated for 3 daily sessions in two participants, and was repeated for 12 daily sessions for 1 participant, who performed a study protocol similar to our Phase I clinical trial. Finally, pre- and post-intervention dorsiflexion active range of motion was measured to ascertain the functional gains.

For the Phase I clinical trial where safety is currently being assessed, a before-and-after study designed was implemented. Specifically, chronic stroke survivors with foot

drop who qualified to participate in the study first underwent baseline neurological and functional assessments (gait velocity, dorsiflexion active range of motion, 6-min walk test) prior to receiving the BCI-FES therapy. Each participant then performed 12 daily sessions of BCI-FES therapy over the course of 4 weeks (3 sessions per week), and interval neurological and functional assessments were performed before every 3rd session. The post-intervention neurological and functional assessments were performed 1 week and 1 month after completing the BCI-FES therapy (see Fig. 3.9 for the study time line). The primary outcome measures for the clinical trial are the proportion of participants who experienced a significant deterioration in their gait velocity at the end of the study, and the secondary outcome measures are the proportion of participants who experienced a deterioration in neurological and functional parameters.

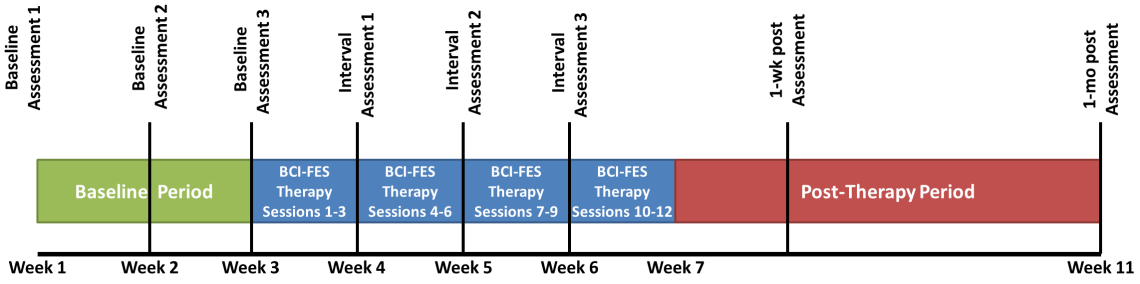

Figure 3.9: Experimental time line of the ongoing Phase I clinical trial.

BCI-FES Integration

To develop a BCI-FES system for the treatment of foot drop in stroke survivors [30], a low-cost, FDA-approved, constant-current neuromuscular stimulator (LG-7000, LG Medical Supplies, Austin, TX) was used for the FES of the neuromuscular system consisting of the deep peroneal nerve and the tibialis anterior muscle (see Fig. 3.8). To facilitate BCI-FES integration, the stimulator's manually controlled "on/off" switch

and analog potentiometer that adjusted the amplitude of the stimulating current was modified to allow for computer control of the stimulator (see Fig. 3.10). To this end, the FES device's analog potentiometer was replaced with a digital potentiometer by utilizing a General Pin Input Output (GPIO) interface. Likewise, the switch function was emulated using a digital relay that kept the stimulating circuit closed/open when electrical stimulation was/was not intended. Both the digital potentiometer and the relay were controlled by a microcontroller unit (Freescale, M52259, Freescale Semiconductors, Austin, TX) in a master-slave configuration. More specifically, a custom-made C-language program was used to instruct the microcontroller unit to listen for command requests from the BCI computer via a DB9 serial port, utilizing a universal asynchronous receiver/transmitter protocol. These requests carried the information of whether to turn the stimulator "on" or "off" (as determined by the prediction model), and the intensity of the electrical stimulation (as determined by the experimenter). Based on the current relay and potentiometer states, the microcontroller generated the appropriate signals needed to achieve the desired results. For example, when real time EEG data were classified as "Dorsiflex", the BCI software sent a series of instructions to the microcontroller that commanded the relay to close the stimulation circuit and the digital potentiometer to decrease its resistance, thereby initiating electrical stimulation. This continued until the real time EEG data were decoded as "Idle", upon which the BCI software sent a series of instructions to the microcontroller to open the relay, thereby opening the stimulation circuit and stopping the electrical stimulation. During operation, the BCI-FES system toggled between these two states.

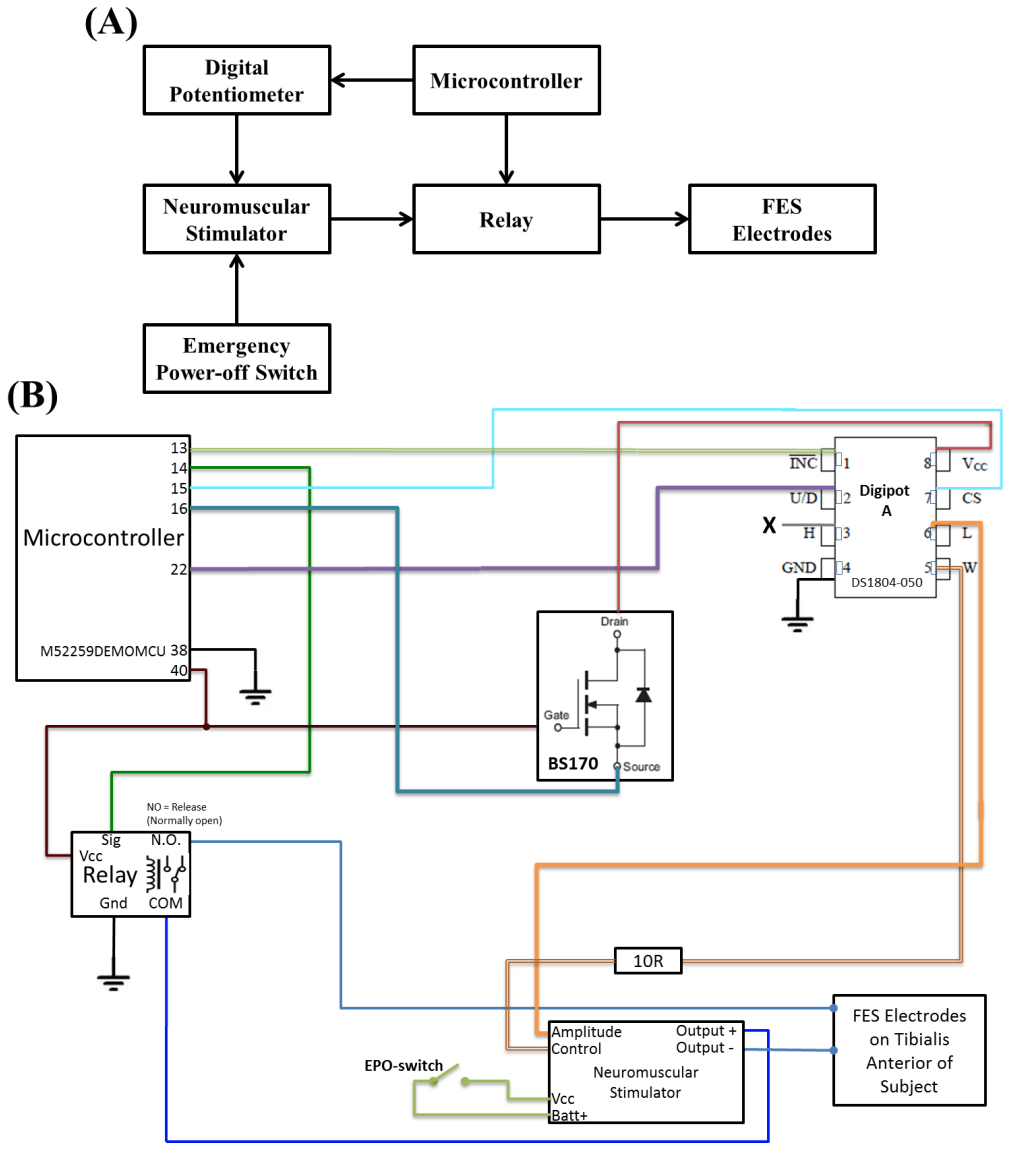

Figure 3.10: (A) The block diagram shows a microcontroller unit interfaced with a digital potentiometer (digipot) and a relay. The digipot modulates the amplitude of the stimulating current, while the relay keeps the circuit between the surface FES electrodes and the stimulator normally open. The relay circuit closes when it receives a logical high from the microcontroller unit (coinciding with the detection of dorsifiexion state by the BCI computer). For safety reasons, a manually operated emergency power-off switch is added to the stimulator power supply circuit. (B) The circuit diagram of the BCI-FES control module showing detailed wiring scheme. The digipots resistance changes from 0 KΩ to 50 KΩ, thereby changing the amplitude of the stimulating current from 0 mA to 100 mA. Not shown in (A) is a field-effect transistor (BS170), used to ensure proper power-on sequence for the digipot [30].

Participant Recruitment and Data Acquisition

Both the able-bodied [30, 31] and stroke population studies [36, 38] were approved by the Institutional Review Board of the University of California, Irvine. For the able-bodied population study [30, 31], recruited participants were able-bodied who are generally healthy with no history of neurological conditions. On the other hand, the stroke population study [36, 38] and Phase I clinical trial recruited chronic stroke survivors (>6 months post-ictus) with foot drop. Exclusion criteria for this study were the presence of electronic implants, peripheral neuropathy, severe contractures, or spasticity, as these conditions may preclude safe and effective FES delivery.

As described in Section 2.2 of Chapter 2, both studies utilized the 63-channel EEG cap to record EEG data, where all impedances were reduced to <10 KΩ. Unlike the able-bodied population studies [30, 31], the stroke population studies [36, 38] used the 32 electrodes presented in Fig. 2.1 of Section 2.2 of Chapter 2. These EEG signals were then streamed in real-time to a computer and re-referenced in a common average mode using one or two linked 32-channel NeXus bioamplifiers (Mind Media, Roermond-Herten, The Netherlands). In addition, for the able-bodied population studies [30, 31], 2 custom-made electrogoniometers [147] were mounted on the dorsum of each ankle to measure foot dorsiflexion; for the stroke population studies [36, 38] and Phase I clinical trial, only 1 electrogoniometer was mounted on the dorsum of the stroke affected ankle. The electrogoniometer signals were then acquired using either a data acquisition system (MP150, Biopac Systems, Goleta, CA) with a sampling rate of 4 kHz and a resolution of 16 bits [30], or using a custom-made Arduino Uno microcontroller (Arduino, SmartProjects, Turin, Italy) [36, 38] similar to the one described in the BCI driven hand orthosis study (Section 3.2). Finally, since much of the electrogoniometer signal was too similar when distinguishing between idling and movement states during the training data procedure in the stroke population

studies [36, 38] and Phase I clinical trial, an audio signal was generated using the above data acquisition system (MP150, Biopac Systems) and used to label the EEG data as "Idle" or "Dorsiflex" given the computer cues. All data was acquired using custom-written Matlab (MathWorks, Natick, MA) programs.

Training Procedure and Decoding Model Generation

For the able-bodied population studies [30, 31], participants alternated between 6-s epochs of repeated foot dorsiflexion and idling given computer cues while their EEG and electrogoniometer data were recorded for a total of 200 epochs (20 min). This training procedure was then repeated using the opposite foot, and the foot that yielded the prediction model with the highest classification accuracy (described in Section 2.4.2 of Chapter 2 and in Appendix B.1) was chosen as the controller foot for the remainder of the study [30]. On the other hand, the stroke population studies [36, 38] and Phase I clinical trial alternated between 6-s epochs of attempted, albeit ineffective, repeated dorsiflexion of the paretic foot and idling given computer cues while their EEG and audio data were recorded for a total of 100 epochs (10 min) to avoid muscle fatigue. Finally, as previously mentioned, the electrogoniometer data was not recorded during this period for the stroke participants, as the attempted foot movement was too weak to distinguish between "Idle" and "Dorsiflex" states.

As mentioned in Section 2.4 of Chapter 2, the training EEG data underwent an automated artifact rejection algorithm to remove channels with excessive EMG activity. For each EEG epoch of the remaining channels corresponding to "Idle" and "Dorsiflex" states (determined by either the electrogoniometer signals [30, 31] or audio signal [36, 38]), the first and last second of data in each epoch were removed to eliminate transient events and visual response from the computer cues. The remaining 4-s-long trials were then transformed into the frequency domain, and the

spatio-spectral features were extracted using the methods described in Section 2.4.1 of Chapter 2 and in Appendix A.3. Finally, a linear Bayesian classifier (described in Section 2.4.2 of Chapter 2 and in Appendix A.4) was used to classify EEG data into "Idle" and "Dorsiflex" states.

Online Signal Analysis and Calibration

During online operation for the able-bodied study [30, 31], stroke population studies [36, 38], and Phase I clinical trial, EEG data were acquired in 0.25 s-long, non-overlapping segments in real time, and the PSDs of the retained EEG channels were used as the input for the feature extraction algorithm described in Section 2.4.1 of Chapter 2 and Appendix A.3. The resulting 1-D spatio-spectral features were then used to calculate the posterior probabilities of "Idle" and "Dorsiflex" state (see Section 2.4.2 of Chapter 2 and Appendix A.4).

Participants from all of the BCI-FES studies [30, 31, 36, 38] underwent the same calibration procedure described in Section 2.5 of Chapter 2. This allowed the experimenter to determine the optimal parameters for online operation, specifically, the thresholds of the binary state machine (described in Section 2.4.2 of Chapter 2), T_I and T_D, where I is the "Idle" class and D is the "Dorsiflex" class. Then, prior to online evaluation, all participants were fitted with a pair of self-adhesive FES surface electrodes on the surface of the skin over the anterior lateral lower leg, covering the approximate course of the deep peroneal nerve (see Fig. 3.8 for placement). Test stimulation was used to confirm that the electrode placement and chosen stimulation parameters were adequate for effective foot dorsiflexion ($\sim$15° to 20°). The stimulation parameters, including the current amplitude, pulse width, and frequency, were empirically determined to achieve the required foot dorsiflexion without causing discomfort to the participant.

Online Sessions and Performance Assessment

To ascertain whether purposeful control of the BCI-FES system is possible in the able-bodied proof-of-concept study [30, 31], participants performed 10 alternating 10-s epochs of idling and repetitive dorsiflexion of the optimally chosen foot to induce BCI-FES mediated dorsiflexion of the contralateral foot. Instructions to perform this task were shown as computerized textual cues, and both the voluntary and BCI-FES mediated foot dorsiflexions were measured by the electrogoniometers for subsequent performance assessment [30]. Finally, note that these able-bodied participants only performed one BCI-FES online session, as this was a proof-of-concept study [30].

For the stroke population studies [36, 38] and Phase I clinical trial, the participants operated the BCI-FES system in real time over multiple online sessions. This allowed for a more complete assessment of the performance in this population, and determined whether stroke individuals could maintain control of the device throughout the experimental day. For each online session, the participants were tasked to perform 10 alternating 10-s-long epochs of idling and BCI-FES mediated dorsiflexion of the stroke affected foot given computer cues. Ideally, during "Idle" epochs, the participant would sit still and the BCI-FES system would provide no electrical stimulation. During "Dorsiflexion" epochs, the participant would attempt foot dorsiflexion of the stroke affected foot, and the system would ideally detect the associated EEG changes and respond by delivering stimulation to elicit foot dorsiflexion. The BCI state transitions throughout the online sessions and the electrogoniometer signals were used to evaluate the online performance [36]. Finally, based on their availability and muscle fatigue, participants performed 1–7 online BCI-FES sessions on each experimental day. The active range of motion of the stroke affected foot was measured before and after the short-term stroke population studies [36, 38] using goniometry. In addition to the dorsiflexion active range of motion, neurological and functional assessments

were performed before every 3rd daily session, 1 week after intervention, and 1 month after intervention.

For the short-term study in the stroke population studies [36], participants underwent 3 daily sessions. On the other hand, for the participant that performed the long-term study as apart of the Phase I clinical trial and the other participants of the Phase I clinical trial, participants performed 12 daily sessions, where as many BCI-FES online runs as possible were performed within a 1 hr period. To emulate a typical physiotherapy schedule for these individuals, these sessions were performed at a rate of 3 times per week over the course of 4 weeks. Dorsiflexion active range of motion, 6 min walk test, 5 m walk tests (gait velocity test, repeated 3 times), and neurological exams were performed at the beginning of the study, at the beginning of each week, and 1 week as well as 1 month after the last session (see Fig. 3.9).

The online performances of both studies were assessed by the following criteria: 1) cross-correlation between BCI-FES decoded states or the electrogoniometer signal changes due to the voluntary foot movement, and the instructional cues or BCI-FES mediated electrogoniometer signal changes; 2) the number of omissions, defined as the failure to activate BCI-FES mediated dorsiflexion during a "Dorsiflexion" cue; 3) the number of false alarms, defined as the activation of BCI-FES mediated dorsiflexion during an "Idle" cue. A detailed description of the cross-correlation analysis, and false alarm and omission analysis, are described in Section 2.7 of Chapter 2 and Appendices B.2 and B.5. Finally, statistical significance of these results was determined by running 10,000 Monte Carlo simulation trials with a chance level classification accuracy (50%). Details of the statistical significance analysis can be found in Section 2.7 of Chapter 2 and Appendix B.3.

In addition to the above performance measures, in the able-bodied population proof-of-concept study [30, 31], the PSDs of the salient electrodes for classification were

also analyzed. To this end, the power spectra of EEG signals under idling and foot dorsiflexion conditions were compared to the signal-to-noise ratio, defined as:

$$\mathrm{SNR}(f) = \frac{(\mu_i(f) - \mu_d(f))^2}{\sigma_i^2(f) + \sigma d^2(f)} \tag{3.1}$$

where f is the frequency, $\mu_i(f)$ and $\mu_d(f)$ are the average powers at the frequency f under idling and dorsiflexion conditions, respectively, and $\sigma_i^2(f)$ and $\sigma_d^2(f)$ are the corresponding variances [77]. Note that this definition is the same signal-to-noise ratio defined in Fig. 3.5 that was also used to understand the salient frequencies and electrodes for classification during BCI operation.

3.3.2 Results

For the able-bodied population study [30, 31], 5 participants were recruited and provided their informed consent to participate in the study. Their demographic data are shown in Table 3.5. The hours of relevant BCI experience and dominant foot are presented in the table.

Table 3.5: The demographics of the 5 able-bodied participants. The columns list: participant number, sex, age, dominant side (L-left, R-right), and number of hours of relevant BCI experience [30, 31].

Participant	Sex	Age (yr)	Dominant Side	BCI Experience (hr)
1	F	24	L	20
2	M	40	R	10
3	M	29	R	5
4	M	28	R	0
5	F	56	R	5

For the stroke population studies [36, 38], 3 male chronic stroke survivors (>6 months post-ictus) with foot drop were recruited for the study. Their demographic data

and stroke information are summarized in Table 3.6. As previously mentioned, the participants of the short-term study, Participants 1 and 2, were both long-term users of the commercial FES system for foot drop (L300, Bioness, Valencia, CA). Finally, note that only 1 participant who performed the long-term study (Phase I clinical trial) is presented in these results, as this participant was excluded from the current Phase I clinical trial due to a recurrent stroke (> 1 month) that was unrelated to the study.

Table 3.6: Summary of the demographics data for the short-term and long-term participants [36, 38] (© 2012 IEEE).

Participant	Age	Study Type	Time from Stroke (mo)	Stroke Location	Clinical Presentation	NIH Stroke Scale
1	60	short	25	left internal capsule	right hemiparesis	4
2	38	short	22	right frontal parietal and temporal lobes MCA territory	left hemiparesis	9
3	83	long	29	left frontal, parietal centrum semiovale	right hemiparesis	4

Offline Performances

For the able-bodied proof-of-concept study [30, 31], the optimal participant-specific EEG decoding models resulted in EEG frequency bands (Table 3.7) that included the μ (8–13 Hz), β (13–30 Hz), and low-γ bands (30–50 Hz). Specifically, for Participant 1, this included the μ (8-13 Hz), β (13-30 Hz), and low-γ (30-38 Hz) bands. For Participant 2, this included the high-β (22-30 Hz) and low-γ (30-50 Hz) bands; for Participant 3, the μ, β and low-γ (30-50 Hz) bands, the μ and β bands for Participant 4, and for Participant 5, the μ, β, and low-γ (30-50 Hz) bands were important frequencies for classification. Finally, the 10-fold cross validation procedure resulted in

classification accuracies that ranged from 85.1% to 97.6%. These results are statistically significant, as the probability of achieving the performance ≥85%, i.e. correctly classifying 170 or more trials (out of 200) by random chance, is only 3.0866×10^{-25}.

Table 3.7: Offline performances of the able-bodied population study [30]. Columns list the foot that was voluntarily dorsiflexed (left, L, or right, R), the EEG frequency band that was used for classification, and the offline classification accuracy.

Participant	Foot	EEG-band (Hz)	Classification Accuracy
1	R	[8-38]	94.4%
2	L	[22-50]	97.6%
3	L	[8-50]	85.1%
4	R	[8-30]	91.9%
5	R	[10-50]	93.6%

Analysis of the participant-specific EEG prediction models revealed that the EEG power changes in the β-band observed over the mid-central areas (i.e. electrode Cz) were the most informative features for classification (see Fig. 3.11), where prominent event-related desynchronization (loss of power) was observed over a broad frequency band (see Fig. 3.12). These observations are consistent with prior studies, where similar event-related desynchronization was observed upon the initiation or imagination of movement [76, 108, 110, 133].

The FES stimulation parameters were similar across participants in the able-bodied population study [30]. Shown in Table 3.8, the FES stimulation parameters ranged from an 88-100 mA current, where 100 mA was the maximum allowable current deliverable by the FES system. In addition, the pulse width ranged from 120–200 Hz, and the frequency ranged from 20–30 Hz. These parameters all allowed for the optimal 15°–20° of FES induced ankle dorsiflexion of the contralateral foot.

The EEG decoding models of the short-term study with stroke individuals [36] resulted in EEG features that deviated from the classical foot representation area seen in Fig. 3.11 for the able-bodied participants. Specifically, it can be seen in Fig. 3.13

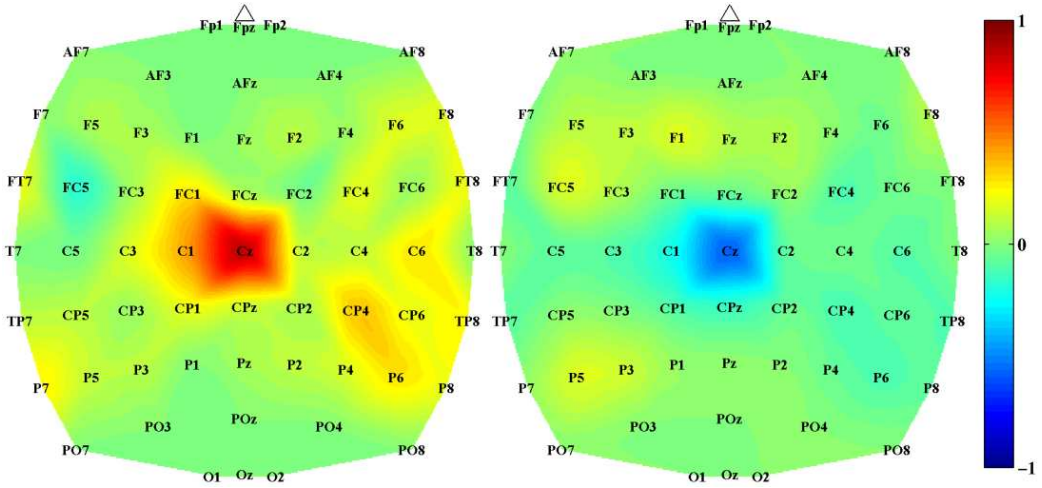

Figure 3.11: Feature extraction mapping, showing salient features for classification (blue, -1, and red, +1) in the high β-band (centered at 29 Hz) for Participant 2 in the able-bodied study [30]. Two maps are presented, one adapted to the idling class (left) and the other to the dorsiflexion class (right).

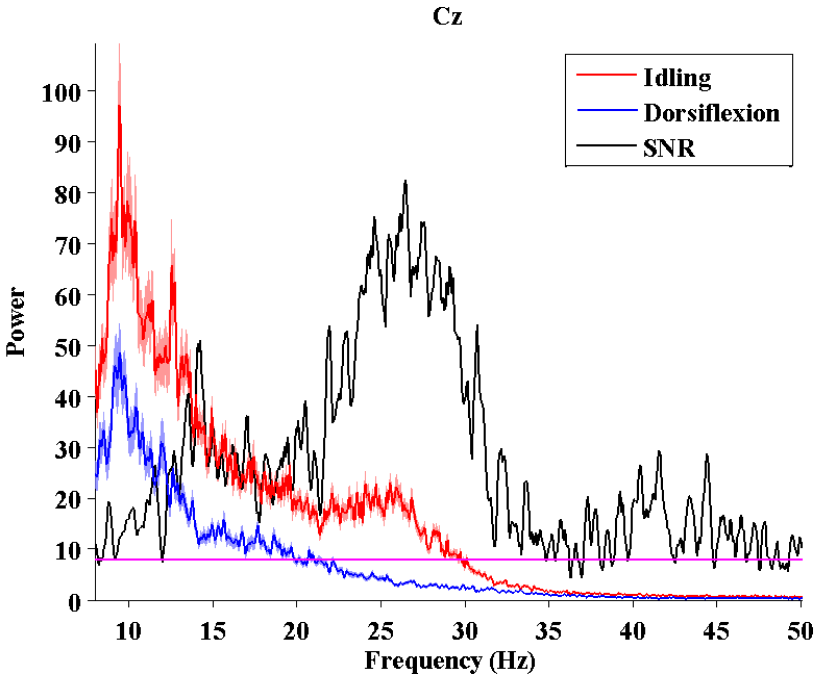

Figure 3.12: PSDs at electrode Cz for the able-bodied study in Participant 2 [30]. A broadband (8–50 Hz) desynchronization of EEG signals is shown. Red and blue traces denote the average ($n = 100$) power spectra of EEG signals under idling and foot dorsiflexion conditions, respectively. The shades represent ± 1 standard error of mean bounds. Black trace represents the signal-to-noise ratio, as defined in Eq. 3.1. The values of the signal-to-noise ratio above the magenta line define the frequencies with a statistically significant difference between the average idling and dorsiflexion powers ($p < 0.001$, paired t-test).

Table 3.8: FES stimulation parameters for the able-bodied population study [30], including the stimulating current amplitude, its pulse width and frequency.

Participant	Current (mA)	Pulse Width (μs)	Frequency (Hz)
1	100	140	20
2	100	200	30
3	90	200	30
4	88	200	20
5	100	120	20

that EEG activity at the midcentral and central-parietal areas in the 20–22 Hz frequency band were salient features for classifying "Idle" and "Dorsiflexion" states. Furthermore, this EEG decoding model revealed salient features in the θ-band (4–6 Hz), also around the midcentral and central-parietal areas of the brain.

The participant with stroke who performed the long-term study as apart of the Phase I clinical trial resulted in EEG decoding models that did not significantly differ from across weeks (Fig. 3.14). At the beginning of the study, the salient features of these decoding models were over the mid-central regions in the 12–14 Hz band, somewhat resembling the EEG decoding models of the short-term study participants [36]. Then, the participant's salient features progressively expanded and became more diffuse over time. Finally, the participant reported a recurrent stroke approximately 1 month after the completion of the study, excluding the participant from the ongoing Phase I clinical trial. However, this adverse event was deemed unrelated to the study, and the other participants' results from the Phase I clinical trial are not shown here as the study is still ongoing.

Online Calibration

Prior to online BCI operation, a brief calibration procedure was performed for the able-bodied [30, 31], stroke [36, 38] studies, and Phase I clinical trial to determine the posterior probability thresholds for optimal online BCI-FES operation. Using the

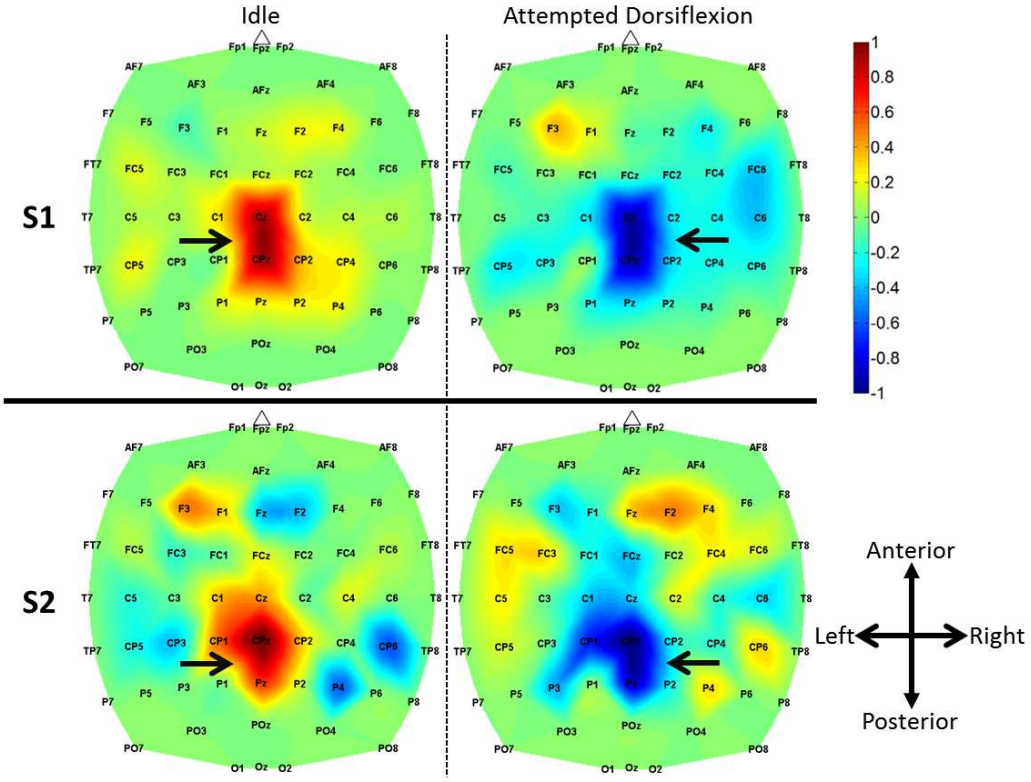

Figure 3.13: Feature extraction mapping of the short-term stroke study [36] (© 2012 IEEE), showing salient features for classification (blue, -1, and red, +1) in the low β-band (centered at 21 Hz) for Participant 1, and in the θ-band (centered at 5 Hz). Both maps show areas over the Cz and CPz electrodes as important features for distinguishing between idling and attempted foot dorsiflexion.

EEG decoding model developed from the training procedure, the participants alternated between idling and dorsiflexion for 3–5 min while their posterior probabilities were recorded. Their histograms were then plotted (Figs. 3.15 and 3.16) to determine the state transition thresholds.

The histograms from the able-bodied population study [30] demonstrated that the posterior probabilities were very separable, although a few false positives could occur (Fig. 3.15). On the other hand, the histograms for the short-term stroke population studies [36] demonstrated that the posterior probabilities during idling epochs were very stable, while the posterior probabilities during dorsiflexion epochs were more

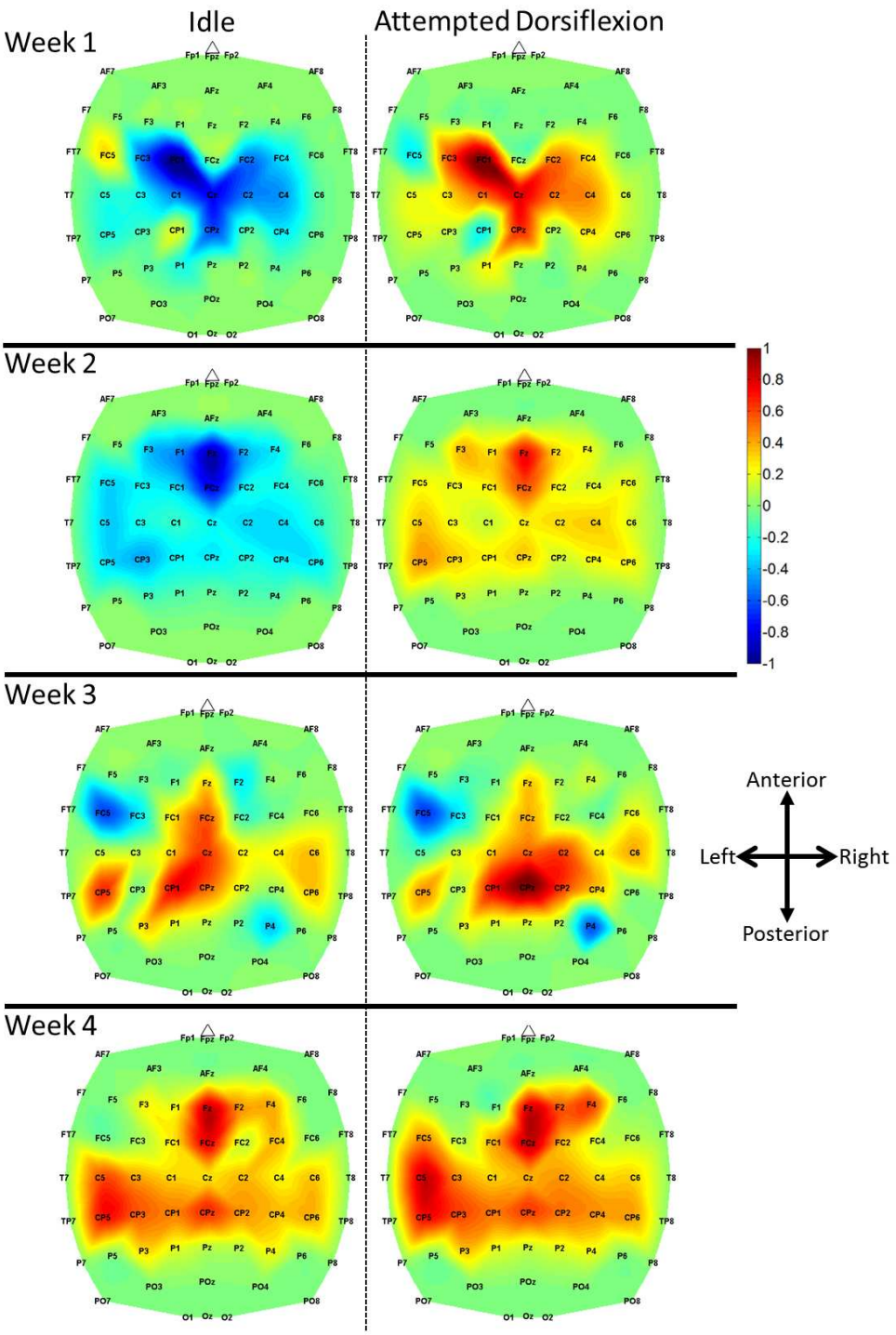

Figure 3.14: Feature extraction for the participant who performed long-term stroke study and Phase I clinical trial, showing salient features in the μ-band (8–12 Hz) and low β-band (12–16 Hz) for Participant 3. The features at Week 1 involved the Cz, CPz, and FC1 electrodes in the 12–14 Hz bin, then features shifted anteriorly at Week 2, and then expanded posteriorly and changed frequencies to the 14–16 Hz bin by Week 3. At Week 4, there was a bilateral and lateral expansion of features, and a return to the 12–14 Hz bin.

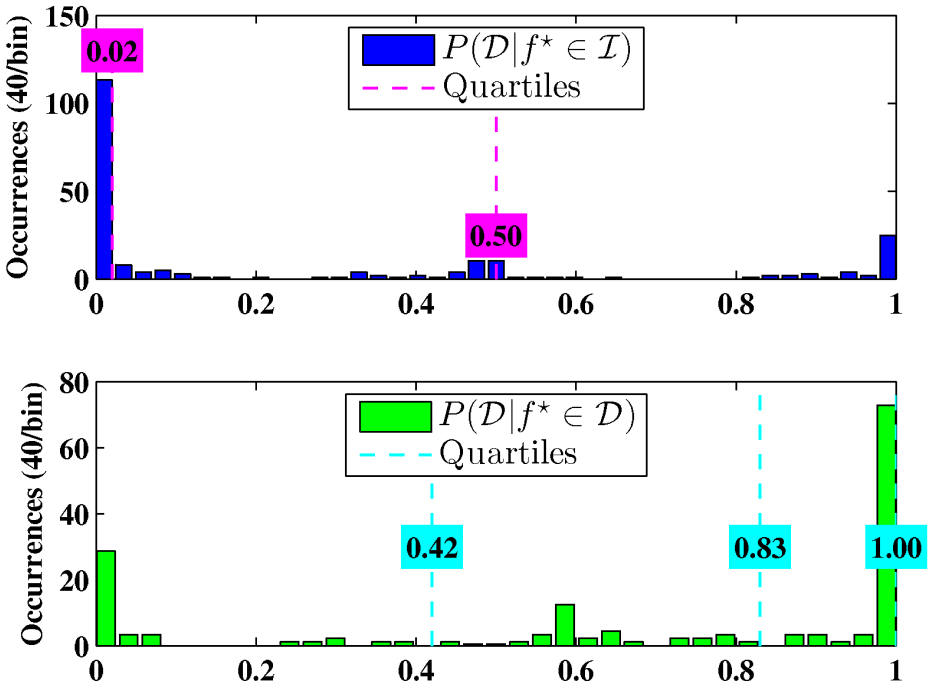

Figure 3.15: Histogram from the able-bodied study, showing the posterior probabilities for Participant 2 [30]. Classes are denoted as dorsiflexion (D) and idling (I). Dashed lines represent the 25%, 50%, and 75% quartiles.

volatile. This resulted in more omissions during BCI-FES online operation, although these errors were mitigated by choosing lower state transition thresholds for these individuals.

Online Performances

For the able-bodied population study [30, 31], participants performed repetitive dorsiflexion of their optimally chosen foot to induce BCI-FES mediated dorsiflexion of the contralateral foot given computer cues. More specifically, each 0.25 s segment of EEG data was acquired and analyzed as explained in the methods section above, and based on the analysis, the computer instructed the FES system to respond. The basic steps of this procedure applied to the training data are illustrated in Fig. 3.17. Note that the pink and green bands in this figure represent the mean ± 2 standard deviations

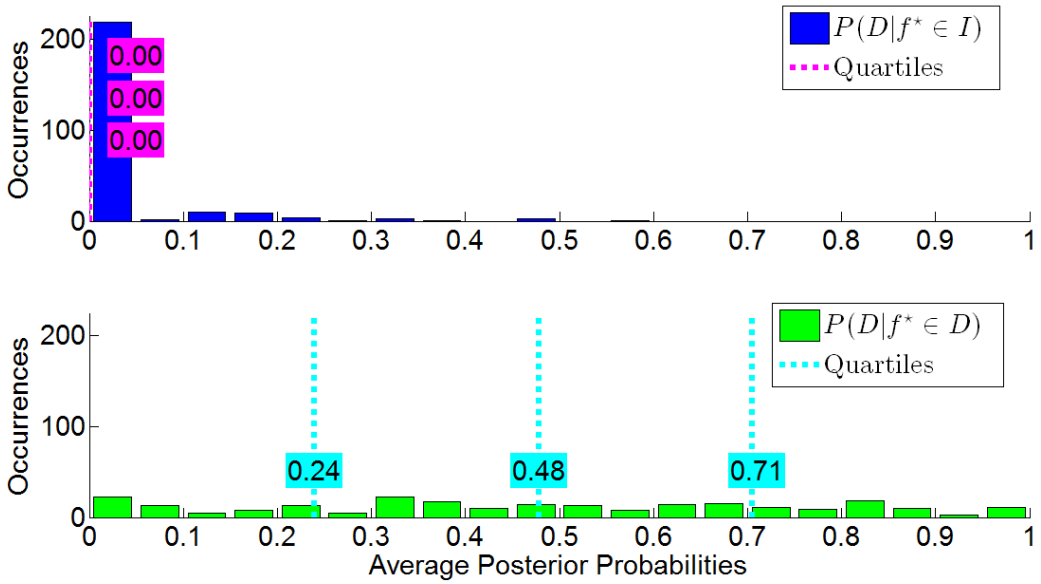

Figure 3.16: Histogram from the short-term stroke study [36] (© 2012 IEEE), showing the posterior probabilities for Participant 1.

of the features corresponding to idling and dorsiflexion training data, respectively. Finally, the dashed lines correspond to the thresholds, T_D (green) and T_I (red), as determined by the calibration procedure, and the pink and red blocks in Fig. 3.17 show the BCI-FES system state, idle (pink) or BCI-FES induced dorsiflexion (green).

To determine the performance of each online session, cross-correlation analysis was performed, and the number of false alarms and omissions were calculated. This resulted in participants being able to perform the task with no omissions and a 100% BCI-FES response (Table 3.9). However, BCI-FES mediated dorsiflexion epochs typically lagged behind the actual dorsiflexion epochs, and the average values of this latency ranged from 1.4 to 3.1 s across all participants. Temporal correlations between the voluntary and BCI-FES mediated dorsiflexion epochs ranged between 0.59 and 0.77, and are also shown in Table 3.9. The statistical significance of these results was confirmed by the 10,000 Monte Carlo simulation trials with a chance level classification accuracy of 50%. The maximum correlation coefficient obtained from the

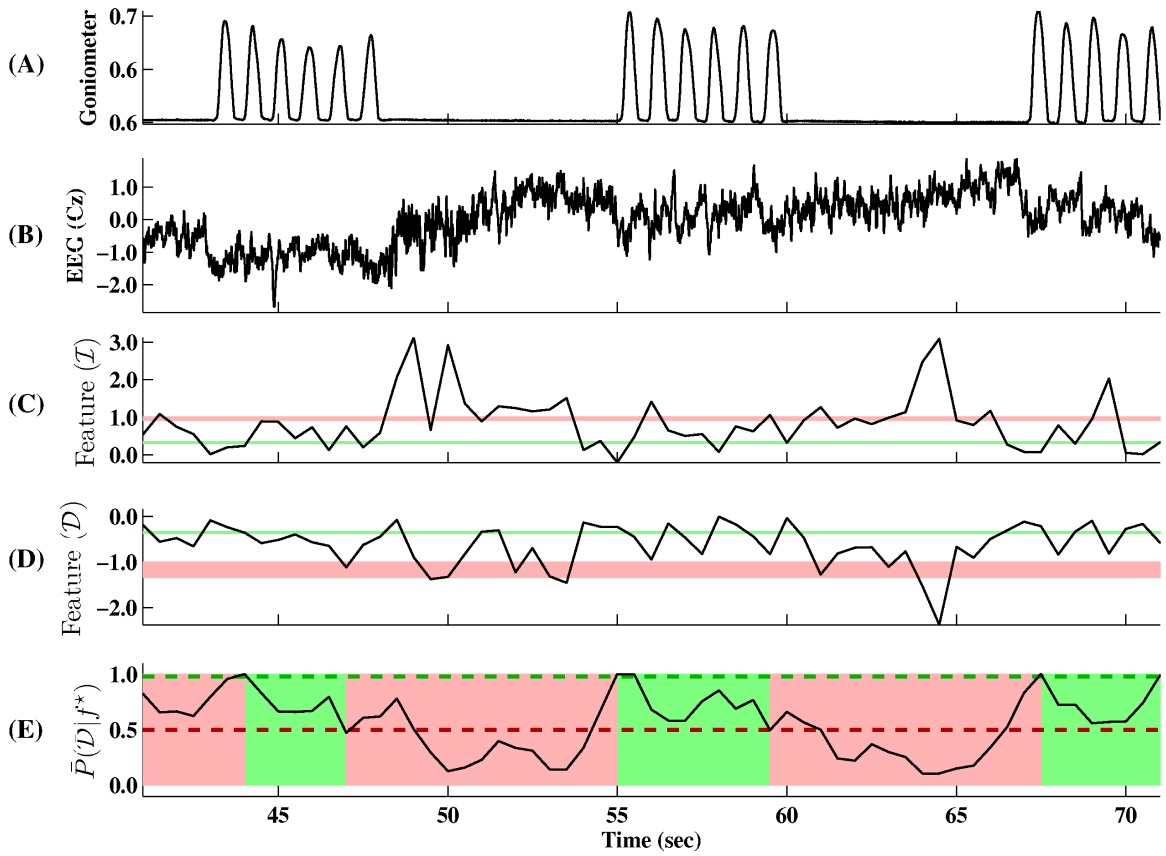

Figure 3.17: (A) A goniometer trace of idling and dorsiflexion states for the able-bodied study [30]. (B) The corresponding EEG signal at the Cz electrode. (C, D) One-dimensional spatio-spectral EEG features in the idling (I) and dorsiflexion (D) subspaces, respectively. (E) The average posterior probability of dorsiflexion given the feature.

simulations was 0.41, and therefore even the lowest correlation coefficient of 0.59 is significant with a p-value $< 10^{-4}$.

The cross-correlation analysis demonstrated that Participants 2 and 5 achieved the highest correlation coefficients, and they also achieved the highest offline classification accuracies. A representative figure of this high performance for Participant 2 can be seen in Fig. 3.18. Conversely, Participant 3 had the lowest classification accuracy and correlation coefficient. This drop in online performance may be attributed to the single false alarm (Table 3.9). Also, the relationship between the offline and online performances indicate that no overfitting occurred during EEG decoding model

Table 3.9: Online performances of the able-bodied study [30]. Cross-correlation between the voluntary and BCI-FES mediated dorsiflexion epochs, corresponding lag at this temporal correlation, total number of omissions (OM), and total number of false alarms (FA) are presented.

Participant	Cross-correlation	Lag (s)	OM	FA
1	0.67	3.1	0	0
2	0.72	1.4	0	0
3	0.59	2.7	0	1
4	0.62	3.0	0	0
5	0.77	2.9	0	0

generation.

The stroke population studies [36, 38] and Phase I clinical trial performed online BCI-FES sessions similar to the able-bodied proof-of-concept study [30, 31]. However, the stroke participants utilized attempted, albeit ineffective, dorsiflexion of the stroke affected foot to cause BCI-FES mediated dorsiflexion of the same foot. The online sessions resulted in the participants who performed the short-term study to complete 9–12 BCI-FES online sessions, and the participant who performed the long-term study as apart of the Phase I clinical trial to complete 102 online sessions (Table 3.10). In addition, the average cross-correlation between the computer cues given to the participants and the BCI-FES response was 0.335 and 0.403 for Participants 1 and 2, respectively. Furthermore, for the participant who performed the long-term study that was excluded from the Phase I clinical trial, the cross-correlation between these two states improved (0.635, see Table 3.10). Finally, dorsiflexion active range of motion improved in all participants, from 5° to 8° in Participant 1, from 0° (no observable dorsiflexion or muscle twitch) to 1° (trace movement) in Participant 2, and from 3° to 12° in the long-term Phase I clinical trial study participant. Note that no adverse events occurred during both the short-term and long-term studies, but a recurrent stroke in the long-term study participant occurred $>$ 1 month after post-therapy follow-up exam and was deemed unrelated to the study.

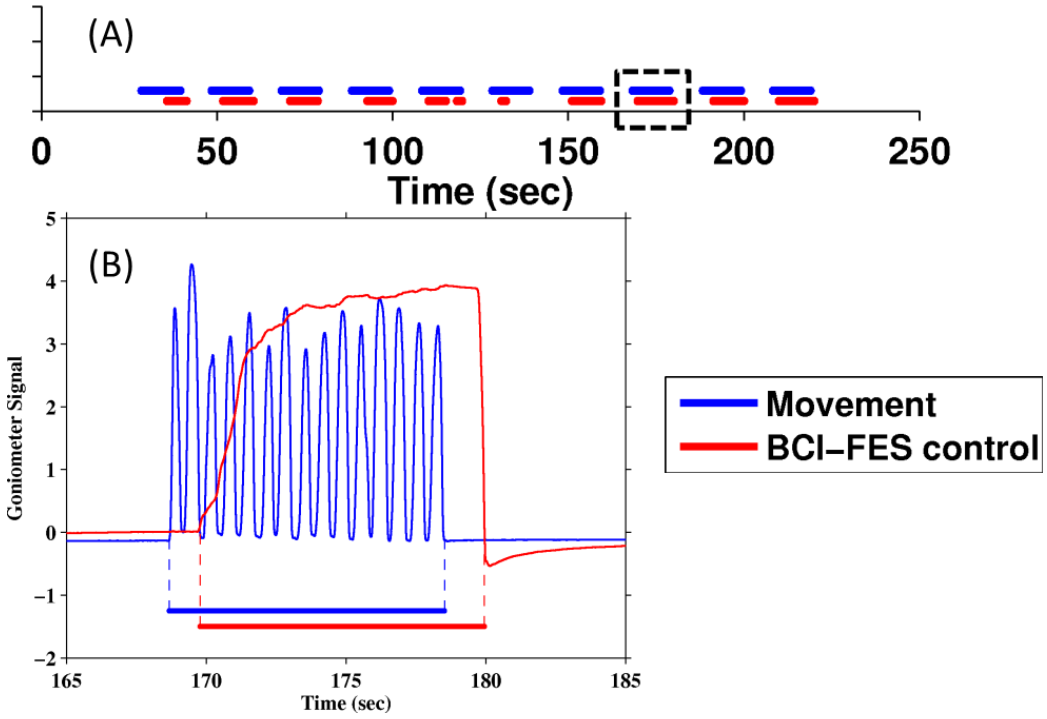

Figure 3.18: Online performance of Participant 2 in the able-bodied study [30]. (A) Blue trace marks the 10 epochs of 10-s-long repetitive foot dorsiflexion, and red trace marks the epochs of BCI-FES mediated dorsiflexion of the contralateral foot. (B) The inset of a single dorsiflexion epoch, showing the goniometer trace corresponding to 15 dorsiflexion cycles (blue) and BCI-FES mediated dorsiflexion (red) of the contralateral foot.

A representative performance of the short-term online sessions [36] can be seen in Fig. 3.19. Depicted in this figure are the computer cues given to the participant (blue blocks), the BCI-FES system response (red blocks), and the corresponding electrogoniometer response on the stroke affected foot. Note that even small dorsiflexion movements were detected by the electrogoniometer immediately prior to larger displacements due BCI-FES mediated dorsiflexion.

The stroke participant who conducted the long-term study and was excluded from the Phase I clinical trial performed 102 total BCI-FES runs over the course of 12 experimental days. A breakdown of these performances and sessions is given in Table 3.11. This participant improved his dorsiflexion active range of motion from 3°

Table 3.10: Summary of online performances for the stroke population studies [36, 38]. Presented are the total number of BCI-FES runs performed, cross-correlation between the computer cues and BCI-FES response (p-value < 0.01), and dorsiflexion active range of motion (AROM) before and after the study. Note that Participant 3 performed the long-term study as apart of the Phase I clinical trial, but was excluded from the clinical trial.

Participant	Total No. of BCI-FES runs completed	Cross-correlation between cues and BCI-FES response	Dorsiflexion AROM (before/after) (°)
1	12	0.335	5/8
2	9	0.403	0/1
3	102	0.635	3/12

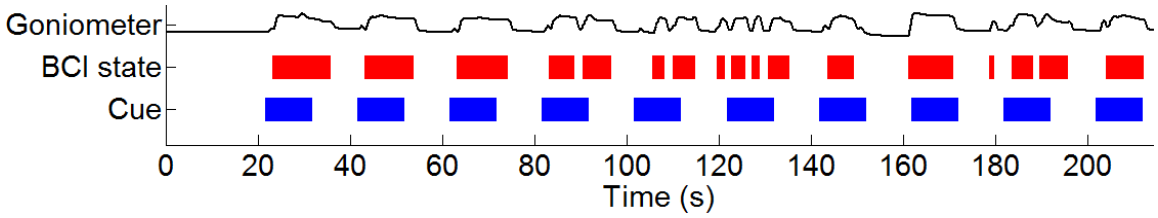

Figure 3.19: Online performance of the stroke individual presented in [36] (© 2012 IEEE) operating the BCI-FES system. Blue blocks correspond to instructional cues to attempt dorsiflexion, and red blocks correspond to BCI-FES mediated dorsiflexion states. Black trace represents the corresponding electrogoniometer trace on the BCI-FES controlled foot.

to 7° after only one week of intervention. His active range of motion continued to improved throughout the study, ultimately reaching 12° one week after the last experimental day. In addition, as described in the methods above, all online sessions were purposeful, and the cross-correlation analysis showed that the participant's ability to control the BCI-FES system improved over time.

3.3.3 Discussion

The results of the able-bodied proof-of-concept study [30, 31] demonstrated the first successful integration of a noninvasive EEG based BCI with a noninvasive FES system

Table 3.11: Number of BCI-FES runs completed, cross-correlation between the computer cues and BCI-FES response, p-value, and dorsiflexion active range of motion (AROM) for each week for the long-term study (Participant 3).

Phase of Study	Total No. of BCI-FES runs completed	Cross-correlation between cues and BCI-FES response	p-value	Dorsiflexion AROM (°)
Baseline	N/A	N/A	N/A	3
Week 1	24	0.635	$p < 0.001$	3
Week 2	25	0.643	$p < 10^{-5}$	7
Week 3	23	0.600	$p < 0.01$	10
Week 4	30	0.658	$p < 0.001$	11
1-week follow up	N/A	N/A	N/A	12

for the lower extremities. The performance of this system was tested in a population of able-bodied individuals and utilized a contralaterally controlled FES paradigm. This paradigm was chosen since ipsilateral dorsiflexion and stimulation in able-bodied participants would produce confounding results, as it would be difficult to resolve voluntary and BCI-FES mediated movements.

The results of the stroke studies [36, 38] provide preliminary evidence that BCI-FES systems may be a useful physiotherapy for stroke survivors. Specifically, all participants learned to successfully operate the BCI-FES system despite their brain injury. In addition, no adverse effects or events were associated with using the BCI-FES system, indicating the safety of the device. However, further analysis from the current participants of the Phase I clinical trial will need to be performed to better assess the level of safety of this system.

The increase in dorsiflexion active range of motion in all participants suggests that operating the BCI-FES system could promote neurological improvements after stroke. Although limited in sample size and lacking analysis of the functional tests that are currently being performed in the Phase I clinical trial, these findings are encouraging. These results are particularly impressive because all the participants were $\sim$2 years post-ictus and therefore at a rehabilitative plateau. Furthermore, since the partici-

pants of the short-term study [36] were long-term users of a commercial FES system for foot drop, these observed improvements were unlikely caused by FES alone.

As seen in the participant who performed the long-term study that was excluded from the Phase I clinical trial, operating the BCI-FES system over a longer time period led to additional improvements. This improvement reached a plateau toward the end of this participant's involvement. This observation indicates that the BCI-FES dorsiflexion system may be applied as a novel physiotherapy, and that approximately 12 experimental sessions may be necessary to achieve optimal neurological outcomes. These results warrant the ongoing formal clinical trials to assess the safety and efficacy of BCI-FES therapies. These trials currently examine whether the improvements in dorsiflexion active range of motion are permanent and whether they translate into gait functional gains by assessing the gait velocity, dorsiflexion active range of motion, and 6-min walk test performed before, during, and after the clinical trials. Finally, future studies will compare the improvements from the BCI-FES therapy to those of conventional physiotherapy.

Offline Performances

The offline EEG decoding models of the able-bodied study [30, 31] corresponding to epochs of repetitive foot dorsiflexion and idling collected during the training procedures revealed that the EEG power in the μ, β, and low-γ bands were responsible for encoding the differences between idling and dorsiflexion states. The change in the signal power was mostly observed over the mid-central area, which likely corresponds to activity within the primary motor cortex's foot representation area (located in the interhemispheric fissure of the brain) and/or supplementary motor area. This was further confirmed by examining the feature extraction maps of the prediction models, which indicated that mid-central brain areas played a prominent role in classifying

idling and dorsiflexion states. While these results are not surprising from an anatomical standpoint, it should be noted that our prediction model is entirely data driven, and so these observations underscore the physiological and anatomical plausibility of our feature extraction maps. It should also be noted that these spatio-spectral EEG signal features are consistent with prior studies [108, 133]. Consequently, idling and dorsiflexion epochs could be predicted from the underlying multi-channel EEG data with an accuracy as high as 97.6%, and all participants achieved performances that were significantly above random chance.

The EEG decoding models generated during the stroke studies [36, 38] that are presented here demonstrate the system's ability to automatically hone in on the frequencies and brain areas underlying dorsiflexion in the post-stroke cortex. Unlike the able-bodied study [30, 31] whose activation areas were consistent with classic motor homunculus, all stroke participants had posterior expansion of their foot representation area. Prior functional studies have reported similar reorganization patterns after stroke [53].

The long-term study in the stroke participant that was excluded from the Phase I clinical trial may have also revealed evidence of motor learning and plasticity, as there was an expansion of salient brain areas in the EEG decoding models though successive weeks of BCI-FES operation. Similar observations have been described in functional magnetic resonance literature, where the learning of a new motor task led to the expansion of relevant brain areas, followed by a decrease in the activation area with continued practice [40]. However, the current study may have not lasted long enough for this contraction to be apparent in the EEG decoding models. Analysis of the features from the EEG decoding models in the ongoing Phase I clinical trial must be performed to confirm this hypothesis.

The automated identification of salient brain areas and frequencies from the feature

extraction techniques presented in these studies and this dissertation reduces the amount of intervention from the experimenter. It also reduces the time necessary for participants to acquire purposeful BCI control by enabling the use of an intuitive "attempted movement" control strategy. The current data-driven feature extraction algorithm may allow BCI-FES operation to accommodate for and complement the brain plasticity process underlying motor learning and recovery. Ultimately, these capabilities of our data-driven feature extraction algorithm may have important implications for stimulating neurological recovery after stroke and future practical clinical applications. It may also be possible to utilize te current feature extraction technique as a new brain mapping tool during this BCI-FES therapy.

Online Performances

The results achieved online during the able-bodied proof-of-concept study [30, 31] demonstrate that BCI-FES mediated foot dorsiflexion can be reliably controlled in a small population of able-bodied individuals. In general, this study suggests that the integration of a noninvasive BCI with a lower-extremity FES system is feasible. In addition to achieving excellent performances, all participants were able to assume immediate control of the interface, requiring only a short training session to develop a EEG decoding model, and a single 3–5 min calibration session. It should be noted that the high performances achieved offline generally transferred into robust online BCI-FES operation, indicating that our cross-validation procedure selected the correct features without overfitting. Finally, the FES-elicited movements during online operation did not interfere with the control of the BCI system. For example, upon cessation of voluntary foot dorsiflexion, it is conceivable that EEG signals due to FES-elicited movements may be confused with those of voluntary movements, which may in turn confuse the classifier and cause the system to remain in the dorsiflexion

state. This type of positive feedback, however, was not observed, perhaps because the EEG signals underlying these types of movements were sufficiently different and did not get misclassified. These differences may reflect spatial separation of cortical representation of FES-induced passive movements (likely localized to sensory cortex areas) and of voluntary movements (originating from more anterior brain motor areas).

For the stroke population studies [36, 38], the online results indicated that stroke individuals were able to achieve immediate and purposeful control of the BCI-FES system regardless of post-stroke cortical reorganization. Furthermore, by coupling the activation of the brain areas reassigned to subserve dorsiflexion with the electrical stimulation of corresponding spinal motor pools via antidromic conduction, this system may provide synaptic strengthening through a Hebbian-like process. This may have contributed to the observed improvement in dorsiflexion active range of motion in the short-term study individuals [36] and the individual excluded from the Phase I clinical trial presented above. More specifically, this BCI-FES system may have allowed for a simultaneous activation of upper motor neurons by means of attempted dorsiflexion with lower motor neurons via antidromic conduction to the anterior horn cells from BCI-mediated FES. Over time, this simultaneous firing may increase the synaptic strength between upper and lower motor neurons. This approach may hold advantages over prior BCI-FES methodologies [24].

3.3.4 Conclusion

The able-bodied proof-of-concept study [30, 31] on the BCI-FES system demonstrates that the integration of a noninvasive EEG based BCI system with a noninvasive FES system for the dorsiflexion of the foot is feasible. The integrated BCI-FES system

shows that EEG signals can be used to enable direct brain control of foot dorsiflexion via FES. This further suggests that it may be feasible to utilize BCI-FES systems to restore lost motor function of the lower extremities in individuals with neurological injury.

The stroke population studies [36, 38] provide preliminary evidence that the operation of a BCI-FES system by chronic stroke individuals may potentially lead to neurological improvements. This approach is based on the Hebbian learning and neural plasticiy principles, which may strengthen the connections between upper and lower motor neurons. Further studies must be performed in addition to the ongoing Phase I clinical trial to formally assess the safety and efficacy of this system as a novel post-stroke neurorehabilitative for the treatment of foot drop. The future work of these clinical trials for this BCI-FES system will be further elaborated upon in Section 5.2.2 of Chapter 5.

Chapter 4

Neurorehabilitation of Ambulation in Spinal Cord Injury

4.1 Overview

Projects 5, 6, 7 of our BCI systems for spinal cord injury (SCI) (Fig. 1.4) focus on neurorehabilitative therapies and neuroprostheses for this patient population. Since these individuals typically have no residual movement in the lost motor functions, these systems rely on kinesthetic motor imagery and attempted movement (without any actual movement occurring) strategies to control the BCI system. Specifically, these systems utilize kinesthetic motor imagery and attempted movement of ambulation (i.e. walking) to control external devices that produce ambulatory movement. For example, the BCI driven walking simulator studies [32, 84, 81, 107, 145, 146] utilized motor imagery of ambulation and attempted walking to control the ambulation of an avatar within a virtual reality environment to determine whether SCI individuals can control ambulation devices using this type of control strategy. Given

the success of these studies, our laboratory has since focused on applying this control strategy to BCI driven ambulation devices for neurorehabilitation therapies and neuroprostheses, such as a robotic gait orthosis (RoGO) [73] or a functional electrical stimulation (FES) device [51, 52] for overground walking (e.g. the Parastep I system, Sigmedics, Fairborn, OH).

The following sections will discuss our BCI systems for ambulation using the kinesthetic motor imagery and attempted walking control strategies. The BCI driven walking simulator studies (Section 4.3) will first be discussed to show how an attempted walking or kinesthetic motor imagery of walking control strategy was determined to be a feasible input for future neurorehabilitative therapies and neuroprostheses for ambulation after SCI. In addition, this system was then used as a training platform for the following BCI driven ambulation devices: the BCI-RoGO [33, 34, 35] (Section 4.4) and the BCI-FES system [80] for overground walking (Section 4.5). Finally, these ambulation systems were both tested in proof-of-concept studies on able-bodied and SCI individuals to determine whether this BCI design could become the first restorative treatment for walking after SCI.

4.2 BCI Systems for Ambulation

SCI can leave the affected individual with severe paraparesis or paraplegia, thus rendering them unable to ambulate. Since there are currently no restorative treatments for this population [39], technological approaches have been sought to substitute for the lost motor functions. Examples of these technologies include RoGOs [73], FES systems [51, 52], and spinal cord simulators (e.g. programmable central pattern generators) [60]. However, these systems lack intuitive able-body-like supraspinal control as they rely on manual controls, and they do not consider neuroplasticity and neu-

rorehabilitative principles of residual or spared spinal connections between the brain, spinal motor pools, spinal cord, and neuromuscular system. As a result, these systems monopolize the upper extremities, which interferes with the user's hand function, and the degree of restoration is minimal. Due to these and other limitations, wheelchairs still remain the primary means of mobility after SCI. Unfortunately, the extended reliance on wheelchairs typically leads to a wide variety of comorbidities (e.g. heart disease, osteoporosis, pressure ulcers) that constitute for the bulk of chronic SCI-related medical care costs [116, 124, 128, 165]. Consequently, to address the above issues associated with the treatment of severe paraparesis and paraplegia after SCI, novel BCI neuroprostheses and neurorehabilitative devices are being pursued by our laboratory. For example, BCIs can be incorporated with programmable central pattern generators, RoGOs, and FES technologies to restore ambulation and lost motor functions in these individuals [168] (see Fig. 4.1). Programmable central pattern generators, however, are not advanced enough yet to integrate with BCIs [67], as they require manual insertion of electrodes, and targeting and aligning the implanted electrodes requires significant improvement before adopting this technology in SCI individuals. Thus, RoGOs and FES systems have become important technologies for restorative treatments after SCI [18], as these systems are noninvasive and can provide immediate ambulation to SCI individuals.

As mentioned in Section 1.2.5 of Chapter 1, BCI driven neuroprostheses differ from neurorehabilitative therapies by directing this technology towards those with complete SCI, as there exists no residual spinal cord connections that can be monopolized. However, these devices still may have several benefits to those with complete SCI. For instance, FES based neuroprostheses can overcome the deficit produced by the lesion in the spinal cord and maintain the integrity of various bodily functions through direct neuromuscular stimulation [58]. Furthermore, BCI driven neuroprostheses can have restorative effects on the strengthening and proprioception of the neuromuscular

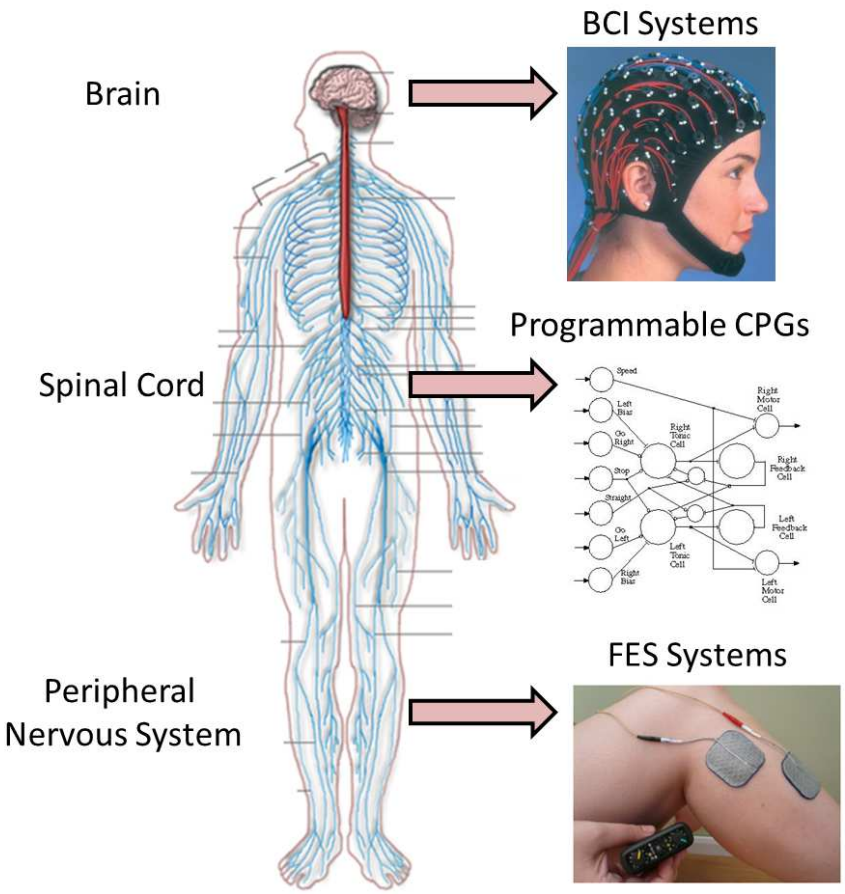

Figure 4.1: Overview of the current technological approaches for restoring ambulation. FES systems and programmable central pattern generators, or reciprocal inhibitory connections that can generate periodic patterns whose frequencies are controlled by the brain [18], can be integrated with current BCI systems for restorative ambulation treatments after SCI.

system [63], as well as hands-free control of the ambulation device.

Recent surveys by [4] and [20] suggest that SCI individuals with paraplegia highly prioritize walking as a function that would improve their quality of life if restored. In addition, survey participants in [20] mentioned that they would be willing to have a surgery to use an implantable BCI driven neuroprosthesis to restore this lost function. To test the feasibility of such a device, an alternative solution is to develop a noninvasive electroencephalogram (EEG) based BCI system for overground walking, as this would be a prerequisite for an implantable BCI system. As a result, our

laboratory has investigated whether an EEG based BCI system could be used to control ambulation, and whether such a system can be integrated with ambulation devices, such as a RoGO [73] or an FES device [51, 52] for overground walking.

4.3 BCI Driven Walking Simulator

The integration of BCIs with lower extremity prostheses and ambulation devices to restore or improve gait function in SCI individuals is envisioned to have intuitive and robust control, as well as minimal user training. For example, an intuitive strategy to control a BCI ambulation device may include attempted walking or kinesthetic motor imagery of walking. The feasibility of such a system, however, is contingent upon the ability to robustly decode neurophysiological patterns underlying these control strategies in the face of potential cortical reorganization following SCI. More specifically, functional magnetic resonance imaging studies suggest that brain areas normally associated with motor imagery of the lower extremity movements or gait may diminish, disappear, or shift following paraplegia due to SCI [1, 22, 68, 123]. This requires a BCI system to accommodate for each user's potentially unique neurophysiology. In addition, a BCI system must be designed to facilitate rapid user training, thereby promoting widespread adoption of this technology. Therefore, we hypothesize that a data-driven method for extracting participant-specific electrophysiological correlates underlying intuitive BCI control strategies will satisfy the above criteria and facilitate a BCI system that is intuitive, robust, and permits rapid user training.

The studies described below [32, 84, 81, 107, 145, 146] present a novel EEG based BCI system for intuitive, self-paced control of the ambulation of a simulator (i.e. avatar) within a virtual reality environment. This BCI-controlled walking simulator employs a data-driven, participant-specific EEG decoding model, which enabled

able-bodied [145] and SCI [81] participants to use kinesthetic motor imagery or attempted walking to achieve intuitive control of the avatar's ambulation after a very brief training session. This simulator provides a similar, albeit virtual, experience of operating a potential BCI-controlled ambulation device without the associated physical risks [91]. In addition, the use of a virtual reality environment in the context of BCI design has been shown to reduce the decoding error [111] and may serve as a training platform for future BCI-controlled lower extremity prostheses [91]. The ability to rapidly achieve purposeful control of an avatar within the virtual reality environment represents a necessary step towards successful integration of an EEG based BCI system and a physical prosthesis for ambulation. Finally, this BCI driven walking simulator may act as the first step in training SCI users to operate such a prosthesis.

4.3.1 Methods

Similar to the BCI-FES system for the treatment of foot drop in stroke survivors described in Section 3.3 of Chapter 3, the BCI driven walking simulator was first tested in an able-bodied population as a proof-of-concept study [32, 84, 107, 145, 146] for 1 daily session, and then in a small SCI population [81] across 5 daily sessions. In addition, the BCI driven walking simulator was tested over a long period of time (i.e. months) in a single SCI individual, however, the results of this study will be described in Section 4.5, as the simulator was used to train the individual to operate the BCI using an attempted walking control strategy for the testing of our system with a FES device for overground walking.

Overview

To determine the feasibility of a BCI system for ambulation, a data-driven, participant-specific decoding methodology (Section 2.4 of Chapter 2) that enables intuitive BCI control was utilized and tested in an able-bodied population [32, 84, 107, 145, 146] followed by an SCI population [81]. To this end, 8 able-bodied participants and 6 SCI participants used kinesthetic motor imagery of walking (for the able-bodied population) or attempted walking (for the SCI population) to operate the ambulation of an avatar within a virtual reality environment. Note that since able-bodied participants are able to walk, they performed kinesthetic motor imagery of walking rather than an attempted walking control strategy, and refrained from making any leg movements. All participants first underwent alternating epochs of kinesthetic motor imagery or attempted walking and idling while their EEG data were collected. Subsequently, the data-driven decoding methodology described in Section 2.4 of Chapter 2 used this training data to extract salient EEG signal features and train the EEG classifier described in Section 2.4.2 of Chapter 2. The training procedure was then followed by several sessions of an online BCI goal-oriented virtual reality walking task, where participants utilized kinesthetic motor imagery or attempted walking and idling to asynchronously control the linear ambulation of an avatar within a virtual reality environment. Note that asynchronous, or self-paced control, means that the participants were able to decide when to turn the BCI system on or off, and did not need to rely on any cues to operate the system. The entire offline and online procedures were repeated for 1 daily session for the proof-of-concept able-bodied study [32, 84, 107, 145, 146], and for 5 daily sessions over the course of several weeks for the SCI population study [81]. Lastly, to assess the attainment of purposeful control, participants' performances were recorded over several online sessions and were compared to random walk Monte Carlo simulations.

BCI Walking Simulator Integration

In order to assess a self-paced BCI kinesthetic motor imagery or attempted walking control strategy for a BCI driven ambulation device, a virtual reality walking simulator was constructed [145]. To this end, the virtual reality environment was created using Garry's Mod™ simulated physics environment (Half-Life 2, Valve Corporation, Bellevue, WA) that consisted of a flat grassland with 10 non-player characters next to traffic cones standing in a straight line. The course length was ∼120 body lengths (∼210 m, assuming a body length of 1.75 m) along the users' avatar linear path (see Fig. 4.2). This design was used to facilitate an asynchronous goal-oriented online task in which the participants utilized kinesthetic motor imagery or attempted walking and idling to walk the avatar forward and stop by each non-player character/cone, a similar virtual reality task conducted in prior studies by other laboratories [91]. Further details of how the performance of this task was evaluated are described in the online signal analysis section below.

To interface the BCI system with the virtual reality environment, a virtual joystick program (Parallel Port Joystick [140] or the vJoy Virtual Joystick [144]) was used. To this end, a C++ dynamic-link library was developed to relay BCI commands from the custom-written Matlab (Mathworks, Natick, MA) programs to move/stop the avatar via the virtual joystick. Finally, a custom-made C# program performed optical character recognition on the position and speed readouts from the virtual reality environment's display (shown in Fig. 4.2) in order to automatically track the participant's online BCI performance while playing the goal-oriented walking task.

Figure 4.2: Screen capture of the virtual reality environment with the BCI-controlled avatar in 3rd person 'over-the-shoulder' view [81]. Shown next to the avatar is a non-player character and a traffic cone. The position and speed readouts used for online performance assessment are shown in the top right corner.

Participant Recruitment and Data Acquisition

Both the able-bodied proof-of-concept study [32, 84, 107, 145, 146] and the SCI population study [81] were approved by the University of California, Irvine Institutional Review Board. For the able-bodied study [32, 84, 107, 145, 146], 8 participants were recruited and gave their informed consent to participate. The SCI population study [81] recruited 5 participants with paraplegia and 1 with tetraplegia due to SCI to participate in the study. These participants were recruited via physician referral from the Long Beach Veterans Affairs Spinal Cord Injury Center and other SCI out-

reach programs, such as Project Walk (Carlsbad, CA). Note that all participants in both studies were BCI näive with only 0–1 hr of prior BCI experience. Finally, for the SCI population study, all participants performed the 5 daily BCI sessions at a rate of approximately 1 session per week, and able-bodied participants performed the BCI session only once.

Prior to online evaluation, each participant underwent the EEG mounting procedure described in Section 2.2 of Chapter 2. Particularly, the participants were positioned 0.8–1 m from a computer screen that displayed textual cues or the virtual reality environment. EEG data were recorded using the 63-channel cap (Medi Factory, Heerlen, The Netherlands) described in Section 2.2 of Chapter 2 and in Fig. 1.3 of Chapter 1. All 63 electrodes were gelled (Compumedics USA, Charlotte, NC) and recorded because the salient brain areas for kinesthetic motor imagery or attempted walking and idling are unknown. The participants then had their 30-Hz impedances between each electrode and the reference electrode reduced to < 10 KΩ. The EEG signals were streamed in real-time to a computer and re-referenced in a common average mode using 2 linked NeXus-32 bioamplifiers (MindMedia, Roermond-Herten, The Netherlands). Data acquisition and analyses were performed using custom-made Matlab (MathWorks, Natick, MA) programs.

Training Procedure and Decoding Model Generation

To facilitate intuitive control of ambulation within a virtual reality environment, an EEG decoding model was developed that differentiates idling and kinesthetic motor imagery (for the able-bodied participants [32, 84, 107, 145, 146]) or attempted walking (for the SCI participants [81]) EEG. As described in Section 2.3 of Chapter 2, training EEG data were acquired while participants underwent alternating 30 s epochs of idling and kinesthetic motor imagery or attempted walking over a 10

min session. Participants were instructed to perform walking or idling via automated textual cues displayed on the screen. For the kinesthetic motor imagery of walking task in the able-bodied study [32, 84, 107, 145, 146], participants were instructed to vividly imagine themselves walking while refraining from moving their own legs. On the other hand, for the attempted walking control strategy in the SCI population study [81], participants were instructed to attempt to perform the cyclic leg movements of walking, although these attempted movements did not produce any motor output.

In order to classify EEG data as either walking or idling, the data were labeled by a corresponding computer signal recorded by an auxiliary data acquisition system (MP150, Biopac Systems, Goleta, CA). The labeling and EEG signals were synchronized by sending a common pulse train to both the MP150 and NeXus-32 data acquisition systems. Electromyogram (EMG) activity was not recorded during either study to monitor for minor limb movements since increased EMG activity is often observed during kinesthetic motor imagery or attempted walking [28, 71, 90, 156]. Instead, the participants were instructed to refrain from moving during the training procedure, which was enforced by observing the procedure and discarding the entire session if it was considered contaminated by overt movements.

Once the training EEG data were collected, the signals were analyzed offline using the methods described in Section 2.4 of Chapter 2 and in Appendix 2.4. First, the EEG channels with excessive EMG activity were excluded from further analysis using the iterative artifact rejection algorithm described in Section 2.4.1 of Chapter 2. The pre-processed continuous 10 min EEG record was then split into 30 s long segments of idling and walking states based on the labeling signal, and were synchronized with this signal using the common synchronization pulse (see Fig. 2.2 in Section 2.2 of Chapter 2). Due to uncertainties in timing between the computer cue and the

participant's reaction, the first 8 s of each state were removed from analysis. Each remaining 22 s EEG segment was then divided into five 4 s long non-overlapping trials for a total of 100 trials.

The labeled EEG trials were transformed using the fast Fourier transform (described in Appendix A.1), and their power spectral densities were integrated in 2 Hz bins from 1–40 Hz. The dimension of the input data was then reduced using the feature extraction techniques described in Section 2.4.1 of Chapter 2 and in Appendix A.3. This resulted in the extraction of 1-D spatio-spectral features, which were then classified using the linear Bayesian classifier described in Section 2.4.2 of Chapter 2 and in Appendix A.4. The classification accuracy of the classifier was then assessed by performing 10 runs of stratified 10-fold cross-validation (described in Section 2.4.2 of Chapter 2 and in Appendix B.1).

For all the SCI neurorehabilitative studies described in this chapter, the above decoding model generation procedure was systematically repeated to find the optimal frequency range [145]. Briefly, the lower frequency bounds was increased in 2 Hz steps until the classifier performance stopped improving, allowing the optimal lower frequency bound, F_L, to be determined. The optimal higher frequency bounds, F_H, was found in a similar manner. This was performed because the important frequency ranges for classification of kinesthetic motor imagery of walking and attempted walking are unknown. The optimal frequency range determined, list of retained channels after artifact rejection, feature extraction mapping and methods used, as well as the classifier parameters – together referred to as the decoding model, were then saved and implemented into the BCI software for real-time BCI operation.

Online Signal Analysis and Calibration

During online operation, 0.5-s-long blocks of EEG data were acquired in real time at a rate of 2 blocks per second (see a similar method described in Section 2.6 of Chapter 2). This rate was limited by the computer processing speed and was empirically found to ensure data acquisition without dropping packets. Of these 0.5 s blocks, 0.75-s-long segments (i.e. the most recent 0.5 s block plus 50% of the previous block) were assembled and processed using the methods described in the offline training section above. Note that this segment length provided an accurate estimation of EEG spectral power even at the lower end of physiological relevant frequencies. Subsequently, the EEG signals were first band-pass filtered, then transformed into the frequency domain, and the power spectral densities over the optimal frequency range were integrated into 2-Hz bins. These spectral data were used as the input for the feature extraction algorithm, and the posterior probabilities of idling and walking were calculated.

Prior to online operation, a short calibration procedure described in Section 2.5 of Chapter 2 was performed. This was necessary to determine the state transition thresholds for the binary state machine that are suitable for self-paced online BCI operation, and to reduce the number of false state transitions during the online walking tasks. Briefly, using the participant-and-day specific EEG decoding model developed during the training procedure, the BCI system was set to run in the online mode (with the virtual reality environment's joystick disabled) while participants were prompted to alternate between idling and kinesthetic motor imagery or attempted walking for $\sim$2 min. The posterior probabilities were then recorded and their histograms were plotted to determine the walking and idling thresholds, T_W and T_I (where W is "Walking" and I is "Idling"), for the binary state machine described in Fig. 2.5 in Section 2.4.2 of Chapter 2. These two thresholds were initially set as the median values from the

histograms, and then were adjusted as necessary based on the participant's feedback and a brief online familiarization test. During online BCI operation, the posterior probabilities corresponding to the most recent 1.5 s of EEG data were averaged and compared to the two thresholds, and the state transitions were executed based on the binary state machine.

Online Sessions and Performance Assessment

To assess the online BCI performance, participants were tasked to move the avatar within 2 body lengths of each non-player character and remain idle at each location for at least 2 s. On each daily session, participants repeated this task for 2–8 online sessions. This depended upon the participant's willingness and availability. In total, each SCI participant underwent between 19 and 29 online sessions over 5 daily sessions [81], and each able-bodied participant performed 5 online sessions in 1 experimental day [32, 84, 107, 145, 146]. Two performance measures were recorded during each session: the time taken to complete the course and the number of successful stops. Participants received one point for idling the avatar within the designated stop for at least 2 s; therefore, the maximum successful stop score was 10 points. In addition, only a fraction of a point was awarded for dwelling between 0.5 and 2.0 s. Note that participants were not penalized for dwelling longer than 2 s, however, this will inevitably increase the completion time and therefore lower the overall performance. A 20 min time limit was enforced, beyond which the online session was interrupted and the number of successful stops achieved thus far was recorded. Ideally, it should take on average 18 s to walk from 1 non-player character to the next without stopping, with the total course completion time of 211 s (191 s for walking and 20 s for idling).

The number of successful stops and completion times were compared to those achieved

by Monte Carlo random walk simulations to determine whether purposeful control was attained. As described in Appendix B.3, random walk performances were simulated using the methods described in Appendix B.3 and applying the state transition rules outlined in Section 2.4.2 of Chapter 2 with the participant-specific threshold values, T_I and T_W. The random walk simulations were also allotted the 20 min time limit, and the number of successful stops was calculated in the same manner as above. To facilitate statistical testing, 1,000 Monte Carlo runs of the random walk simulation (Appendix B.3) were performed. The participants' performances were then compared to those of the Monte Carlo simulation, and empirical p-values were calculated. An additional control experiment consisted of an able-bodied participant manually performing the same task with a physical joystick.

The 2-D probability density function (PDF), with number of successful stops and completion times as variables, of each participants' simulated random walk from the Monte Carlo simulations (Appendix B.3) was estimated using the Parzen window method [42, 13]. Through each participant's observed performance point (consisting of a successful stops and completion time pair), a constant-value PDF contour was drawn. The volume under the PDF outside the contour was then found by numerical integration, effectively defining the p-value (the null hypothesis being that the participants' performances are no different from random walk). Purposeful control was defined as the ability to complete the task within 20 min with performances significantly different from random walk.

In addition to the above Monte Carlo simulation analysis to assess purposeful control, and since it is difficult to interpret multivariate performance measures across participants and sessions, a single composite score was defined as the following geometric

mean:

$$c = \sqrt{c_s c_t} \tag{4.1}$$

where c_s and c_t are the normalized performance measures for the number of successful stops and completion times, respectively. Further details of how the composite score is calculated can be found in Appendix B.4. As a recap, the values of c_s and c_t are obtained by:

$$\begin{aligned} c_s &= \frac{s}{s_{\max}} \\ c_t &= \frac{t_{\max} - t}{t_{\max} - t_{\min}} \end{aligned} \tag{4.2}$$

Here, s is the participant's number of successful stops, $s_{\max} = 10$ is the maximum number of successful stops, t is the participant's completion time, $t_{\max} = 1200$ s is the maximum allowed time, and $t_{\min} = 201.52$ s is the minimum time required to complete the course while achieving 10 successful stops. The values of c_s and c_t, and consequently c, range from 0 to 100%, where 100% corresponds to a prefect performance. Note that the the geometric mean used here favors a performance that is balanced over a performance that sacrifices one performance measure over the other (e.g. when a participant finishes the course in a short time while failing to make stops). Also, the normalization of c_s and c_t ensures that the performance measures are unitless.

4.3.2 Results

Eight able-bodied participants [32, 84, 107, 145, 146], 5 SCI participants [81] with paraplegia, and 1 SCI participant with tetraplegia [81] participated in this study. The demographic data for the able-bodied study [32, 84, 107, 145, 146] are presented in

Table 4.1, and the demographic data for the SCI population study [81] are shown in Table 4.2. Note that the participant with tetraplegia suffered from syringomyelia (Participant 3 in Table 4.2).

Table 4.1: Demographic data of the able-bodied study [32, 84, 107, 145, 146], including gender, age, and hours of BCI experience.

Participant	Sex	Age	BCI Experience
1	M	40	∼1 hr
2	M	29	∼1 hr
3	F	23	∼1 hr
4	F	57	0 hr
5	F	24	0 hr
6	M	21	0 hr
7	M	25	0 hr
8	M	32	0 hr

Table 4.2: Demographic data of the SCI population study [81], including gender, age, and SCI status. ASIA = American Spinal Injury Association impairment scale. Note that all SCI participants were BCI näive with 0 hours of BCI experience.

Participant	Sex	Age	SCI Status
1	M	34	T11, ASIA A, 8 yr. post injury
2	M	46	T1, ASIA B, 4 yr. post injury
3	M	43	C5, Syringomyelia, 14 yr. post onset
4	M	59	T1, ASIA B, 2 yr. post injury
5	M	21	T11, ASIA B, 1 yr. post injury
6	F	27	T8, ASIA B, 11 yr. post injury

Offline Performances

The stratified 10-fold cross-validation of the participant-specific EEG decoding models in the able-bodied study [32, 84, 107, 145, 146] resulted in classification accuracies that ranged from 64.3% to 88.3% (Table 4.3), with p-values < 0.01 (the null hypothesis being defined as having a chance level classification accuracy of 50%). The average offline performance of the able-bodied participants was 75.1% [32, 84, 107, 145, 146]. Finally, note that these accuracies represent the probability of correctly classifying

a trial given the feature, $f^\star$, in other words, $P(\text{correct}|f^\star) = P(I|f^\star \in I)P(I) + P(W|f^\star \in W)P(W)$, where $P(I|f^\star \in I)$ and $P(W|f^\star \in W)P(W)$ are the posterior probabilities of idling (I) or walking (W) given that the observed feature belongs to the idle or walk class, respectively, and $P(I)$ and $P(W)$ are the prior probabilities of idling and walking classes, respectively. Details of this procedure are described in Section 4.3.1 above and in Appendix B.1.

Table 4.3: Offline performances represented as classification accuracies estimated by the cross-validation procedure for the able-bodied study [32, 84, 107, 145, 146].

Participant	$P(\text{correct}\|f^\star)$	p-value
1	88.3±0.7%	1.27×10^{-16}
2	86.6±0.8%	6.56×10^{-15}
3	76.0±1.3%	9.05×10^{-8}
4	80.9±1.2%	1.35×10^{-10}
5	67.4±2.2%	2.04×10^{-4}
6	72.5±1.6%	2.35×10^{-6}
7	64.3±1.1%	1.76×10^{-3}
8	64.5±1.8%	1.80×10^{-3}
All	75.1±9.5%	–

The offline performances of the EEG decoding models in the SCI population study [81] revealed similar classification accuracies that ranged from 60.5% to 94.5% across all participants (Table 4.4). These accuracies had corresponding p-values between 0.018 and 10^{-20}, thus indicating that the classifier performances were well above the chance level (50%). In addition, the participants' average offline performances were 82.3%, 71.8%, 82.3%, 82.5%, and 82.2%, respectively. As a clarification, note that due to time constraints of the participant, SCI Participant 6 was only able to perform 1 day of the study, whose offline classification accuracy was 94.5%. Finally, the overall average classification accuracy across all 6 participants was $80.8 \pm 8.90\%$ ($n = 26$).

Further analysis of the participant-specific feature extraction maps of the able-bodied study [32, 84, 107, 145, 146] demonstrated that the most informative features for classification of kinesthetic motor imagery of walking were the EEG powers in the 4–18

Table 4.4: Offline performances of the SCI population study [81]. $P(\text{correct}|f^\star)$ and p-value are presented for each participant on each experimental day.

Participant	Day	$P(\text{correct}\|f^\star)$	p-value
1	1	71.9±2.2%	6.29×10^{-6}
	2	89.4±1.2%	1.53×10^{-17}
	3	83.9±2.0%	1.30×10^{-12}
	4	84.0±1.9%	1.30×10^{-12}
	5	82.2±1.7%	6.55×10^{-12}
	Avg.	82.3±6.4%	1.26×10^{-6}
2	1	62.2±1.8%	6.00×10^{-3}
	2	62.0±1.8%	1.05×10^{-2}
	3	60.5±2.0%	1.76×10^{-2}
	4	91.6±1.7%	1.60×10^{-19}
	5	82.5±1.6%	6.55×10^{-12}
	Avg.	71.8±14.3%	6.82×10^{-3}
3	1	90.3±1.3%	1.66×10^{-18}
	2	83.9±1.1%	1.30×10^{-12}
	3	72.8±2.9%	2.35×10^{-6}
	4	81.0±2.1%	1.35×10^{-10}
	5	83.3±1.2%	1.30×10^{-12}
	Avg.	82.3±6.3%	4.69×10^{-7}
4	1	74.7±1.7%	2.82×10^{-7}
	2	92.3±1.6%	1.36×10^{-20}
	3	81.5±1.3%	3.07×10^{-11}
	4	80.5±2.0%	1.35×10^{-10}
	5	83.5±2.2%	1.30×10^{-12}
	Avg.	82.5±6.4%	5.64×10^{-8}
5	1	82.7±1.3%	6.55×10^{-12}
	2	86.3±1.3%	6.56×10^{-15}
	3	78.9±1.4%	2.17×10^{-9}
	4	82.2±1.5%	6.55×10^{-12}
	5	81.0±1.3%	1.35×10^{-10}
	Avg.	82.2±2.7%	4.30×10^{-10}
6	1	94.5±0.8%	6.26×10^{-23}

Hz frequency range over the lateral central/centro-parietal areas (see Fig. 4.3). Based on the brain areas underlying these features, the motor imagery control strategies utilized by the able-bodied participants likely correspond to motor imagery of arm swinging or arm movement produced during walking.

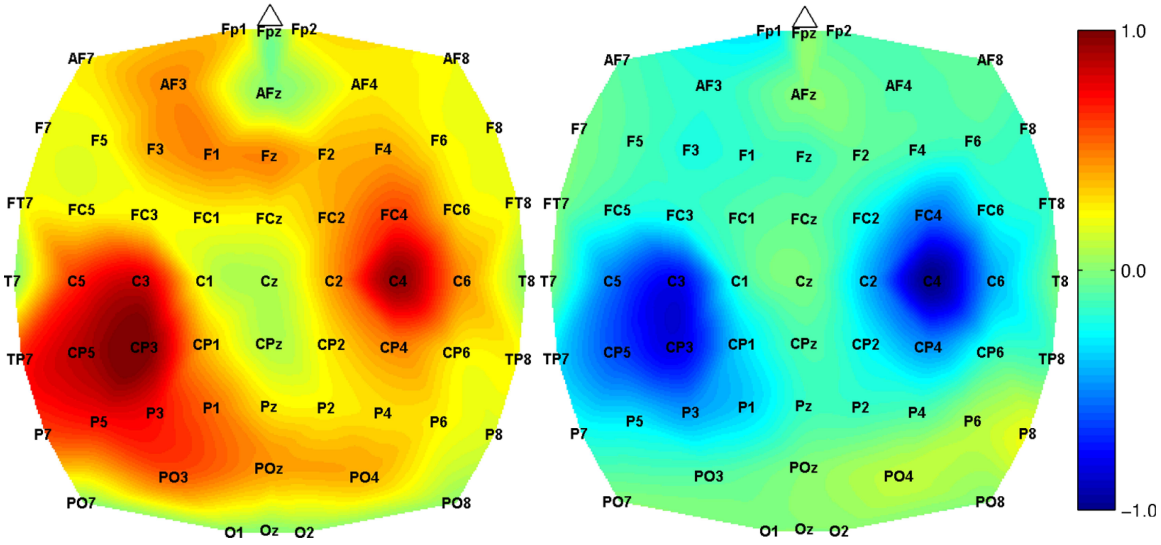

Figure 4.3: Spatio-spectral feature extraction maps corresponding to the 12–14 Hz frequency range for Participant 2 in the able-bodied study [32, 84, 107, 145, 146]. There are 2 maps presented, 1 for idling (left) and the other for kinesthetic motor imagery of walking (right).

Unlike the able-bodied participants' control strategy of kinesthetic motor imagery of walking, the SCI participants utilized an attempted walking control strategy. This resulted in salient frequencies in the μ (8–12 Hz) frequency band [81]. Furthermore, qualitative analysis of these topographic maps revealed significant variations in the brain areas utilized by the participants while performing the attempted walking and idling task. For example, Participant 2 used mostly the Cz area (Fig. 4.4), whereas Participant 5 used areas C3 and C4 (Fig. 4.5). Furthermore, the utilized brain areas and frequency bands evolved for each participant over the 5 experimental days. For instance, Participant 2 had growing activation of mid-frontal areas (over Cz or FCz and adjacent electrodes) mostly in the μ (8–12 Hz) and low-β (12–16 Hz) bands.

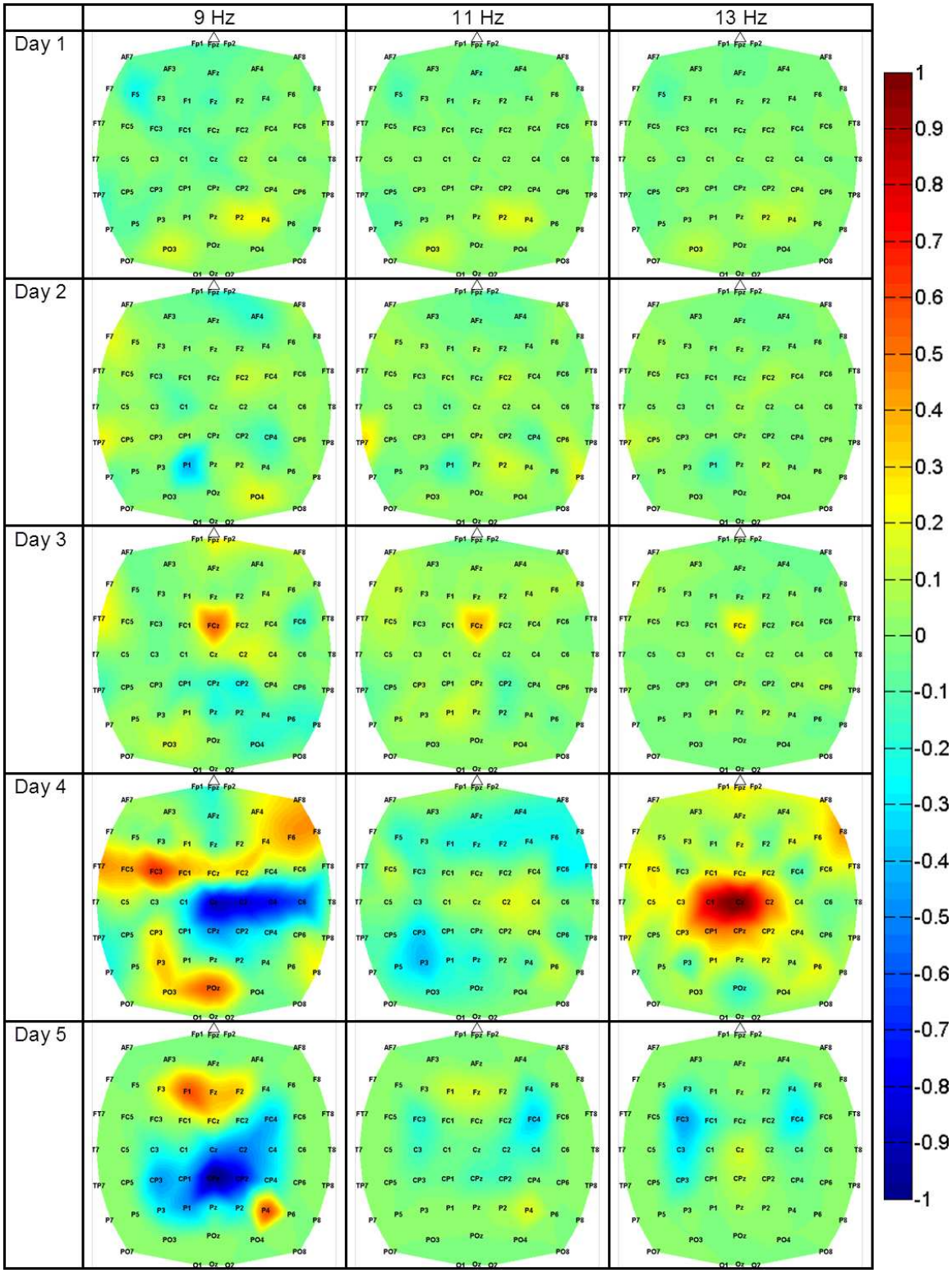

Figure 4.4: Feature extraction maps of Participant 2 for all experimental days [81]. The EEG power in the 9–13 Hz bins in the central (Cz) and centro-parietal (CPz) areas were the most salient.

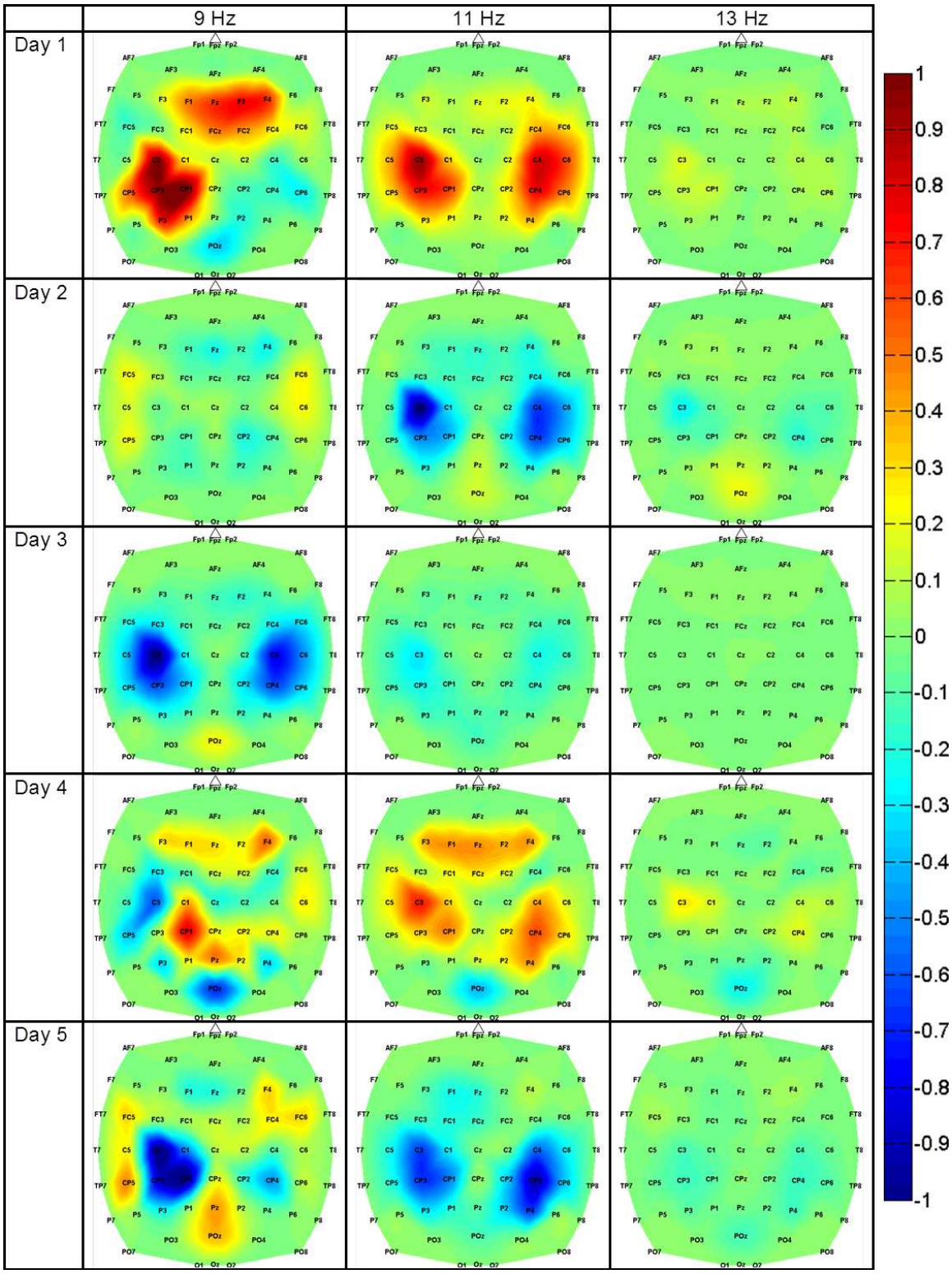

Figure 4.5: Feature extraction maps of Participant 5 for all experimental days [81]. The EEG power in the 9–13 Hz bins in the mid-frontal (Fz), lateral central (C3 and C4), and lateral centro-parietal (CP3 and CP4) areas were most salient.

Online Calibration

The short calibration procedure (Section 4.3.1) in the able-bodied study [32, 84, 107, 145, 146] resulted in histograms representative of Fig. 4.6. Note that in an ideal situation, the distribution of $P(W|f^\star \in W)$ should cluster around 1, whereas $P(W|f^\star \in I)$ should cluster around 0. However, in reality, due to the inherent noise in EEG, these distributions will have some overlap. The state transition thresholds, T_I and T_W, were then determined and their values are shown in Table 4.5. Also, if EEG data carried no class information, the two thresholds would be equal to $P(W)$ (0.5 in the study). On the other hand, if classes could be perfectly decoded from EEG data, the threshold values T_I and T_W would approach 0 and 1, respectively. The values of T_I and T_W varied across participants from 0.19 to 0.55, and from 0.43 to 0.91, respectively. As apparent in Table 4.5, the thresholds of all participants were separable. In addition, the calculated values of T_W were found to correlate with the offline performances shown in Table 4.3 ($\rho = 0.87$, p-value = 0.002). On the other hand, the same was not true for T_I ($\rho = 0.87$, p-value = 0.90). Finally, it was found that the offline performances also correlated with the separability of T_W and T_I (i.e. $T_W - T_I$), resulting in a correlation coefficient of 0.80 (p-value = 0.009). Note, however, that these tests were based on only 9 samples.

Table 4.5: The chosen values of the state transition thresholds, T_I and T_W, for the able-bodied study [32, 84, 107, 145, 146].

Participant	T_I	T_W
1	0.53	0.91
2	0.24	0.64
3	0.19	0.56
4	0.43	0.58
5	0.55	0.57
6	0.53	0.61
7	0.41	0.43
8	0.19	0.45

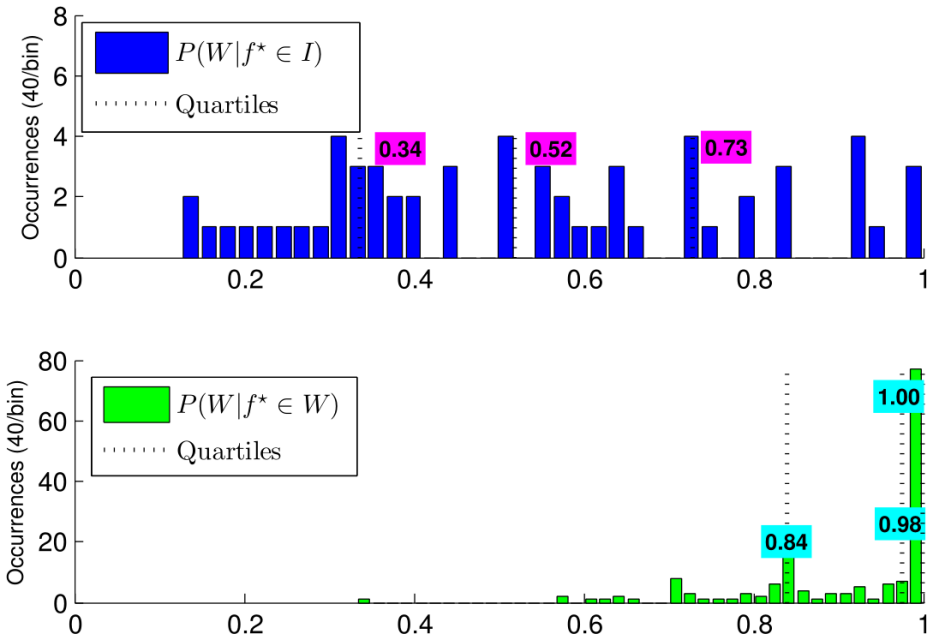

Figure 4.6: Representative histogram for Participant 1 from the able-bodied study [32, 84, 107, 145, 146]. The dotted lines denote quartiles.

For the SCI population study [81], the state transition thresholds, T_I and T_W, were also separable (except for Participant 2 on the 1st experimental day). A representative example of these thresholds can be seen in Fig. 4.7. Specifically, as seen in Table 4.6, the values of T_I and T_W ranged from 0.07 to 0.70 and from 0.09 to 0.90, respectively. In addition, the average thresholds across all participants on all experimental days was 0.40 and 0.62 for T_I and T_W, respectively.

Online Performances

As described in Section 4.3.1, the online performances of all participants operating the BCI-controlled walking simulator were evaluated by comparing the task completion times and successful stops to those of the simulated random walk. Three short videos demonstrating the walking simulator task can be seen at `<http://www.youtube.com/user/UCIBCI>`, where the videos are titled "Able-bodied Subject Operates BCI-controlled Avatar", "Subject with Tetraplegia Operates BCI-controlled

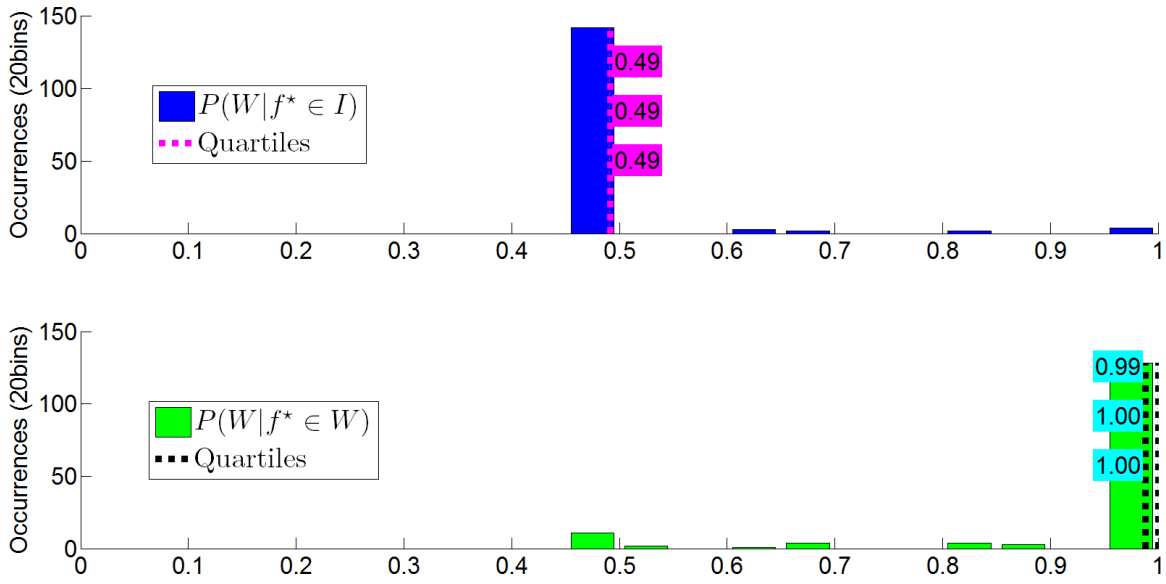

Figure 4.7: Representative histogram for Participant 3 from the SCI population study [81] for the attempted walking control strategy. The dotted lines denote quartiles.

Avatar", and "Subject with Paraplegia Operates BCI-controlled Avatar". After completing 1,000 Monte Carlo random walk simulations (Appendix B.3) per participant with the threshold parameters given in Tables 4.5 and 4.6, the 2D-PDF contours were constructed and the empirical p-values of the participant's online performances (numbers of successful stops and completion time) were calculated. The online performances, corresponding empirical p-values, and random walk PDF contours of 4 representative able-bodied participants are shown in Fig. 4.8. Overall, in 43 out of the 45 online sessions of the able-bodied study [32, 84, 107, 145, 146], participants achieved performances that were significantly different (i.e. 'outside of the contours') from those of random walk simulations ($p < 0.01$). At a significance level of 0.05, performances were different from random walk in 44 sessions (able-bodied Participant 7 had a single session with a non-significant performance). In addition, the average completion times and successful stops are summarized in Table 4.7. Note that the completion time consists of a fixed walking time (191 s) and a variable amount of idling time.

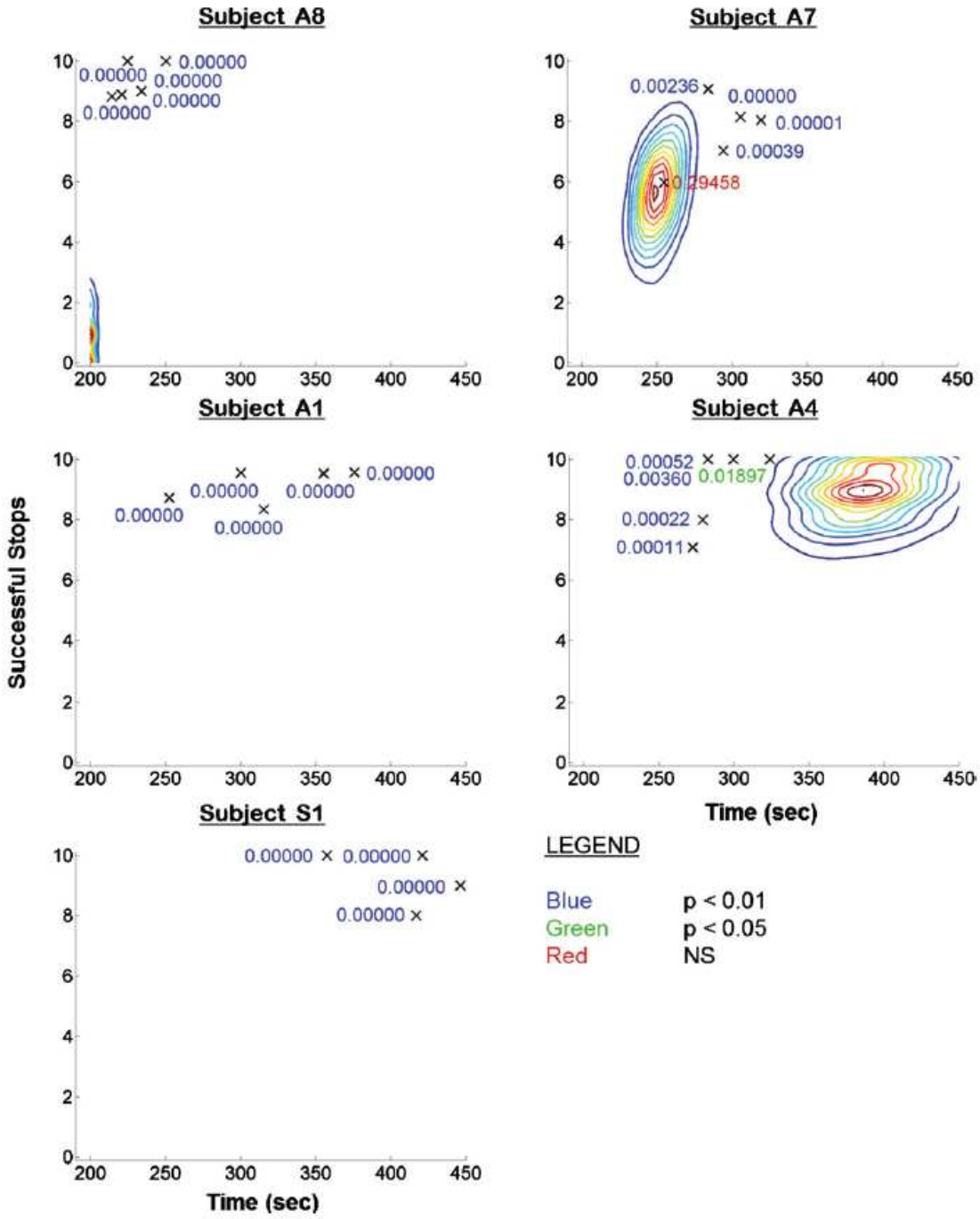

Figure 4.8: Representative online performances of 4 participants in the able-bodied study [32, 84, 107, 145, 146]. Each cross corresponds to 1 online session's completion time and successful stops. The numbers next to the crosses indicate the empirical p-values colored by significance level. The random walk PDFs are displayed as contours. For Participant 1, the random walk simulation did not complete the task within the allotted 20 min time limit, so contours are not shown.

Table 4.6: Online state transition thresholds, T_I and T_W, for online operation for the SCI population study [81].

Participant	Day	T_I	T_W
1	1	0.37	0.47
	2	0.42	0.67
	3	0.45	0.55
	4	0.22	0.39
	5	0.35	0.44
2	1	0.50	0.50
	2	0.07	0.09
	3	0.42	0.45
	4	0.60	0.70
	5	0.60	0.66
3	1	0.20	0.30
	2	0.57	0.62
	3	0.26	0.75
	4	0.70	0.90
	5	0.40	0.90
4	1	0.62	0.80
	2	0.61	0.80
	3	0.38	0.45
	4	0.40	0.60
	5	0.58	0.65
5	1	0.30	0.85
	2	0.40	0.70
	3	0.30	0.70
	4	0.40	0.80
	5	0.30	0.85
6	1	0.32	0.87

The participants in the able-bodied study [32, 84, 107, 145, 146] achieved the following online performances. For Participant 1, purposeful control was achieved with superior performance for both completion time and successful stops. Participants 4, 5, and 6 achieved purposeful control with superior performance in completion time only. On the other hand, Participant 2, 3, 7, and 8 achieved purposeful control with superior performance in the number of successful stops, although they required more time to complete the task. Finally, to demonstrate the performance level achievable by manual control, an able-bodied participant performed the task with a physical

Table 4.7: Average online performances of the participants in the able-bodied study [32, 84, 107, 145, 146] compared to those of random walk simulations (RW). Note that the random walk composite scores were not calculated because the raw data was not saved.

Participant	Completion Time (s) mean ± std.	Successful Stops mean ± std.	Composite Score (%)
1	319.8±48.3	9.14±0.57	89.7±2.54
1-RW	>1200	0.24±0.43	–
2	266.7±10.8	7.80±1.10	85.2±6.04
2-RW	224.4±18.1	1.47±1.09	–
3	291.9±19.3	8.03±1.08	85.3±6.03
3-RW	219.3±9.8	2.46±1.37	–
4	291.7±20.6	9.01±1.39	90.3±6.49
4-RW	383.4±26.7	9.15±0.82	–
5	325.4±54.2	8.10±0.94	84.0±4.92
5-RW	602.6±38.5	9.89±0.24	–
6	318.2±27.3	8.09±1.06	84.3±5.38
6-RW	699.0±53.4	9.91±0.24	–
7	291.5±24.4	7.65±1.19	83.2±6.03
7-RW	251.6±9.8	5.62±1.24	–
8	228.8±14.0	9.34±0.60	95.3±2.70
8-RW	193.9±2.3	0.39±0.54	–
All Participants	292.4±41.4	8.39±1.12	87.1±6.17
Joystick	205.07±4.2	9.38±0.85	96.5±3.81

joystick. The manual joystick performance was significantly different and superior to the BCI performances in terms of completion times ($p = 0.0002$), but was not significantly different in terms of the number of successful stops ($p = 0.086$).

Fig. 4.9 shows a representative time-space course of 1 online session for Participant 8 in the able-bodied study [32, 84, 107, 145, 146]. In this session, not only did the participant complete the course with the maximum number of successful stops and a short completion time, but the participant also had only 2 false alarms (i.e. the avatar walking when it was not supposed to) and no omissions (i.e. the avatar stopping when it is not supposed to). Over the 5 online sessions performed by this participant during 1 experimental day, the participant averaged 0.4 false alarms and 2.5 omissions. By factoring in the duration of false alarms and omissions, as well as the completion time,

these values correspond to error rates of 0.42% and 3.34%, respectively. The online performances of the other participants in the able-bodied study [32, 84, 107, 145, 146] were not recorded with this level of detail because the computer code was modified in the late stage of this particular study to accommodate for this function, and so it was not possible to state their exact false start and stop rates. Since Participant 8 achieved the best online performance, it is likely that the other participants' error rates were higher than the numbers reported above. Therefore, while not universally applicable, the results presented in Fig. 4.9 illustrate the level of control achievable by able-bodied participants using the BCI system and a kinesthetic motor imagery of walking control strategy.

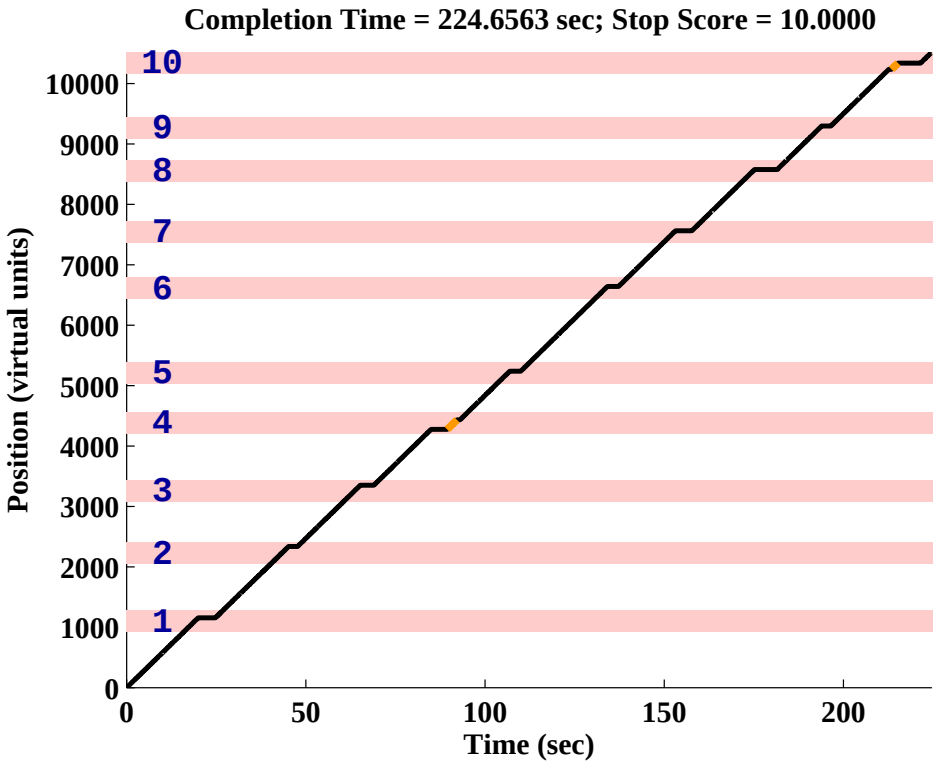

Figure 4.9: Time-space course of a representative online session for Participant 8 in the able-bodied study [32, 84, 107, 145, 146]. The pink areas mark designated stopping zones. Orange segments mark false starts. In order to finish the course, the participant is required to walk out of the last stopping zone.

For the SCI population study [81], all participants were able to achieve purposeful

online performances immediately (on experimental day 1), with the exception of Participant 2, who achieved purposeful control by day 2. The online performances for each participant across all experimental days are shown in Table 4.8. The average stop score was 7.4 ± 2.3, and the average completion time was 277 ± 56.3 s across all online sessions (n = 128). Furthermore, the average composite score was 81.4 ± 13.5%. As previously mentioned, note that ideally, the course should be completed within 211 s with a fixed 191 s of walking time and 20 s of idling time, so the additional time spent to complete the course was due to errors (e.g. false alarms and omissions). These errors may have be due to difficulty transitioning to the walk state or due to overestimating the 2 s dwelling time at each character. Also, only minimal lapses in BCI control occurred, as only 5 out of the 128 online sessions (∼4%) were non-purposeful ($p \geq 0.01$), and 123 sessions were purposeful ($p < 0.01$). Specifically, Participant 1 had 3 non-purposeful online sessions out of the 26 sessions performed, and Participants 2 and 4 had 1 non-purposeful session out of the 24 and 18 sessions performed, respectively.

Examples of the best online performances for Participants 1–5 are shown in Fig. 4.10 below [81]. In addition to these performances, the random walk PDFs are also displayed. Note that only the contour for Participant 1 is shown, as all other random walk PDFs fell outside of the allotted 20 min time limit. For additional comparison, the average number of successful stops achieved by a manual joystick was 9.38 ± 0.85 (Table 4.8 above), and on their best day, Participants 3, 4, and 5 achieved a similar number of successful stops. However, no participants were able to complete the course as fast as the manually controlled joystick.

In addition to the random walk PDFs of the best online performances for Participants 1–5 in Fig. 4.10 above, Fig. 4.11 shows 2 time-space courses of the best online sessions for Participants 3 and 5. Note that Participant 3 only had a single false alarm and

Table 4.8: Average online performances for the SCI population study [81]. Shown are the total number (n) of sessions performed, participants' best day's performances, and the random walk (RW) performances. Note that random walk composite scores were not calculated because the raw data was not saved, and Participant 6 only performed 1 experimental day.

Participant		Completion Time (s) mean±std.	Successful Stops mean±std.	Composite Score (%)
1	n=29	275±45	6.2±1.8	74.7±10.2
	Best Day 5	298±77	6.8±2.3	76.9±11.0
	RW	227±7	5.0± 1.3	–
2	n=25	271±66	5.7±2.3	71.0±13.6
	Best Day 5	293±26	8.1±1.2	85.4±4.9
	RW	1445±118	9.0±0.9	–
3	n=24	277±65	9.4±1.3	92.8±8.0
	Best Day 4	231±8	10.0±0.0	98.4±0.4
	RW	>1200	0.1±0.3	–
4	n=19	289±43	8.3±1.8	86.0±10.2
	Best Day 1	264±12	8.9±0.3	91.5±1.5
	RW	>1200	4.3±0.7	–
5	n=27	258±31	7.7±2.1	84.4±12.3
	Best Day 4	260±17	10.0±0.0	96.9±0.8
	RW	>1200	5.1±1.4	–
6	n=4	410.6±33	9.25±0.8	85.4±4.9
	RW	>1200	4.52±1.6	–
All Participants		277±56.3	7.4±2.3	81.4±13.5
Joystick		205.07±4.2	9.38±0.85	96.5±3.81

a single omission, while Participant 5 had no false alarms and only 2 omissions. Also, the online performances of the other participants were not recorded with this level of detail, as the computer code was modified in the late stage of this study to accommodate for this function. It is likely that the other participants' false alarms and omissions were higher than those reported in Fig. 4.11. Therefore, while not universally applicable, these results illustrate the level of control achievable by this BCI system in SCI individuals [81].

The composite scores calculated from the online performances measures presented in Table 4.8 demonstrated that a high level of performance was achievable by all SCI individuals [81]. In general, the performances improved significantly over time.

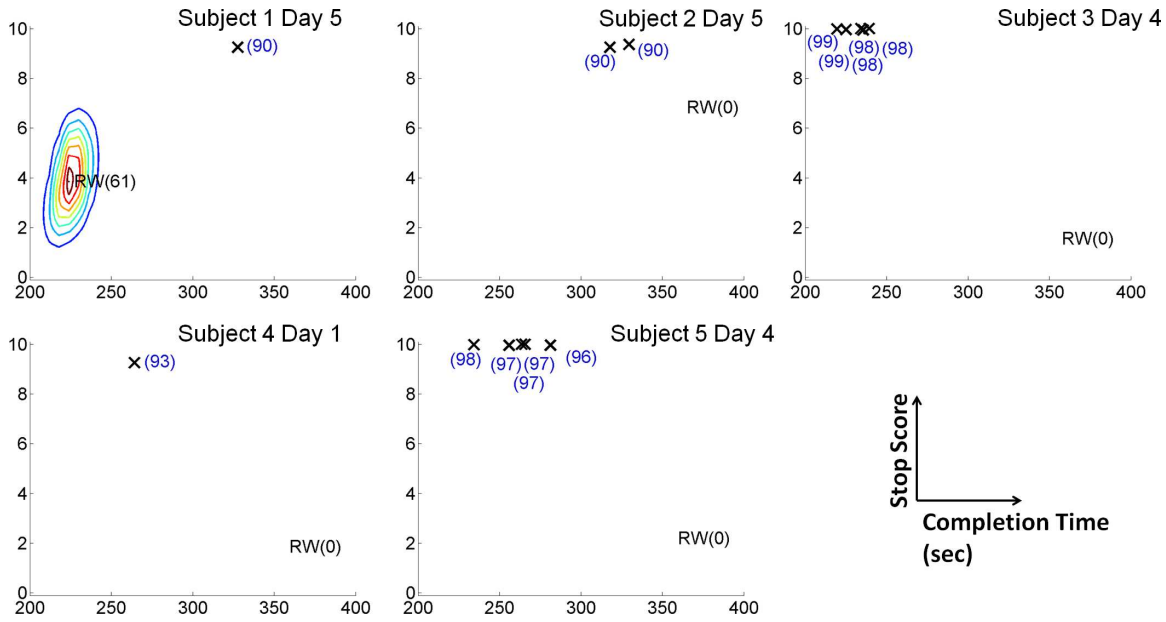

Figure 4.10: The best online performances for Participants 1 through 5 for the SCI population study [81]. Each cross corresponds to 1 online session's completion time and successful stops. The numbers in parentheses next to the crosses indicate the composite score (in %) and are colored by significance level ($p < 0.01$). The random walk PDFs are displayed as contours for Participant 1, but are absent for other participants as the contours lie outside of the allotted 20 min time limit.

The average score on day 1 for all participants was 77.8%, and the average score on day 5 was 85.7% ($p = 0.0302$). For comparison, the composite score of the joystick task was $96.5 \pm 3.8\%$. On their best days, Participants 3, 4, and 5 achieved performances similar to those of the manually controlled joystick, reaching nearly perfect performances (100%). Specifically, Participant 3 had a best online composite score of 99.0%, Participant 4 had a best score of 96.1%, and Participant 5 had a best score of 98.3%.

4.3.3 Discussion

The results of the able-bodied study [32, 84, 107, 145, 146] demonstrated that the self-paced BCI driven walking simulator can be purposefully controlled in real time

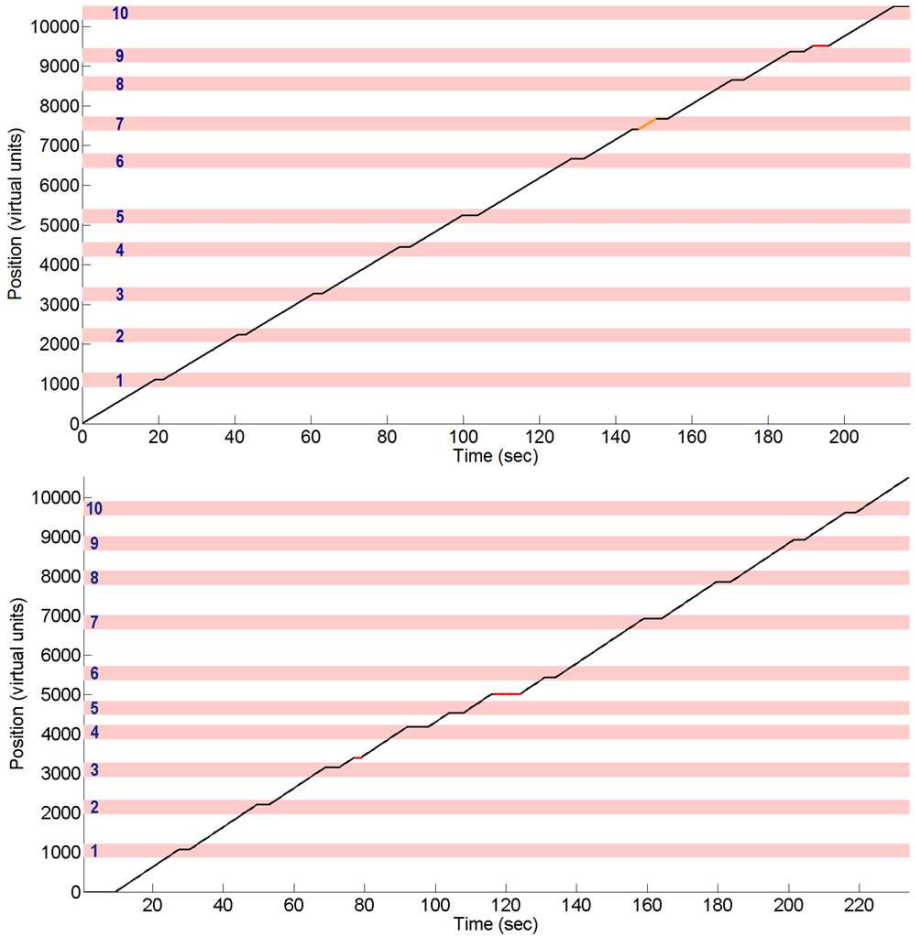

Figure 4.11: Time-space course of a representative online session for Participants 3 and 5 in the SCI population study [81]. The pink areas mark designated stopping zones. Orange segments mark false starts. In order to finish the course, the participant is required to walk out of the last stopping zone.

by 8 able-bodied participants using an intuitive kinesthetic motor imagery of walking control strategy. All participants were able to achieve purposeful control of the avatar's linear ambulation after only a 10 min training session followed by a 2 min calibration session. The rapid training and acquisition of purposeful BCI control were facilitated by a data-driven machine learning method to generate participant-specific EEG decoding models. The decoding models were validated first offline and then during online BCI operation. These results indicate that the system may satisfy the proposed requirements of an ideal BCI-lower extremity prosthesis, i.e. robustness,

intuitiveness, and short training time.

The SCI population study [81] further demonstrated that the self-paced BCI-controlled walking simulator can be purposefully controlled in real time by SCI individuals using an intuitive attempted walking control strategy. All participants gained purposeful control on the first experimental day after undergoing the 10 min training session and 2 min calibration session, with the exception of Participant 2, who did not attain control until the 2nd experimental day. In addition, BCI control was maintained over the course of the study, and the performance improved in 4 out of 5 participants. These findings suggest that a BCI-controlled lower extremity neuroprosthesis or neurorehabilitative therapy for gait rehabilitation after SCI may be feasible.

Offline Performances

It follows from the offline performances of the able-bodied [32, 84, 107, 145, 146] and SCI population [81] studies that idling and walking kinesthetic motor imagery or attempted walking states can be decoded from underlying EEG signals with moderate to high accuracy. Furthermore, the 10 min training session was sufficient for the data-driven machine learning algorithm to generate participant-specific EEG decoding models. These models achieved offline classification accuracies in the able-bodied study [32, 84, 107, 145, 146] between 64.3% and 88.3% (mean: 75.1%), which were significantly superior to random chance (50%), and with p-values as small as 10^{-16}. In addition, the offline classification accuracies in the SCI population study [81] ranged from 62.0% to 94.5% (mean: 80.5%), with p-values as small as 10^{-23}. Finally, this was true even for BCI-näive participants with 0 hours of BCI experience.

The EEG decoding models of the able-bodied participants [32, 84, 107, 145, 146] also yielded feature extraction maps that could be used to uncover the brain areas and

frequency bands that differentiate the idling and kinesthetic motor imagery of walking behaviors. Particularly, the EEG features responsible for encoding the differences between the 2 states in the able-bodied participants were the powers in the μ (8 – 12 Hz) and β (13 – 30 Hz) EEG bands over the lateral central and lateral centro-parietal electrodes. The activity measured by these electrodes is most likely localized to the lateral sensorimotor cortex, which is typically associated with hand and arm movements.

Unlike the features salient for classification between idling and kinesthetic motor imagery of walking in the able-bodied participants [32, 84, 107, 145, 146], the participants from the SCI population study [81] had informative features in the μ and β bands over the mid-central as well as lateral central electrodes. These electrodes are likely to record the activity originating from the medial sensorimotor and supplementary motor cortices, where the leg and foot cortical representation areas are classically located. Hence, it appears that there is a divergence between the brain areas employed by the able-bodied participants and the SCI participants while undergoing kinesthetic motor imagery of walking and attempted walking control strategies. It is possible that these differences are simply caused by the different mental strategies employed by the SCI and able-bodied participants. This may because unlike simple motor imageries often used in BCI studies, such as fist clenching [99, 111] or foot tapping [111], walking kinesthetic motor imagery and attempted walking emulates a highly complex set of upper and lower extremity movements for which there may not be a universal motor imagery strategy. Based on their feature extraction maps, it can be hypothesized that able-bodied participants predominantly imagined the arm swinging process of walking as opposed to the leg movement component. It is also possible that due to the extremely small sample size (only 100 training EEG trials), the relative contribution of other potential brain representation areas (e.g. lower extremity motor areas) was masked by a more dominant arm swing imagery in these

maps. In contrast, due to motor paraplegia or tetraplegia in the SCI participants, attempted walking may be a mental task that is as vivid as attempted leg movements or executed walking. However, given the limited population sizes of these 2 studies, these hypotheses could not be formally tested.

The proposed data-driven machine learning methodology was able to produce participant-specific decoding models that accommodate for the neurophysiological variations across participants. This is especially important for BCI users with SCI, as post-injury cortical reorganization can occur. Namely, recent functional magnetic resonance imaging studies [1, 22, 68, 123] reported significant changes in motor cortical representation areas for lower extremity motor imagery following SCI. This may explain the evolution of salient features across experimental days in the SCI participants (Figs. 4.4 and 4.5). On the other hand, the changes in salient features may be due to differences in imageries employed by each participant, for instance, the attempted walking instructions may have been interpreted differently by each participant and across experimental days. Nevertheless, their activation during attempted walking is consistent with functional imaging studies, such as the study reported in [89].

The spatio-spectral variations of attempted walking activation patterns demonstrate the necessity of the data-driven machine learning approach for rapid acquisition of intuitive BCI control. First, our approach accommodates for the variations of these activity patterns across participants, as well as their evolution over time. Second, it facilitates rapid acquisition of online BCI control, presumably by enabling participants to utilize intuitive mental strategies. The user training time necessary to acquire purposeful BCI control in this study is significantly shorter than those of other BCI studies where users must learn a completely new cognitive skill to modulate pre-selected EEG features, such as the μ-rhythm over lateral central areas [161]. Finally, this approach carries a significant potential value in the future practical im-

plementation of BCIs for ambulation, as it may drastically reduce the training time needed to attain purposeful and useful control of self-paced BCIs from a timescale of weeks to months to one of minutes to days. This in turn may significantly reduce the cost of training users to operate future BCI driven lower extremity neuroprostheses and neurorehabilitative therapies.

Online Performances

The online performance from the able-bodied study [32, 84, 107, 145, 146] had average online performances that ranged from 228.8 to 410.6 s for completion time and from 7.65 to 9.34 for number of successful stops, with Participant 8 achieving the highest number of successful stops. Furthermore, in all but 1 online session (out of 45), all participants demonstrated purposeful BCI control. These results were similar in the SCI population study [81], as purposeful control was maintained in 96% of all online sessions. In addition, 4 out of 6 SCI participants achieved successful stop scores similar to those obtained using a manually controlled joystick. Even though no participants were able to complete the course as fast as manual control, it is encouraging that the average composite scores increased significantly over the course of the SCI study [81]. Particularly, for Participants 3 and 5, the average composite scores approached 100% by the end of the study. Therefore, not only was online control significantly different from random walk, it was also meaningful. Given this trend, additional training and practice may help further improve performance, possible to the point of approaching that of a manually controlled joystick.

While there is a positive correlation between the offline classification accuracy and online performance measures, the offline and online performances were only moderately coupled (e.g. only 21% of the variance in the able-bodied study [32, 84, 107, 145, 146] can be accounted for by the completion times and number of successful stops). This

may be due to several underlying causes. First, the high variability of online performances may cause a poor linear regression fit. Second, linear regression may not be the best model to link offline and online performances. Lastly, the presence of outliers may cause the parameters of the linear regression model to be chosen suboptimally.

As an example of the above discrepancy, the best able-bodied participant (Participant 8) and the best SCI participant (Participant 3), had an offline performance of only 65% and 82.3 $\pm$ 6.3%, respectively, and yet they both were able to achieve a level of online control that nearly matched that of a manual joystick. This discrepancy may be caused by physiological and behavioral factors. It may be hypothesized that a relatively low offline performance reflects the participant's inconsistency in generating kinesthetic motor imagery or attempted walking and/or occasional lapses in attention. Since offline training is done without feedback, the participants may not be aware of these issues. Ultimately, this may lead to a decoding model that is suboptimal and hence yield low offline performances. When online, the feedback is always present, allowing the participants to hone their mental strategies and presumably utilize kinesthetic motor imagery and attempted walking control strategies that are more consistent with the models. The participants' abilities to adapt and achieve good performances during online BCI operation may also indicate that the decoding model retains useful kinesthetic motor imagery or attempted walking features despite being suboptimal.

In general, the BCI performances were inferior to those of a manually controlled physical joystick. However, note that some participants (e.g. Participant 8 in the able-bodied study [32, 84, 107, 145, 146] and Participants 3 and 5 in the SCI population study [81]), all BCI näive users, were only slightly slower than the joystick with equivalently numbers of successful stops. Therefore, additional training and online practice may help further reduce the completion time, possibly to the point of

approaching that of manual control. Should this goal be achieved, it could further justify the pursuit of BCI-controlled lower extremity neuroprostheses and neurorehabilitative therapies for ambulation after SCI.

Comparison with Other Studies

The BCI driven walking simulator studies [32, 84, 81, 107, 145, 146] represent the first demonstration of integrating an EEG based BCI with a virtual reality walking simulator. A comparison between this study and related BCI-virtual reality environment studies [91, 111] is given in Table 4.9. Note that the present approach utilizes kinesthetic motor imagery or attempted walking and idling as a control strategy, which intuitively matches the walking task. On the other hand, the study in [91], and especially the one presented in [111], were less intuitive. Furthermore, the present approach requires a significantly shorter training time before participants were able to gain online BCI control. With the present approach, BCI-näive participants were able to achieve purposeful online BCI control within minutes as opposed to the months of training required in the other studies [91, 111]. In addition, this system has been tested in a substantially larger population of able-bodied and SCI participants, suggesting that it may be generalizable. Finally, a direct comparison of the results between this study and related BCI-virtual reality environment studies is not possible due to variations in experimental designs.

Table 4.9: Comparison of our virtual reality walking simulator studies to similar studies in the field [81]. AB = able-bodied, SCI = spinal cord injury participants.

Study	Mental Strategy	Training Time	Sample Size
Our present studies [32], [84, 81, 107, 146, 145]	Imagery or attempted walking/idling	10 min	8 AB, 6 SCI
Leeb et al. [91]	Imagery of foot/idling	4 months	1 SCI
Pfurtscheller et al. [111]	Imagery of foot/hand	3–5 months	3 AB

4.3.4 Conclusion

In summary, the BCI-controlled walking simulator presented in the able-bodied [32, 84, 107, 145, 146] and SCI population [81] studies show that participants can purposefully operate the self-paced virtual reality ambulation system in real time. More importantly, these studies satisfy the proposed criteria of a practical BCI system, namely, intuitiveness, robustness, and short training time. The operation of the system was intuitive as it enabled participants to use kinesthetic motor imagery or attempted walking to control the ambulation of the avatar. The system was robust in that the data-driven decoding methodology was able to successfully accommodate for participant-to-participant and day-to-day variations in the neurophysiological underpinnings of idling and kinesthetic motor imagery or attempted walking behaviors (e.g. differences between able-bodied and SCI participants). In addition, the data-driven methodology was able to overcome the potential problems associated with variations in neurophysiology due to cortical reorganization after SCI, learning and plasticity processes, and differences in kinesthetic motor imagery and attempted walking strategies. The SCI participants were also able to maintain purposeful online control over the course of several weeks, further underscoring the system's robustness over time. Finally, the system required only a short training time, as BCI control was attained after only a 10 min long training data collection procedure followed by a 2 min calibration session in all but 1 SCI participant on the 1^{st} experimental day.

The high level of control achieved by the SCI participants [81] over the course of the study indicates that BCI-controlled lower extremity neuroprostheses and neurorehabilitative therapies for ambulation after SCI may be feasible. The proposed BCI-virtual reality system may also serve as a training platform for BCI-controlled ambulation devices once they become widely available. Furthermore, the intuitive kinesthetic motor imagery and attempted walking strategies were proven to be viable

control strategies for these future prostheses and neurorehabilitative devices.

4.4 BCI-Robotic Gait Orthosis

After determining that kinesthetic motor imagery and attempted walking is a viable control strategy for our BCI system [32, 84, 81, 107, 145, 146], our laboratory translated this technology from virtual reality to a physical prosthesis [33, 34, 35]. It is envisioned that a combination of an invasive brain signal acquisition system and implantable system for ambulation, such as an implantable FES system, can potentially act as a permanent BCI prosthesis. However, for safety reasons, the feasibility of brain-controlled ambulation must first be established in noninvasive systems. Thus, we integrated our noninvasive EEG based BCI system with a noninvasive RoGO before testing this system with FES technologies [51, 52] (e.g. Parastep I system, Sigmedics, Fairborn, OH). This was done for safety reasons, as it does not require intensive physiotherapy to improve cardiovascular and respiratory systems, a requirement for ambulation devices that use FES.

Commercially available RoGOs were explored prior to implementing our BCI system with a noninvasive FES device for overground walking. These lower extremity prostheses included the ReWalk (Argo Medical Technologies, Inc., Marlborough, MA) and Lokomat [73] (Hocoma, Volketswil, Switzerland). The Lokomat device was ultimately chosen because of its availability as well as it's body-weight support system, which allows for a much safer and easier test bed for early development of a BCI-prosthesis for ambulation. After integrating our BCI system with the Lokomat device, it was tested in able-bodied and SCI participants as a proof-of-concept study [33, 34, 35].

4.4.1 Methods

Similar to the BCI driven walking simulator studies mentioned above, the BCI-RoGO was first tested in an able-bodied participant, and then in an SCI participant [33, 34, 35]. Both participants performed the experiment over 1 experimental day, as this study was intended to be a proof-of-concept study to see if operation of a BCI-controlled RoGO was possible.

Overview

To determine the feasibility of a BCI driven RoGO using a kinesthetic motor imagery or attempted walking control strategy, EEG data were recorded from participants as they engaged in alternating epochs of idling and kinesthetic motor imagery of walking (for the able-bodied participant) or attempted walking (for the SCI participant) [33, 34, 35]. These data were then analyzed offline to generate a participant-specific EEG decoding model for online BCI operation. The commercial RoGO system, suspended over a treadmill using a body-weight support system, was interfaced with the BCI computer to allow for computerized control. In a series of five, 5-min-long online tests, the participants were tasked to ambulate using the BCI-RoGO system when prompted by computerized cues. This was different from the self-paced walking simulator tests [32, 84, 81, 107, 145, 146], as it allowed for a better assessment of the performance of the system and the response between the BCI and RoGO. The performance of this system was finally assessed by calculating the cross-correlation and latency between the computerized cues and BCI-RoGO response, as well as the omission and false alarm rates (Appendix B).

BCI-RoGO Integration

To comply with the institutional restrictions that prohibit software installation, the RoGO computer was interfaced with the BCI using a pair of microcontrollers (Arduino, SmartProjects, Turin, Italy) to perform mouse hardware emulation. Microcontroller #1 relayed commands from the BCI computer to microcontroller #2 via an Inter-Integrated Circuit (I^2C) connection [33, 34, 35]. Microcontroller #2 then acted as a slave device programmed with mouse emulation firmware [56] to automatically manipulate the RoGO's user interface. This setup enabled the BCI computer to directly control the RoGO idling and walking functions.

Participant Recruitment and Data Acquisition

Ethical approval was obtained from the Institutional Review Board at the Long Beach Veterans Affairs Medical Center and the University of California, Irvine. Participants were recruited from a population of able-bodied individuals, or those with chronic, complete motor paraplegia due to SCI (>12 months post-injury) [33, 34, 35]. The exclusion criteria for participants with SCI were severe spasticity, contractures, restricted range of motion, or fractures in the lower extremities, pressure ulcers, severe osteoporosis, or orthostatic hypotension. These criteria were ruled out in a safety screening evaluation consisting of an interview, a physical exam, lower extremity dual-energy X-ray absorptiometry (DEXA) scan and X-rays, and a tilt-table exam.

The actively shielded 64-channel EEG cap (Medi Factory, Heerlen, The Netherlands) described in Section 2.2 of Chapter 2 and in Fig. 1.3 of Chapter 1 was mounted on the participants' head and impedances were reduced to <10 KΩ. All 64 electrodes were used, so the EEG signals were streamed in real-time to a computer and re-referenced in a common average mode using two linked NeXus-32 bioamplifiers (MindMedia,

Roermond-Herten, The Netherlands) at a sampling rate of 256 Hz. The participants were suspended in a treadmill-equipped RoGO (Lokomat, Hocoma, Volketswil, Switzerland) using partial weight unloading (see Fig. 4.12).

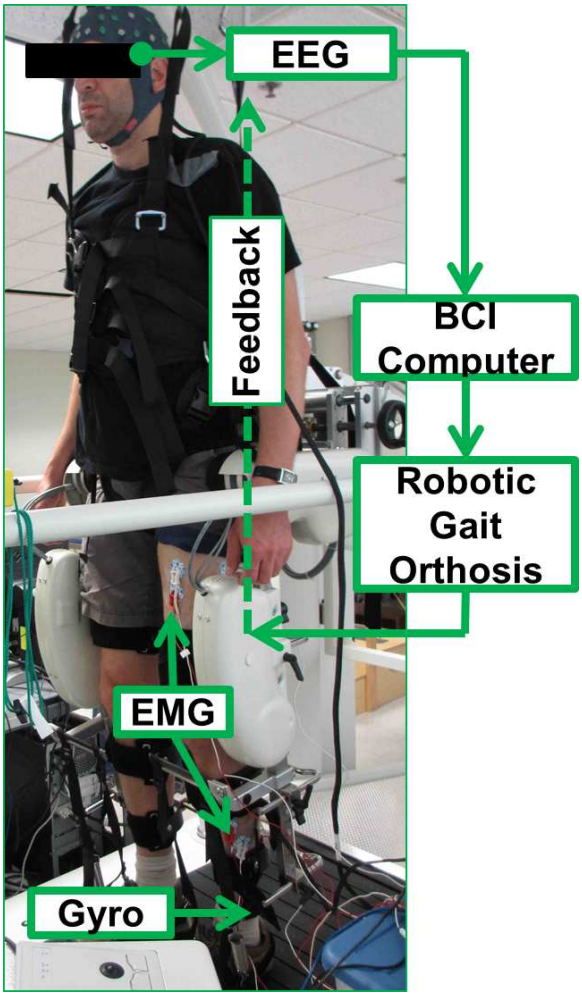

Figure 4.12: Experimental setup showing a participant suspended in the RoGO while wearing an EEG cap, surface electromyogram (EMG) electrodes, and a gyroscope on the left leg. A monitor (not shown), placed in front of the participant at eye-level, presented instructional cues [34].

Training Procedure and Decoding Model Generation

Similar to the training procedure described in the BCI walking simulator studies [32, 84, 81, 107, 145, 146] (Section 4.3), EEG data were collected as the participants

alternated between 30-s epochs of idling and kinesthetic motor imagery (for the able-bodied participant) or attempted (for the SCI participant) walking for a total of 10 min, as directed by computer cues [33, 34, 35]. This entailed vivid imagination of walking during kinesthetic motor imagery of walking cues, or attempted walking movements without using the arms or making excessive movements for the SCI participant during the walking cues. For the idling cues, both participants were tasked with remaining relaxed and refraining from movements. During this entire procedure, the able-bodied participant stood still with his arms at his side, while the SCI participant stood still with his arms resting on the arm rests of the treadmill for postural stability.

As described in Section 2.3 of Chapter 2, in order to classify EEG data as either walking or idling, the data were labeled by a corresponding computer signal recorded by an auxiliary data acquisition system (MP150, Biopac Systems, Goleta, CA). The labeling and EEG signals were synchronized by sending a common pulse train to both the MP150 and NeXus-32 data acquisition systems. Electromyogram (EMG) activity was not recorded during either study to monitor for minor limb movements since increased EMG activity is often observed during kinesthetic motor imagery or attempted walking [28, 71, 90, 156]. Instead, the participants were instructed to refrain from moving during the training procedure, which was enforced by observing the procedure and discarding the entire session if it was considered contaminated by overt movements.

Once the training EEG data were collected, the signals were analyzed offline using the methods described in Section 2.4 of Chapter 2 and in Appendix 2.4. First, the EEG channels with excessive EMG activity were excluded from further analysis using the iterative artifact rejection algorithm described in Section 2.4.1 of Chapter 2. The EEG epochs corresponding to the "Idling" and "Walking" states were then trans-

formed into the frequency domain, and their power spectral densities (PSD) were integrated over 2 Hz bins. As described in Section 2.4 of Chapter 2, the data then underwent dimensionality reduction using a combination of classwise principal component analysis (CPCA) and approximate information discriminant analysis (AIDA). A linear Bayesian classifier, described in Section 2.4.2 of Chapter 2, was then designed in the feature domain, and the performance of the Bayesian classifier (Appendix B.1), expressed as a classification accuracy, was assessed by performing stratified 10-fold cross-validation. Finally, the optimal frequency range was found using the methods described in Section 4.3.1 above. This was performed because the important frequency ranges for classification of kinesthetic motor imagery of walking and attempted walking were still unknown. The optimal frequency range determined, list of retained channels after artifact rejection, feature extraction mapping and methods used, as well as the classifier parameters, were saved and implemented into the BCI software for real-time BCI operation.

EMG and Leg Movement Measurement

EMG was measured to rule out BCI control by voluntary leg movements in the able-bodied participant during real-time online operation [33, 34, 35]. To this end, baseline lower extremity EMG were measured under 3 conditions: *active walking* (the participant voluntarily walks while the RoGO servos are turned off), *cooperative walking* (the participant walks synergistically with the RoGO), and *passive walking* (the participant is fully relaxed while the RoGO makes walking movements). Three pairs of surface EMG electrodes were placed over the left quadriceps, tibialis anterior, and gastrocnemius (Fig. 4.12), and signals were acquired with a bioamplifier (MP150, Biopac Systems, Goleta, CA), bandpass filtered (0.1–1000 Hz), and sampled at 4 KHz. In addition, leg movements were measured by a gyroscope (Wii Motion Plus,

Nintendo, Kyoto, Japan) with a custom wristwatch-like enclosure, strapped to the distal left lower leg (proximal to the ankle, shown in Fig. 4.12) [3]. Approximately 85% body-weight unloading was necessary for proper RoGO operation, and the walking velocity was set to 2 km/hr.

Online Signal Analysis and Calibration

Methods similar to the walking simulator studies described above (Section 4.3) and in Section 2.6 of Chapter 2 were used during online BCI-RoGO operation [33, 34, 35]. Specifically, 0.75 s segments of EEG data were acquired every 0.25 s in a sliding overlapping window. The PSD of the retained EEG channels were calculated for each of these segments and used as the input for the signal processing algorithms described above. The posterior probabilities of "Idling" and "Walking" classes were calculated using the Bayes rule (Eq. 2.2 in Section 2.4.2 of Chapter 2).

To calibrate the BCI-RoGO system prior to online operation and performance assessment, methods similar to the walking simulator studies [32, 84, 81, 107, 145, 146] described above (Section 4.3) and in Section 2.5 of Chapter 2 were used. This step was necessary to reduce the noise during online BCI operation and to minimize the mental workload of the participants. To this end, the posterior probability was averaged over 2 s of EEG data, and was compared to 2 thresholds, T_I and T_W, to initiate state transitions. The values of T_I and T_W were determined by setting the system to run in the online mode (with the RoGO walking disabled, but all systems turned on) as the participant alternated between idling and kinesthetic motor imagery or attempted walking for $\sim$5 min. The values of the posterior probabilities were then plotted in a histogram to empirically determine the values of T_I and T_W, and a brief familiarization online session with feedback was used to further fine-tune these threshold values.

Online Sessions and Performance Assessment

To assess the performance of the BCI-RoGO system, participants were mounted in the RoGO and used idling/kinesthetic motor imagery or attempted walking to elicit BCI-RoGO driven idling/walking. Unlike the walking simulator studies [32, 84, 81, 107, 145, 146] described above (Section 4.3), the self-paced BCI-RoGO system was tested using 5 alternating 1 min epochs of computerized textual cues [33, 34, 35]. This was done instead of a self-paced game to better assess the performance and latency of the BCI-RoGO system. During these computer-cued online tests, the underlying EEG changes during kinesthetic motor imagery or attempted walking should ideally initiate and maintain the BCI-RoGO walking until the kinesthetic motor imagery or attempted walking stops. The participants were instructed to make no voluntary movements and to keep their arms still (for the able-bodied participant, he kept his arms at his side, and for the SCI participant, he kept his arms resting on the arm rests for postural stability). Left leg EMG and movements were measured as described above. This online test was performed 5 times in a single experimental day for each participant.

Online performance was assessed using the following metrics [33, 34, 35]:

1. Cross-correlation between the cues and BCI-RoGO walking
2. Omissions – failure to activate BCI-RoGO walking during the "Walk" cues
3. False Alarms – initiation of BCI-RoGO walking during the "Idle" cues

Details of these analysis are described in Section 2.7 of Chapter 2 and in Appendix B.

For the able-bodied participant [33, 34, 35], analysis of EMG and leg movement data was performed to ascertain whether RoGO walking was entirely BCI controlled.

First, to demonstrate that covert movements were not used to initiate BCI-RoGO walking, gyroscope and rectified EMG data (in the 40-400 Hz band) were compared to the BCI decoded "Walking" states in each session. Ideally, the initiation of these states should precede EMG activity and leg movements. Then, to establish whether voluntary movements were used to maintain BCI-RoGO walking, EMG during these epochs were compared to the baselines (i.e. active, cooperative, and passive walking). To this end, EMG data were segmented by individual steps based on the leg movement pattern [3], as measured by the gyroscope. The PSD of these EMG segments were then averaged and compared to those of the baseline walking conditions. Ideally, the EMG power during BCI-RoGO walking should be similar to that of *passive walking* and different from those of *active* and *cooperative walking*.

To determine the significance of each online BCI-RoGO session's performance, the cross-correlation between the cues and BCI-RoGO were compared to 10,000 Monte Carlo trials. A detailed description of how the nonlinear auto-regressive model was created is described in Appendix B.3. Finally, an empirical p-value was defined as the fraction of Monte Carlo trials whose maximum correlation was higher than that of the online session.

4.4.2 Results

As previously mentioned, 2 participants (1 able-bodied and 1 with paraplegia due to SCI) were recruited for this study and provided their informed consent to participate. Their demographic data are described in Table 4.10 below. Participant 2, who was affected by paraplegia due to SCI, underwent the screening evaluation and met all study criteria.

Table 4.10: Demographic data of the BCI-RoGO study participants [33, 34, 35]. ASIA = American Spinal Injury Association.

Participant	Age	Gender	Prior BCI Experience	SCI Status
1	42	Male	∼5 hours	N/A
2	25	Male	∼3 hours	T6 ASIA B

Offline Performances

All participants successfully underwent the training EEG procedure. Their EEG decoding models were generated based on the training EEG data. This offline analysis resulted in a model classification accuracy of 94.8 ± 0.8% and 77.8 ± 2.0% for Participants 1 and 2, respectively (chance: 50%). The EEG feature extraction maps are shown in Fig. 4.13. As seen in Fig. 4.13, the able-bodied participant (Participant 1) utilized mostly channels over the arm representation areas, e.g. channels C5 and C6, over the μ-band (8-12 Hz), while the SCI participant (Participant 2) utilized channels over the arm and leg representation areas, e.g. channels C4 and C5 as well as channel CPz, also over the μ-band.

Online Calibration

After the short calibration procedure, a histogram of the posterior probabilities was plotted. Fig. 4.14 shows the resulting histograms for both participants. From these histograms and the familiarization session with feedback, the respective values of T_I and T_W were set to 0.04 and 0.65 for Participant 1, and 0.50 and 0.90 for Participant 2, respectively. It should be noted that both threshold sets for each participant were highly separable, which led to smooth online BCI-RoGO operation.

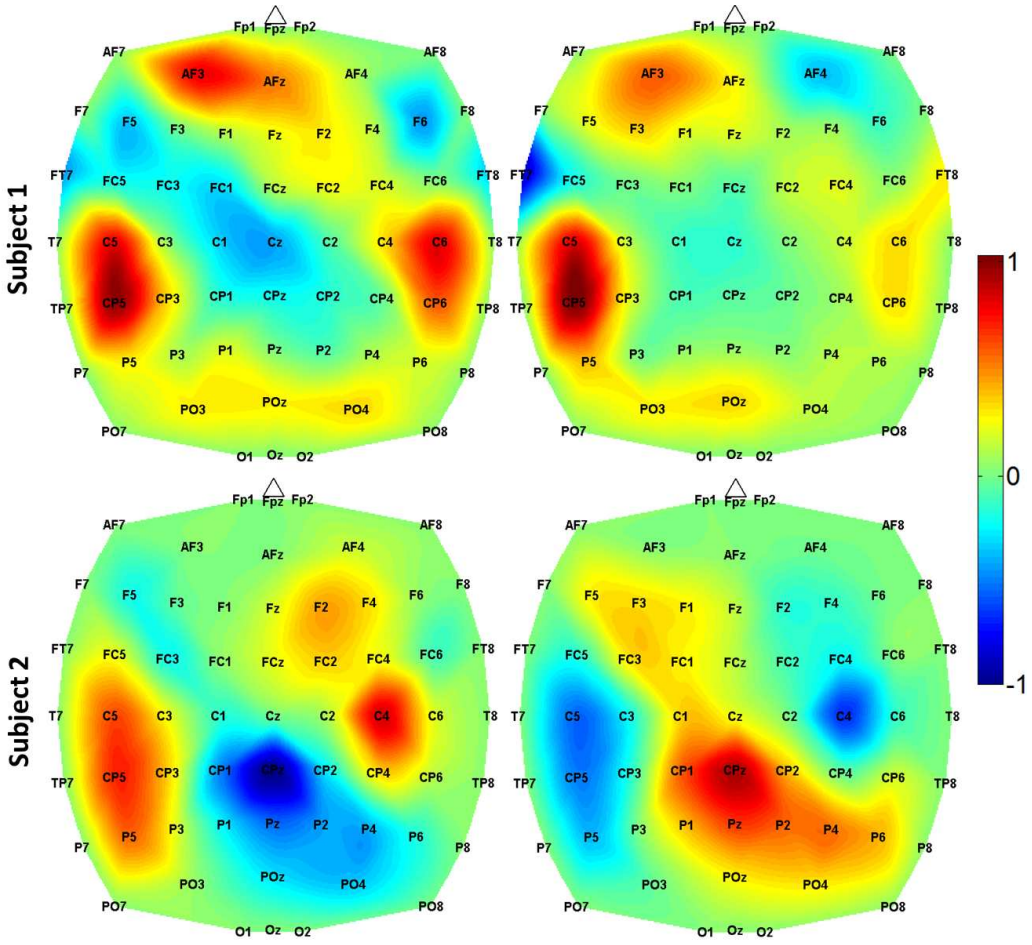

Figure 4.13: The CPCA+AIDA feature extraction maps for both participants of the BCI-RoGO study [34]. Since feature extraction is piecewise linear, there is 1 map for each class. Brain areas with values close to +1 or -1 are most salient for distinguishing between "Idling" and "Walking" classes at this frequency. The most salient features were in the 8-10 Hz bin for Participant 1 and the 10-12 Hz bin for Participant 2.

Online Performances

The performances from the 5 online sessions for both participants are summarized in Table 4.11. The average cross-correlation between the computer cues and the participants' BCI-RoGO walking epochs was 0.812 ± 0.048. As a control, the maximum cross-correlation between the instructional computer cues and simulated BCI operation using 10,000 Monte Carlo trials were 0.438 and 0.498 for Participants 1 and 2, respectively. This indicates that all of the cross-correlations in Table 4.11

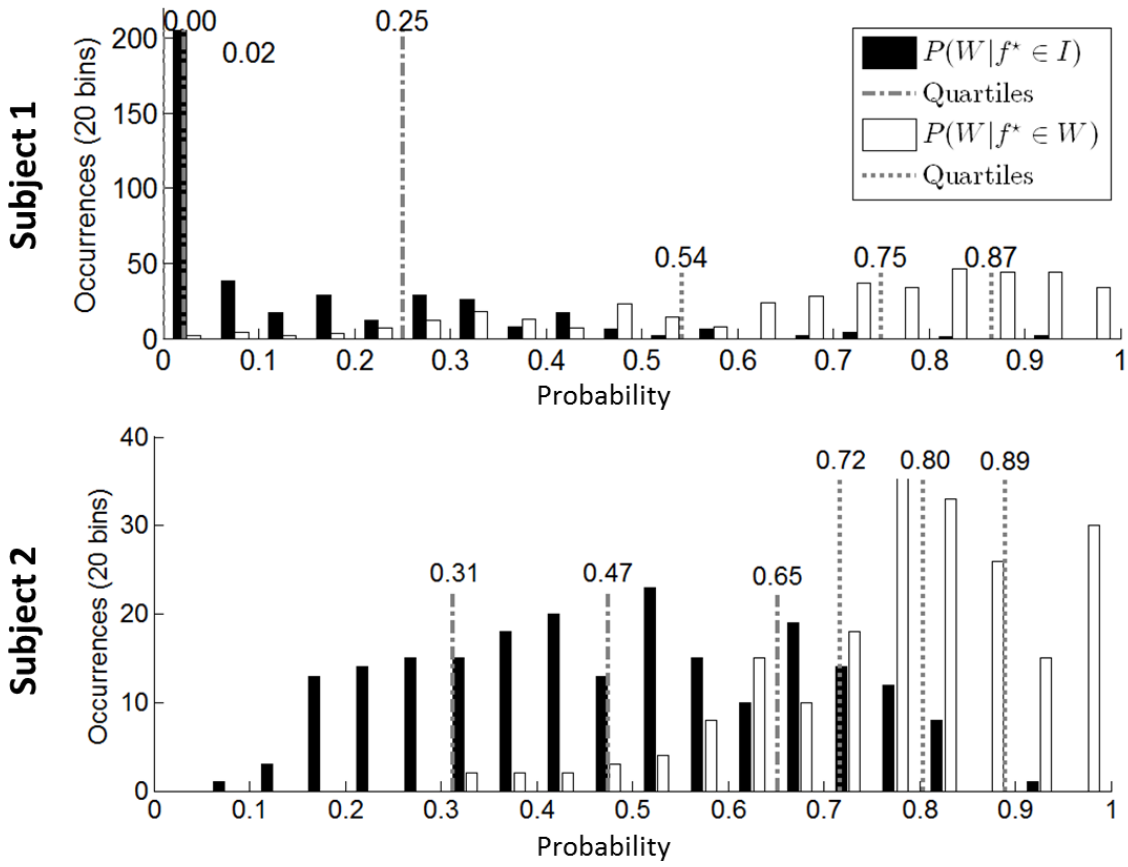

Figure 4.14: The histograms of the averaged posterior probabilities for both participants of the BCI-RoGO study [34].

were significant with an empirical p-value $< 10^{-4}$. Also, there were no omissions for either participant. The false alarm rate averaged 0.8 across all online sessions and participants. While the duration of these false alarm epochs averaged 7.42 $\pm$ 2.85 s, much of this time can be attributed to the RoGO's locked-in startup sequence ($\sim$5 s). In addition, each participant managed to achieve 2 sessions with no false alarms. Videos of a representative online session for the able-bodied participant (Participant 1) and for the participant with SCI (Participant 2) can be found at `<http://www.youtube.com/user/UCIBCI>`, where the videos are titled "BCI RoGO" and "Person with Paraplegia Uses a Brain-Controlled Orthosis to Regain Walking (4x)", respectively.

Table 4.11: Online performances of the BCI-RoGO study [34], showing the cross-correlation between the BCI-RoGO walking and computer cues at specific lags, number of false alarms and omissions, and the average duration of the false alarm epochs.

Participant	Session	Cross-Correlation (lag in s)	Omissions	False Alarms (avg. duration in s)
1	1	0.771 (10.25)	0	1 (12.00)
	2	0.741 (4.50)	0	2 (5.50±0.00)
	3	0.804 (3.50)	0	1 (5.30)
	4	0.861 (4.50)	0	0
	5	0.870 (12.00)	0	0
	Avg.	0.809±0.056 (6.95±3.89)	0	0.8 (7.08±3.28)
2	1	0.781 (6.25)	0	1 (8.80)
	2	0.878 (6.75)	0	0
	3	0.782 (6.25)	0	0
	4	0.851 (14.25)	0	1 (5.50)
	5	0.785 (5.75)	0	2 (8.40±4.10)
	Avg.	0.815±0.046 (7.85±3.60)	0	0.8 (7.76±2.80)
	Overall	0.812±0.048 (7.40±3.56)	0	0.8 (7.42±2.85)

For the able-bodied participant (Participant 1), the EMG and leg movement data from the online sessions were analyzed as described above. EMG and gyroscope measurements indicated that no movement occurred prior to the initiation of BCI decoded "Walking" states (see Fig. 4.15). When compared to the baselines, the EMG during online BCI-RoGO walking in all 3 muscle groups were statistically different from those of *active* or *cooperative walking* conditions ($p < 10^{-13}$), and were not different from those of *passive walking* ($p = 0.37$). These results confirm that the BCI-RoGO system was wholly BCI controlled. Note that *passive walking* is known to generate EMG activity [98], hence a similar level of activity during BCI-RoGO walking (Fig. 4.16) is expected. Furthermore, since the participant with SCI (Participant 2) does not have any voluntary motor control of the lower extremities, there was no need to perform EMG measurements and analysis.

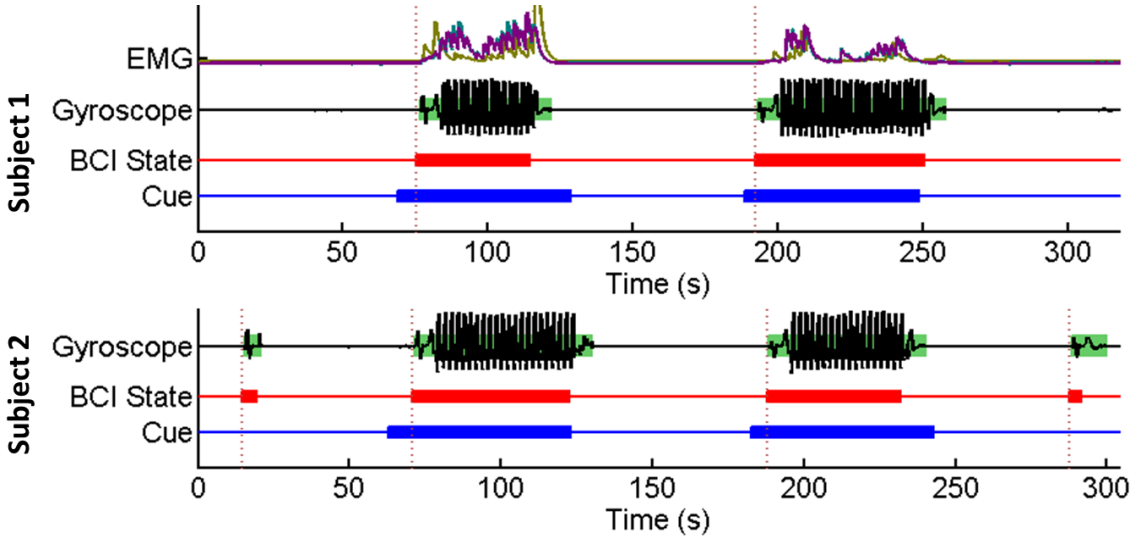

Figure 4.15: Time course of a representative session for each participant in the BCI-RoGO study [34], showing epochs of idling and BCI-RoGO walking determined from the gyroscope trace (green blocks). The red trace represents the decoded BCI states, while the blue trace represents the computer cues. The thick/thin blocks indicate walking/idling. Corresponding EMG (gold: quadriceps, teal: tibialis anterior, purple: gastrocnemius) are also shown. Note that EMG was not measured for Participant 2.

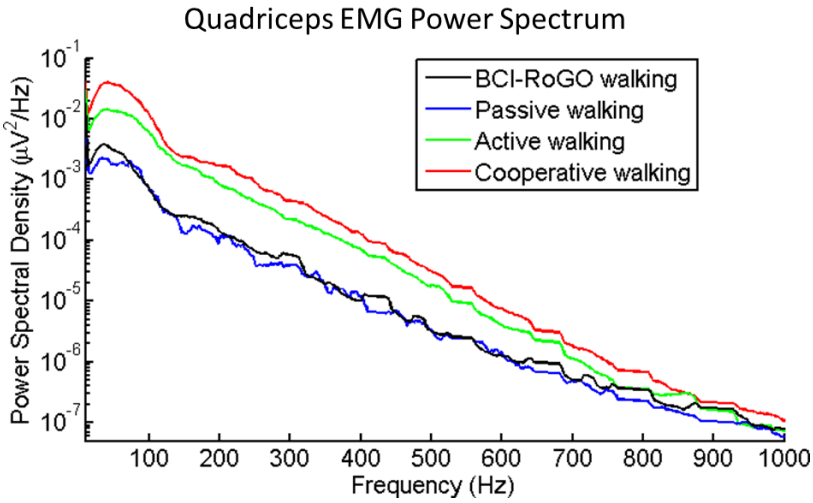

Figure 4.16: EMG power spectral density of Participant 1 in the BCI-RoGO study [34], showing representative EMG PSD of the quadriceps. The spectra demonstrates that EMG during BCI-RoGO walking are different from active or cooperative walking baseline conditions, and are similar to passive walking.

4.4.3 Discussion

The results of the BCI-RoGO study [33, 34, 35] demonstrate that BCI-controlled lower extremity neuroprostheses and neurorehabilitative devices for walking after SCI are feasible. Both participants gained purposeful and highly accurate control of the BCI-RoGO system on their first attempt. It is particularly notable that the participant with paraplegia due to SCI (Participant 2) was able to accomplish this with minimal prior BCI experience and after only a brief 10 min training data acquisition session. This study represents the first-ever demonstration of a person with paraplegia due to SCI re-gaining brain-driven basic ambulation and completing a goal-oriented walking task using a RoGO.

Offline Performances

The EEG decoding models for both participants in this study had a high offline classification accuracy. In the case of Participant 1, the performance was higher than his performances in prior BCI walking avatar studies (e.g. Participant 1 in [146] and in [145]). Note that the gain in this performance was achieved despite the participant being suspended in the RoGO (as opposed to being seated in the BCI walking simulator studies [146, 145]). Examination of the EEG decoding models also revealed that the salient brain areas underlying kinesthetic motor imagery of walking and attempted walking differed between able-bodied and SCI participants (Fig. 4.13). Collectively, these areas likely overlie the pre-frontal cortex, supplementary motor, and the leg and arm sensorimotor representation areas, and are consistent with those previously reported. For example, activation of the pre-frontal cortex and supplementary motor area during walking motor imagery has been described in previous functional imaging studies [89]. Similarly, involvement of the leg and bilateral arm

areas during attempted or kinesthetic motor imagery of walking have been previously reported in the walking simulator studies [32, 84, 81, 107, 145, 146], and may be associated with leg movement and arm swing imagery. This EEG decoding model was further validated by generating highly separable posterior probability distributions (Fig. 4.14) and facilitating highly accurate online BCI-RoGO control. Finally, since it was generated through our data-driven procedure, the modeling approach is participant-specific and may accommodate for the neurophysiological variability across participants [32, 84, 81, 107, 145, 146].

Online Performances

Both participants attained highly accurate online control of the BCI-RoGO system. This was achieved immediately on each participants' first attempt and generally improved through the course of the 5 online sessions. The average online cross-correlation between the computer cues and BCI response (0.812) was higher than those achieved with lower (0.67) and upper (0.78) extremity BCI-prostheses (i.e. the BCI-FES system for foot dorsiflexion [30] and the BCI driven hand orthosis system [83] in Sections 3.3 and 3.2 of Chapter 3, respectively), despite EEG being acquired under more hostile (ambulatory) conditions. Furthermore, not only did the participant with paraplegia attain immediate BCI-RoGO control, but he also had a higher average online performance than the able-bodied participant. This implies that future BCI-prostheses for restoring overground walking after SCI may be feasible. Additionally, all of the participants' online BCI-RoGO sessions were purposeful with a 100% response rate (no omissions). Although Participant 1 had no false alarms by the end of the experiment, Participant 2 experienced false alarms in the final online session. These false alarms were few in number and short in duration, however, they carry the risk of bodily harm, and this problem must be addressed in the develop-

ment of future BCI-prostheses for overground walking. Table 4.11 also shows that the maximum correlation was attained at an average lag of 7.4 s. Most of this lag can be attributed to the RoGO's locked-in power-down sequence (∼5 s), and minor sources of delay include a combination of user response time and the 2-s long posterior probability averaging window.

With no more than ∼5 hr of relevant BCI experience (operating the BCI walking simulator described in Section 4.3 above), both participants attained a high level of control of the BCI-RoGO system after undergoing a series of short procedures (i.e. 10 min training data acquisition, 5 min calibration, and 5 min of familiarization). This indicates that a data-driven EEG decoding model as well as prior virtual reality training using our BCI driven walking simulator [32, 84, 81, 107, 145, 146] may have facilitated this rapid acquisition of BCI control. In addition, this model enables BCI operation using an intuitive control strategy, i.e. kinesthetic motor imagery or attempted walking to induce walking and idling or relaxation to stop. This is in contrast to requiring participants to undergo months of training in order to acquire a completely new skill of modulating pre-selected EEG signal features as frequently done in operant conditioning BCI studies [91, 111].

Based on the above observations, our data-driven BCI approach may be necessary for intuitive and practical BCI-controlled lower extremity prostheses and neurorehabilitative therapies for those with SCI. This approach enables participants with SCI to use intuitive BCI control strategies such as kinesthetic motor imagery or attempted walking. Similar to Participant 2 in this BCI-RoGO study [33, 34, 35], this can be accomplished with minimal user training and supervision from the experiment operator.

4.4.4 Conclusion

In conclusion, the results from the BCI-RoGO study [33, 34, 35] provide convincing evidence that BCI control of ambulation after SCI is possible, which warrants future studies to test the function of this system in a population of participants with SCI. Since participants with SCI were able to operate the BCI walking simulator [32, 84, 81, 107, 145, 146], it is expected that they can readily transfer these skills to the BCI-RoGO system, similar to Participant 2. In addition, this system justifies the development of BCI-controlled lower extremity prostheses for free overground walking for those with complete motor SCI. Finally, the current BCI-RoGO system can also be applied to gait rehabilitation in incomplete motor SCI. It can be hypothesized that coupling the behavioral activation of the supraspinal gait areas via the BCI and spinal cord gait central pattern generators using feedback via the RoGO may provide a unique form of Hebbian learning. This novel neurorehabilitative therapy could improve neurological outcomes after incomplete SCI beyond those of standard gait therapy.

4.5 BCI-FES System for Overground Walking

After providing convincing evidence that BCI control of ambulation after SCI is possible through the BCI-RoGO [33, 34, 35] and BCI walking simulator studies [32, 84, 81, 107, 145, 146], our laboratory decided to explore lower extremity prostheses for *overground* walking. To this end, FDA-approved and commercially available RoGOs and noninvasive FES devices for overground walking were explored. This included the ReWalk (Argo Medical Technologies, Inc., Marlborough, MA) and the Parastep (Sigmedics, Fairborn, OH) systems, both FDA-approved overground walking devices for those with paraplegia due to SCI. The Parastep device, an FES system for over-

ground walking, was ultimately chosen because this system allows for activation of lower motor neurons using orthodromic and antidromic stimulation. The orthodromic stimulation allows for muscle activation of the lower extremities, while the antidromic stimulation allows for stimulation towards the anterior horn cells of the spinal cord. By integrating such a system with our BCI system, direct brain control of ambulation may be possible, and a neurorehabilitative system that allows for simultaneous firing of both the upper motor neurons (via the BCI) and lower motor neurons (via the antidromic stimulation from the FES) may be possible. If integrated and the feasibility of such a system is possible in an SCI individual with paraplegia, this may become the first restorative treatment for overground walking for those with incomplete motor SCI, and may become the first neuroprosthesis for those with motor complete SCI.

In addition to becoming the first neuroprosthesis or neurorehabilitative device for overground walking after SCI, the BCI driven Parastep device may determine whether an implantable BCI device is feasible, as SCI participants are willing to have a surgery for an implantable BCI driven neuroprosthesis to restore the lost walking function [4, 20]. However, to first test the feasibility of such a system, our laboratory integrated the BCI system with the Parastep device, and assessed the performance of this system over multiple sessions and experimental days on participants with paraplegia due to SCI [79, 80, 82].

4.5.1 Methods

Overview

To ensure safe and proper use of the BCI-Parastep system, an intensive screening process was first performed. Following the participant screening process, BCI walking simulator and Parastep FES training were performed over the course of several weeks

for participants to be able to control both the BCI and FES systems while being weight loaded and overground [79, 80, 82]. Once participants were able to walk the length of the overground walking course using the Parastep system, and were able to purposefully control the BCI walking simulator in the self-paced virtual reality walking course (Section 4.3 above), the BCI and Parastep systems were integrated and evaluated during unloading and overground weight loading conditions [79, 80, 82]. Finally, a complete performance assessment of the system during both of these conditions was performed.

Participant Screening

Since the Parastep system is an FDA-approved device, intensive screening requirements were performed on all recruited participants. Most of the screening tests were performed to ensure safe and proper use of the Parastep system during weight loading, and are described below.

Ethical approval was obtained from the University of California, Irvine. Individuals with paraplegia due to SCI (those with complete loss of motor function in the lower extremities, levels T6–T11) were recruited via physician referral from the University of California, Irvine Medical Center, as well as from Institutional Review Board approved recruitment fliers posted at Project Walk (Carlsbad, CA) and on campus. Exclusion criteria were osteoporosis, fractures, unable to tolerate FES, inability to control the BCI walking simulator, presence of any electronic implant (e.g. pacemaker), presence of pressure ulcers, orthostatic hypotension, poor truncal control, spasms, contractures, or orthopedic malformations that may prevent proper use of the FES system, and any neuromuscular disease, cauda equino syndrome, or pregnancy.

To ascertain the above inclusion and exclusion criteria, recruited participants also underwent several screening exams and imaging to ensure safe use of the Parastep system. This included a dual energy X-ray absorptiometry (DEXA) scan and lower extremity X-rays, tilt table exam, pregnancy test, BCI screening using the BCI driven walking simulator (Section 4.3 above), FES tolerance test, and orthopedic-neurological exams. These procedures were performed to ensure the participant's ability to safely tolerate the FES from the Parastep system as well as weight bearing during ambulation. Finally, the BCI screening was used to ensure that the participant could use our BCI system to control the Parastep device.

DEXA Scan and Lower Extremity X-Rays: Potential users underwent a DEXA scan and lower extremity X-rays to ensure that they are not at risk for developing fractures. To this end, both X-rays and the DEXA scan were performed using standard clinical practices. For the DEXA scan, a Hologic QDR Discovery-A DEXA fan-beam scanner (Hologic, Waltham, MA) and Hologic enhanced software (version 13.3.0.1) were used to calculate the bone mineral density of the entire body and both hips. The T-scores of the measurements (provided by the manufacturer) were used to determine their risk of fracture given their ethnicity, gender, and age. Finally, bilateral knee, ankle, hip, femur, and tibia/fibula X-rays were performed using a General Electric MVP 80 diagnostic X-ray unit (General Electric, Fairfield, CT) with Fuji computed radiography imaging plates (Fujifilm USA, Cypress, CA) to determine if there were any deformities or fractures in the lower extremities.

Tilt Table Exam: To assess orthostatic hypotension and weight bearing ability, a tilt table exam was performed using standard clinical practices. During this test, participants must not have exhibited symptoms of orthostatic hypotension with a gradual or immediate elevation to 90°, a drop in systolic blood pressure by more than 20 points, or a drop in diastolic blood pressure by more than 10 points after 3 min.

FES Screening: A Parastep FES tolerance test was performed prior to training to determine if any adverse responses (e.g. autonomic dysreflexia) would occur during Parastep FES training. To this end, FES electrodes were applied to the bilateral quadriceps, tibialis anteriors, and gluteal muscles. The test unit of the Parastep system (provided by the manufacturer) was then used to stimulate these muscle groups. The participant's ability to tolerate FES stimulation as well as their level of discomfort and pain were recorded, along with their ability to generate an effective muscle response.

BCI Screening: To determine whether participants could use our BCI system to control Parastep induced walking, the BCI walking simulator system [32, 84, 81, 107, 145, 146] (Section 4.3 above) was used. Briefly, the actively shielded 64-channel EEG cap (Medi Factory, Heerlen, The Netherlands) described in Section 2.2 of Chapter 2 and in Fig. 1.3 of Chapter 1 was mounted on the participants' head and impedances were reduced to $<$10 KΩ. Note that only 24 channels were selected (Fig. 2.1 in Section 2.2 of Chapter 2) because: (i) the EEG amplifier could only handle 24 channels over wireless bluetooth communication, (ii) they are less prone to motion and electromyogram (EMG) artifacts, and (iii) most of the chosen channels are located over the motor cortex while still covering other brain areas. An EEG amplifier (Mind Media, Roermond-Herten, The Netherlands) was then used to amplify (gain: 20), band-pass filter (0.01-50 Hz), and digitize (sampling rate: 256 Hz, resolution: 22 bits) the EEG signals. They were finally wirelessly streamed to the computer in real-time via bluetooth connection, and subsequently re-referenced in a common average mode.

Prior to online operation of the BCI walking simulator system, participants first underwent the same short 10 min offline training procedure as described in the BCI walking simulator studies [32, 84, 81, 107, 145, 146] (Section 4.3 above). Fig. 4.17

depicts a screen shot of the offline training procedure, where participants performed alternating epochs of attempted walking and idling while their EEG were recorded while following computer cues. In addition to their EEG, audio and synchronization signals were recorded via an auxiliary data acquisition system (MP150, Biopac Systems, Goleta, CA) to be able to distinguish between "Idle" and "Walk" states (Fig. 4.17). Finally, participants were asked to remain still during the entire procedure, and their movement was monitored by the experimenter. If overt movements were observed, the participant was asked to repeat the entire training procedure without making the undesired movements.

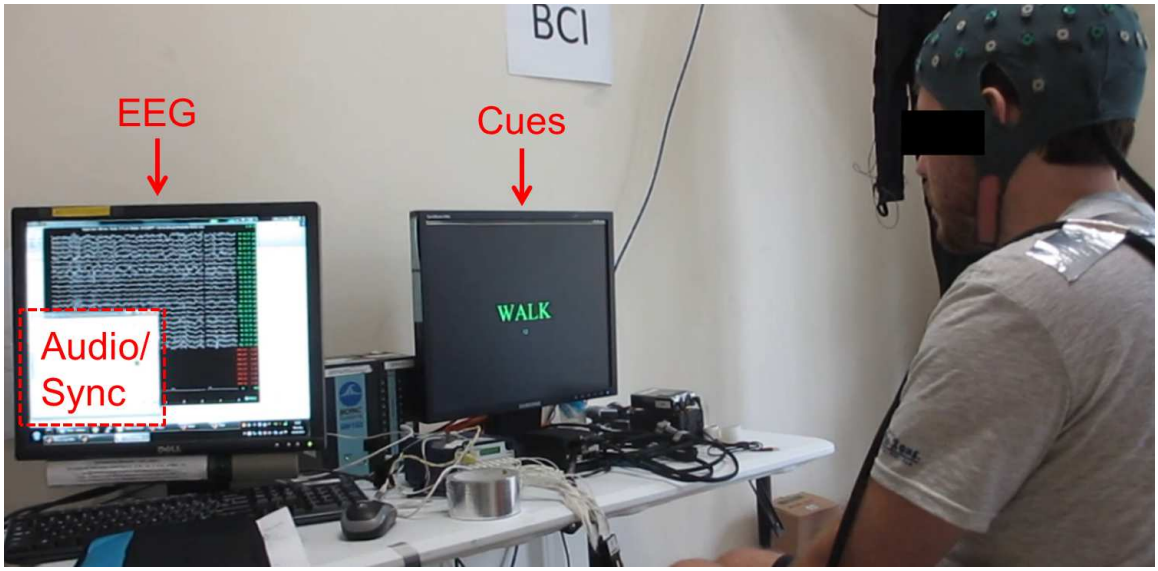

Figure 4.17: Screen capture of the offline training procedure. Note that the screen with the EEG and the synchronization and audio cues was not visible for the participants.

After the short training procedure, participant-specific EEG decoding models similar to the BCI driven walking simulator studies [32, 84, 81, 107, 145, 146], and described in Section 2.4 of Chapter 2, were developed. To this end, EEG and audio signals (the audio was turned on during a "Walk" cue and off during an "Idle" cue) were synchronized using the common pulse train, and then segmented into ∼4 s long trials of "Idling" and "Walking" using the audio data. The EEG trials were then

transformed into the frequency domain, and their PSDs were integrated over 2-Hz bins from 6-40 Hz. The data then underwent dimensionality reduction using CPCA, and discriminating features were extracted using either Fisher's linear discriminant analysis [47] (LDA) or AIDA. A detailed description of these techniques are described in Section 2.4.1 of Chapter 2 and in Appendix A.3. Finally, a linear Bayesian classifier was designed in the feature domain (Section 2.4.2 of Chapter 2 and Appendix A.4), and the performance of the classifier was determined through stratified 10-fold cross-validation (Appendix B.1).

During online operation, 0.75 s segments of EEG data were acquired in real time via bluetooth communication every 0.25 s in a sliding window. The PSD of the EEG channels were calculated for each of these segments, and was used as the input for the EEG decoding models. The posterior probabilities of "Idling" and "Walking" classes given the observed EEG feature were calculated using the Bayes' rule (Eq. 2.2 in Section 2.4.2 of Chapter 2), and were averaged over a 1.5 – 2.0 s sliding window to minimize the false alarm and omission rates.

Prior to performing the online BCI walking simulator experiments, a brief calibration session was performed to reduce noise during online operation. As mentioned in the previous BCI walking simulator studies [32, 84, 81, 107, 145, 146] and BCI-RoGo study [33, 34, 35] presented above (Sections 4.3 and 4.4), the BCI system was ran in the online mode (with the walking simulator turned off) while the participant alternated between idling and attempted walking for $\sim$5 min. The values of the averaged posterior probabilities were then plotted in a histogram to determine the values of the thresholds for the binary state machine, T_I and T_W, and these values were fine-tuned in a brief familiarization session.

For the online experiments, participants performed 1–5 online sessions of the goal-oriented and self-paced BCI walking simulator task within the virtual reality envi-

ronment described in Section 4.3 above [32, 84, 81, 107, 145, 146]. Specifically, participants were instructed to utilize attempted walking and idling to control the linear ambulation of an avatar and make 10 sequential stops at designated points within the virtual reality environment (see Fig. 4.2). Note that participants were able to choose either 1st or 3rd person view to operate the avatar, and the screen shot in Fig. 4.2 is in 3rd person view. The results of this task (i.e. the number of successful stops and course completion time) were compared to random walk Monte Carlo simulations to assess purposeful control (Section 4.3 above). If purposeful control was not achieved by the 5th BCI screening session, the participant was excluded from the rest of the study.

BCI Walking Simulator Training

The BCI walking simulator training session was performed in a similar manner to the BCI screening experiments above and the BCI walking simulator studies [32, 84, 81, 107, 145, 146] described in Section 4.3. Specifically, participants underwent the short 10 min offline training procedure where they alternated between epochs of attempted walking and idling while their EEG were recorded on each BCI training day [79, 80, 82]. Then, a participant-specific EEG decoding model was developed and a brief calibration procedure was performed to find the optimal parameters for online operation for that day. Once the models and parameters were determined, participants then performed 1–5 online sessions of the goal-oriented and self-paced BCI walking simulator task described in Section 4.3 above [32, 84, 81, 107, 145, 146]. To this end, the participants utilized attempted walking and idling to control the linear ambulation of an avatar while making 10 sequential stops at designated points within the virtual reality environment (Fig. 4.2 in Section 4.3). This entire procedure was repeated until the BCI-FES integration and evaluation sessions to ensure that

the participants could retain the learned brain-controlled attempted walking task.

Parastep Training

The guidelines of the Parastep system required the participants to recondition their muscles prior to gait training and BCI-FES evaluation. This allowed the participants to improve the efficiency of their cardiovascular and respiratory systems, as well as reduce their level of muscle atrophy in the lower extremities. To this end, participants performed strength training of the quadriceps with a physical therapist and at-home exercises using the E-unit FES device to develop endurance. Once the physical therapist determined that the participant regained sufficient strength and endurance, and demonstrated the ability to stand using the Parastep, the training sessions progressed to the movements required for overground gait training.

Quadriceps Strengthening Exercises: The purpose of the quadriceps strength training exercises was to ensure the participant's ability to stand with 85% of their weight bearing in their legs. To accomplish this, participants performed FES stimulation of the quadriceps to extend their leg while seated. This was repeated with increasing ankle weights until the participant was able to fully extend the leg while bearing 10% of his/her body weight without fatiguing.

At-Home Exercises: Participants were encouraged during the duration of the study to perform daily at-home exercises using the E-unit FES device. This device delivered stimulation to the quadriceps, and could be switched to stimulation of the step reflex via FES of the tibialis anteriors while preventing the user from walking. Depending on their strength and endurance, participants were encouraged to perform 10–15 s of FES stimulation of the quadriceps while wearing weights around the ankle until he or she fatigued. Note that the amount of weight lifted from the ankle via ankle weights

depended on the participant's strength. In addition, participants were instructed to perform leg extension exercises by stimulating the tibialis anteriors for 10 – 15 s, and repeating this procedure until each leg fatigued. These exercises were performed to improve the strength of both quadriceps and tibialis anteriors, and instructions were adjusted depending on the participant's current strength and endurance during overground gait training.

Overground Gait Training: The overground gait training for the Parastep system with the physical therapist first focused on learning the specific coordination of movements that result in standing and walking. This included the following biomechanical requirements:

1. Standing posture: anterior-posterior alignment, left-right alignment while standing
2. Weight-bearing support: standing 85% of the body's weight through the legs
3. Dynamic balance: standing and walking without toppling over
4. Gait cycle: the ability to perform toe off, swing through, and heel strike
5. Weight transfer: the ability to transfer weight in the anterior-posterior direction and in the lateral direction for advancement and body weight transfer, respectively
6. Walker management: progress and place the walker properly during standing and walking
7. Locomotion and ambulation: perform walking without the intervention of another person for a distance of >3.66 m (>12 ft)

Once the participant was able to comfortably perform all of the above tasks, overground gait training was continued until the participant could walk the length of the overground walking course (3.66 m, 12 ft) without any intervention from the physical therapist. This procedure continued throughout the study to ensure safe and proper use of the Parastep system during BCI-Parastep operation. Also, all of the above procedures were performed while the participant was mounted in a ZeroG body weight support system (Aretech LLC., Ashburn, VA) to prevent any falls during Parastep training and BCI-Parastep evaluation. The ZeroG system was set to a 2 in fall distance and 60% body weight support, values empirically determined by the limitations of the system itself (it would not catch the person unless weight unloading was applied) and the experimenters during Parastep training and BCI-Parastep evaluation.

BCI-Parastep Integration and Physical Sensor Development

In order to facilitate BCI control of the Parastep system, the Parastep device was integrated with the computer via a microcontroller (Arduino, SmartProjects, Torino, Italy). This was accomplished by replacing the 3 manual switches (i.e. sit/stand, left step, and right step) of the Parastep system with digital relays (Relay shield V2.0, Seeed Technology Inc., Shenzhen, China) that were interfaced with the microcontroller (Fig. 4.18). Then, via a wireless bluetooth connection (Bluetooth Mate Silver, Sparkfun Electronics, Boulder, CO), the Parastep system was wirelessly controlled by the computer and microcontroller. Finally, to simulate linear ambulation, the step timings from the Parastep training sessions were analyzed via video recordings from the overground gait training, and a custom C++ program was uploaded to the microcontroller to execute an automatic, cyclic stepping pattern that closely mimicked the FES induced stepping pattern of the participant. The microcontroller

only executed these movements upon commands given by custom written Matlab (Mathworks, Natick, MA) programs.

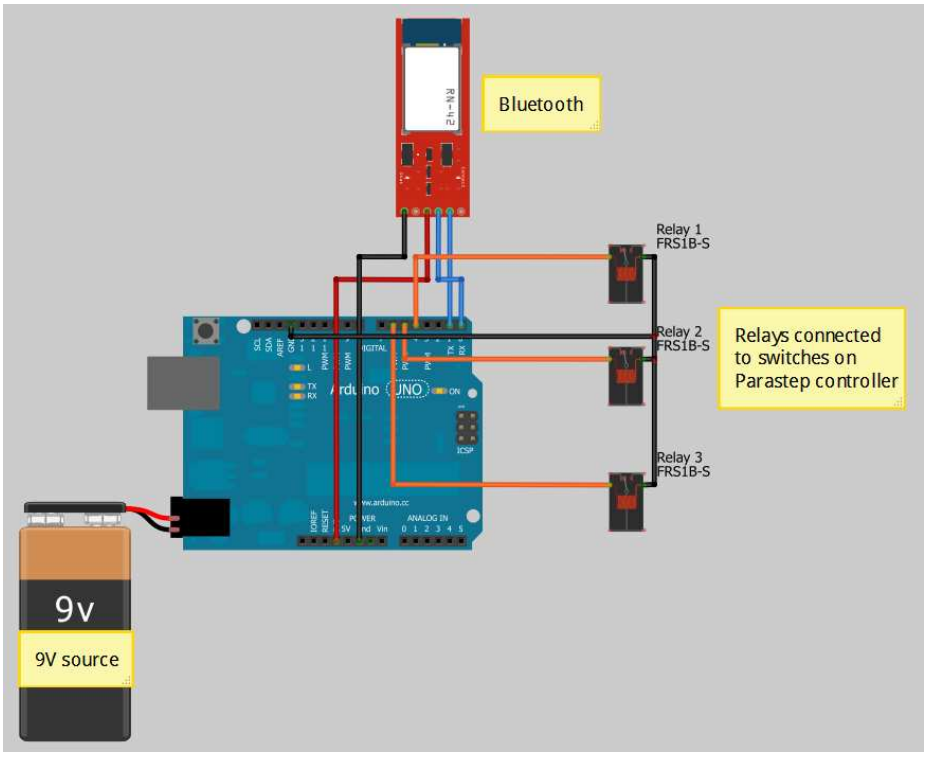

Figure 4.18: Overview schematic of the microcontroller used to wirelessly control the Parastep system using the BCI system.

In addition to integrating the BCI system with the Parastep device, a physical sensor measurement system was developed to be able to analyze the real-time control of the BCI-Parastep system. To this end, 2 gyroscopes (L3G4200D, STMicroelectronics, Geneva, Switzerland) and a laser distance meter (411D Laser Distance Meter, Fluke Corporation, Everett, WA) connected to a microcontroller (LR3 Laser Rangefinder Interface, Porcupine Electronics LLC., Cedar Park, TX) were integrated with a master microcontroller unit (Arduino). A synchronization signal was also integrated with the master microcontroller unit, and wired to the EEG amplifier of the BCI-Parastep system to be able to align all real-time data for subsequent analysis. Then, via another wireless bluetooth communication (Bluetooth Mate Silver), the master mi-

crocontroller unit sent gyroscope, laser, and synchronization data to the computer in real time. This data was plotted and saved using custom written Matlab (Mathworks) programs.

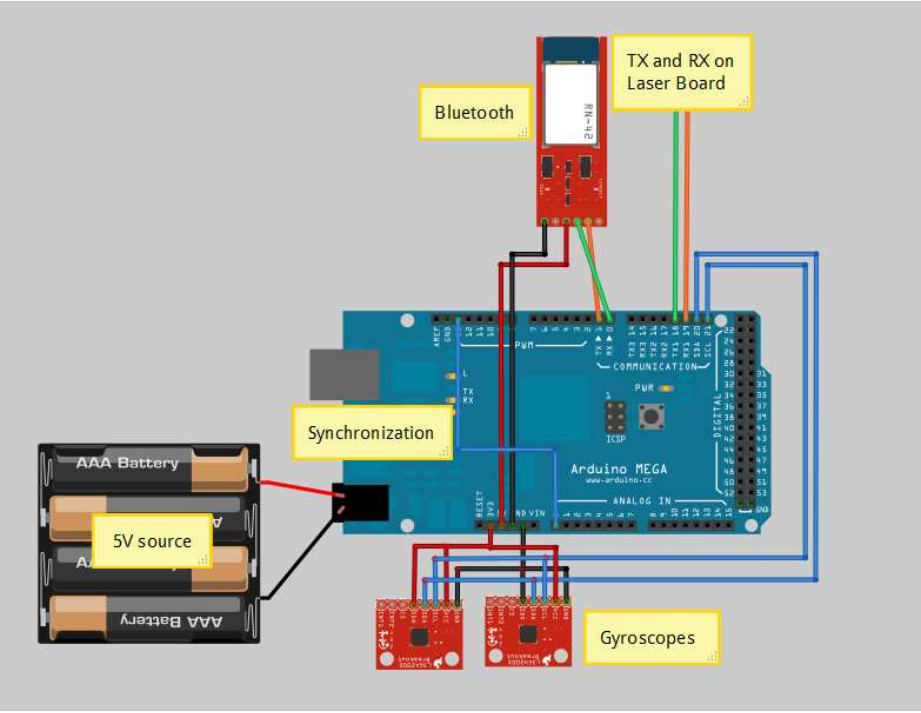

Figure 4.19: Overview schematic of the physical sensor measurement microcontroller unit and system for BCI-Parastep evaluation.

The BCI-Parastep system and physical measurement system were mounted on the participants using a custom-made belt pack and backpack. The custom-made belt pack housed the Parastep microcontroller unit, while the custom-made backpack housed the EEG amplifier and physical sensor system. Once all of these devices were mounted on the participant, postural stability was assessed and Parastep induced standing and walking was tested to ensure safe and proper use of the BCI-Parastep system. Finally, all real time experiments were videotaped, and these video recordings were aligned with all data using the synchronization signal and an light emitting diode (LED) mounted on the walker of the Parastep.

BCI-Parastep Online Experiments

The BCI-Parastep experiments were only performed after the experimenters and physical therapist determined that the participant could safely walk the length of the overground walking course while being weight loaded. After BCI and Parastep training were deemed complete, participants performed several suspended walk tests in which they conducted alternating epochs of idling and BCI-Parastep mediated walking while following computer cues [79, 80, 82]. Participants then performed overground walking tests over the course of several weeks to months in which they used BCI-Parastep mediated standing and walking to idle and walk in a self-paced overground course [79, 80, 82].

Suspended Walking Tests: Prior to performing the overground walking course using the BCI-Parastep system, participants performed suspended walking tests in which they performed BCI-Parastep mediated walking and idling (i.e. standing) while being completely suspended off the ground using the ZeroG system. Specifically, participants were positioned 1 m from a computer monitor, and the ZeroG unloaded the participants so that their toes were > 5 cm off the ground (see Fig. 4.20). This, along with the Parastep walker, allowed the participants to perform BCI-mediated Parastep walking without moving toward or away from the computer screen. Participants were then asked to perform 5 trials of alternating 30 s epochs of idling and attempted walking to control the BCI-Parastep system in real time. The performance of this experiment was assessed using the video recordings, BCI, and physical sensor data.

Overground Walking Course: The 3.66 m (12 ft) overground walking course [79, 80, 82] consisted of 3 cones positioned 1.83 m (6 ft) apart (see Fig. 4.21). To test the BCI-Parastep system in a self-paced real time condition, participants were asked to remain idle at each of the 3 cones for 10–20 s given verbal cues by the experimenter.

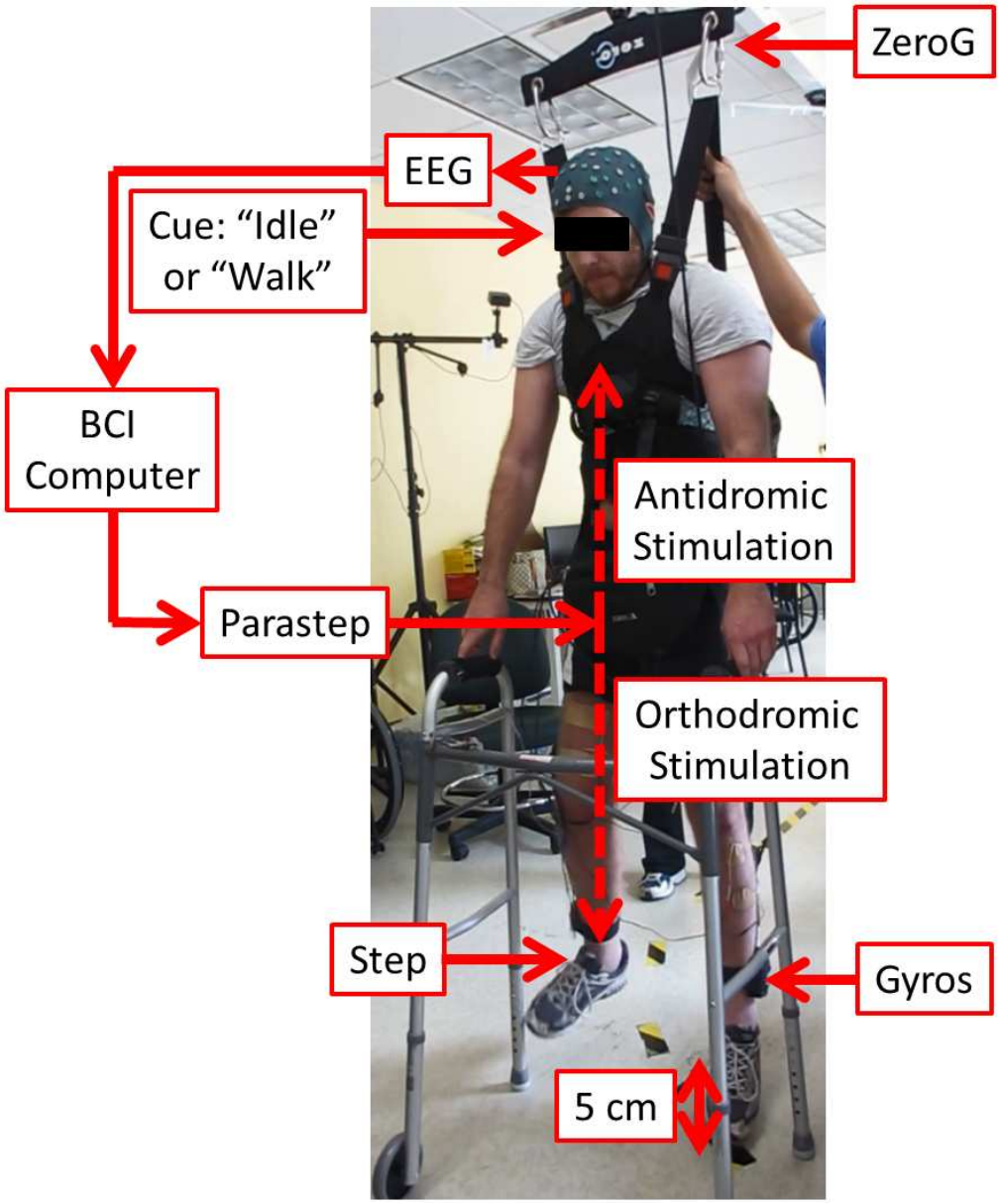

Figure 4.20: Experimental setup of the suspended walking tests for the BCI-Parastep study, showing the the participant suspended 5 cm off the ground in the ZeroG while wearing an EEG cap, the Parastep system, and gyroscopes on each leg. A monitor (not shown), placed in front of the participant at eye-level, presented instructional cues. Note that the walker was used by the participant for balance while suspended.

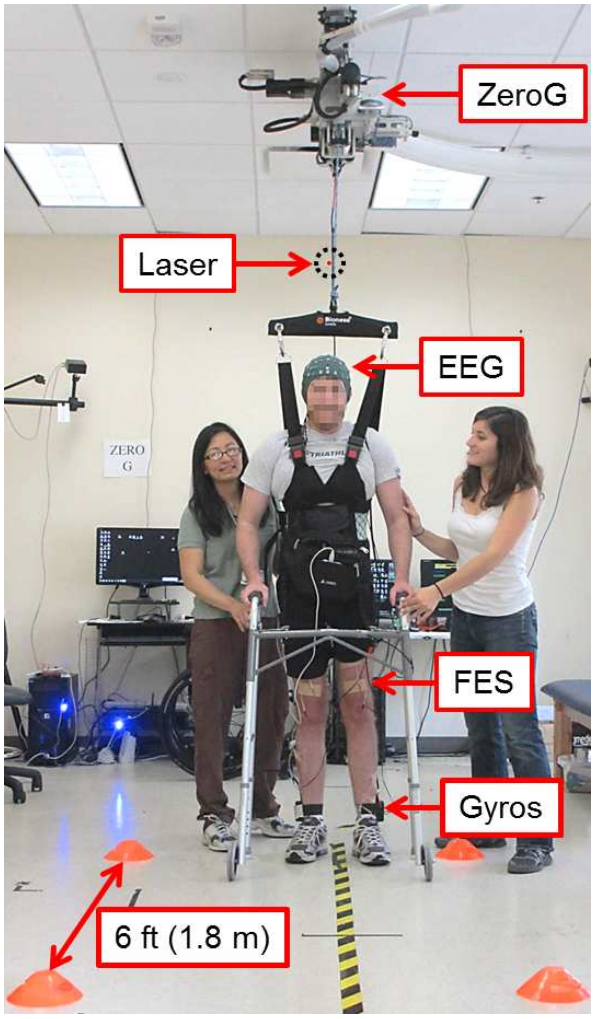

Figure 4.21: Schematic of the overground walking course, depicting the EEG based BCI system, Parastep FES device and walking, the gyroscopes and laser distance meter, and the ZeroG body weight support system. Note that only 2 of the 3 cones are shown in the figure [79, 80, 82] (© 2014 IEEE).

Then, the participant used BCI-Parastep mediated walking to walk to the next cone. Note that verbal cues were only given by the experimenter to help guide the user through the course, help assess the timing of the idling periods, and the duration of idling was randomized to prevent any anticipation by the participant. Also, the participants were weight loaded (2 in fall distance, 60% unloading), as the ZeroG was used in this condition solely to prevent any falls.

Performance Assessment

To assess the performance of all the BCI tests (i.e. the walking simulator, suspended walking tests, and the overground walking experiments), analysis of the BCI, physical sensors, and video recordings was performed [79, 80, 82]. This was accomplished by first aligning the data using the common synchronization signal. Then, the performance of the BCI system, as well as the integrated BCI-Parastep system, were analyzed using the aligned data with custom written Matlab (Mathworks, Natick, MA) programs. Finally, Monte Carlo simulations (Appendix B.3) were used to assess whether these performances were purposeful.

BCI Walking Simulator Analysis: The performance of the BCI driven walking simulator during both BCI training and BCI screening was assessed using 2 performance measures [32, 84, 81, 107, 145, 146]: (i) the number of successful stops and (ii) the course completion time. As described in Section 4.3 above, the number of successful stops ranged between 0–10 points, where 1 point was given for dwelling at the designated stop for at least 2 s, only a fraction of a point was given for dwelling at the designated stop between 0.5 and 2 s (increasing proportionally with the dwelling time), and no point was given for dwelling less than 0.5 s. Finally, a full point was awarded for dwelling longer than 2 s, but this inherently increased the course completion time.

Similar to the BCI walking simulator studies [32, 84, 81, 107, 145, 146], the number of successful stops and course completion time were combined to create a single composite score (Appendix B.4, Section 4.3) to the BCI walking simulator performances. As previously mentioned, the composite score ranged from 0 to 100%, where 100% corresponds to a perfect performance. Note that the composite score used the geometric mean of the successful stop score and course completion time, ensuring a

unitless measurement to compare performances across participants and experimental days.

To determine purposeful control [32, 84, 81, 107, 145, 146], the composite score of the BCI walking simulator online sessions was compared to random walk simulations. This was done by comparing the composite score of each online session to 10,000 Monte Carlo simulations. The Monte Carlo simulations described in Appendix B.3 and further described in Section 4.3 above, were then used to empirically determine the p-value, the fraction of Monte Carlo runs that achieved a higher performance than the participants' online session.

Suspended Walking Analysis: The suspended walking tests were analyzed by performing cross-correlation and information transfer rate (ITR) analyses on the aligned BCI, physical sensor, and video recording data. Specifically, cross-correlation analysis (Appendix B.2) between the computer cue and BCI-Parastep mediated walking and idling was performed to determine the latency (lag) and maximal temporal correlation (ρ). From this data, the number of false alarms and omissions, as well as the duration of these errors, were also calculated (Appendix B.5), and purposeful control was assessed through 10,000 Monte Carlo simulations using the methods described in Appendix B.3. As previously mentioned, a false alarm was defined as the initiation of BCI-Parastep mediated walking within any idling epoch; an omission was defined as the absence of BCI-Parastep mediated walking within any "Walk" computer cue epoch. Finally, the ITR (in bits/s) was calculated using equal priors (0.5) at the lag determined from the cross-correlation analysis (Appendix B.4).

Overground Walking Analysis: The overground walking tests were assessed by performing cross-correlation and ITR (at the lag determined from the cross-correlation analysis) analyses between the verbal cues (as recorded by the video data) and the state of the BCI (i.e. "Idle" or "Walk"). In addition to these analyses, cross-

correlation analysis between the verbal cues and gyroscopes, and between the BCI state and gyroscopes, were performed. The number of false alarms and omissions were also calculated as explained in the suspended walk analysis described above. Finally, 10,000 random walk Monte Carlo simulations were used to assess purposeful control of each overground BCI-Parastep mediated walking performance.

4.5.2 Results

Participant Screening

Four SCI participants were recruited for this study, and their demographic data are shown in Table 4.12. Out of these recruited participants, only 1 was eligible for the study. This is because the participants were either unable to comply with the experimental protocol, physically unable to safely tolerate FES stimulation and weight bearing due to a high risk of autonomic dysreflexia, or were unable to commit to the experimental time requirements.

Table 4.12: Demographics of the recruited participants for the BCI-Parastep study. Note that the participant (Pt.) with a * was the only participant that passed the screening evaluation and participated in the full study.

Pt.	Age	Sex	SCI Status
1	23	Male	T11, ASIA B, 3 yrs. post injury
2*	26	Male	T6, ASIA B, 5 hrs. post injury
3	25	Female	T3–T4, ASIA B, 2 yrs. post injury
4	33	Male	T6, ASIA B, 5 yrs. post injury

The participant that passed the screening evaluation was an active 26 year old male with paraplegia. After a traumatic injury of the spinal cord in 2008, he has a complete motor lesion below T6 and an incomplete sensory lesion below T7 (ASIA B). Also, the participant has full passive range of motion in the hips, knees, and ankles, but has a slight contracture in his left leg.

Training

The BCI and Parastep screening and training resulted in the time line shown in Fig. 4.22 for the selected SCI participant. Note that the Parastep training took the longest time for this participant, as up to 32 one hour sessions are encouraged by the Parastep manual to be able to master the biomechanical requirements of overground walking. However, the participant was able to master these requirements after only 15 Parastep training sessions, or 22.5 hours of physical therapy. In addition, even though the participant obtained perfect BCI control of the walking simulator after only 11 hours of training, the BCI training continued until the end of the study to ensure that the participant could maintain the attempted walking control strategy and high-level of BCI performance.

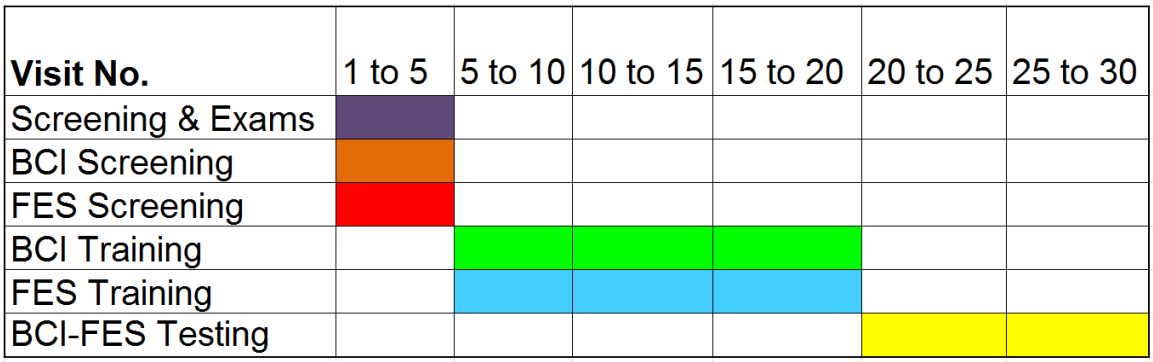

Figure 4.22: Experimental time line of the SCI participant that participated in the full BCI-Parastep study.

BCI Walking Simulator Training

The BCI training sessions described above were performed in conjunction with each Parastep training session to ensure the participant's ability to retain the learned attempted walking control strategy. On each training day, a participant-specific EEG decoding model was developed and a brief calibration procedure was performed to

determine the optimal parameters for online BCI operation. After performing cross-validation on these decoding models, it was found that the offline EEG decoding models improved over time. Specifically, the classification accuracies presented in Fig. 4.23 show that the participant was able to learn the BCI-walking task on the 1st experimental day (chance level being 50%), and was able to achieve a perfect offline classification accuracy (100.00±0.0%) by the 15th BCI training day.

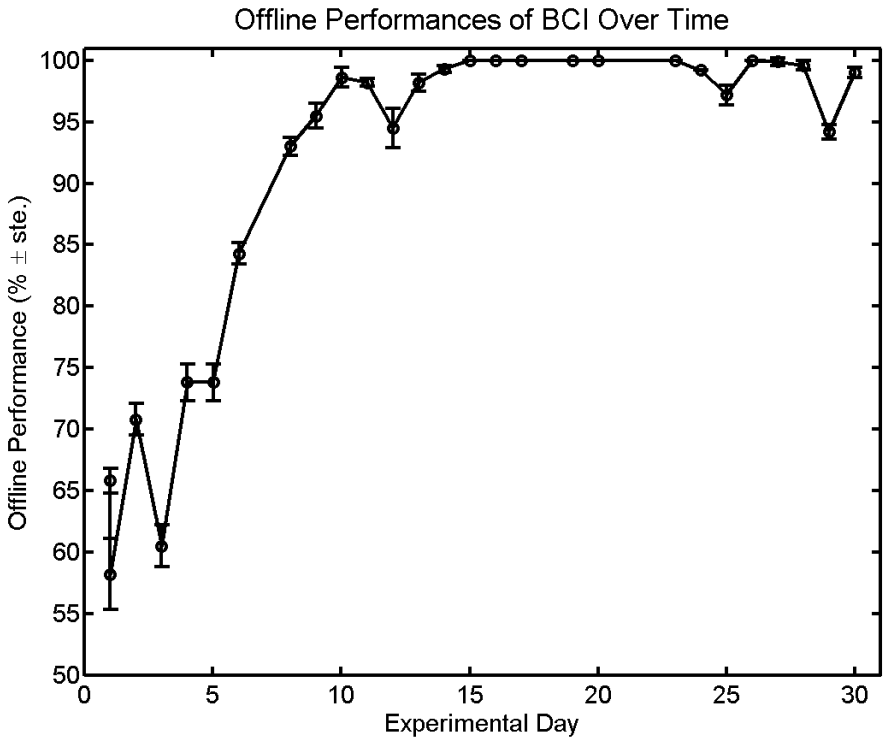

Figure 4.23: Offline performances (in %) of the BCI training sessions for the SCI participant in the BCI-Parastep study. Standard errors of the mean (ste.) are displayed as error bars.

The participant-specific offline EEG decoding models resulted in spatio-spectral features that converged to similar frequencies and brain areas across experimental days. This can be seen in Fig. 4.24, where salient features were found in the low-β (13 – 16 Hz) and high-β (20 – 28 Hz) frequency bands over the C3 and C4 electrodes and the Cz and CPz electrodes, respectively [82]. Furthermore, these features varied during the first 10 – 15 experimental days of BCI training, and then converged to

features similar to that of Fig. 4.24 towards the end of the study. Even though the EEG decoding models converged to similar features toward the end of the study, the BCI training procedure was still performed on each experimental day to optimize the online performance of the BCI-Parastep overground walking tests.

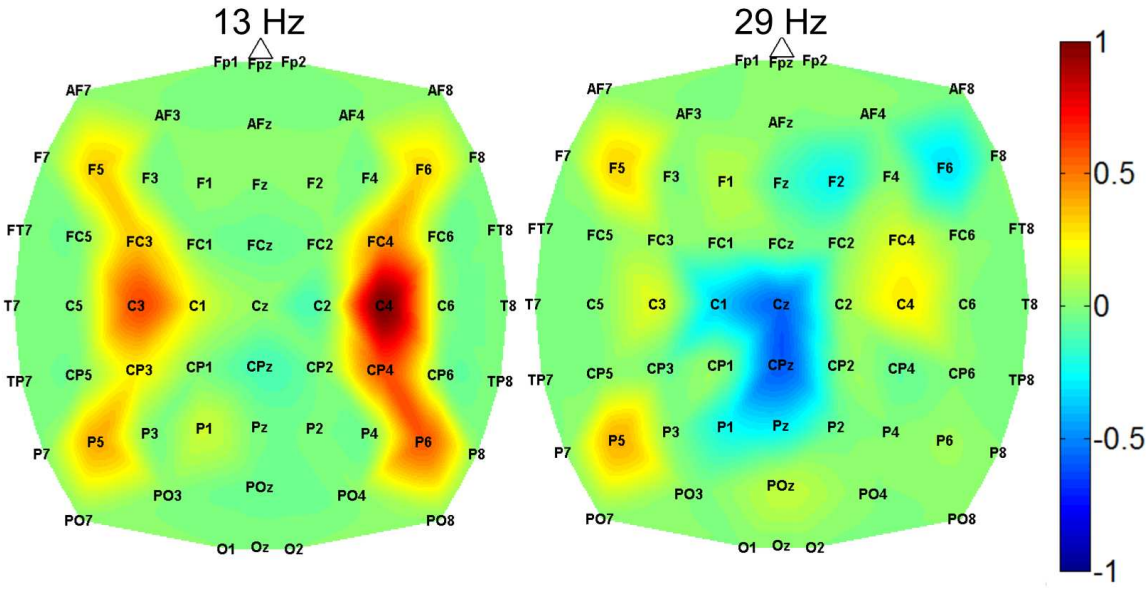

Figure 4.24: Offline feature extraction images of the SCI participant on the 24$^{\text{th}}$ experimental day [82] (© 2014 IEEE). Two images are presented, one for the 13 Hz bin and the other for the 29 Hz bin for the "Walk" class.

The BCI walking simulator online tests resulted in online performances that also improved over time. For instance, the number of successful stops approached 10 points (a perfect score) and the course time approached the manual joystick time (205.07±4.2 s, see Table 4.7 in Section 4.3) by the 11$^{\text{th}}$ experimental day. This can be seen in Fig. 4.25, which shows the mean and variance of the cone stop score and course time for each experimental day during the BCI training sessions. Specifically, the figure shows that the variance of the walking simulator online scores decreased over time, while the mean cone score improved and the mean course time decreased toward the end of the study.

The combined cone stop score and course time of the BCI walking simulator training

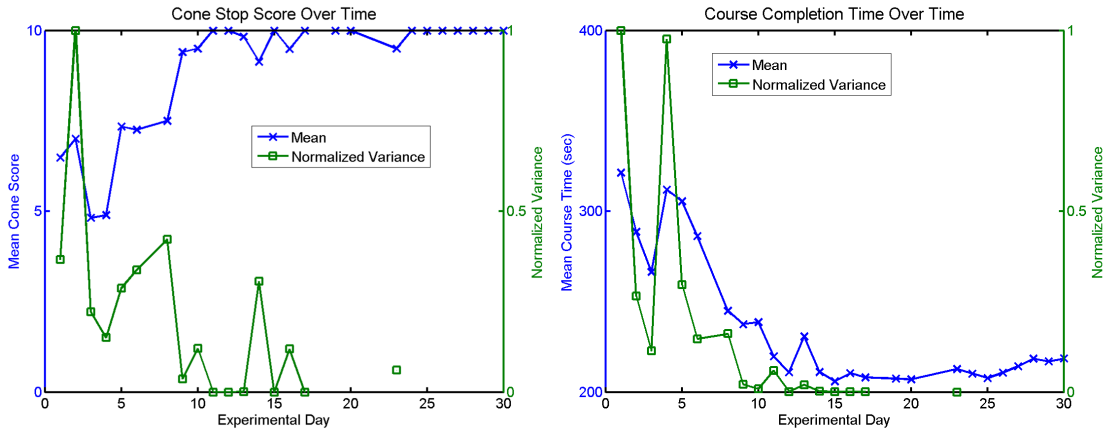

Figure 4.25: Cone score (left plot) and course times of the BCI training sessions for the SCI participant in the BCI-Parastep study. The mean (blue) and normalized variance (green) are presented for each experimental day.

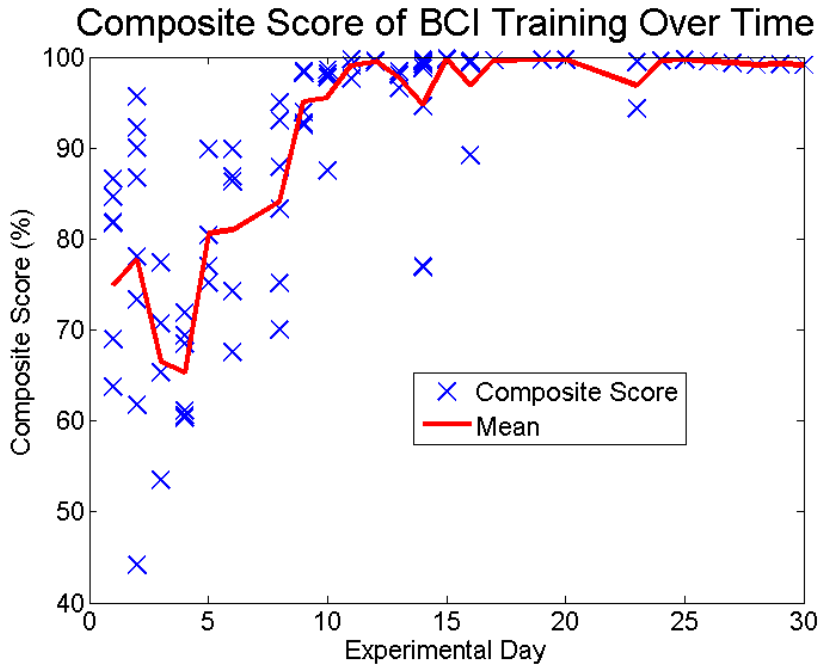

Figure 4.26: Composite scores of the BCI training sessions for the SCI participant in the BCI-Parastep study [82] (© 2014 IEEE). Individual performances are blue, and the mean for each experimental day is red.

resulted in a composite score that ranged from 0% to 100%, where 100% corresponds to a perfect performance. Since the number of successful stops and course time of the BCI walking simulator training improved over time, the composite scores also improved. This can be seen in Fig. 4.26, where the mean and normalized variance of the composite score are depicted [82]. The composite scores also approached a perfect performance (100%) by the 11^{th} experimental day. Finally, as determined from the Monte Carlo simulations (p-value$< 10^{-4}$), all composite scores were deemed purposeful since the 1^{st} experimental day.

Parastep Training

The Parastep training required the SCI participant to perform FES strength training with a physical therapist and at-home exercises to develop strength and endurance prior to overground gait training. Specifically, the participant's strength and endurance were first assessed during the FES screening process in which the physical therapist and neurologist assessed several factors, including spasticity, active range of motion, and contractures. It was noted that the SCI participant that performed the full study had a slight contracture in his left leg, but it was determined that he was still physically capable of performing Parastep FES training and could participate in the full BCI-Parastep study.

After the screening process, the SCI participant was instructed to perform at-home quadricep exercises in which he used the E-unit FES device to lift 1-10 lbs for 15 s, and rested for 30 s in between each lift until his quadriceps fatigued. Once the participant was able to do this comfortably without fatiguing quickly (this occurred by the 15^{th} experimental day), the participant was then instructed to perform triple flexion response exercises in addition to the quadricep exercises. The purpose of this additional exercise was to improve the participant's strength and endurance in

his tibialis anteriors, as reliably obtaining the triple flexion response was difficult during physical therapy due to the contracture in his left leg. Finally, in addition to the above at-home exercises, the participant was encouraged to perform as many standing sessions as possible using his standing frame at home to improve his muscle strength during standing as well as his postural stability.

Table 4.13: Experimental days taken for each Parastep FES movement training task. Note that the 1st BCI-Parastep experimental session occurred on the 20th experimental day, as the participant was able to comfortably use the Parastep system to walk >3.66 m (>12 ft), on experimental day 19, reaching up to 23.01 m (75.5 ft).

Experimental Days	Parastep FES Movement Training
5–10	Standing posture: anterior-posterior alignment and left-right alignment while standing
11–12	Weight-bearing support: standing 85% of the body's weight through the legs
11–12	Dynamic balance: standing and walking without toppling over
13–14	Gait cycle: the ability to perform toe off, swing through, and heel strike
11–14	Weight transfer: the ability to transfer weight in the anterior-posterior direction and in the lateral direction for advancement and body weight transfer, respectively
15–16	Walker management: progress and place the walker properly during standing and walking
16–19	Locomotion and ambulation: perform walking without the intervention of another person for a distance of >3.66 m

For the Parastep FES physical therapy, the SCI participant performed 1 – 2 weekly sessions of FES training to be able to obtain the ability to stand, support his body weight, postural stability and weight transfer, and progress safely down the overground walking course using the FES system. A breakdown of these weekly sessions and his ability to properly use the Parastep system to ambulate down the overground walking course can be seen in Table 4.13. Note that since the Parastep device is an FDA-approved device, these FES sessions were based on the guidelines of the Parastep system presented in the overground gait training section above.

BCI-Parastep Online Experiments

Once the BCI and physical therapy with the Parastep system were deemed complete, as the SCI participant was able to safely ambulate down the overground walking course, the BCI and Parastep systems were integrated and the suspended and overground walking experiments were performed. This occurred after the 19^{th} experimental day. Prior to performing the overground walking course using the integrated BCI-Parastep system, the suspended walking tests were performed. Here, the participant utilized BCI-Parastep mediated walking and idling in response to textual cues on a screen while completely suspended off the ground using the ZeroG system. After performing 2 suspended walking tests on the 20^{th} and 21^{st} experimental days [79, 80, 82], an ITR as high as 3.643 bits/s was obtained (Table 4.14). Additionally, the SCI participant was able to perform this task purposefully (p-value$< 10^{-4}$) with cross-correlation coefficients as high as 0.957 at a 4.25 s lag, and with no omissions and false alarms during the 2^{nd} suspended walking test. Finally, the suspended walking tests resulted in an average cross-correlation of 0.937 at a 3.630 s lag, 1 false alarm for 1.750 s across both tests, 0 omissions across both tests, and an average ITR of 3.342 bits/s (Table 4.14).

Table 4.14: Performances of the 2 online suspended walking tests [79, 80, 82] (© 2014 IEEE). The participant alternated between 5 trials of 30 s of idling and attempted walking while completely suspended off the ground given textual cues. Cross-correlation (ρ, lag, p-value$< 10^{-4}$ for all sessions) and ITR (at the lag determined by the cross-correlation analysis and using equal priors) between the cues and the participant's FES induced walking are shown. False alarms (FA and duration, dur.) and omissions (OM) were also determined for each test.

Expm. Date No.	ρ	Lag (s)	FA	FA Dur.	OM (s)	ITR (bits/s)
20	0.917	3.00	1	1.75	0	3.041
21	0.957	4.25	0	0	0	3.643
Avg.	0.937	3.630	0.500	0.880	0	3.342

Given the promising results from the BCI-Parastep suspended walk tests shown above, the participant performed the overground walking tests on the same experimental days (starting on day 20), and continued to perform these tests until the end of the study, on the 30th experimental day. A video describing one of the best overground walking tests can be seen at <http://www.youtube.com/user/UCIBCI>, where the video is titled "Person with Paraplegia Uses a Brain-Computer Interface to Regain Overground Walking". In addition, the time course plot of this particular session, depicting the laser, gyroscope, verbal cues (as determined from the video recording), and BCI data can be seen in Fig. 4.27. As seen in the video and representative time course plot, the participant was able to idle and walk to each cone without any false alarms or omissions, and only stopped 0.17 m away from the 2nd cone due to the distance of his stride length using the Parastep FES system. For comparison, a representative time course plot of the 3rd overground walking test on the 23rd experimental day is shown in Fig. 4.28 [82]. It can be seen in this plot that the participant had 0 omissions and 1 very small false alarm at the start of the 2nd "Walk" cue, but was able to stop perfectly at each cone.

Overall, the SCI participant was able to perform 1 – 6 overground walking tests each experimental day, and his endurance and ability to perform more overground walking tests improved over time (see Fig. 4.29), resulting in 30 overground walking sessions total. From the cross-correlation analysis, it was found that the participant averaged a 0.797 ± 1.658 correlation at a 2.561 ± 4.154 s lag between the verbal cues and BCI state, and a 0.773 ± 0.174 correlation at a 2.987 ± 4.196 s lag and 0.775 ± 0.164 correlation at a 2.861 ± 4.229 s lag between the left and right gyroscopes and the verbal cues, respectively. Furthermore, the participant averaged 0.865 ± 0.100 correlation at a 0.914 ± 1.349 s lag between the BCI state and left gyroscope, and a 0.868 ± 0.089 correlation at a 0.706 ± 1.297 s lag between the BCI state and right gyroscope. A breakdown of these cross-correlation results can be seen in Table 4.15.

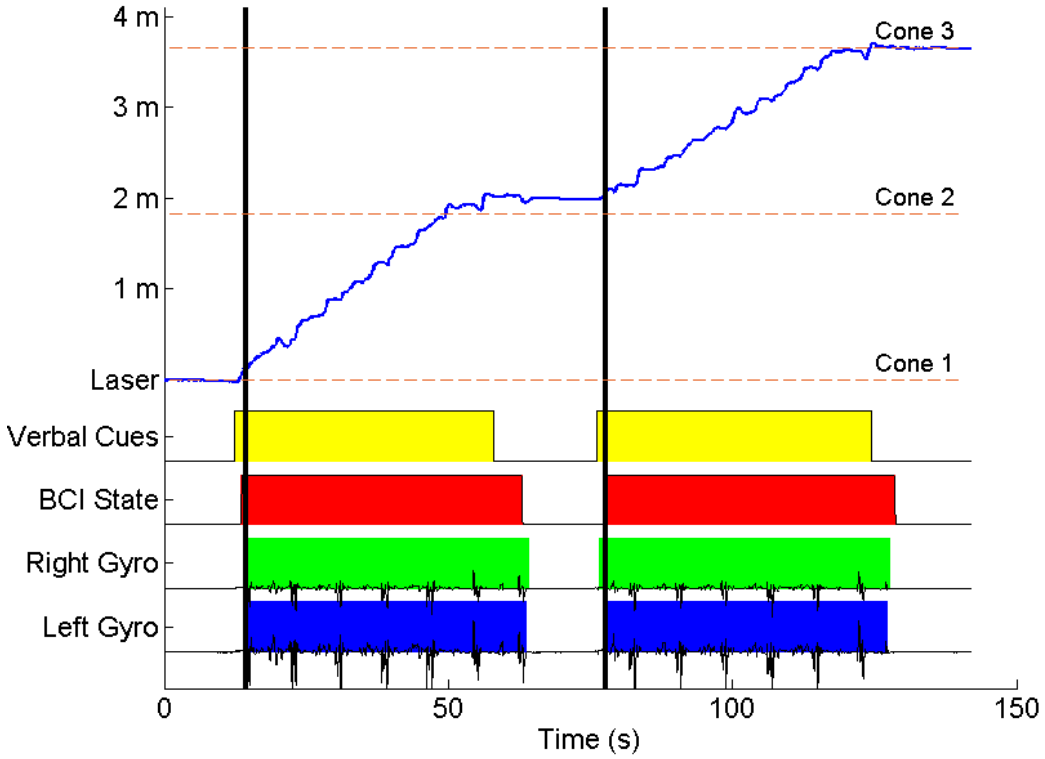

Figure 4.27: The best overground walking test for the BCI-Parastep study, depicting the gyroscope data, BCI state, verbal cues given by the experimenter, and the laser data for the 2nd walking test on the 27th experimental day. Note that the participant overestimated the location of the 2nd cone.

For further analysis, the number of false alarms and omissions were determined for each session, and Monte Carlo simulations were performed to determine whether the participant had purposeful control during each overground BCI-Parastep mediated walking session. This resulted in no omissions during any overground walking test, and a 2.333 $\pm$ 2.039 average number of false alarms across sessions and experimental days. The Monte Carlo simulations also revealed that 4 out of the 30 overground walking sessions were non-purposeful (p-value $< 10^{-4}$). Furthermore, the ITR analysis at the lag determined from the cross-correlation results above revealed that the SCI participant was able to achieve ITRs similar to that of the suspended walking tests. Specifically, the participant had an average ITR of 2.298 $\pm$ 0.889 bits/s across all overground walking tests and experimental days, and he achieved a maximum ITR

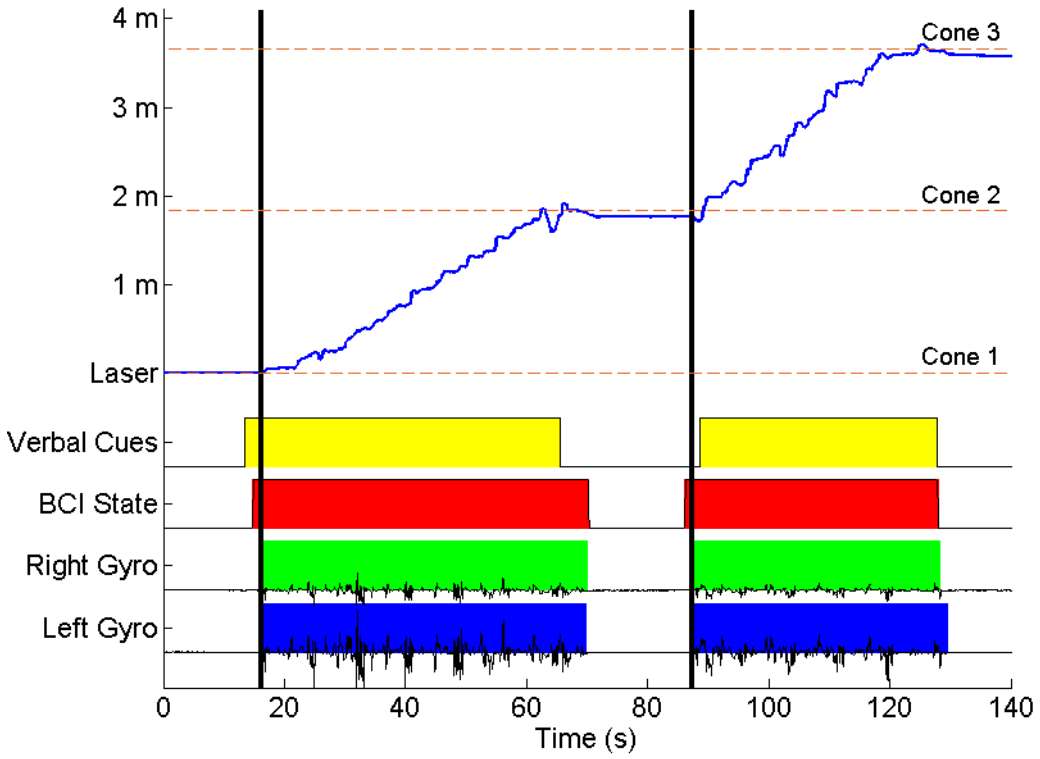

Figure 4.28: Representative overground walking test for the BCI-Parastep study [82] (© 2014 IEEE), depicting the gyroscope data, BCI state, verbal cues given by the experimenter, and the laser data for the 3rd walking test on the 23rd experimental day. Note the very small false alarm on the 2nd "Walk" trial.

of 3.676 bits/s on the 2nd overground walking session on the 28th experimental day. An overview of the ITR results, number false alarms, and the false alarm durations (given that the participant was told to idle at each cone for 10–20 s) is given in Table 4.16.

To determine the source of the false alarms during the overground walking tests, the power spectrum at each channel was plotted to determine the source of the error. It was found that there was a desynchronization in the β-band (13 – 30 Hz) over electrode Cz and in the μ-band (8 – 12 Hz) over electrodes C3 and C4 during the false alarms. This was consistent with the features determined during the offline feature extraction images described in Fig. 4.24. Thus, it was determined that these false alarms may have occurred due to purposeful attempted walking or postural

Table 4.15: Cross-correlation analysis results of the BCI-Parastep study, showing the maximal correlation value at a specific lag (in s) between the verbal cues and BCI state, verbal cues and each gyroscope, and between the BCI state and each gyroscope.

Cross-Correlation Between	Average	Std. Dev.	Max.	Min.
Cues vs. State	0.797	0.166	0.985	0.300
Lag Cues vs. State (s)	2.561	4.154	18.152	0
Cues vs. Gyro 1	0.774	0.174	0.996	0.337
Lag Cues vs. Gyro 1 (s)	2.987	4.196	20.000	0
Cues vs. Gyro 2	0.775	0.164	0.987	0.347
Lag Cues vs. Gyro 2 (s)	2.861	4.229	20.000	0
State vs. Gyro 1	0.865	0.100	0.989	0.622
Lag State vs. Gyro 1 (s)	0.914	1.349	6.875	0.105
State vs. Gyro 2	0.868	0.089	0.975	0.667
Lag State vs. Gyro 2 (s)	0.706	1.297	4.379	0

Table 4.16: ITR (in bits/s), number false alarms, and false alarm duration (Dur., in number of false alarms/s) for the 30 BCI-Parastep overground walking tests performed. Note that the ITR was calculated using equal priors and the lag determined from the cross-correlation analysis, and the false alarm rates were determined from the minimum (10 s) and maximum (20 s) durations of idling at each cone. Also, no omissions occurred during any overground walking session.

	Average	Std. Dev.	Max.	Min.
ITR (bits/s)	2.298	0.904	3.676	0.207
No. False Alarms	2.333	2.073	7	0
Min. False Alarm Rate (FA/s)	0.039	0.034	0.116	0
Max. False Alarm Rate (FA/s)	0.078	0.069	0.233	0

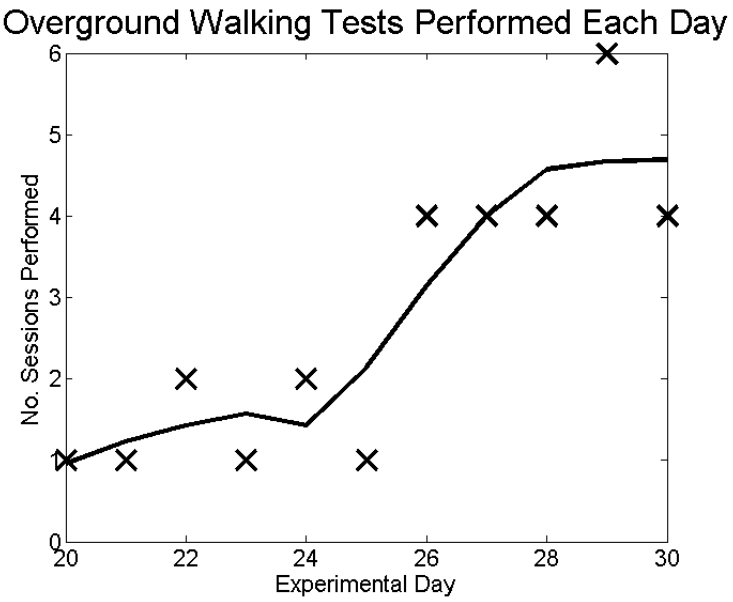

Figure 4.29: Total number of overground walking tests across experimental days.

stability during standing, and were not artifact or noise driven.

4.5.3 Discussion

The results of the BCI-Parastep study [79, 80, 82] indicate that a BCI-FES system for overground walking after paraplegia due to SCI is feasible. The SCI individual with paraplegia that participated in the study was able to purposefully operate the BCI-Parastep system during both suspended and overground walking conditions. Furthermore, the SCI individual was able to produce and maintain a high level of control during both walking and idling states across 10 experimental days. Specifically, the suspended walk tests resulted in high ITRs and correlations, as well as very low false alarm and omission rates. This translated into purposeful real-time control of the BCI-Parastep system during the overground walking tests.

Screening

Out of the 4 SCI individuals with paraplegia recruited for this study, only 1 participant was eligible for full participation. This low number of recruited participants was due to the strict inclusion and exclusion requirements of the study. In addition, the guidelines of the FDA-approved Parastep system required an intensive screening process to ensure safe and proper use of the system during weight loading. This limited the population of SCI individuals who were recruited (Table 4.12) to only 1 SCI participant to be able to safely participate in the full BCI-Parastep study. Therefore, this study was reduced to a single case study to assess the feasibility of the BCI-Parastep device.

Training

As seen in Fig. 4.22 from the results above, the majority of the time taken to perform the BCI-Parastep study with the single SCI participant was due to the BCI and Parastep training sessions. This was likely due to the intensive FES physical therapy required to be able to perform sit-to-stand and stand-to-walk functions using the Parastep system, as 22.5 hours of physical therapy was needed for the participant to safely walk the 3.66 m overground walking course. In order to reduce this training time, longer and more intense sessions of physical therapy could be performed, or the user could increase the duration and intensity of the at-home FES quadricep exercises to improve his strength and endurance more quickly. However, since the SCI participant required much less physical therapy than the recommended 32 hours given by the Parastep guidelines to be able to safely walk the overground walking course, we believe that this duration of training was necessary to properly learn the overground walking task, and may have been optimal for this particular SCI

individual.

BCI Training: The EEG decoding models and offline performances of these decoding models (as determined by cross-validation) indicate that the participant was able to learn the attempted walking and idling control strategy for the BCI system on the 1st experimental day, and was able to improve his control strategy to that of a perfect offline performance after only 15 BCI training days. These offline EEG decoding models resulted in salient features over the arm and foot representation areas of the brain (Fig. 4.24), and these features became consistent across experimental days after the 15th day. Furthermore, the perfect offline performances translated into very high online performances using the BCI walking simulator (see the composite scores in Fig. 4.26). Conversely, the low offline performances in the beginning of the BCI training resulted in low online performances. This indicated that no overfitting occurred using the data-driven feature extraction procedure of the BCI system across experimental days. Finally, since the SCI participant was able achieve a perfect online performance using the BCI walking simulator after only 11 experimental days, this indicates that SCI individuals with paraplegia may be able to more rapidly obtain purposeful BCI control of the BCI-Parastep system by training on the virtual reality walking simulator system. This virtual reality environment is a much safer test bed for an attempted walking BCI control strategy, and should be utilized for lower extremity neuroprostheses and neurorehabilitative walking devices in the future.

Parastep Training: The results of the Parastep training sessions, performed in conjunction with the BCI training, demonstrated that the SCI participant was able to obtain standing and walking functions of his legs using the FES system after only 22.5 out of the 32 recommended hours of physical therapy. It can be noted from Table 4.13 that many of the physical therapy sessions performed focused on standing posture, weight transfer, and ambulation. This was due to the need to

perform postural stability while shifting weight in the anterior-posterior directions for walker advancement, and in the lateral direction for stepping. Also, the triple flexion response of the FES during the swing-through phase of the ambulation task was highly sensitivity to the amount weight transfer, so optimizing the level of weight transfer for ambulation required several hours of therapy and practice by the participant. Finally, the SCI participant had a slight contracture in his left leg, which caused placement of the FES over the tibialis anterior muscle to cause a triple flexion response to be difficult. This was a consistent issue during the ambulation physical therapy sessions, as well as during the BCI-Parastep overground walking tests, and required several tests of the left leg triple flexion response prior to each BCI-Parastep overground walking experimental day.

Online Experiments

After 22.5 hours of physical therapy and BCI training, the SCI participant performed both suspended and overground walking online experiments where he utilized attempted walking and idling to control the BCI-Parastep system in real time. These tests revealed that the participant was able to achieve very high ITRs and correlation values, demonstrating the high-level of control achievable by this system and an attempted walking control strategy. Since such a high-level of control was achievable by this participant, this warrants further investigation with other SCI individuals with paraplegia.

Suspended Walking Tests: The suspended walking tests revealed that the SCI participant was able to use attempted walking and idling to control the BCI-Parastep system while being completely unloaded and following computer cues. The very low number of false alarms (only 1 across both sessions) and no omissions, as well as the low latency (3.00 – 4.25 s) between the cues and state of the BCI, resulted in very

high ITRs and correlation values (> 3 bits/s, > 0.9, respectively). These results also revealed that the SCI participant was able to turn the BCI system "off" (i.e. switch the BCI-Parastep system from walking to standing) even while being stimulated to perform FES-mediated standing during the idle cues. Conversely, even though he was completely suspended, the SCI participant was able to perform BCI-Parastep mediated stepping and walking without any omissions or confounding issues. This experimental paradigm was important to test the feasibility of such a system prior to the overground walking tests because if the participant was unable to turn the device from stand-to-walk or walk-to-stand while being suspended off the ground, he would be less likely to perform these actions while being weight loaded during the overground walking tests. If this occurred, then the participant would not be able to start at the beginning of the course or be able to stop at the end of the course, which would be unsafe when trying to allow the participant to go back to a sitting position to stop the experimental session. Finally, since this experimental paradigm required the participant to follow computer cues and not perform a task in a more self-paced manner such as during the overground walking tests or walking simulator sessions, these results better assessed the performance achievable by the system itself.

Overground Walking Tests: Similar to the suspended walk tests, the ITRs and correlations achievable during the overground walking tests were > 3 bits/s (best ITR: 3.676 bits/s, see Fig. 4.27) and > 0.9 (best correlation between cue and BCI state: 0.985), respectively. However, although the participant was able to achieve a high level of control during the overground walking tests, the false alarm rate increased and average correlation decreased when progressing from the suspended to overground walking tests [82]. This may be due to the low number of suspended walking sessions performed in comparison to the overground walking tests, or due to issues with postural stability during weight loading. Since the EEG decoding model shown in Fig. 4.24 revealed salient features over the arm and leg representation areas

of the brain, it was found that these regions were similarly activated during the false alarms, and may have been due to the participant using his arms for postural stability during standing or due to purposeful attempted walking.

When comparing the cross correlation analysis between the suspended and overground walking tests, it should be noted that the SCI participant was able to control the BCI-Parastep system with only a ∼2.861 s latency between the verbal cues given by the experimenter and the walking movement recorded by the gyroscopes. This is lower than the latency determined from the suspended walking tests (average: 3.630 s), and may have been due to the participant's ability to better learn the overground walking task. Since the suspended walking tests were performed prior to the overground walking tests, the BCI walking simulator training better mimicked the self-paced goal-oriented overground walking tests, and the participant performed more overground walking tests than suspended tests, so the difference in latency may be explained by these confounding issues.

In addition to the above analyses that demonstrated the high-level of control and low latency as well as false alarms and omissions achieved during the overground walking tests, the number of overground walking tests increased across experimental days. This was likely due to an improvement in the SCI participant's endurance when using the BCI-Parastep system to induce FES-mediated walking and standing. Also, the SCI participant was able to better control the system towards the end of the study, as he was able to better understand the task and the strategies necessary to best control the system during overground weight loading conditions. This improvement in endurance is encouraging, as future BCI driven neuroprostheses and neurorehabilitative devices for ambulation should minimize fatigue to maximize the duration (and distance) of overground walking and/or therapy being performed.

Comparison with Other Studies

The overground walking tests using the BCI-Parastep system revealed that the participant was able to achieve ITRs as high as 3.676 bits/s. When compared to our other BCI studies, such as the P300 speller study where ∼3 bits/s was achieved by an able-bodied participant [148] (Section 1.2.3 in Chapter 1), these results exceed our own previous BCI studies. Furthermore, the ITRs achievable in this study were ∼3 times higher than the best bit rates achieved with other BCI speller systems [138], BCI 2-D cursor control systems [161], and SSVEP [48] based BCI systems. Table 4.17 shows a comparison of these ITRs for several selected BCI studies [48, 161], our P300 speller study [148], and our BCI-Parastep study [79, 80, 82]. Since this high-level of control and communication rate is necessary for future BCI driven neuroprostheses and neurorehabilitative devices for overground walking, the methodologies described in this chapter and in Chapter 2 should be utilized in future BCI systems for ambulation.

Table 4.17: Comparison of the current BCI-Parastep study [79, 80, 82] with other BCI studies in the field, showing the type of BCI system, type of study participants (SCI or able-bodied, SCI), control paradigm utilized by the participant, and maximum achievable ITR (bits/s).

Study	Type of BCI	Study Participants	Control Paradigm	ITR (bits/s)
King et al. [79, 80, 82]	BCI-FES Walking	1 SCI	Attempted Walking	3.676
Wang et al. [148]	P300 Speller	6 AB	Oddball	3.038
Wolpaw et al. [161]	2D Cursor	2 SCI, 2 AB	Hand Imagery	1.249
Gao et al. [48]	2D Cursor	1 AB	SSVEP	1.133

4.5.4 Conclusion

The BCI-Parastep study [79, 80, 82] presented here represents the very first study where a SCI individual with paraplegia used his brain waves to control the FES of

his own muscles to induce walking. Furthermore, the participant with paraplegia due to SCI was able to purposefully operate the device in real time using an intuitive attempted walking and idling control strategy after only minimal training. The high level of control achievable by this participant during the overground walking tests demonstrates that a BCI driven neuroprosthesis or neurorehabilitative device for ambulation after SCI is feasible. However, to determine whether this system could become a restorative tool or neuroprosthesis for overground walking in SCI individuals, this device will need to be tested in a much larger population. If successful, this system may become the first restorative treatment or neuroprosthesis for overground walking in SCI individuals, thus greatly improving their quality of life.

Chapter 5

Future Work

5.1 Overview

The remaining chapters will conclude upon the high performance BCI systems for neurorehabilitation discussed in the previous chapters, and will highlight the future work that will be performed for each of these systems. The future work discussed below includes the following BCI systems for stroke and spinal cord injury (SCI): i) BCI driven hand orthosis, ii) BCI-functional electrical stimulation (FES) system for foot dorsiflexion, iii) BCI driven walking simulator, iv) BCI driven robotic gait orthosis (RoGO), and v) BCI-FES system for overground walking. First, the BCI systems for the neurorehabilitation of stroke will be discussed, where the populations to be tested, future experimentation and control experiments, assessment of the electroencelphalogram (EEG) features and brain changes while using the BCI system, and future improvements to the study design will be highlighted. Future work for

the BCI systems for neurorehabilitation and neuroprostheses for SCI individuals will then follow, highlighting the future work with larger SCI populations and longer durations of the studies, assessment of brain changes while using these devices, and future implementations of the system with other devices for ambulation. If these improvements are implemented, then our BCI system may become a novel neurorehabilitative tool for stroke and SCI individuals, ultimately restoring motor behavior to these individuals and greatly improving their quality of life.

5.2 Stroke Neurorehabilitation

The BCI systems designed for the neurorehabilitation of stroke individuals presented in Chapter 3 utilized attempted or actual movement to initiate the movement of an external device, such an orthosis or FES system. These studies focused on only one type of attempted movement that is simple, and assessed both the movement and non-movement states of the elementary behavior in real time. The BCI systems also attempted to control the movements over a long period of time, i.e. several seconds, to ensure that coactivation of upper and lower motor neurons would occur during each attempted movement trial, thus capitalizing on Hebbian-like neuroplasticity. If successful in causing coactivation during the therapies, these BCI systems may lead to lasting functional improvements in post-stroke individuals.

The following sections will describe the future work necessary to develop the BCI systems from Chapter 3 into novel neurorehabilitative therapies that can utilize coactivation of upper and lower motor neurons to cause functional improvements. If tested in larger populations, and if the brain changes over time are assessed, these therapies

may lead to adaptive neuroplastic changes in the post-stroke brain of stroke individuals. These systems may also provide a new therapeutic tool for these individuals beyond that of standard physiotherapy, which may restore their motor functions and improve their quality of life.

5.2.1 BCI Driven Hand Orthosis

To apply the BCI driven hand orthosis system described in Section 3.2 of Chapter 3 to the neurorehabilitation of chronic stroke survivors with hand weakness, an ipsilateral BCI control paradigm should be used. Through the use of attempted or residual movements of the affected hand, followed by the activation of the orthosis, post-stroke individuals may be able to restore hand grasping behavior in an intuitive manner. However, the post-stroke brain is expected to have undergone cortical reorganization that may result in EEG signal features that deviate from classical features underlying hand grasping behavior. Unlike previous BCI stroke studies that rely on able-bodied brain anatomy [24, 118], the data-driven feature extraction method demonstrated in Chapter 2 can find optimal combinations of EEG signal features directly associated with hand grasping behavior in the post-stroke cortex. This method may facilitate reliable BCI operation of the orthosis and in turn, help reinforce connections between the post-stroke brain areas underlying hand grasping and the corresponding spinal motor pools. Finally, successful implementation of ipsilateral BCI-hand orthosis grasping in a population of post-stroke individuals with hand motor impairment may potentially allow to this system to become a new neurorehabilitation tool.

Previous BCI stroke studies for upper extremity weakness [15, 118] did not decode during both movement and non-movement states, so they may not have reached the

full potential of BCI systems for neurorehabilitation. By improving our data-driven feature extraction technique as well as the implementation of movement and non-movement states in the design of our future stroke therapies, we may provide more intuitive BCI operation and improvements beyond those achieved with current BCI studies [15, 24, 118]. These improvements may potentially lead to better and longer lasting functional improvements.

In addition to implementing an ipsilateral control paradigm and the above features, our online experimental paradigm will need to consist of longer "Grasping" and "Idling" epochs. This lengthy duration of each state may help pair intentions and movements over a significant period of time despite the $\sim$2 s lag between the initiation of voluntary and BCI-mediated movements (Table 3.4 in Section 3.2 of Chapter 3). In the long-term, the co-activation of the motor cortex (intentions) and proprioceptive pathways (BCI-mediated movements) may either reinforce the existing or create novel synaptic connections [131], ultimately restoring hand grasping to chronic stroke individuals.

Other future work for the BCI driven hand orthosis study will include the testing of this device on a large population of stroke individuals with distal upper extremity weakness. If proven feasible and safe in this patient population, then several control studies will be performed to determine the efficacy of the neurorehabilitative therapy. These control studies will include a sham study, where one group of stroke individuals will receive randomized hand orthosis grasping and extension while performing attempted movement and non-movement of the hand to control the BCI system. Another type of control study may include training stroke individuals to perform attempted motor movements to control the BCI while keeping the hand orthosis turned off. Finally, other control studies that must be performed in the future include performing standard physiotherapies for the hand, such as bilateral arm training [97] or

constraint-induced movement therapy [139, 158], to test these standards against our BCI driven hand orthosis neurorehabilitative therapy.

5.2.2 BCI-FES System for Foot Dorsiflexion

The BCI-FES system for foot dorsiflexion may be used in future seated therapeutic exercises to facilitate neural repair in stroke individuals who are affected by foot drop. By pairing the activation of the motor cortex associated with attempted, but impaired, foot dorsiflexion with the electrical stimulation of foot dorsiflexion (via antidromic electrical stimulation of the deep peroneal nerve towards the anterior horn cell of the spinal cord), it can be hypothesized that spared connections between the post-injury motor cortex and the spinal motor pools that correspond to the motor control of foot dorsiflexion will be reinforced through Hebbian-like neuroplasticity. This plasticity process associated with the BCI-FES therapy may translate into the improvement of unassisted dorsiflexion strength and gait function in this population.

The applicability of the BCI-FES therapy for the neurorehabilitation of foot drop through Hebbian learning or other neuroplastic changes raises significant concerns about eliminating the latency between the onset of voluntary movement and BCI-FES mediated movement. The observed latency from the BCI-FES system is partly caused by the averaging of the posterior probability over a 1.5 s period during online operation. Reducing the averaging window may help decrease this latency, although it would come at the expense of lowering the online performance (i.e. higher false positive and omission rates). Note that the observed latency is also consistent with the natural delay of maximal event-related desynchronization and synchronization of EEG sensorimotor rhythms [110, 133], and it may be partially responsible for the

delay in the BCI-FES system response. A potential solution to this problem may be to use our data-driven algorithm to search for relevant time domain EEG features, such as readiness potentials [95]. These slow negative potential shifts may be observed as early as 1 s before the initiation of a self-paced motor behavior [95], and they can potentially be used for earlier classification of dorsiflexion and idling. Also, a combination of temporal and spectral features may be used in the future to eliminate the latency while ensuring a high performance. However, further research is required, as changes in both the training paradigm and signal processing methodology will need to be implemented such that novel EEG features associated with movement intentions can be reliably detected.

The ideal BCI-FES system for neurorehabilitation should mimic foot dorsiflexion in a 1:1 temporal fashion, in which a single foot dorsiflexion cycle translates into a single BCI-FES mediated dorsiflexion cycle. To achieve this, changes in both the training paradigm and signal processing methodology will need to be implemented such that transient EEG changes associated with foot dorsiflexion and relaxation can be reliably detected and utilized to govern the BCI-FES system state transitions. If these implementations are made, the BCI-FES system may become a more intuitive BCI neurorehabilitatitive therapy.

In addition to improving the current automated identification algorithms and signal processing methodologies, the BCI-FES system should also monitor the EEG signal changes that occur over time. This may be accomplished through the use of the feature extraction maps from our signal processing methodologies, functional magnetic resonance (fMRI), functional near infrared spectroscopy (fNIRS), magnetoencephalogram (MEG), or positron emission tomography (PET). By monitoring the brain before, during, and after the BCI-FES therapy sessions, we may be able to better induce adaptive neuroplastic changes, thus better improving their motor

function.

If the above improvements are made, this system should then be tested on a much larger population of stroke individuals. Safety and efficacy (Phase I clinical trial) must contain a much larger population of study participants (20 – 80) than those presented in Chapter 3. Thus, the current BCI-FES study will more actively enroll participants in the Phase I clinical trial. Furthermore, after the Phase I clinical trial deems the BCI-FES system for foot dorsiflexion to be safe, the study will become a Phase II clinical trial, where the efficacy of the therapy will need to be determined through 100 – 300 study participants. To accomplish this, several control experiments will need to be performed. For instance, a sham study will need to be performed, where participants who are post-stroke and affected by foot drop will receive randomized FES while performing intentional attempted foot dorsiflexion and idling using the BCI system. This will help determine if the improvement in active range of motion of dorsiflexion is due to use of the BCI-FES system or due to FES alone. Also, another control study that will need to be performed is the use of the BCI system to monitor attempted foot dorsiflexion and idling while the FES does not provide any stimulation to see the effects of BCI use and intentional foot dorsiflexion and idling practice. Finally, the last control study during the Phase II clinical trial will include performing standard physiotherapies to stroke individuals, such as exercise with a physical therapist (e.g. toe-to-heel rocking, isometric dorsiflexion and stretching), to compare these current standards to our BCI-FES neurorehabilitative therapy.

In addition to the above control studies, it would be beneficial to compare the BCI-FES therapy for foot drop against current ankle-foot orthotics and FES systems on the market. For instance, it would be beneficial to compare the functional improvements from using a commercially available Bioness FES system (L300, Bioness Inc., Valencia, CA) to our own system. Also, a comparison of our system to the benefits of current

ankle-foot orthoses, the other standard for the treatment of foot drop, would also be beneficial, as much of these standards have no lasting functional improvements when used. If this system is proven to be effective, then it may become a novel neurorehabilitative therapy for stroke individuals affected by foot drop.

5.3 Neurorehabilitation of Ambulation in Spinal Cord Injury

The BCI systems for neurorehabilitative therapies and neuroprostheses described in Chapter 4 focused on ambulation applications for SCI individuals. By utilizing attempted walking and kinesthetic motor imagery as control strategies, these systems focused on an intuitive control strategy for BCI driven ambulation devices. In order to determine whether these intuitive control strategies could control our BCI system, the system and strategies were first tested using a virtual reality environment, a safe test bed for ambulation devices. It was found from these walking simulator studies (Section 4.3 in Chapter 4) that the BCI system could be controlled using both kinesthetic motor imagery and attempted walking control strategies by SCI individuals, which could be used as a training platform for BCI ambulation systems.

By utilizing the BCI driven walking simulator in a virtual reality environment as a training platform, SCI individuals were able to purposefully operate both a BCI driven RoGO and a BCI driven FES device for ambulation. The success of these proof-of-concept studies indicates that BCI driven neuroprostheses and neurorehabilitative devices for ambulation after SCI are feasible. Furthermore, if tested on a much larger SCI population, this BCI system and control strategy may become the first step

towards an implantable BCI system for overground walking, and thus a restorative solution to walking after paraplegia due to SCI. This may be accomplished through the use of spinal cord stimulators (e.g. programmable central pattern generators), invasive FES systems, or other invasive ambulation devices.

5.3.1 BCI Driven Walking Simulator

The results of the BCI driven walking simulator studies described in Section 4.3 of Chapter 4 suggest that attempted walking or kinesthetic motor imagery of walking strategies to control our BCI system are usable input control strategies for BCI driven ambulation. To further test this control strategy as well as our BCI virtual reality system, this device should be further tested in a much larger SCI population. Specifically, if the BCI driven walking simulator is tested in several more SCI individuals with paraplegia, and if this system is tested on a much longer time scale in each of these individuals (similar to the duration of the BCI training presented in the BCI-Parastep system described in Section 4.5 of Chapter 4), then it may become a useful training platform for future BCI ambulation systems.

In addition to the above increase in participant sample size and duration of the study, the brain changes associated with cortical reorganization due to use of our BCI driven walking simulator training platform should be examined over time. This could be accomplished through several different signaling modalities, such as fMRI, fNIRs, MEG, PET, or even the feature extraction maps from our signal processing methodologies. If these brain changes are closely monitored during extensive use of our BCI training platform, then maladaptive neuroplastic changes may be prevented. Also, the control of the system may be optimized by focusing on the anatomically

plausible brain areas and frequencies determined for each SCI individual. By limiting the electrodes and frequencies to these areas, cortical reorganization may be better facilitated and lead to functional improvements, and the control of the system may be optimized for each SCI user.

If the brain changes associated with BCI use are monitored, and the duration and sample size of the study are increased, it may be possible to also optimize the duration necessary to obtain perfect BCI control of the walking simulator. This may in turn assist with the development of a BCI training platform for ambulation devices that could be implemented quickly in any SCI individual. Furthermore, the larger SCI population study may also fine-tune the inclusion and exclusion criteria for future BCI ambulation systems. For instance, if the SCI individual is unable to obtain purposeful control after a certain number (determined by the long term study) of BCI walking simulator tests and experimental sessions, then this participant may be excluded from the BCI ambulation study or clinical use of the device. This would improve the level of success in using a BCI ambulation device, and may become an important enrollment tool for future implantable BCI systems.

Once the BCI driven walking simulator system becomes a training platform for BCI driven ambulation devices in SCI individuals with paraplegia, future work will include integrating this BCI system with other ambulation devices and use the training platform to train the SCI participants of future studies prior to testing with the actual BCI-ambulation device. Similar to the BCI driven RoGO (Section 4.4 of Chapter 4) and BCI-Parastep (Section 4.5 of Chapter 4) studies, this training platform can be used to screen the SCI individual and determine whether the future BCI-ambulation device would be an appropriate solution for this particular individual prior to actual integration and testing. This will save time and money in the development of ambulation devices, and would allow for long term training and testing of the BCI system

to occur on only those individuals who would succeed and benefit from a BCI driven ambulation device.

If these future BCI ambulation systems are successfully tested in a large SCI population beyond those tested in the BCI driven RoGO and BCI-Parastep studies, clinical trials to develop a commercial BCI driven neuroprosthesis or neurorehabilitative device would be warranted. These future research efforts may ultimately lead to the development of an implantable BCI neuroprosthesis for ambulation; for example, the integration of an invasive BCI system with an invasive FES system or programmable central pattern generator for ambulation. This type of system would eliminate the need for any preparation or mounting of EEG, while potentially achieving better performances and long term use of the system, thus becoming a restorative treatment for overground walking after paraplegia due to SCI.

In conclusion, the above improvements and future studies may allow the BCI driven walking simulator system to become an important tool for future implantable BCI driven neuroprotheses and neurorehabilitative devices for ambulation. The results from these future studies will help determine the appropriate training duration using the BCI driven walking simulator, the salient brain areas and frequencies for each SCI individual, and whether the enrolled SCI participant can use an attempted walking control strategy to control our BCI. By utilizing noninvasive and virtual reality environments as our training platform, this system may help optimize future implantable BCI ambulation systems by allowing the experimenter to adjust and test the parameters necessary for optimal control for each SCI individual prior to implantation and integration of the invasive BCI neuroprosthesis. If successful, then it may be feasible to develop an appropriate restorative treatment for overground walking after paraplegia due to SCI.

5.3.2 BCI-Robotic Gait Orthosis

After determining that SCI individuals can use attempted and kinesthetic motor imagery of walking to control the BCI driven walking simulator (Section 4.3 of Chapter 4), this system was integrated with a RoGO to test the feasibility of a BCI driven ambulation device. The Lokomat system (Hocoma, Volketswil, Switzerland) was first integrated with the BCI system because of its availability and body-weight support system, which made it a much safer and easier test bed for early development of a BCI driven neuroprosthesis or neurorehabilitation therapy for ambulation. The proof-of-concept study of this system in an able-bodied and SCI individual resulted in purposeful real time control of the BCI driven RoGO. Thus, this study suggests that a BCI-controlled lower extremity neuroprosthesis or neurorehabilitation therapy for walking after SCI is feasible.

To make the BCI driven RoGO more successful as a neurorehabilitative therapy for those with incomplete motor SCI, the latency between the user's intention and the BCI-mediated RoGO walking must be minimized. Similar to the BCI-FES studies for the neurorehabilitation of foot drop in stroke individuals (Section 3.3 of Chapter 3), the applicability of this system for neurorehabilitation of ambulation through Hebbian learning or other neuroplastic changes raises concerns about eliminating the latency between the onset of neural intention from upper motor neurons and the output behavior from the RoGO. This delay can potentially be minimized with additional user training in a controlled environment. Also, reducing the posterior probability averaging window may eliminate some of the delay, but this would be at the expense of increasing the false alarm and omission rates. This trade-off should be examined in future studies to make this system become a more intiutive BCI neurorehabiltitative

therapy for those with incomplete motor SCI.

The EEG decoding models generated from idling and kinesthetic motor imagery or attempted walking must also be improved to make them immune to EEG perturbations caused by other simultaneous cognitive and behavioral processes common during ambulation (e.g. talking, head turning, postural stability). Anecdotally, no disruption of BCI operation was observed during the BCI-RoGO study and the BCI driven walking simulator studies (Section 4.3 of Chapter 4) when the participants engaged in brief conversations or hand and arm gestures during the familiarization sessions. However, formalized testing of this hypothesis is necessary and should performed in future studies.

If the above implementations are made, and similar improvements mentioned in the other studies above are also implemented, then the BCI driven RoGO should be further tested in a much larger population of SCI individuals. Currently, only 1 SCI participant and 1 able-bodied participant have participated in the study. To truly assess the feasibility of such a device, further testing in several more SCI individuals is necessary. This may difficult, however, as the Lokomat device is only available for research and experimentation on the weekends after clinical use, which may become conflicting for the SCI participant's schedule. Furthermore, the BCI driven RoGO system should also be tested over a much longer period of time, so future studies should assess the performance of the device in SCI individuals over the course of several weekends.

Since the Lokomat system allows for weight unloading during ambulation, this device may provide a safe training platform for future weight loaded overground walking devices, such as the BCI-Parastep system described in Section 4.5 of Chapter 4. The screening requirements of these future devices may be further fine-tuned after testing each SCI participant in the BCI driven RoGO, as this system would allow

the experimenters to determine whether the participant can perform BCI mediated ambulation in a safer and weight unloaded test bed. Finally, if the brain changes associated with using this device are monitored over time (similar to the future studies described in the BCI driven walking simulator studies above), then this system may become a BCI ambulation training platform for future overground BCI ambulation systems.

If the BCI-RoGO system is successful in a large population of SCI individuals, such a system may justify the future development of BCI-controlled lower extremity neuroprostheses for free overground walking for those with complete motor SCI, such as the Parastep device (Sigmedics, Fairborn, OH). However, to make this system usable for this type of application, issues such as additional degrees of freedom (e.g. turning, velocity modulation, transitioning between sitting and standing), as well as appropriate solutions for signal acquisition (e.g. invasive recordings such as electrocorticogram (ECoG) signals) must be addressed. Finally, the current BCI-RoGO system can also be applied to gait rehabilitation in incomplete motor SCI as a neurorehabilitative therapy. It can be hypothesized that coupling the behavioral activation of the supraspinal gait areas (via the BCI) and spinal cord gait central pattern generators (feedback driving via the RoGO) may provide a unique form of Hebbian learning. This could potentially improve neurological outcomes after incomplete motor SCI beyond those of standard gait therapy. However, further improvements in the system design and latency between intention and actual movement via the RoGO must be made prior to testing this as a neurorehabilitative therapy.

In summary, the BCI driven RoGO must be drastically improved and tested on a larger population of SCI individuals with both complete and incomplete motor SCI. If it is successful in either of these patient populations, then it could become a novel neurorehabilitative therapy in those with incomplete SCI, or serve as a test bed to

determine whether an SCI participant can use the BCI system to operate an overground walking neuroprosthesis, such as the Parastep system. If successful, this device may become a useful neurorehabilitative therapy and neuroprosthesis for overground walking after paraplegia due to SCI, and potentially a restorative treatment towards walking, thus greatly improving the quality of life in this population.

5.3.3 BCI-FES System for Overground Walking

Both the BCI driven walking simulator (Section 4.3 of Chapter 4) and the BCI driven RoGO (Section 4.4 of Chapter 4) studies provide preliminary evidence that a BCI driven overground walking device for those with paraplegia due to SCI is feasible. Thus, the BCI system was integrated with the Parastep system (Sigmedics, Fairborn, OH), an FDA-approved noninvasive FES system for overground walking, and tested in an individual with complete motor paraplegia due to SCI. The results from this study (Section 4.5 of Chapter 4) demonstrated that the SCI individual was able to use his EEG of attempted walking and idling to control the FES of his muscles to induce walking and standing. The high level of control achieved by this participant using the BCI-Parastep system to perform overground walking demonstrated that a BCI driven neuroprosthesis or neurorehabilitative device for ambulation after SCI is feasible.

To be able to better assess the performance and feasibility of the BCI-Parastep system, this device must be tested on a larger population of SCI individuals with paraplegia. However, this may be difficult in future studies because of the strict screening requirements for loaded overground FES driven walking using the Parastep system. Also, since the duration of BCI and FES training is intense, many SCI individuals may not

be willing to perform the time requirements of the study. In order to reduce these issues with participant recruitment, the at-home exercises and physical therapy can be improved, allowing for a shorter time commitment for the BCI and FES training period. In addition, the inclusion and exclusion criteria and screening process of the study could be improved and optimized. Since the Parastep is an FDA-approved device, these improvements must satisfy the guidelines of the Parastep system.

In addition to an increase in study participants to better assess performance and feasibility, the BCI-Parastep system will also need to be improved to reduce the latency between attempted walking and FES mediated walking. Since the BCI-Parastep system can allow for coactivation of the upper and lower motor neurons via intention from attempted walking and antidromic stimulation via the FES, Hebbian-like neuroplasticity may be promoted. However, the latency between these actions should be minimized by reducing the posterior probability averaging window and analysis duration, but this would be at the expense of increasing the false alarm and omission rates during real time operation. Thus, future studies should examine this trade-off as well as more computationally efficient data-driven techniques that search for relevant time domain EEG features, such as readiness potentials [95].

Once the latency between intention and BCI-Parastep mediated walking and standing is reduced, the amount of fatigue from using the Parastep FES system for overground walking must also be reduced. This fatigue is due to the high energy demand from use of the FES system, and could be reduced by better optimizing the stimulation parameters of the FES prior to walking. Also, the fatigue during BCI-Parastep use and the issues during FES overground walking may be reduced by optimizing the location of the FES stimulation pads. This may be accomplished through semi-permanent medical tattoos (e.g. similar to those used in cancer therapies [117]) or other semi-permanent landmarks. If these FES parameters are optimized, then

the fatigue experienced by the SCI individual can be reduced, thus allowing the participant to perform BCI-Parastep mediated overground walking for a much longer distance and duration, a requirement for an ideal neuroprosthesis.

If the above improvements are made and this system is proven feasible in a much larger SCI population, then a Phase I clinical trial can begin. This would require determining whether this system is more appropriate to apply to SCI individuals as a neurorehabilitative therapy or as a neuroprosthesis. If it is determined that this system should act as a neurorehabilitative therapy, then the safety of the therapy will first need to be tested in several participants (20 – 80) with incomplete motor SCI. On the other hand, if this device proves to perform better as a neuroprosthesis for those with complete motor SCI, then it would be feasible to consider more invasive methodologies of recording to create a more permanent and long-term solution.

If the noninvasive neurorehabilitative therapy or invasive neuroprosthesis are determined to be safe, the efficacy of the system in both of these applications will then need to be determined. This would be determined through a Phase II clinical trial (100 – 300 study participants), where further evaluation of safety as well as efficacy would be performed. Several control should be performed during this phase of the clinical trials. First, a control experiment where participants perform other cognitive and behavioral processes while operating the system (e.g. talking, head turning, postural stability) should be performed to see if the BCI is robust against noise perturbations in the EEG caused by these actions. It was noted during this study, however, that the SCI participant was able to talk to the experimenter during BCI-Parastep operation, and these perturbations did not cause any changes in the state of the BCI system. Nevertheless, formalized testing during larger population studies should be considered.

In addition to the above control experiment, several other control experiments must

also be performed during the clinical trials. For instance, during the Phase II clinical trial, the BCI-Parastep neurorehabilitative therapy in incomplete motor SCI individuals should be compared to other standard physiotherapies for overground walking after SCI. Since there currently are no restorative treatments for this motor behavior in this patient population, this may include comparing the therapy to other research-level therapies [141], such as spinal cord stimulators [60], transcranial magnetic stimulation [57] during robotic-assisted locomotor training (e.g. using the Lokomat system) or physical therapist-assisted locomotor training, or the Re-Walk system (Argo Medical Technologies, Inc., Marlborough, MA). Also, the BCI-Parastep system should be compared against a sham control group, where the BCI and Parastep system will be used to allow the participant to perform attempted walking neural intention to induce FES-mediated walking, but the state of the FES system (i.e. walk or stand) will be completely randomized and not dependent on the output of the BCI. Finally, the BCI-Parastep system will need to be tested against standard lower-extremity FES therapy and use of the Parastep system alone [51, 52].

Future work may also consist of translating this device into an invasive BCI-walking system as a neuroprosthesis rather than a neurorehabilitative therapy. This will require further research and improvements in implantable neural recording units, such as microelectrode arrays (e.g. Utah Array, Blackrock Microsystems, Salt Lake City, UT) or ECoG grids (e.g. Wireless ECoG Microelectrode Array, Lawrence Livermore National Laboratory, Livermore, CA), and implementation of these neural recordings with our BCI system. If attempted walking and idling can be used to reliably control the BCI system using these invasive recordings, and if these systems can more reliably record neural data over time, then this proposed system may lead to a long-term implantable BCI system for overground walking after SCI. The external device or output of the BCI system must also be optimized. This may include implantable spinal cord stimulators [60] or implantable FES systems [59]. Thus, if the BCI system

and external overground walking device become implantable, then this system may lead to the first neuroprosthesis for overground walking, which may in turn restore walking to SCI individuals with paraplegia and greatly improve their quality of life.

Chapter 6

Conclusion

The BCI systems presented in this dissertation have the potential to serve as neurorehabilitative therapies and neuroprostheses in stroke and spinal cord injury (SCI) individuals. If proven successful in larger populations and compared to other standard physiotherapies, this system may lead to novel therapies and prostheses for both populations, thus restoring motor functions to these individuals. Furthermore, the data-driven decoding methodologies presented here may serve as a future brain mapping tool during use of our BCI system. If the neuroplastic brain changes during rehabilitation or use of the BCI system can be monitored, then this system may be able to optimize the therapeutic use or location of long-term signal recordings for neuroprosthetic design, thus optimizing the system for both types of applications. Furthermore, the optimization of this system may lead to the promotion of neuroplasticity and cortical reorganization, which would in turn lead to motor function improvements and an increase in independence. This may improve the quality of life of stroke and SCI individuals beyond that of current rehabilitation.

The systems for the neurorehabilitation of stroke individuals presented in Chapter 3

attempted to improve the function of elementary motor movements that commonly exhibit weakness or paralysis in chronic ($>$ 6 months post-ictus) stroke survivors. For instance, the BCI system was applied to the treatment of foot drop as well as hand weakness in the studies presented in Chapter 3. These systems also attempted to control the elementary movements over a significant duration to promote coactivation of upper and lower motor neurons, and to try to capitalize on a Hebbian-like neuroplastic process. If both of these systems are proven feasible in a large population of chronic stroke survivors, these BCI systems may novel neurorehabilitative therapies that lead to lasting functional improvements in post-stroke individuals.

The hand orthosis study (Section 3.2 of Chapter 3) was able to allow a population of able-bodied individuals control their hand via an orthosis purposefully in real time. In addition, this system was able to allow these individuals to obtain intuitive real time control for the entire experimental day after only minimal training and calibration. However, to determine if this system could become an applicable neurorehabilitative therapy for stroke individuals, it needs to be tested on a population of chronic stroke individuals with hand weakness. If proven feasible and effective in this population, then this BCI-hand orthosis system may become a viable treatment for distal upper extremity weakness in those affected by stroke.

The preliminary evidence shown in the BCI driven functional electrical stimulation (FES) studies for the treatment of foot drop (Section 3.3 in Chapter 3) suggests that chronic stroke survivors can safely use the BCI-FES system. More importantly, an improvement in their active range of motion of foot dorsiflexion in the impaired foot was observed in those stroke individuals who performed the short-term study (3 daily sessions of 1 hr BCI-FES therapy). Additional improvements in motor function were seen in the participant who performed the long-term (12 daily sessions) BCI-FES study as apart of the Phase I clinical trial. The results of all the studies for this

system warrant future formal clinical trials on stroke individuals to further assess the safety and efficacy of this novel therapy to improve foot dorsiflexion and gait function in stroke individuals affected by foot drop.

For the neurorehabilitation of SCI individuals, the BCI systems shown in Chapter 4 focused on neurorehabilitative therapies and neuroprostheses for ambulation. These studies demonstrated that BCI driven walking is feasible and can be purposefully operated by SCI individuals in real time. Furthermore, these systems can be controlled after minimal training using an intuitive control strategy, i.e attempted or kinesthetic motor imagery of walking. This control strategy was first deemed feasible in a virtual reality environment in a population of able-bodied and SCI individuals. After obtaining this preliminary evidence, the BCI system was then further tested by integrating it with a robotic gait orthosis (RoGO) and overground FES system. These proof-of-concept studies were proven successful, as they obtained a very high level of control by the able-bodied and SCI participants. However, future studies should be performed to test the feasibility of these systems as neurorehabilitative therapies and neuroprostheses in a larger population of incomplete and complete motor SCI individuals.

The BCI driven walking simulator studies (Section 4.3 of Chapter 4) were originally developed to determine the feasibility of using an attempted or kinesthetic motor imagery of walking strategy to control the BCI system. Since it controlled a virtual reality environment rather than an ambulation device, this provided a safe test bed for assessing the feasibility of BCI controlled ambulation. The results of this study demonstrated that both able-bodied and SCI individuals can control the system using these strategies, and can purposefully operate a virtual reality avatar in a self-paced manner. This system became the first step in developing a BCI driven ambulation system, as well as becoming an important BCI training platform for future BCI

ambulation studies.

Once the attempted walking control strategy was determined feasible from the BCI driven walking simulator studies, the BCI system was integrated with a RoGO. This system allowed for safe testing in a weight unloaded condition, where able-bodied and SCI participants used attempted walking and idling to control the BCI-RoGO system in real time. Moreover, these individuals were able to use an intuitive strategy to obtain a high level of control of the system after only minimal training on the first experimental day. The success of this proof-of-concept study indicates that a BCI-controlled lower extremity prosthesis for walking may be feasible. Future studies will need to be performed to further assess this feasibility, as well as determine the safety of the device. If successful, this system may be marketed towards either incomplete or complete motor SCI with paraplegia as a neurorehabilitative therapy or training tool for a future overground walking neuroprosthesis.

The success of both the BCI driven RoGO and BCI driven walking simulator studies discussed above (Sections 4.4 and 4.3 of Chapter 4, respectively) led to the development of a BCI driven FES system for overground walking in those with paraplegia due to SCI. The feasibility of such a device was tested in an SCI individual with complete motor SCI (T6, ASIA B), and became the first successful instance of an SCI individual with paraplegia to be able to control the overground walking function of his own muscles using his brain waves. Specifically, this individual was able to purposefully operate the BCI-FES device for overground walking in real time using his brain waves and an intuitive attempted walking control strategy after only minimal training. The high level of control achieved by this participant during this study demonstrates that a BCI driven neurorehabilitative therapy or neuroprosthesis for overground ambulation after paraplegia due to SCI is feasible. If tested in a much larger population of both complete and incomplete motor SCI individuals, then this

system may become the first restorative treatment for overground walking after SCI.

Since the BCI driven walking simulator system was determined to be an excellent training platform for the BCI driven RoGO and BCI driven FES system for overground walking, future work with these systems will be directed towards further development of the RoGO and FES overground walking system. In addition, the testing of this device in SCI individuals will lead to determining the applicability and efficacy of using these systems for neurorehabilitative therapies or neuroprostheses. The BCI driven RoGO may become a viable neurehabilitative therapy in those with incomplete motor SCI by promoting coactivation of upper and lower motor neurons via attempted walking brain waves from the BCI and spinal cord central pattern generator stimulation via feedback from the RoGO. On the other hand, this device may become an important tool in developing future implantable neuroprostheses for overground walking. This system may be used as a training platform for these future devices by determining optimal electrode placement for salient brain waves (as recorded by the EEG and from the BCI prediction model) and training the SCI individual to perform overground walking in a weight unloaded and safe ambulation conditioning paradigm.

Unlike the BCI driven RoGO, the BCI-FES system for overground ambulation may become a better novel neurorehabilitative therapy in incomplete motor SCI individuals, as it has the potential to coactivate the upper and lower motor neurons via attempted walking neural signals and antidromic FES stimulation towards the propriospinal connections and anterior horn cell of the spinal cord. Alternatively, the BCI-FES system for overgound walking (i.e. the BCI-Parastep system) may serve as a noninvasive solution to a neuroprosthesis for overground walking after SCI, or as an important feasibility step in developing an implantable neuroprosthesis for overground walking. Since this system is closer to able-bodied-like walking as it performs

overground walking in weight loaded conditions, the BCI-FES system for overground walking may better determine the feasibility of an implantable neuroprosthesis by assessing the performance of such a system under noninvasive conditions, thus greatly improving the potential sample size of such a study. However, implantable devices for both ambulation and neural recordings must be further developed in conjunction with these future tests to provide a long-term, robust, and ideal neuroprosthesis solution for overground walking after paraplegia due to SCI.

All of the aforementioned BCI systems for stroke and SCI neurorehabilitation provide restorative treatments for functional motor paresis and paralysis. Particularly, the BCI systems for stroke individuals provide restorative solutions for the treatment of hand weakness and foot drop, while the BCI systems for SCI focus on restoring ambulation in these individuals. These systems together further elucidate the capabilities of our BCI system, as well as provide novel therapeutic treatments and prostheses to these individuals. Since our BCI prediction model procedure is data driven and has found anatomically relevant features across both types of study populations, this BCI system may advance neuroscience by providing a new brain mapping tool to assess neurophysiogical changes from BCI use. Furthermore, if these BCI systems are optimized, they may provide novel neurorehabilitative therapies in stroke and SCI individuals, potentially improving their functional motor deficits, and in turn, their quality of life. They may also provide evidence to further the investigation of implantable neuroprostheses in these individuals, restoring the functional motor behavior to individuals while possibly providing some form of neuroplasticity to enhance long term functional improvements. If these systems are proven successful and research on neurorehabilitative therapies and neuroprostheses is continued, then restorative treatments for these motor deficits can be developed.

In summary, the BCI systems described in this dissertation provide preliminary ev-

idence for future neurorehabilitative therapies and neuroprostheses. By focusing on SCI and stroke individuals, the marketability of our BCI system was greatly expanded beyond those traditionally used for communication [41]. Furthermore, by focusing on coactivation of neural intention and corresponding output motor behavior, these BCI systems may promote Hebbian-like neuroplasticity and lead to better functional motor improvements than the standard physiotherapies and substitutive devices typically used by these individuals. This may in turn improve the daily functional tasks post-stroke and SCI individuals can perform, which may then greatly improve their quality of life.

Bibliography

[1] H. Alkadhi, P. Brugger, S. Hotz Boendermaker, G. Crelier, A. Curt, M. C. Hepp-Reymond, and S. S. Kollias. What disconnection tells about motor imagery: evidence from paraplegic patients. *Cereb. Cortex*, 15:131–140, 2005.

[2] B. Z. Allison, D. J. McFarland, G. Schalk, S. D. Zheng, M. M. Jackson, and J. R. Wolpaw. Towards an independent brain–computer interface using steady state visual evoked potentials. *Clin. Neurophys.*, 119(2):399–408, 2008.

[3] K. Aminian, B. Najafi, C. Büla, P. F. Leyvraz, and P. Robert. Spatio–temporal parameters of gait measured by an ambulatory system using miniature gyroscopes. *J. Biomech.*, 35(5):689–699, 2002.

[4] K. D. Anderson. Targeting recovery: Priorities of the spinal cord–injured population. *J. Neurotraum.*, 21(10):1371–1383, 2004.

[5] K. K. Ang, C. Guan, K. S. G. Chua, B. T. Ang, C. W. K. Kuah, C. Wang, K. S. Phua, Z. Y. Chin, and H. Zhang. A large clinical study on the ability of stroke patients to use an EEG–based motor imagery brain-computer interface. *Clin. EEG Neurosci.*, 42(4):253–258, 2011.

[6] T. Ball, A. Schreiber, B. Feige, M. Wagner, C. Hermann Lücking, and R. Kristeva-Feige. The role of higher-order motor area in voluntary movement as revealed by high-resolution EEG and fMRI. *Neuroimage*, 10:682–694, 1999.

[7] J. D. Bayliss and D. H. Ballard. A virtual reality testbed for brain–computer interface research. *IEEE T. Rehabil. Eng.*, 8(2):188–190, 2000.

[8] H. Benz, H. Zhang, A. Bezerianos, S. Acharya, N. Crone, X. Zheng, and N. Thakor. Connectivity analysis as a novel approach to motor decoding for prosthesis control. *IEEE T. Neur. Sys. Reh.*, 20(2):143–152, 2012.

[9] N. Birbaumer. Breaking the silence: Brain-computer interfaces (BCI) for communication and motor control. *Psychophysiology*, 43(6):517–532, 2006.

[10] N. Birbaumer, N. Ghanayim, T. Hinterberger, I. Iversen, B. Kotchoubey, A. Kübler, J. Perelmouter, E. Taub, and H. Flor. A spelling device for the paralysed. *Nature*, 398(6725):297–298, 1999.

[11] B. Blankertz, R. Tomioka, S. Lemm, M. Kawanabe, and K. R. Muller. Optimizing spatial filters for robust EEG single–trial analysis. *IEEE Signal Proc. Mag.*, 25(1):41–56, 2008.

[12] S. J. Boniface and U. Ziemann, editors. *Plasticity in the Human Nervous System: Investigations with Transcranial Magnetic Stimulation*. Cambridge University Press, 2003.

[13] Z. I. Botev. A novel nonparametric density estimator. Postgraduate Seminar Series, School of Physical Sciences at The University of Queensland, 2006.

[14] D. Broetz, C. Braun, C. Weber, S. R. Soekadar, A. Caria, and N. Birbaumer. Combination of brain–computer interface training and goal–directed physical therapy in chronic stroke: a case report. *Neurorehab. Neural Re.*, 24(7):674–679, 2010.

[15] E. Buch, C. Weber, L. G. Cohen, C. Braun, M. A. Dimyan, T. Ard, J. Mellinger, A. Caria, S. Soekadar, and A. Fourkas. Think to move: a neuromagnetic brain-computer interface (BCI) system for chronic stroke. *Stroke*, 39(3):910–917, 2008.

[16] N. Caporale and Y. Dan. Spike timing–dependent plasticity: A Hebbian learning rule. *Annu. Rev. Neurosci.*, 31(1):25–46, 2008.

[17] C. W. Chen, C. C. K. Lin, and S. J. Ming. Hand orthosis controlled using brain–computer interface. *J. Med. Biol. Eng.*, 29:234–241, 2009.

[18] G. Cheron, M. Duvinage, C. De Saedeleer, T. Castermans, A. Bengoetxea, M. Petieau, K. Seetharaman, T. Hoellinger, B. Dan, T. Dutoit, and Y. Ivanenko. From spinal central pattern generators to cortical network: Integrated BCI for walking rehabilitation. *Neural Plast.*, 2012:1–13, 2012.

[19] C. Chin, M. Popovic, A. Thrasher, T. Cameron, A. Lozano, and R. Chen. Identification of arm movements using correlation of electrocorticographic spectral components and kinematic recordings. *J. Neural Eng.*, 4(2):146–158, 2007.

[20] J. L. Collinger, M. L. Boninger, T. M. Bruns, K. Curley, W. Wang, and D. J. Weber. Functional priorities, assistive technology, and brain–computer interfaces after spinal cord injury. *J. Rehabil. Res. Dev.*, 50(2):145, 2013.

[21] T. M. Cover and J. A. Thomas. *Elements of Information Theory*. Wiley Interscience, 1991.

[22] S. C. Cramer, L. Lastra, M. G. Lacourse, and M. J. Cohen. Brain motor system function after chronic, complete spinal cord injury. *Brain*, 128:2941–2950, 2005.

[23] S. C. Cramer, M. Sur, B. H. Dobkin, C. O'Brien, T. D. Sanger, J. Q. Trojanowski, J. M. Rumsey, R. Hicks, J. Cameron, D. Chen, W. G. Chen, L. G.

Cohen, C. deCharms, C. J. Duffy, G. F. Eden, E. E. Fetz, R. Filart, M. Freund, S. J. Grant, S. Haber, P. W. Kalivas, B. Kolb, A. F. Kramer, M. Lynch, H. S. Mayberg, P. S. McQuillen, R. Nitkin, A. Pascual-Leone, P. Reuter-Lorenz, N. Schiff, A. Sharma, L. Shekim, M. Stryker, E. V. Sullivan, and S. Vinogradov. Harnessing neuroplasticity for clinical applications. *Brain*, 134(6):1591–1609, 2011.

[24] J. J. Daly, R. Cheng, J. Rogers, K. Litinas, K. Hrovat, and M. Dohring. Feasibility of a new application of noninvasive brain computer interface (BCI): a case study of training for recovery of volitional motor control after stroke. *J. Neurol. Phys. Ther.*, 33(4):203–211, 2009.

[25] J. J. Daly and J. R. Wolpaw. Brain–computer interfaces in neurological rehabilitation. *Lancet Neurol.*, 7(11):1032–1043, 2008.

[26] K. Das and Z. Nenadic. Approximate information discriminant analysis: A computationally simple heteroscedastic feature extraction technique. *Pattern Recogn.*, 41(5):1565–1574, 2008.

[27] K. Das, S. Osechinskiy, and Z. Nenadic. A classwise PCA–based recognition of neural data for brain–computer interfaces. *IEEE Eng. Med. Bio.*, 2007:6520–6523, 2007.

[28] R. Dickstein, M. Gazit-Grunwald, M. Plax, A. Dunsky, and E. Marcovitz. EMG activity in selected target muscles during imagery rising on tiptoes in healthy adults and poststroke hemiparetic patients. *J. Motor Behav.*, 37:475–483, 2005.

[29] H. R. Dinse, G. H. Recanzone, and M. M. Merzenich. Alterations in correlated activity parallel ICMS induced representational plasticity. *NeuroReport*, 5:173–176, 1993.

[30] A. H. Do, P. T. Wang, A. Abiri, C. E. King, and Z. Nenadic. Brain–computer interface controlled functional electrical stimulation system for ankle movement. *J. Neuroeng. Rehabil.*, 8(49), 2011.

[31] A. H. Do, P. T. Wang, A. Abiri, C. E. King, and Z. Nenadic. Brain computer interface control of functional electrical stimulation to restore foot dorsiflexion. In *The 63rd American Academy of Neurology Annual Meeting*, Honolulu, HI, 2011.

[32] A. H. Do, P. T. Wang, C. E. King, L. A. Chui, and Z. Nenadic. Asynchronous BCI control of a walking simulator. In *the 4th International Brain–Computer Interface Meeting*, Asilomar, CA, 2010.

[33] A. H. Do, P. T. Wang, C. E. King, S. N. Chun, and Z. Nenadic. Brain–computer interface controlled robotic gait orthosis. In *IEEE EMB/CAS/SMC Workshop on Brain-Machine-Body Interfaces*, San Diego, CA, 2012.

[34] A. H. Do, P. T. Wang, C. E. King, S. N. Chun, and Z. Nenadic. Brain–computer interface controlled robotic gait orthosis. *J. Neuroeng. Rehabil.*, 10(111), 2013.

[35] A. H. Do, P. T. Wang, C. E. King, A. Schombs, S. N. Chun, and Z. Nenadic. Brain–computer interface controlled robotic gait orthosis. In *the 5th International Brain–Computer Interface Meeting*, Asilomar, CA, 2013.

[36] A. H. Do, P. T. Wang, C. E. King, A. Schombs, S. C. Cramer, and Z. Nenadic. Brain–computer interface controlled functional electrical stimulation device for foot drop due to stroke. In *IEEE Eng. Med. Bio.*, pages 6414–6417, San Diego, CA, 2012.

[37] A. H. Do, P. T. Wang, C. E. King, A. Schombs, J. J. Lin, M. Sazgar, F. P. K. Hsu, S. J. Shaw, D. E. Millett, C. Y. Liu, A. A. Szymanska, L. A. Chui, and Z. Nenadic. Sensitivity and specificity of upper extremity movements decoded from electrocorticogram. In *IEEE Eng. Med. Bio.*, pages 5618–5621, Osaka, Japan, 2013.

[38] A. H. Do, P. T. Wang, C. E. King, A. Schombs, Z. Nenadic, and S. C. Cramer. Brain–computer interface controlled functional electrical stimulation as a novel approach to improving foot–drop after stroke. In *International Stroke Conference*, Honolulu, HI, 2013.

[39] B. H. Dobkin. *The Clinical Science of Neurologic Rehabilitation*. Oxford University Press, 2nd edition, 2003.

[40] Y. Dong, C. J. Winstein, R. Albistegui-DuBois, and B. H. Dobkin. Evolution of fMRI activation in the perilesional primary motor cortex and cerebellum with rehabilitation training–related motor gains after stroke: a pilot study. *Neurorehab. Neural Re.*, 21(5):412–428, 2007.

[41] G. Dornhege. *Toward Brain–Computer Interfacing*. Neural Information Processing Series. MIT Press, 2007.

[42] R. O. Duda, P. E. Hart, and D. G. Stork. *Pattern Classification*. Wiley–Interscience, 2001.

[43] P. W. Duncan and S. M. Lai. Stroke recovery. *Top. Stroke Rehabil.*, 4(3):51–58, 1997.

[44] C. Enzinger, S. Ropele, F. Fazekas, M. Loitfelder, F. Gorani, T. Seifert, G. Reiter, C. Neuper, G. Pfurtscheller, and G. Müller-Putz. Brain motor system function in a patient with complete spinal cord injury following extensive brain-computer interface training. *Exp. Brain Res.*, 190(2):215–223, 2008.

[45] L. A. Farwell and E. Donchin. Talking off the top of your head: toward a mental prosthesis utilizing event–related brain potentials. *Electroen. Clin. Neuro.*, 70(6):510–523, 1988.

[46] B. J. Fisch and R. Spehlman. *Fisch and Spehlmann's EEG Primer: Basic Principles of Digital and Analog EEG*. Elsevier Ltd., 3 edition, 1999.

[47] R. A. Fisher. The use of multiple measurement in taxonomic problems. *Ann. Eugenic.*, 7(2):179–188, 1936.

[48] X. Gao, D. Xu, M. Cheng, and S. Gao. A BCI–based environmental controller for the motion–disabled. *IEEE T. Neur. Sys. Reh.*, 11(2):137–140, 2003.

[49] A. Goffer. Gait–locomotor apparatus, 2006.

[50] M. Gongora, C. Peressutti, S. Machado, S. Teixeira, B. Velasques, and P. Ribeiro. Progress and prospects in neurorehabilitation: clinical applications of stem cells and brain computer interface for spinal cord lesions. *Neurol. Sci.*, 34(4):427–433, 2013.

[51] D. Graupe, R. Davies, H. Kodylewski, and K. H. Kohn. Ambulation by traumatic T4–12 paraplegics using functional neuromuscular stimulation. *Crit. Rev. Neurosurg.*, 8:221–231, 1998.

[52] D. Graupe and K. H. Kohn. Functional neuromuscular stimulator for short–distance ambulation by certain thoracic–level spinal–cord–injured paraplegics. *Surg. Neurol.*, 50(3):202–207, 1998.

[53] J. B. Green. Brain reorganization after stroke. *Top. Stroke Rehabil.*, 10(3):1–20, 2003.

[54] F. E. Grubbs. Procedures for detecting outlying observations in samples. *Technometrics*, 11(1):1–21, 1969.

[55] C. Guan, M. Thulasidas, and J. Wu. High performance P300 speller for brain–computer interface. In *IEEE International Workshop on Biomedical Circuits and Systems*, 2004.

[56] A. Hacking. Arduino UNO mouse HID version 0.1, 2011.

[57] N. Hajela, C. K. Mummidisetty, A. C. Smith, and M. Knikou. Corticospinal reorganization after locomotor training in a person with motor incomplete paraplegia. *Biomed. Res. Int.*, 2013:516427, 2013.

[58] S. Hamid and R. Hayek. Role of electrical stimulation for rehabilitation and regeneration after spinal cord injury: an overview. *Eur. Spine J.*, 17(9):1256–1269, 2008.

[59] E. Hardin, R. Kobetic, L. Murray, M. Corado-Ahmed, G. Pinault, J. Sakai, S. N. Bailey, C. Ho, and R. J. Triolo. Walking after incomplete spinal cord injury using an implanted FES system: A case report. *J. Rehabil. Res. Dev.*, 44(3):333–346, 2007.

[60] S. Harkema, Y. Gerasimenko, J. Hodes, J. Burdick, C. Angeli, Y. Chen, C. Ferreira, A. Willhite, E. Rejc, R. G. Grossman, and V. R. Edgerton. Effect of epidural stimulation of the lumbosacral spinal cord on voluntary movement, standing, and assisted stepping after motor complete paraplegia: a case study. *Lancet*, 377(9781):1938–1947, 2011.

[61] D. Hebb. *The Organization of Behaviour: A Neuropsychological Theory*. Wiley, 1949.

[62] D. A. Heldman, W. Wang, S. S. Chan, and D. W. Moran. Local field potential spectral tuning in motor cortex during reaching. *IEEE T. Neur. Sys. Reh.*, 14(2):180–183, 2006.

[63] S. Hesse. Locomotion therapy in neurorehabilitation. *NeuroRehabilitation*, 16(3):133–139, 2001.

[64] L. Hochberg, M. Serruya, G. Friehs, J. Mukand, M. Saleh, A. Caplan, A. Branner, D. Chen, R. D. Penn, and J. Donoghue. Neuronal ensemble control of prosthetic devices by a human with tetraplegia. *Nature*, 442(7099):164–171, Jul 2006.

[65] L. R. Hochberg, D. Bacher, B. Jarosiewicz, N. Y. Masse, J. D. Simeral, J. Vogel, S. Haddadin, J. Liu, S. S. Cash, P. van der Smagt, and J. P. Donoghue. Reach and grasp by people with tetraplegia using a neurally controlled robotic arm. *Nature*, 485(7398):372–375, 2012.

[66] U. Hoffmann, J.-M. Vesin, T. Ebrahimi, and K. Diserens. An efficient P300–based brain–computer interface for disabled subjects. *J. Neurosci. Meth.*, 167(1):115–125, 2008.

[67] B. J. Holinski, K. A. Mazurek, D. G. Everaert, R. B. Stein, and V. K. Mushahwar. Restoring stepping after spinal cord injury using intraspinal microstimulation and novel control strategies. In *IEEE Eng. Med. Bio.*, pages 5798–5801, Boston, MA, 2011.

[68] S. Hotz-Boendermaker, M. Funk, P. Summers, P. Brugger, M. C. Hepp-Reymond, A. Curt, and S. S. Kollias. Preservation of motor programs in paraplegics as demonstrated by attempted and imagined foot movements. *NeuroImage*, 39:383–394, 2008.

[69] P. J. Huber. *Robust Statistics*. Wiley Series in Probability and Statistics–Applied Probability and Statistics Section Series. Wiley, 2004.

[70] T. E. Hutchinson, K. P. White, W. N. Martin, K. C. Reichert, and L. A. Frey. Human–computer interaction using eye–gaze input. *IEEE T. Syst. Man. Cyb.*, 19(6):1527–1534, 1989.

[71] E. Jacobson. Electrical measurements of neuromuscular states during mental activities: Imagination of movement involving skeletal muscle. *Am. J. Physiol.*, 91:567–608, 1930.

[72] H. H. Jasper. Report of the committee on methods of clinical examination in electroencephalography: 1957. *Electroen. Clin. Neuro.*, 10(2):370–375, 1958.

[73] S. Jezernik, G. Colombo, T. Keller, H. Frueh, and M. Morari. Robotic orthosis Lokomat: a rehabilitation and research tool. *Neuromodulation*, 6(2):108–115, 2003.

[74] H. S. Jørgensen. The copenhagen stroke study experience. *J. Stroke Cerebrovasc.*, 6(1):5–16, 1996.

[75] H. S. Jørgensen, H. Nakayama, H. O. Raaschou, and T. S. Olsen. Recovery of walking function in stroke patients: The copenhagen stroke study. *Arch. Phys. Med. Rehab.*, 76(1):27–32, 1995.

[76] S. Kanoh, K. Miyamoto, and T. Yoshinobu. Development of brain-computer interface (BCI) system for bridging brain and computer. In *13th International Conference on Biomedical Engineering*, volume 23, pages 2264–2267, Singapore, 2009.

[77] S. M. Kay. *Fundamentals of Statistical Signal Processing: Detection Theory*, volume 2. Prentice-Hall, New Jersey, 07458, 1998.

[78] C. E. King, K. R. Dave, P. T. Wang, M. Mizuta, D. J. Reinkensmeyer, A. H. Do, S. Moromugi, and Z. Nenadic. Performance assessment of a brain–computer interface driven hand orthosis. *Ann. Biomed. Eng.*, (in revision), 2014.

[79] C. E. King, C. M. McCrimmon, P. T. Wang, C. C. Y. Chou, A. H. Do, and Z. Nenadic. Noninvasive brain–computer interface driven functional electrical stimulation device for ambulation. In *Orange County Graduate Women in Science Spring Conference*, Irvine, CA, 2014.

[80] C. E. King, C. M. McCrimmon, P. T. Wang, C. C. Y. Chou, Z. Nenadic, and A. H. Do. Brain–computer interface driven functional electrical stimulation system for overground walking: a case report. In *American Academy of Neurology Annual Meeting*, Philadelphia, PA, 2014.

[81] C. E. King, P. T. Wang, L. A. Chui, A. H. Do, and Z. Nenadic. Operation of a brain–computer interface walking simulator by users with spinal cord injury. *J. Neuroeng. Rehabil.*, 10(77), 2012.

[82] C. E. King, P. T. Wang, C. M. McCrimmon, C. C. Y. Chou, A. H. Do, and Z. Nenadic. Brain computer interface driven functional electrical stimulation system for overground walking in spinal cord injury participant. In *IEEE Eng. Med. Bio.*, Chicago, IL, 2014 (accepted).

[83] C. E. King, P. T. Wang, M. Mizuta, D. J. Reinkensmeyer, A. H. Do, S. Moromugi, and Z. Nenadic. Noninvasive brain–computer interface driven hand orthosis. In *IEEE Eng. Med. Bio.*, pages 5786–5789, Boston, MA, 2011.

[84] C. E. King, P. T. Wang, Z. Nenadic, and A. H. Do. BCI controlled walking simulator for a BCI driven FES device. In *The 39th Neural Interfaces Conference*, Long Beach, CA, 2010.

[85] R. Kohavi. A study of cross–validation and bootstrap for accuracy estimation and model selection. In *Int. Joint C. Art. Int.*, pages 1137–1145, 1995.

[86] A. Kostov and M. Polak. Parallel man–machine training in development of EEG–based cursor control. *IEEE T. Rehabil. Eng.*, 8(2):203–205, 2000.

[87] D. J. Krusienski, E. W. Sellers, D. J. McFarland, T. M. Vaughan, and J. R. Wolpaw. Toward enhanced P300 speller performance. *J. Neurosci. Meth.*, 167(1):15–21, 2008.

[88] J. Kubánek, K. J. Miller, J. G. Ojemann, J. R. Wolpaw, and G. Schalk. Decoding flexion of individual fingers using electrocorticographic signals in humans. *J. Neural Eng.*, 6(6):066001, 2009.

[89] C. La Fougère, A. Zwergal, A. Rominnger, S. Förster, G. Fesl, M. Dieterich, T. Brandt, M. Strupp, P. Bartenstein, and K. Jahn. Real versus imagined locomotion: a 18F-FDG PET-fMRI comparison. *Neuroimage*, 50(4):1589–1598, 2010.

[90] F. Lebon, D. Rouffet, C. Collet, and A. Guillot. Modulation of EMG power spectrum frequency during motor imagery. *Neurosci. Lett.*, 435:181–185, 2008.

[91] R. Leeb, D. Friedman, G. R. Müller-Putz, R. Scherer, M. Slater, and G. Pfurtscheller. Self-paced (asynchronous) BCI control of a wheelchair in virtual environments: a case study with a tetraplegic. *Comput. Intell. Neurosci.*, page 79642, 2007.

[92] E. C. Leuthardt, G. Schalk, J. W. Wolpaw, J. G. Ojemann, and D. W. Moran. A brain–computer interface using electrocorticographic signals in humans. *J. Neural Eng.*, 1:63–71, 2004.

[93] M. F. Levin, J. A. Kleim, and S. L. Wolf. What do motor "recovery" and "compensation" mean in patients following stroke? *Neurorehab. Neural Re.*, 23(4):313–319, 2009.

[94] N. Liang and L. Bougrain. Decoding finger flexion from band–specific ECoG signals in humans. *Front. Neurosci.*, 6(6), 2012.

[95] B. Libet, C. Gleason, E. Wright, and D. Pearl. Time of conscious intention to act in relation to onset of cerebral activity (readiness–potential). *Brain*, 106:623–642, 1983.

[96] K. C. Lin, Y. F. Chang, C. Y. Wu, and Y. A. Chen. Effects of constraint–induced therapy versus bilateral arm training on motor performance, daily functions, and quality of life. *Neurorehab. Neural Re.*, 23(5):441–448, 2009.

[97] A. R. Luft, S. McCombe-Waller, and J. Whitall. Repetitive bilateral arm training and motor cortex activation in chronic stroke: A randomized controlled trial. *JAMA- J. Am. Med. Assoc.*, 292(15):1853–1861, 2004.

[98] S. Mazzoleni, G. Stampacchia, E. Cattin, E. Bradaschia, M. Tolaini, B. Rossi, and M. C. Carrozza. Effects of a robot–mediated locomotor training on EMG activation in healthy and SCI subjects. In *11^{th} IEEE Int. Conf. Rehab. Robotics*, pages 378–382, 2009.

[99] D. McFarland, L. Miner, T. Vaughan, and J. Wolpaw. Mu and beta rhythm topographies during motor imagery and actual movements. *Brain Topography*, 12:177–186, 2000.

[100] D. J. McFarland, W. A. Sarnacki, and J. R. Wolpaw. Electroencephalographic (EEG) control of three-dimensional movement. *J. Neural Eng.*, 7(3):036007, 2010.

[101] M. Middendorf, G. McMillan, G. Calhoun, and K. S. Jones. Brain–computer interfaces based on the steady–state visual–evoked response. *IEEE T. Rehabil. Eng.*, 8(2):211–214, 2000.

[102] S. Moromugi, K. Kawakami, K. Nakamura, T. Sakamoto, and T. Ishimatsu. A tendon–driven glove to restore finger function for disabled. In *ICROS-SICE Int. Joint. Conf.*, Fukuoka, Japan, 2009.

[103] G. Müller-Putz, R. Scherer, G. Pfurtscheller, and R. Rupp. EEG-based neuroprosthesis control: a step towards clinical practice. *Neurosci Lett*, 382(1-2):169–174, 2005.

[104] G. R. Müller-Putz, R. Scherer, C. Brauneis, and G. Pfurtscheller. Steady-state visual evoked potential (SSVEP)-based communication: impact of harmonic frequency components. *J. Neural Eng.*, 2(4):123–130, 2005.

[105] A. R. Murguialday, V. Aggarwal, A. Chatterjee, Y. Cho, R. Rasmussen, B. O'Rourke, S. Acharya, and N. V. Thakor. Brain-computer interface for a prosthetic hand using local machine control and haptic feedback. In *IEEE International Conference on Rehabilitation Robotics*, pages 609–613, Nice, France, 2008.

[106] Z. Nenadic. Information discriminant analysis: Feature extraction with an information–theoretic objective. *IEEE T. Pattern Anal.*, 29(8):1394–1407, 2007.

[107] Z. Nenadic, P. T. Wang, C. E. King, A. H. Do, and L. A. Chui. Asynchronous brain–computer interface control of ambulation simulator. In *Soc. Neurosci. Abstr.*, San Diego, CA, 2010.

[108] C. Neuper and G. Pfurtscheller. Post–movement synchronization of beta rhythms in the EEG over the cortical foot area in man. *Neurosci. Lett.*, 216:17–20, 1996.

[109] R. Ortner, B. Z. Allison, G. Korisek, H. Gaggl, and G. Pfurtscheller. An SSVEP BCI to control a hand orthosis for persons with tetraplegia. *IEEE T. Neur. Sys. Reh.*, 19(1):1–5, 2011.

[110] G. Pfurtscheller and A. Aranibar. Evaluation of event-related desynchronization (ERD) preceding and following voluntary self–paced movement. *Electroen. Clin. Neuro.*, 46(2):138–146, 1979.

[111] G. Pfurtscheller, R. Leeb, C. Keinrath, D. Friedman, C. Neuper, C. Guger, and M. Slater. Walking from thought. *Brain Res.*, 1071:145–152, 2006.

[112] G. Pfurtscheller, G. Müller, J. Pfurtscheller, H. Gerner, and R. Rupp. 'thought'–control of functional electrical stimulation to restore hand grasp in a patient with tetraplegia. *Neurosci. Lett.*, 351(1):33–36, 2003.

[113] G. Pfurtscheller and C. Neuper. Event–related synchronization of mu rhythm in the EEG over the cortical hand area in man. *Neurosci. Lett.*, 174:93–96, 1994.

[114] G. Pfurtscheller, C. Neuper, C. Andrew, and G. Edlinger. Foot and hand area mu rhythms. *Int. J. Psychophysiol.*, 26:121–135, 1997.

[115] T. Pistohl, A. Schulze-Bonhage, A. Aertsen, C. Mehring, and T. Ball. Decoding natural grasp types from human ECoG. *NeuroImage*, 59(1):248–260, 2012.

[116] M. M. Priebe, M. Martin, L. A. Wuermser, T. Castillo, and J. McFarlin. The medical management of pressure ulcers. In V. W. Lin, D. D. Cardenas, and N. C. Cutter, editors, *Spinal Cord Medicine–Principles and Practice*, pages 567–590. Demos Medical Publishing, New York, NY, 2003.

[117] H. Probst, D. Dodwell, J. C. Gray, and M. Holmes. An evaluation of the accuracy of semi–permanent skin marks for breast cancer irradiation. *Radiography*, 12(3):186–188, 2006.

[118] A. Ramos-Murguialday, D. Broetz, M. Rea, L. Läer, Ö. Yilmaz, F. L. Brasil, G. Liberati, M. R. Curado, E. Garcia-Cossio, and A. Vyziotis. Brain–machine–interface in chronic stroke rehabilitation: a controlled study. *Ann. Neurol.*, 74:100–108, 2013.

[119] I. H. Robertson and J. M. J. Murre. Rehabilitation of brain damage: brain plasticity and principles of guided recovery. *Psychol. Bull.*, 125(5):544–575, 1999.

[120] D. Romilly, C. Anglin, R. Gosine, C. Hershler, and S. Raschke. A functional task analysis and motion simulation for the development of a powered upper–limb orthosis. *IEEE T. Rehabil. Eng.*, 2(3):119–129, 1994.

[121] S. T. Roweis and L. K. Saul. Nonlinear dimensionality reduction by locally linear embedding. *Science*, 290(5500):2323–2326, 2000.

[122] D. N. Rushton. Functional electrical stimulation and rehabilitation–an hypothesis. *Med. Eng. Phys.*, 25(1):75–78, 2003.

[123] P. Sabbah, S. De Schonen, C. Leveque, S. Gay, F. Pfefer, C. Nioche, J. L. Sarrazin, H. Barouti, M. Tadie, and Y. S. Cordoliani. Sensorimotor cortical activity in patients with complete spinal cord injury: a functional magnetic resonance imaging study. *J. Neurotraum.*, 19:53–60, 2002.

[124] S. Sabharwal. Cardiovascular dysfunction in spinal cord disorders. In V. W. Lin, D. D. Cardenas, and N. C. Cutter, editors, *Spinal Cord Medicine–Principles and Practice*, pages 179–192. Demos Medical Publishing, New York, NY, 2003.

[125] M. Salvaris and F. Sepulveda. Visual modifications on the P300 speller BCI paradigm. *J. Neural Eng.*, 6(4):046011, 2009.

[126] G. Santhanam, S. I. Ryu, B. M. Yu, A. Afshar, and K. V. Shenoy. A high–performance brain–computer interface. *Nature*, 442(7099):195–198, 2006.

[127] G. Schalk. Sensor modalities for brain–computer interfacing. In J. A. Jacko, editor, *Human-Computer Interaction: Novel Interaction Methods and Techniques*, volume 5611 of *Lecture Notes in Computer Science*, pages 616–622. Springer Berlin Heidelberg, 2009.

[128] J. K. Schmitt and D. L. Schroeder. Endocrine and metabolic consequences of spinal cord injuries. In V. W. Lin, D. D. Cardenas, and N. C. Cutter, editors, *Spinal Cord Medicine–Principles and Practice*, pages 221–235. Demos Medical Publishing, New York, NY, 2003.

[129] E. W. Sellers, D. J. Krusienski, D. J. McFarland, T. M. Vaughan, and J. R. Wolpaw. A P300 event–related potential brain–computer interface (BCI): the effects of matrix size and inter stimulus interval on performance. *Biol. Psychol.*, 73(3):242–252, 2006.

[130] H. Serby, E. Yom-Tov, and G. F. Inbar. An improved P300–based brain–computer interface. *IEEE T. Neur. Sys. Reh.*, 13(1):89–98, 2005.

[131] S. Silvoni, A. Ramos-Murguialday, M. Cavinato, C. Volpato, G. Cisotto, A. Turolla, F. Piccione, and N. Birbaumer. Brain–computer interface in stroke: a review of progress. *Clin. EEG Neurosci.*, 42(4):245–252, 2011.

[132] E. Smith and M. Delargy. Locked–in syndrome. *Brit. Med. J.*, 330(7488):406–409, 2005.

[133] T. Solis-Escalante, G. Müller, and G. Pfurtscheller. Overt foot movement detection in one single Laplacian EEG derivation. *J. Neurosci. Meth.*, 175:148–153, 2008.

[134] S. Sutton, M. Braren, J. Zubin, and E. R. John. Evoked–potential correlates of stimulus uncertainty. *Science*, 150(700):1187–1188, 1965.

[135] K. Takano, T. Komatsu, N. Hata, Y. Nakajima, and K. Kansaku. Visual stimuli for the P300 brain–computer interface: a comparison of white/gray and green/blue flicker matrices. *Clin. Neurophysiol.*, 120(8):1562–1566, 2009.

[136] D. M. Taylor, S. I. Tillery, and A. B. Schwartz. Direct cortical control of 3D neuroprosthetic devices. *Science*, 296(5574):1829–1832, 2002.

[137] K. Torkkola. Feature extraction by non–paramatric mutual information maximization. *J. Mach. Learn. Res.*, 3:1415–1438, 2003.

[138] G. Townsend, B. K. LaPallo, C. B. Boulay, D. J. Krusienski, G. E. Frye, C. K. Hauser, N. E. Schwartz, T. M. Vaughan, J. R. Wolpaw, and E. W. Sellers. A novel P300–based brain–computer interface stimulus presentation paradigm: moving beyond rows and columns. *Clin. Neurophysiol.*, 121(7):1109–1120, 2010.

[139] J. H. van der Lee, R. C. Wagenaar, G. J. Lankhorst, T. W. Vogelaar, W. L. Deville, and L. M. Bouter. Forced use of the upper extremity in chronic stroke patients: Results from a single–blind randomized clinical trial. *Stroke*, 30:2369–2375, 1999.

[140] D. van der Westhuysen. Parallel port joystick, 2011.

[141] H. J. A. van Hedel and V. Dietz. Rehabilitation of locomotion after spinal cord injury. *Restor. Neurol. Neuros.*, 28(1):123–134, 2010.

[142] B. Várkuti, C. Guan, Y. Pan, K. S. Phua, K. K. Ang, C. W. K. Kuah, K. Chua, B. T. Ang, N. Birbaumer, and R. Sitaram. Resting state changes in functional connectivity correlate with movement recovery for BCI and robot–assisted upper–extremity training after stroke. *Neurorehab. Neural Re.*, 62(1):53–62, 2013.

[143] F. B. Vialatte, M. Maurice, J. Dauwels, and A. Cichocki. Steady–state visually evoked potentials: Focus on essential paradigms and future perspectives. *Prog. Neurobiol.*, 90(4):418–438, 2010.

[144] vJoy. vjoy virtual joystick, 2014.

[145] P. T. Wang, C. E. King, L. A. Chui, A. H. Do, and Z. Nenadic. Self–paced brain–computer interface control of ambulation in a virtual reality environment. *J. Neural Eng.*, 9(5):056016, 2012.

[146] P. T. Wang, C. E. King, L. A. Chui, Z. Nenadic, and A. H. Do. BCI controlled walking simulator for a BCI driven FES device. In *RESNA Annual Conference*, Las Vegas, Nevada, 2010.

[147] P. T. Wang, C. E. King, A. H. Do, and Z. Nenadic. A durable, low–cost electrogoniometer for dynamic measurement of joint trajectories. *Med. Eng. Phys.*, 33(5):546–552, 2011.

[148] P. T. Wang, C. E. King, A. H. Do, and Z. Nenadic. Pushing the communication speed limit of a noninvasive brain–computer interface. *ArXiv CoRR*, abs/1212.0569, 2012.

[149] P. T. Wang, C. E. King, A. Schombs, J. J. Lin, M. Sazgar, F. P. K. Hsu, S. J. Shaw, D. Millett, C. Y. Liu, L. A. Chui, Z. Nenadic, and A. H. Do. Electrocorticogram encoding of upper extremity movement trajectories. In *IEEE Eng. Med. Bio. Neural Eng.*, pages 1429–1432, San Diego, CA, 2013.

[150] P. T. Wang, C. E. King, A. Schombs, J. J. Lin, M. Sazgar, F. P. K. Hsu, S. J. Shaw, D. E. Millett, C. Y. Liu, L. A. Chui, Z. Nenadic, and A. H. Do. Electrocorticographic gamma band power encodes the velocity of upper extremity movements. In *The 5th International Brain–Computer Interface Meeting*, volume Article ID: 120, Asilomar, CA, 2013.

[151] P. T. Wang, C. E. King, S. J. Shaw, D. E. Millett, C. Y. Liu, L. A. Chui, Z. Nenadic, and A. H. Do. A co–registration approach for electrocorticogram electrode localization using post–implantation MRI and CT of the head. In *IEEE Eng. Med. Bio. Neural Eng.*, pages 525–528, San Diego, CA, 2013.

[152] P. T. Wang, E. J. Puttock, C. E. King, A. Schombs, J. J. Lin, M. Sazgar, F. P. K. Hsu, S. J. Shaw, D. E. Millett, C. Y. Liu, L. A. Chui, A. H. Do, and Z. Nenadic. State and trajectory decoding of upper extremity movements from electrocorticogram. In *IEEE Eng. Med. Bio. Neural Eng.*, San Diego, CA, 2013.

[153] Q. Wang, Z. Ji, K. Miller, and G. Schalk. Prior knowledge improves decoding of finger flexion from electrocorticographic signals. *Front. Neurosci.*, 5(127), 2011.

[154] Z. Wang, A. Gunduz, P. Brunner, A. Ritaccio, Q. Ji, and G. Schalk. Decoding onset and direction of movements using electrocorticographic (ECoG) signals in humans. *Front. Neuroeng.*, 5(15), 2012.

[155] Z. Warraich and J. A. Kleim. Neural plasticity: The biological substrate for neurorehabilitation. *Phys. Med. Rehabil.*, 2(12):S208–S219, 2010.

[156] T. Wehner, S. Vogt, and M. Stadler. Task-specific EMG–characteristics during mental training. *Psychol. Res.*, 46:389–401, 1984.

[157] J. A. Wilson, E. A. Felton, P. C. Garell, G. Schalk, and J. C. Williams. ECoG factors underlying multimodal control of a brain–computer interface. *IEEE T. Neur. Sys. Reh.*, 14(2):246–250, 2006.

[158] S. L. Wolf, C. J. Winstein, J. P. Miller, E. Taub, G. Uswatte, D. Morris, C. Giuliani, K. E. Light, and D. Nichols-Larsen. Effect of constraint–induced movement therapy on upper extremity function 3 to 9 months after stroke. *J. Am. Med. Assoc.*, 296(17):2095–2104, 2006.

[159] J. R. Wolpaw, N. Birbaumer, D. J. McFarland, G. Pfurtscheller, and T. M. Vaughan. Brain–computer interfaces for communication and control. *Clin. Neurophysiol.*, 113(6):767–791, 2002.

[160] J. R. Wolpaw, G. Loeb, B. Z. Allison, E. Donchin, O. F. do Nascimento, W. J. Heetderks, F. Nijboer, W. Shain, and J. Turner. BCI meeting 2005–workshop on signals and recording methods. *IEEE T. Neur. Sys. Reh.*, 14(2):138–141, 2006.

[161] J. R. Wolpaw and D. J. McFarland. Control of a two–dimensional movement signal by a noninvasive brain–computer interface in humans. *P. Natl. Acad. Sci. USA*, 101(51):17849–17854, 2004.

[162] J. Wright. The FIM, 2000.

[163] W. Wu, Y. Gao, E. Bienenstock, J. Donoghue, and M. Black. Bayesian population decoding of motor cortical activity using a Kalman filter. *Neural Comput.*, 18:80–118, 2006.

[164] T. Yanagisawa, M. Hirata, Y. Saitoh, H. Kishima, K. Matsushita, T. Goto, R. Fukuma, H. Yokoi, Y. Kamitani, and T. Yoshimine. Electrocorticographic control of a prosthetic arm in paralyzed patients. *Ann. Neurol.*, 71(3):353–361, 2012.

[165] Y. Zehnder, M. Lüthi, D. Michel, H. Knecht, R. Perrelet, I. Neto, M. Kraenzlin, G. Zäch, and K. Lippuner. Long–term changes in bone metabolism, bone mineral density, quantitative ultrasound parameters, and fracture incidence after spinal cord injury: a cross-sectional observational study in 100 paraplegic men. *Osteoporos. Int.*, 15(3):180–189, 2004.

[166] R. Zerafa, T. Camilleri, O. Falzon, and K. P. Camilleri. Comparison of plain and checkerboard stimuli for brain computer interfaces based on steady state visual evoked potentials. In *IEEE Eng. Med. Bio. Neural Eng.*, pages 33–36, San Diego, CA, 2013.

[167] D. Zhang, X. Gao, S. Gao, A. K. Engel, and A. Maye. An independent brain–computer interface based on covert shifts of non–spatial visual attention. In *IEEE Eng. Med. Bio.*, pages 539–542, Minneapolis, MN, 2009.

[168] D. Zhang, G. Liu, G. Huan, J. Liu, and X. Zhu. A hybrid FES rehabilitation system based on CPG and BCI technology for locomotion: A preliminary study. In M. Xie, Y. Xiong, C. Xiong, H. Liu, and Z. Hu, editors, *Intell. Rob. App.*, volume 5928 of *Lecture Notes in Computer Science*, pages 1073–1084. Springer Berlin Heidelberg, 2009.

Appendices

A Our Current Methodology

The following algorithms must be performed to be able to develop a prediction model and classify EEG signals in real time:

1. Remove electromyogram (EMG) contaminated channels.
2. Transform the data into the frequency domain using the fast Fourier transform (FFT) or take 400 ms after the onset of the stimulus of temporal data for the P300 speller system (see Section 1.2.2 in Chapter 1 for differences between our cue and self-paced BCI systems).
3. Vertically reshape the data.
4. Apply classwise principal component analysis (CPCA) [27] to extract the salient features and reduce the dimensions of the data to m dimensions.
5. Apply approximate information discriminant analysis (AIDA) [26] or Fisher's linear discriminant analysis (LDA) [47] to further reduce the dimensions of the data to a $c-1$ dimensional feature, where c are the total number of classes.
6. Use a linear Bayesian classifier to classify the resulting feature.

7. Send the output BCI decision to the external device or interface.

A.1 Fast Fourier Transform (FFT)

For the self-paced BCI systems (i.e. all systems except for the P300 speller system), once the channels whose EEG data contains excessive EMG are removed (see Section 2.4.1 of Chapter 2), FFT must be performed in order to transform the data into the frequency domain using the following equation:

$$FFT(x_k) = \sum_{n=0}^{N-1} x_n e^{-i2\pi k \frac{n}{N}} \tag{A.1}$$

for $k = 0, \ldots, N-1$. After the data is transformed into the frequency domain, its power spectral density (PSD) is integrated in 2 Hz bins (ω), centered at $\frac{N}{2} + 1$. Specifically, the power spectral density at each of these frequencies is calculated using the Fourier transform of the autocorrelation function, i.e.:

$$PSD(\omega_k) = \frac{1}{N^2}[|FFT(x_k)|^2 + |FFT(x_{N-k})|^2] \tag{A.2}$$

for $k = 1, 2, \ldots, (\frac{N}{2} - 1)$. Also, $FFT(x)$ is the transform described in Eq. A.1 and ω_k is the frequency bins defined above (has B total bins).

A.2 Vertical Reshape

To be able to perform CPCA on the data in the frequency or temporal domain, the data matrix must first be vertically reshaped.

Let A be a B by C matrix,

$$\mathbf{A} = \begin{pmatrix} a_{11} & a_{12} & \cdots & a_{1C} \\ a_{21} & a_{22} & \cdots & a_{2C} \\ \vdots & \ddots & \ddots & \vdots \\ a_{B1} & a_{B2} & \cdots & a_{BC} \end{pmatrix} \tag{A.3}$$

Then, $\bar{a}$ is the vertically reshaped version of $\mathbf{A}$, which is defined as:

$$\bar{a} = \begin{bmatrix} a_{11} & a_{21} & \cdots & a_{B1} & a_{12} & a_{22} & \cdots & a_{B2} & \cdots & a_{1C} & a_{2C} & \cdots & a_{BC} \end{bmatrix}^T \tag{A.4}$$

The resulting vector consists of the first column of the matrix, followed by the second column, and so on.

A.3 Feature Extraction

Once the data is vertically reshaped, CPCA [27] is performed to reduce the dimensions of the data and extract the salient features. This is done using the following steps:

1. Calculate the class-specific covariance matrix:

$$\mathbf{\Sigma_i} = \bar{a}\bar{a}^T \tag{A.5}$$

   where $\bar{a}$ is the trial or observation. Calculate this covariance matrix for $i = 1, \ldots, c$, where c is the total number of classes.

2. Calculate the eigenvalues and eigenvectors of the class-specific covariance ma-

trix:

$$\mathbf{\Sigma_c} V = \lambda V \tag{A.6}$$

where λ are the eigenvalues and V are the eigenvectors of the class-specific covariance matrix.

3. Reduce the dimensions of the data using a mean eigenvalue threshold, $\bar{\lambda}$. Then, remove the eigenvectors corresponding to the eigenvalues that are less than the mean.

4. Calculate the between class covariance matrix:

$$\mathbf{\Sigma_b} = \sum_{i=1}^{c} p_i (\mu_i - \mu)^T (\mu_i - \mu) \tag{A.7}$$

where μ_i are the means of the individual classes and the prior probabilities of each class are p_i, which is the number of samples in the class divided by the total number of samples:

$$p_i = \frac{\text{number of samples in the class}}{\text{total number of samples}} \tag{A.8}$$

Also, the global mean, μ is defined as:

$$\mu = \sum_{i=1}^{c} p_i \mu_i \tag{A.9}$$

5. Perform principal component analysis (PCA) on the between class covariance matrix, $\mathbf{\Sigma_b}$, using the same methods above (steps 2 and 3).

6. Augment the eigenvectors belonging to each class to the between class eigenvectors.

7. Orthonormalize the resulting matrix.

8. Use the resulting orthonormalization to define $\mathbf{\Phi_C}(d)$.

Finally, to reduce the dimension of the data to a 1-D feature, f, the following AIDA [26] *or* LDA [47, 42] algorithms are used. Note that AIDA or LDA is chosen as the appropriate algorithm to use during the cross-validation procedure described in Appendix B.1. Specifically, the following steps are performed during AIDA:

1. Calculate the empirical prior probabilities using the known class labels (same as p_i described above for the CPCA algorithm), the m-dimensional class means, μ_i, and their covariances, $\mathbf{\Sigma_i}$, for $i = 1, \ldots, c$. See the CPCA algorithm above for how to calculate $\mathbf{\Sigma_i}$.

2. Calculate the global mean, μ, and the within class covariance matrix, $\mathbf{\Sigma_w}$.

$$\mathbf{\Sigma_w} = \sum_{i=1}^{c} p_i \Sigma_i \tag{A.10}$$

   Note that the global mean, μ, is described in the CPCA algorithm above.

3. Calculate the between class covariance matrix, $\mathbf{\Sigma_b}$, as described in the CPCA algorithm above.

4. Decorrelate the between class covariance matrix using the covariance of the parameters, $\mu\mu^T$:

$$\mathbf{\Sigma_b} = \mathbf{\Sigma_b} - \mu\mu^T \tag{A.11}$$

5. Calculate the total covariance matrix, $\mathbf{\Sigma}$:

$$\mathbf{\Sigma} = \mathbf{\Sigma_w} + \mathbf{\Sigma_b} \tag{A.12}$$

where the within class covariance matrix $\mathbf{\Sigma_w}$ and the between class covariance matrix $\mathbf{\Sigma_b}$ are used.

6. Calculate the inverse square root of the within class covariance matrix, $\mathbf{\Sigma_w}^{-\frac{1}{2}}$.

7. Calculate $\mathbf{S}_{DA}$, the approximate μ-measure [26], using the following equation:

$$\mathbf{S}_{DA} = \log(\mathbf{\Sigma_w}^{-\frac{1}{2}}\mathbf{\Sigma}\mathbf{\Sigma_w}^{-\frac{1}{2}}) - \sum_{i=1}^{c} p_i \log(\mathbf{\Sigma_w}^{-\frac{1}{2}}\mathbf{\Sigma_i}\mathbf{\Sigma_w}^{-\frac{1}{2}}) \tag{A.13}$$

8. Reduce the number of dimensions in $\mathbf{S}_{DA}$ to m (usually 2) dimensions by performing PCA on $\mathbf{S}_{DA}$ and retaining only the m largest eigenvectors, V.

9. Calculate $\mathbf{T}_{DA}$, the transformation matrix, using the following equation:

$$\mathbf{T}_{DA} = V^T \mathbf{\Sigma_w}^{-\frac{1}{2}} \tag{A.14}$$

where V are the eigenvectors and $\mathbf{\Sigma_w}$ is the within class covariance matrix.

10. If AIDA produces a better performance than LDA from the cross-validation procedure described in Appendix B.1, then use the following combination of CPCA and AIDA:

$$f^\star = \mathbf{T}_{DA}\mathbf{\Phi}_C(d) \tag{A.15}$$

where $\mathbf{T}_{DA}$ is the AIDA transformation matrix.

For the LDA algorithm, the following steps are used [42, 47]:

1. Compute the m-dimensional class means, prior probabilities, and covariances, μ_i, $\mathbf{\Sigma_i}$, and p_i, where m is the dimension of the data after CPCA feature extraction. Also, compute the within class covariance matrix, $\mathbf{\Sigma_w}$ and the between

class covariance matrix $\mathbf{\Sigma_b}$ as described in the AIDA and CPCA algorithms above, respectively.

2. Find the criterion function, $J(.)$, or the generalized Rayleigh quotient [42]:

$$J(\mathbf{w}) = \frac{\mathbf{w}^T \mathbf{\Sigma_b} \mathbf{w}}{\mathbf{w}^T \mathbf{\Sigma_w} \mathbf{w}} \tag{A.16}$$

where $\mathbf{w}$ is the optimal direction of the projection of the samples onto a discriminating line. To find the vector, $\mathbf{w}$, that maximizes $J(.)$, we must satisfy the following equation:

$$\mathbf{\Sigma_b} \mathbf{w} = \lambda \mathbf{\Sigma_w} \mathbf{w} \tag{A.17}$$

where λ are the eigenvalues.

3. If the within class covariance matrix, $\mathbf{\Sigma_w}$, is non-singular, then use the conventional eigenvalue problem and solve for $\mathbf{w}$:

$$\mathbf{\Sigma_w}^{-1} \mathbf{\Sigma_b} \mathbf{w} = \lambda \mathbf{w} \tag{A.18}$$

4. Thus, if $\mathbf{\Sigma_w}$ is non-singular, and can be inverted, then the criterion function is maximized when the LDA transformation matrix, $\mathbf{T}_{DA}$, is composed of the eigenvectors of:

$$\mathbf{\Sigma_w}^{-1} \mathbf{\Sigma_b} \tag{A.19}$$

Note that there will be at most $c - 1$ eigenvectors with non-zero real corresponding eigenvalues. From these eigenvectors, we have obtained $\mathbf{w}$ for Fisher's linear discriminant [47], a linear function that yields the maximum ratio of the between-class to within-class scatter, i.e. covariances. Also, we have now

mapped an m-dimensional data set onto $c-1$ dimension for a c class system.

5. If LDA produces a better performance than AIDA from the cross-validation procedure described in Appendix B.1, then use the following combination of CPCA and LDA:

$$f^\star = \mathbf{T}_{DA}\mathbf{\Phi}_C(d) \tag{A.20}$$

where $\mathbf{T}_{DA}$ is the $c-1$ dimensional projection in direction $\mathbf{w}$, or the LDA transformation matrix, described in the steps above.

A.4 Classification

Once the feature, $f^\star$, is extracted, classification can be performed using a linear Bayesian classifier [42]. This formula (Eq. 2.2 in Section 2.4.2 of Chapter 2) can be derived using the overall risk [42]:

$$R = \int R(\alpha(f^\star)|f^\star)P(f^\star)df^\star \tag{A.21}$$

where $\alpha(f^\star)$ is the decision function of action α, which assumes a value for the input feature $f^\star$. The conditional risk associated with action α is then:

$$\begin{aligned} R(C_1|f^\star) &= \lambda_{C_1,C_2}P(C_2|f^\star) \\ R(C_2|f^\star) &= \lambda_{C_2,C_1}P(C_1|f^\star) \end{aligned} \tag{A.22}$$

where $R(C_1|f^\star)$ is the conditional risk of classifying the feature $f^\star$ as "Class 1". Then, decide that the feature $f^\star$ belongs to "Class 1" if $R(C_1|f^\star) < R(C_2|f^\star)$ (i.e. the likelihood ratio test [42]). In terms of the posterior probabilties, we decide the

feature $f^\star$ belong to class C_1 if:

$$(\lambda_{C_2,C_1} - \lambda_{C_1,C_1})P(C_1|f^\star) > (\lambda_{C_1,C_2} - \lambda_{C_2,C_2})P(C_2|f^\star) \tag{A.23}$$

where the factors $\lambda_{C_1,C_2} - \lambda_{C_1,C_1}$ and $\lambda_{C_1,C_2} - \lambda_{C_2,C_2}$ are positive. Thus, in practice, the decision is generally determined by employing the Bayes' formula:

$$P(C_i|f^\star) = \frac{p(f^\star|C_i)P(C_i)}{p(f^\star)} \tag{A.24}$$

where $C_i = C_1, C_2$ are the classes. The Bayes' formula can be expressed informally as the posterior probability of "Class i" given the feature $f^\star$ is the likelihood ($p(f^\star|C_i)$) times the prior ($P(C_i)$) divided by the evidence ($p(f^\star)$). By replacing the posterior probabilities with the prior probabilities and the conditional densities from the two equations above, the following rule can be found. Decide class C_1 if:

$$(\lambda_{C_2,C_1} - \lambda_{C_1,C_1})p(f^\star|C_1)P(C_1) > (\lambda_{C_1,C_2} - \lambda_{C_2,C_2})p(f^\star|C_2)P(C_2) \tag{A.25}$$

and decide class C_2 otherwise. In order to implement this into our binary state machine, we can assume $(\lambda_{C_2,C_1} - \lambda_{C_1,C_1})$ and $(\lambda_{C_1,C_2} - \lambda_{C_2,C_2})$ are equal, as the likelihood of false alarms and omissions are equal in our binary state machine. Also, if we assume equal prior probabilities for each class, as this is true in the case of our self-paced BCI systems (note that $P(C_1) = \frac{1}{7}$ and $P(C_2) = \frac{6}{7}$ in the P300 speller system described in Section 1.2.3 of Chapter 1), the decision rule becomes:

$$\frac{P(f^\star|C_1)}{P(f^\star|C_2)} \begin{array}{c} C_1 \\ > \\ < \\ C_2 \end{array} 1 \tag{A.26}$$

Finally, the posterior probabilities, $P(f^\star|C_1)$ and $P(f^\star|C_2)$ are calculated from:

$$P(f^\star|C_1) = \frac{f_{PDF}(f^\star|C_1)P(C_1)}{f_{PDF}(f^\star)} \tag{A.27}$$

where $P(C_1)$ is the prior probability of "Class 1" trials and $f_{PDF}(f^\star|C_1)$ is the conditional probability density function (PDF) of features under "Class 1". A similar expression is derived for $P(f^\star|C_2)$. Finally, the parameters of the linear Bayesian classifier can be estimated by assuming features that are conditionally Gaussian, i.e. $f|C_1 \sim \mathbb{N}(\hat{\mu_{C_1}}, \hat{\sigma}^2)$ and $f|C_2 \sim \mathbb{N}(\hat{\mu_{C_2}}, \hat{\sigma}^2)$, where $\hat{\mu_{C_1}}$ and $\hat{\mu_{C_2}}$ are the conditional sample means of the features under "Class 1" and "Class 2" classes, respectively, and $\hat{\sigma}^2$ is the unconditional sample variance of the features [42].

B Statistical Analyses and Performance Measurements

B.1 Cross-Validation

To assess the performance of the feature extraction and classification methods on the training data, stratified 10-fold cross-validation is performed [85]. Specifically, the following steps are performed to determine the number of misclassified trials and the probabilities of false alarm and omission errors:

1. Randomly separate the EEG trials from the training data into 10 groups of equal size, or 10 folds, while preserving the ratio of the class labels (1:1 for our self-paced BCI systems, and 1:6 for our P300 speller system). Note that the word *stratified* in our cross-validation method allows proportion of these labels

to be maintained.

2. Train the parameters of CPCA, AIDA or LDA, and linear Bayesian classifier using the data from 9 folds and the methods described in Appendix A.

3. Transform the remaining fold of data into the feature domain and classify this fold assuming an equal cost of omissions and false alarm probabilities (see below for definition). Calculate the cross-validation estimate of accuracy as the overall number of correct classifications divided by the number of instances in the data. Formally, if D_i is the test fold that includes instances $x_i = \langle C_{1,i}, C_{2,i} \rangle$, then the cross-validation estimate of accuracy is defined as:

$$\mathbf{acc_{CV}} = \frac{1}{N} \sum_{\langle C_{1,i}, C_{2,i} \rangle \in D} \delta(\mathcal{I}(\frac{D}{D_{(i)}, C_{1,i}}), C_{2,i}) \tag{B.28}$$

where $\mathcal{I}$ is the inducer on data set D, which maps the given data set onto the linear Bayesian classifier.

4. Repeat steps 2 and 3 above until all 10 folds are exhausted, each time designating a different fold for classification. The number of misclassified trials is used to calculate the probabilities of false alarm and omission errors using the following confusion matrix:

Table B.1: Confusion matrix where T and D are the true and decoded labels of trials.

T \ D	$\hat{C}_1$	$\hat{C}_2$
C_1	$p(\hat{C}_1 \mid C_1)$	$p(\hat{C}_2 \mid C_1)$
C_2	$p(\hat{C}_1 \mid C_2)$	$p(\hat{C}_2 \mid C_2)$

where C_1 and C_2 are classes "Class 1" and "Class 2", respectively. Also, note that $p(\hat{C}_1|C_1)$ is the fraction of correctly decoded "Class 1" trials, and $p(\hat{C}_2|C_1) = 1 - p(\hat{C}_1|C_1)$ is the probability of an omission. Similarly, $p(\hat{C}_2|C_2)$

is the fraction of correctly decoding "Class 2" trials, and $p(\hat{C}_1|C_2) = 1-p(\hat{C}_2|C_2)$ is the probability of a false alarm. By combining these two types of errors, the probability of misclassification can be defined as:

$$p_e = p(\hat{C}_2|C_1)p(C_1) + p(\hat{C}_1|C_2)p(C_2) \tag{B.29}$$

Finally, the probability of correct classification is defined as $p_c = 1 - p_e$, or Eq. B.28 given above.

5. Estimate the standard deviation of these errors by repeating the 10-fold cross validation procedure 10 times, each time re-randomizing the grouping of trials into folds.

6. Determine the parameters for optimal online operation by maximizing the output classification accuracy (Eq. B.28) from the stratified 10-fold cross-validation procedure. This includes finding the best discriminant analysis method, AIDA *or* LDA, to use for the given training data set.

B.2 Cross-Correlation Analysis

In order to assess the performance of our self-paced BCI systems, cross-correlation analysis is performed. To this end, the following steps are conducted to determine the maximal correlation at the optimal lag:

1. Remove all dropped packets and outliers from the data sets. This is accomplished by calculating Grubb's test statistic [54] for outliers:

$$G = \frac{\max|x[i] - \bar{x}|}{\sigma} \tag{B.30}$$

where $\bar{x}$ is the sample mean and σ is the standard deviation, respectively. Note that this test statistic is the largest absolute deviation from the sample mean in units of the sample standard deviation. Finally, remove these outliers and interpolate using the known sampling rate to obtain smooth and continuous data for each data set.

2. Determine which physical sensor data set, audio data, or state of the BCI system to use for cross-correlation analysis. Specifically, for the physical sensor data, if more than one trace is used to assess the intended movement, choose the data set that has the maximum difference between the 95^{th} and 5^{th} percentiles of the data. In other words, calculate the k^{th} percentile by ordering all the values in the data set from smallest to largest. Then multiply k percent by the total number of values in the data set, N. Finally, count the values in your data set until you reach the k^{th} percent. After determining each k^{th} percentile, find the maximum of the difference between the 95^{th} and 5^{th} percentiles:

$$x = \max(\text{percentile}(x, 95\%) - \text{percentile}(x, 5\%)) \tag{B.31}$$

3. After choosing the appropriate data sets for intended movement and the output control device movement, determine the epochs of idling and movement using a manual threshold crossing from the physical sensor readings, audio, or state of the BCI system. Note that this manual threshold is determined by plotting the data and empirically determining the appropriate threshold that crosses movement epochs and is above the idling data.

4. Define a time series, x, that describes the intended movement as:

$$x[i] = \begin{cases} -1, & \text{if} \quad i \in C_1 \\ 1, & \text{if} \quad i \in C_2 \end{cases} \tag{B.32}$$

where $i = 1, 2, \ldots, N$, and N is the number of samples in the physical sensor trace. A time series, y, describing the output control device movement, is similarly defined as:

$$y[i] = \begin{cases} -1, & \text{if} \quad i \in C_1 \\ 1, & \text{if} \quad i \in C_2 \end{cases} \tag{B.33}$$

5. Calculate the normalized cross-covariance function between the times series x and y:

$$\rho_{xy}(m) = \begin{cases} \frac{\sum_{n=1}^{N-m} x_{n+m} y_n}{N-m} & m \geq 0 \\ \frac{\sum_{n=1}^{N+m} x_n y_{n-m}}{N+m} & m < 0 \end{cases} \tag{B.34}$$

where $m \in [-N+1, N-1]$ is the lag between the sequences x and y.

6. Find the latency between the two sequences by determining the lag with maximal cross-covariance:

$$m^\star = \arg \max_{-L \leq m \leq L} \rho_{xy}(m) \tag{B.35}$$

where L is the lag cutoff. Subsequently, the maximal temporal correlation between x and y at the optimal lag is determined as:

$$\rho^\star_{xy} = \rho_{xy}(m^\star) \tag{B.36}$$

B.3 Monte Carlo Simulations

To assess the significance of the online performances, Monte Carlo simulations are performed [34]. This is done using the following steps:

1. Define the following auto-regressive model:

$$\begin{aligned} X_{k+1} &= \alpha X_k + \beta W_k \quad X_0 \sim U(0,1) \\ Y_k &= h(X_k) \end{aligned} \tag{B.37}$$

   where X_k is the state variable, $W_k \sim U(0,1)$ is uniform white noise, Y_k is the simulated posterior probability, and h is a piecewise linear saturation function that ensures $y_k \in [0,1]$.

2. Find the coefficients α and β so that the mean, $\mu\{Y_k\}$, and the lag-one (i.e. "one off") correlation coefficient, $\rho(Y_{k+1}, Y_k)$, match those of the posterior probability sequence, $\bar{P}$, observed in the online sessions. Specifically, by assuming that the sequence of simulated posterior probabilities, $\bar{P}_k = \bar{P}(C_2|f_k^\star)$, are wide-sense stationary with mean μ and variance σ^2, the coefficients α and β can be determined from:

$$\begin{aligned} \alpha &= \rho \\ \alpha\mu + \tfrac{\beta}{2} &= \mu \end{aligned} \tag{B.38}$$

   where ρ is the correlation coefficient between $\bar{P}_{k+1}$ and $\bar{P}_k$.

3. Using the above coefficients, feed the simulated posterior probabilities, $\{Y_k\}$, into the binary state machine (Fig. 2.5 in Section 2.4.2 of Chapter 2). This results in a simulated sequence of "Class 1" and "Class 2" states for each Monte Carlo run.

4. Find the cross-correlation between the intended movement and the simulated BCI states using the cross-correlation methods described above to find the Monte Carlo temporal correlation, $\rho^{\star}_{xy}$.

5. Repeat the above steps for several Monte Carlo runs, typically 10,000 runs, for each online session.

6. Determine the empirical p-value by finding the fraction of Monte Carlo runs that achieved a higher temporal correlation than the online session's $\rho^{\star}_{xy}$.

B.4 Information Transfer Rate and Performance Measures

In addition to the above performance measures, we also calculate the information transfer rate (ITR) as well as other performance measures for our BCI systems. Particularly, we calculate the ITR and the below performance measure for the P300 speller system described in Section 1.2.3 of Chapter 1, the BCI driven walking simulator system described in Section 4.3 of Chapter 4, and the BCI-FES system for overground walking described in Section 4.5 of Chapter 4. For the ITR calculations, the following steps are performed:

1. Given the law of total probability and the confusion matrix described in Table B.1, the following unconditional probabilities of the decoded data can be found:

$$\begin{aligned} p(\hat{C}_1) &= p(\hat{C}_1|C_1)p(C_1) + p(\hat{C}_1|C_2)p(C_2) \\ p(\hat{C}_2) &= p(\hat{C}_2|C_1)p(C_1) + p(\hat{C}_2|C_2)p(C_2) \end{aligned} \tag{B.39}$$

where $\hat{C}_1$ and $\hat{C}_2$ are the outputs of the binary state machine given in Fig. 2.5

in Section 2.4.2 of Chapter 2.

2. Calculate the unconditional entropy [21]:

$$H(\text{out}) = -[p(\hat{C}_1)\log_2 p(\hat{C}_1) + p(\hat{C}_2)\log_2 p(\hat{C}_2)] \tag{B.40}$$

3. Estimate the conditional entropy, $H(\text{out}|\text{in})$, from [21] using the following equation:

$$\begin{aligned} H(\text{out}|\text{in}) &= H(\text{out}|\text{in} = C_1)p(C_1) + H(\text{out}|\text{in} = C_2)p(C_2) \\ &= -[p(\hat{C}_1|C_1)\log_2 p(\hat{C}_1|C_1) + p(\hat{C}_2|C_1)\log_2 p(\hat{C}_2|C_1)]p(C_1) \\ &\quad -[p(\hat{C}_1|C_2)\log_2 p(\hat{C}_1|C_2) + p(\hat{C}_2|C_2)\log_2 p(\hat{C}_2|C_2)]p(C_2) \end{aligned} \tag{B.41}$$

4. Use the mutual information to calculate the reduction in the output uncertainty by subtracting $H(\text{out}|\text{in})$ from $H(\text{out})$ given in the above equations:

$$I(\text{out}, \text{in}) = H(\text{out}|\text{in}) - H(\text{out}) \tag{B.42}$$

5. If the observed features, $f^\star$, carry no class-relevant information, then the confusion matrix entries in Table B.1 become:

$$\begin{aligned} p(\hat{C}_1|C_1) &= p(\hat{C}_1|C_2) = 0 \\ p(\hat{C}_2|C_2) &= p(\hat{C}_2|C_1) = 1 \end{aligned} \tag{B.43}$$

In addition to the above entries, the chance-level performance of the Bayesian classifier is $p_e = p(C_1)$ and $p_c = p(C_2)$. For the self-paced BCI systems, given a 1:1 ratio of each class, the chance performance $p_c = 50\%$. Conversely, for the P300 speller system, given a 1:6 ratio of each class, the chance performance $p_c = 85.7\%$. Finally, given the equations above and using l'Hôpital's rule, it readily follows that $H(\text{out}) = 0$, $H(\text{out}|\text{in}) = 0$, and $I(\text{in}, \text{out}) = 0$.

6. To calculate the theoretical maximum for each communication channel and for a perfect classifier, we have:

$$p(\hat{C}_1|C_1) = p(\hat{C}_2|C_2) = 1 \tag{B.44}$$

From the law of total probability explained above, we obtain $p(\hat{C}_1) = p(C_1)$ and $p(\hat{C}_2) = p(C_2)$. Thus, since the output is no longer considered random and the input is known, it follows that $H(\text{out}|\text{in}) = 0$. Finally, assuming that the class ratio for the P300 speller system is 1:6 and is 1:1 for our other self-paced BCI systems, the theoretical maxima for these systems are $I(\text{out}, \text{in}) = 0.5917$ bits/transmission and $I(\text{out}, \text{in}) = 1$ bit/transmission, respectively.

It can be shown in the methods above that unless the communication channel is symmetric (i.e. $p(\hat{C}_2|C_1) = p(\hat{C}_1|C_2)$), $I(\text{in}, \text{out})$ *cannot* be expressed as a function of p_e and p_c (see the cross-validation procedure described in Appendix B.1). Note that $p(\hat{C}_2|C_1) = p(\hat{C}_1|C_2)$ is true in the case of our self-paced BCI systems for movement vs. idling, but not in the case of our P300 speller system.

Given the above explanation, the ITR analysis described in [159] uses a symmetric binary communication channel to model their BCI system, similar to our self-paced BCI systems (i.e. the prior probabilities are equal given an equal number of instances of "Class 1" and "Class 2" in the data set). However, the system described in [159] is a P300 speller system, which given definition of the oddball paradigm [45], this system *cannot* have equal probabilities of oddball and non-oddball classes. Thus, the equation from [159]:

$$I(\text{in}, \text{out}) = \log_2 C + p_c \log_2 p_c + p_e \log_2(\frac{p_e}{C-1}) \tag{B.45}$$

where C are the number of classes in the system (i.e. $C = 2$), is not adequate

in the context of P300 speller BCI systems. However, this equation can be used for our self-paced BCI systems, where the expression above reduces to $I(\text{in}, \text{out}) = 1 + p_c \log_2 p_c + p_e \log_2 p_e$. Finally, this equation represents the capacity, i.e. the maximal achievable ITR, of a binary *symmetric* channel [21], and thus should not be used for practical ITR calculations for our BCI systems.

The performance measures for the BCI driven walking simulator described in Section 4.3 of Chapter 4 and the BCI-FES system for overground walking described in Section 4.5 of Chapter 4 utilizes a composite score to assess the performance of a self-paced BCI system in a self-paced manner. To this end, the goal-oriented tasks result in two performance measures: course completion time and cone score or number of successful stops. To combine these scores into a single performance measure, a composite score is defined. This is accomplished by performing the following steps:

1. Given the difficulty of interpreting multivariate performance measures across participants and sessions, the following geometric mean is used:

$$c = \sqrt{c_s c_t} \tag{B.46}$$

   where c_s and c_t are the normalized performance measures for the number of successful stops and the course completion time, respectively.

2. Determine c_s and c_t by normalizing each variable with the limits of the goal-oriented task:

$$c_s = \frac{s}{s_{max}} \tag{B.47}$$

$$c_t = \frac{t_{max} - t}{t_{max} - t_{min}} \tag{B.48}$$

where s is the participant's number of successful stops, s_{max} is the maximum number of successful stops (e.g. 10 in the BCI driven walking simulator), t is the participant's completion time, t_{max} is the maximum allowed time (e.g. 1200 s in the BCI driven walking simulator), and t_{min} is the minimum time required to complete the course while achieving all successful stops (e.g. 201.52 s in the BCI driven walking simulator). The values of c_s and c_t, and consequently c, range from 0 to 100%, where 100% corresponds to a perfect performance. Finally, note that the use of the geometric mean favors a performance that is balanced over a performance that sacrifices one performance measure over the other, and the normalization of c_s and c_t ensures that the performance measures are unitless.

B.5 False Alarms and Omissions

To determine the number of false alarms and omissions during online BCI operation, the bounds of the cues, states and physical sensor data must first be determined. This is accomplished by the following steps:

1. Determine which physical sensor data is best for extracting the bounds of the movement.

2. Check the input dimension and plot the data in time using the known sampling rate.

3. If the signal is an audio signal (i.e. for the cue signal), calculate the signal

power. Then, set the resulting low and high values to -1 and 1, respectively.

4. If the signal is a binary signal that ranges from 0 to 1, set the 0 values to -1.
5. Filter the signal from 0.001 to 35 Hz using a Butterworth band pass filter.
6. Manually determine the appropriate threshold to extract the bounds by plotting the signal.
7. Find the rising and falling edges of the signal using the determined threshold.
8. Extract the timing boundaries from the rising and falling edges of the signal.

Once the bounds of the data are extracted, the signals are converted into sequences x and y based on the bounds:

$$x[i], y[i] = \begin{cases} -1, & \text{if } i \in C_1 \\ 1, & \text{if } i \in C_2 \end{cases} \tag{B.49}$$

where $i = 1, 2, \ldots, N$, and N is the number of samples in the signals.

Once the signals are converted, the number of false alarms and omissions for each online session can be calculated. A false alarm is defined as the initiation of a BCI response within any C_1 epoch (e.g. C_1 is "idle" for the movement based BCIs). Similarly, an omission is defined as the absence of a BCI response within any C_2 epoch (e.g. C_2 is "move" for the movement based BCIs). To find these errors, the following steps are performed:

1. Determine which signal is the test signal and reference signal. Typically, the reference signal is the cue given to the participant, and the test signal is the BCI state or physical sensor signals.

2. Convert the reference and test signals to 0 and 1's.

3. Using the methods described above, extract the timing bounds of the reference and test signals.

4. Determine the maximum possible number of omissions and false alarms based on the size of the signals, and decrease this number by looking at the reference and test signal. If a test signal is on when the reference signal is on, delete the number of omissions for this epoch.

5. Decrease the number of false alarms by determining whether the test signal is off when the reference signal is off, and deleting the number of false alarms for this epoch.

6. Look through all of the reference epochs, and determine if the test signal is "stuck" on during this epoch to determine the number of times the BCI response is stuck on during an off epoch.

7. Look through all of the reference epochs using the edges of the bounds, and determine if a false activation or deactivation occurs by determining when the falling edges of the bounds in the test data occur.

8. Plot the reference and test signals to verify the number of false alarms, omissions, false activations, false deactivations, and the number of times the BCI is "stuck" in its current state.